EPFL

Thèse n° 9253

The complex winds of the Alps: an unseen asset for the energy transition

Présentée le 27 octobre 2021

Faculté de l'environnement naturel, architectural et construit
Laboratoire des sciences cryosphériques
Programme doctoral en génie civil et environnement

pour l'obtention du grade de Docteur ès Sciences

par

Jérôme François Sylvain DUJARDIN

Acceptée sur proposition du jury

Prof. S. Takahama, président du jury
Prof. M. Lehning, directeur de thèse
Prof. J. Lundquist, rapporteuse
Dr I. Gouttevin, rapporteuse
Prof. A. Davison, rapporteur

École polytechnique fédérale de Lausanne

2021

For a successful technology,
reality must take precedence over public relations,
for Nature cannot be fooled.
— Richard Feynman

For my son Robin and the coming generations,...

Acknowledgements

My journey as a Ph.D. student started with my beloved partner in life Annelen Kahl, and as such I must start my acknowledgments with her, because without her I would not be submitting this thesis today. We started as climbing partners when she was a Ph.D. student herself, and it evolved almost instantly into being partners in all aspects of life. It only took her five years to convince my stubborn mind to leave the industrial sector for a more fulfilling position in academia, and since that moment we have also been partners in science. During the last four years she has provided optimism and precious guidance to me through the ups and downs of completing this thesis. I cannot thank her enough for bringing me back to academia, introducing me to the extraordinary scientific community I am now a part of, and pushing me into a fulfilling career addressing the most critical issues facing our planet today.

Second, I would like to thank my Ph.D. supervisor Michael Lehning, an amazing leader and scientist. This thesis would have not been possible without him. Despite my atypical background, he offered me a position as a scientific collaborator to work on a subject that I consider very important: the transition away from fossil fuels. I am profoundly grateful that, more than five years ago, he placed his trust in me. More than bringing me into academia, he convinced me to pursue a Ph.D. and offered me the opportunity and privilege to do so. Along the way he gave me the freedom to shape my own research and to explore topics that interested me. Thanks to him, I also got the opportunity, and honor, to join the Japanese expedition JARE60 to Antarctica. This was a unique and quite incredible experience that I will never forget. I am looking forward to our continuing collaboration on this project in the coming years, and to a lifelong friendship through our shared passion for creating a better future for our planet through renewable energy.

Stuart Bartlett, my first colleague at EPFL, was the initiator of the electrical system modeling described in Part I. I want to thank him for the time he spent introducing me to this research topic and for our collaboration that led to the interesting models described in this thesis. As I was working on my Ph.D., my interest for atmospheric sciences and for wind energy progressively grew. Varun Sharma and Bert Kruyt, colleagues at EPFL and SLF, sparked and nourished my interest for these topics. Our many interesting conversations were a true source of inspiration, and I learned a lot by their side. I also want to thank two other colleagues at EPFL, Adrien Michel and Mahdi Jafari, for all the fun times and for their support during some difficult moments.

Finally, I will write something about my son Robin, hoping he will read it in a few years. Having a little baby in the last year of the Ph.D. was a challenging endeavor to say the least, but being

such a sweet boy and a good sleeper made me feel he tried his best to keep me sane during this hectic, but rewarding, time in my life. Thank you, my boy, for that! Scientists around the world are working tirelessly to find solutions to the burdens that our civilization is inflicting on future generations. Robin gives me strength and motivation to work harder, and I hope the world will be on a better path by the time he reads these lines.

Lausanne, October 2, 2021 J. D.

Abstract

Wind energy has played a major role in the development of our society since 5000 BC when the first sail boats travelled the Nile River. Wind technology continued to advance with the invention of wind-powered pumps and mills in China and the Middle East as early as 200 BC, and by the late 19^{th} century the first electricity-generating wind turbines were built. Today the effects of human driven climate change are pushing the world to transition from a fossil fuel dominated energy diet to a menu composed of a variety of technologies powered by renewable energies, including wind power. While this transition is a global challenge for all sectors of society, incorporating the variety of renewable resources into an efficient and reliable electric grid will be one of the greatest challenges our society faces. Our consumption habits and the historical design of our electricity grids were based on relatively few, centralized, and controllable power plants that use various fossil or nuclear fuels to generate power on demand to match real time use. The weather driven nature and low energy density of renewable sources like solar, wind and hydro lead to a more distributed and fluctuating electricity generation, which results in multiple problems: In Switzerland, under the foreseen future where photovoltaic (PV) panels are predominantly installed in urban areas, the nuclear phase-out will cause large deficits of electricity in winter. This thesis contributes to the solution of these important challenges in two ways: first by presenting a model that combines a variety of renewable energy sources to form a reliable and efficient electrical system, and secondly by improving the assessment of wind power potential in the Alps.

The first two parts of this thesis are concerned with the simulation and optimization of the Swiss electrical system, in which the nuclear reactors are replaced by a combination of solar and wind energy sources. A spatially explicit approach is required to consider the spatio-temporal variability in renewable sources. Storage hydropower is a remarkable asset for the energy transition, and thus occupies a central role in the manner the system is modeled and operated (Part I). A novel algorithm explores how the whole system reacts under various combinations of PV and wind energies (Part II). By simultaneously optimizing the generation mix and location of PV panels and wind turbines, while considering the electrical grid and land use, this algorithm showed that a large number of carefully located wind turbines and a small number of PV panels located in the Alps can provide a much more balanced system than the conventional, urban PV scenario. This approach reduces the seasonal imbalance between production and consumption by 80%, while keeping cross-border electricity exchanges at current levels.

Part III of this thesis addresses the difficulty of wind power potential assessment in moun-

tainous terrain. On such terrain, high horizontal resolution is required in the numerical models that simulate the air flows. This constraint, and the need for long time series, prohibit the simulation of large domains and thus the identification of the best locations for wind turbines in the entire Swiss Alps. Downscaling models for wind are often used to obtain high resolution and long time series, but perform poorly on such terrain. In order to improve these models, a new method based on deep learning is presented. It downscales the outputs of the operational numerical model COSMO-1 used for the Swiss weather forecast, which has a resolution of 1.1 km, to a 50-meter resolution. The validation at 60 measurement stations shows that wind speeds and directions are more accurate than COSMO-1 and present many of the expected orographic effects like deflection, sheltering and ridge acceleration.

Résumé

L'énergie éolienne a joué un rôle majeur dans le développement de notre société depuis 5000 avant J.-C., lorsque les premiers bateaux à voile naviguaient sur le Nil. La technologie éolienne a continué à progresser avec l'apparition de pompes et de moulins alimentés par le vent en Chine et au Moyen-Orient dès 200 avant J.-C., et à la fin du 19^{e} siècle, les premières éoliennes génératrices d'électricité ont été construites. Aujourd'hui, les effets du changement climatique provoqué par l'homme poussent le monde à passer d'un régime énergétique dominé par les combustibles fossiles à un menu composé d'une variété de technologies alimentées par des énergies renouvelables, dont l'énergie éolienne. Si cette transition est un défi mondial pour tous les secteurs de la société, l'intégration des multiples ressources renouvelables dans un réseau électrique efficace et fiable sera l'un des plus grands défis que notre société devra relever. Nos habitudes de consommation et la conception historique de nos réseaux électriques reposent sur des centrales électriques relativement peu nombreuses, centralisées et contrôlables, qui utilisent divers combustibles fossiles ou nucléaires pour produire de l'énergie à la demande en fonction de l'utilisation en temps réel. La nature des conditions météorologiques et la faible densité énergétique des sources renouvelables comme le solaire, l'éolien et l'hydroélectricité conduisent à une production d'électricité plus distribuée et fluctuante, ce qui entraîne de multiples problèmes : En Suisse, si les panneaux photovoltaïques (PV) continuent d'être majoritairement installés dans les zones urbaines, la sortie du nucléaire entraînera d'importants déficits d'électricité en hiver. Cette thèse contribue à la solution de ces défis importants de deux manières : d'abord en présentant un modèle qui combine plusieurs énergies renouvelables pour former un système électrique fiable et efficace, et ensuite en améliorant l'évaluation du potentiel éolien dans les Alpes.

Les deux premières parties de cette thèse portent sur la simulation et l'optimisation du système électrique suisse, dans lequel le parc nucléaire est remplacé par une combinaison de sources d'énergie solaire et éolienne. Une approche distribuée spatialement est nécessaire pour considérer la variabilité spatio-temporelle des sources renouvelables. L'hydroélectricité à accumulation est un atout remarquable pour la transition énergétique, et occupe donc un rôle central dans la manière dont le système est modélisé et géré (partie I). Un nouvel algorithme explore la manière dont l'ensemble du système réagit à diverses combinaisons d'énergies PV et éolienne (partie II). En optimisant simultanément la proportion et l'emplacement des panneaux PV et des éoliennes, tout en tenant compte du réseau électrique et de l'utilisation des sols, cet algorithme a montré qu'un grand nombre d'éoliennes judicieusement placées et un peu nombre de panneaux PV situés dans les Alpes peuvent fournir un système beaucoup

plus équilibré que le scénario conventionnel de PV urbain. Cette approche réduit de 80% le déséquilibre saisonnier entre la production et la consommation, tout en maintenant les échanges transfrontaliers d'électricité aux niveaux actuels.

La partie III de cette thèse aborde la difficulté de l'évaluation du potentiel éolien en terrain montagneux. Sur de tels terrains, une haute résolution horizontale est nécessaire dans les modèles numériques qui simulent les flux d'air. Cette contrainte, et le besoin de longues séries temporelles, empêchent la simulation de grands domaines et donc l'identification des meilleurs emplacements pour les éoliennes dans l'ensemble des Alpes suisses. Des modèles de réduction d'échelle pour le vent sont souvent utilisés pour obtenir une haute résolution et de longues séries temporelles, mais ils sont peu performants sur un tel terrain. Afin d'améliorer ces modèles, une nouvelle méthode basée sur l'apprentissage profond est présentée. Elle permet de réduire l'échelle des sorties du modèle numérique opérationnel COSMO-1 utilisé pour les prévisions météorologiques suisses, qui a une résolution de 1,1 km, à une résolution de 50 mètres. La validation à 60 stations de mesure montre que les vitesses et les directions du vent sont plus précises que celles de COSMO-1 et présentent un grand nombre des effets orographiques attendus.

Contents

Acknowledgements i

Abstract (English/Français) iii

1 Introduction: Context and throughline 1
- 1.1 Preamble . . . 1
- 1.2 The energy transition in Switzerland . . . 1
  - 1.2.1 Overview of the Swiss electricity system . . . 2
  - 1.2.2 Modeling and optimizing the electricity system . . . 3
  - 1.2.3 Synergies between energy sources . . . 5
- 1.3 Towards better estimates of wind energy potentials in the Alps . . . 7
  - 1.3.1 Uncertainties in wind potential assessment . . . 7
  - 1.3.2 Downscaling methods . . . 9
  - 1.3.3 A quick introduction to deep learning . . . 10
  - 1.3.4 Wind-Topo: a new downscaling method for highly complex terrain . . . 11

I Charting the course: A possible route to a fully renewable Swiss power system 21

2 Main text 23
- 2.1 Introduction . . . 25
- 2.2 Model construction . . . 27
  - 2.2.1 Overview . . . 27
  - 2.2.2 Hydropower . . . 29
  - 2.2.3 Solar . . . 30
  - 2.2.4 Geothermal . . . 32
  - 2.2.5 Wind . . . 32
  - 2.2.6 Nuclear . . . 32
  - 2.2.7 Grid and demand . . . 33
- 2.3 Results . . . 34
  - 2.3.1 Summary analysis . . . 34
  - 2.3.2 Temporal dynamics . . . 38
  - 2.3.3 Spatial dynamics . . . 41
- 2.4 Discussion . . . 43

2.5 Conclusions . . . 46
2.6 Further work . . . 47

II Synergistic optimization of renewable energy installations through evolution strategy 55

3 Main text 57
3.1 Introduction . . . 59
3.2 Data and Methods . . . 61
3.2.1 Test scenario . . . 61
3.2.2 Constraints and objective function . . . 61
3.2.3 Genetically encoded generation mix and installation locations . . . 62
3.2.4 Power and energy balance models and objective function . . . 62
3.2.5 Electricity generation from PV panels and wind turbines . . . 64
3.2.6 GIS analysis for installation potential . . . 64
3.2.7 Evolution Strategy . . . 66
3.3 Results . . . 68
3.3.1 Wind dominated evolution . . . 69
3.3.2 A solution for the benefit of all . . . 70
3.3.3 Grid constraints . . . 71
3.4 Conclusion and discussion . . . 74

4 Supplementary Information 81

III Wind-Topo: Downscaling near-surface wind fields to high-resolution topography in highly complex terrain with deep learning 95

5 Main text 97
5.1 Introduction . . . 99
5.2 Methods . . . 101
5.2.1 General approach . . . 101
5.2.2 Model inputs . . . 101
5.2.3 New topographic descriptors . . . 102
5.2.4 Data flow . . . 104
5.2.5 Deep learning architecture . . . 105
5.2.6 Loss function . . . 108
5.2.7 Making predictions . . . 109
5.3 Results . . . 109
5.3.1 Aggregated scores . . . 110
5.3.2 Disaggregated scores . . . 112
5.3.3 Selected stations . . . 114
5.3.4 Generated wind fields . . . 117

5.4 Conclusion . . . 120

6 Supplementary Information **127**

Summary, Conclusion and Outlook **139**

A Interplay between photovoltaic, wind energy and storage hydropower in a fully renewable Switzerland **145**
A.1 Introduction . . . 147
A.1.1 Mixing ratios of wind and solar . . . 147
A.1.2 Import/export . . . 148
A.1.3 Selected scenario . . . 149
A.1.4 Outline . . . 149
A.2 Methods . . . 150
A.2.1 Data . . . 150
A.2.2 Strategy for balancing supply and demand as a function of PV-wind mixing ratio . . . 156
A.3 Results . . . 164
A.3.1 Short-term storage capacity required to compensate for excess production 164
A.3.2 Annual required import and export . . . 166
A.3.3 Solutions to limit the annual required import . . . 167
A.3.4 Results for the years 2009-2015 . . . 170
A.4 Conclusion . . . 173
A.5 Add-on: Optimized formulation for the energy storage . . . 177

B Optimized market value of alpine solar photovoltaic installations **183**
B.1 Introduction . . . 185
B.2 Literature Review . . . 187
B.3 Methods . . . 188
B.3.1 Models . . . 189
B.3.2 Scenarios . . . 191
B.4 Results . . . 195
B.4.1 Increased market value . . . 195
B.4.2 Spatial distribution of PV installations . . . 198
B.4.3 Weather driven performance . . . 199
B.4.4 Spatial heterogeneity of market value . . . 200
B.5 Discussion and conclusion . . . 202

Curriculum Vitae **209**

1 Introduction: Context and throughline

1.1 Preamble

This thesis explores the role that alpine wind energy could play in the European energy transition, more specifically in Switzerland. The initial motivation is rooted in the seasonal imbalance in central Europe between winter-peaking electricity consumption and summer-peaking hydropower and photovoltaic (PV) productions. Given the weather regimes in this region, the stronger winds in winter could be an asset for the reduction of this imbalance. However, wind power is generally not considered to be a valuable resource in Switzerland, partially because of the intricacy of the winds in its complex topography and because of low public acceptance. Appendix A shows that wind power is a better complement to the Swiss hydropower system than PV, at least if the electrical grid is not involved. Part I presents a model of the Swiss electrical grid and how it reacts under high shares of distributed renewable generators. Part II builds on this model to optimize the generation mix between PV and wind energies and the locations of the generators. A high share of wind energy located in the mountains has the potential to almost entirely eliminate the seasonal imbalance. Given the difficulty of obtaining accurate wind potentials in highly complex terrain like the Alps, a new downscaling method for near surface wind fields was developed and is presented in Part III.

1.2 The energy transition in Switzerland

The world is on the verge of a global crisis caused by rapid climate change, and is now trying to reduce anthropogenic greenhouse gas emissions. Almost all nations and economic sectors are facing unprecedented challenges in addressing this crisis. In response to these challenges, industries traditionally dominated by fossil fuel combustion such as transportation and heating are transitioning to electricity, but this electricity is still largely derived from fossil fuel or nuclear generation facilities, which emit large amounts of greenhouse gases or have

unresolved issues with spent fuel disposal (nuclear). To address these problems, the Swiss Confederation made an ambitious challenge to the nation: Power the country with renewable sources by 2050. If achieved successfully, this could be an inspiring example for the rest of the world in its course to reduce fossil fuel dependency (5; 16; 23; 49). With its high share of storage hydropower and its diversity of landscapes and climates, Switzerland is well equipped to take up the challenge.

1.2.1 Overview of the Swiss electricity system

Switzerland is part of the synchronous grid of Continental Europe, the largest collection of interconnected grids in the world, reliably providing electricity to 400 million customers in 24 countries. The Continental European grid transmits alternating current electricity at 50 Hz, so all existing and future sources must deliver electricity at this frequency and must be in phase, like musicians in an orchestra rigorously following the beat. Switzerland is centrally located in this jewel of engineering, and all changes to its own system must be compatible with the Continental European grid at large.

For half a century Switzerland relied on hydropower and nuclear energy for its electricity production. Hydropower accounts for approximately 60% of the consumption on an annual basis, almost equally split between non-dispatchable run-of-river power plants and dispatchable storage hydropower plants. Until the end of 2019 nuclear power satisfied the remaining 40% of production on an annual basis. The combination of these two sources produced approximately 60 TWh/year (12). In December 2019, the country began its nuclear phaseout with the decommissioning of the nuclear reactor of Mühleberg, the first of five reactors to be decommissioned by 2035. To fulfill the Paris Agreement and climate policy packages such as the European Commission's "Fit-for-55" (11), Switzerland will have to either replace its nuclear reactors by renewable generators or to rely strongly on its neighbors for large imports of electricity.

One of the biggest challenges in achieving this goal is balancing the various renewable energy sources and storage mechanisms to provide on-demand power to consumers throughout the year, regardless of the current weather conditions. The existing system was designed around a few, centralized, dispatchable power plants from which electricity is distributed in a controlled manner to consumers via an arborescent grid of progressively smaller transmission capacity. The integration of high shares of renewable generators is a real challenge for the electrical system, because of this distributed nature. On the one hand, renewable energies can be a threat on very short time scales (seconds, minutes) for power regulation across the grid, and on the other hand they can generate strong mismatches between production and demand on time scales ranging from minutes to years.

Future Swiss electricity generation will be characterized by two important items: energy storage and generation from large storage hydropower facilities, and a high share of generation from photovoltaic and wind energy. As hydropower in Switzerland is already almost fully

exploited, it is expected that solar and wind will replace what the nuclear fleet has provided until now. Switzerland's complex topography is a challenge for accurate estimates of production potential, but at the same time this high variability presents opportunities for the energy transition. The complementarity between various renewable energy sources and the decorrelation between generators installed in various microclimates are examples of such opportunities.

1.2.2 Modeling and optimizing the electricity system

Aggregated approach

Modeling the entire European electrical system with a level of detail that can resolve all time scales (seconds to years), for all types of sources (dispatchable and non-dispatchable), at a resolution that can capture all the spatio-temporal fluctuations of nature-driven sources (hydro, solar, wind), while considering the whole grid (transmission, distribution) and the electricity market is a Herculean task. Scientists have adopted many different approaches to this problem, each one focusing on a few aspects only. One approach, the so-called copper plate assumption, assumes unrestricted transmission capacities and does not consider the electrical grid linking production and consumption. Many researchers in the energy modeling field use this approach to optimize the generation mix between the various sources (like solar and wind) to achieve various goals: maximize revenue, minimize amount of backup generation or storage. In Europe, (20) optimized the installed capacities of PV and wind in each country to reduce storage requirements, and (39) investigated the same goal with an aggregated approach. (3) optimized the cost of electricity from PV and wind installations in the USA. (28; 7) also optimized the generation portfolio for a fully renewable USA.

Switzerland has an asset that most countries do not possess: a robust storage hydropower system. With more than 10 GW of turbine capacity connected to hydroelectric reservoirs and electricity consumption varying between 4 and 10 GW, the country is well placed to compensate for the intermittencies of PV and wind energy. However, absorbing the overproduction from renewables is currently limited to the 3.6 GW of pumping capacity. Furthermore, the reservoirs associated to these pumps are rather small and can smooth the fluctuations on time scales ranging from a few hours to a few days only. The largest reservoirs, used for turbining, also have a limited total capacity which corresponds to about a month of electricity demand. As most of them are filled with water from snow melt, the general situation is a saturation of the reservoirs at the end of October and a depletion at the end of April. Because of the relatively small capacity of the reservoirs, Switzerland has been a net exporter of electricity in summer and a net importer in winter. With more PV energy entering the system in summer, this imbalance will only increase in the foreseen future. Wind energy, however, can show a production profile that does not coincide with the summer peaks of hydropower production. Wind turbines located in areas that present a high yield in winter could be particularly effective in reducing the seasonal imbalance.

This complex interplay between generation mix (PV and wind) and hydropower system (water inflow, reservoir capacity, pumping) requires a detailed modeling of each component to capture the dynamic of the system as a whole. Appendix A presents such a model and shows how various combinations of PV and wind energies impact the seasonal imbalance and the required exchanges with neighboring countries. It also explores the impacts of oversized PV and wind generation (with more production than demand on an annual basis) and of increased reservoir capacity. With its copper plate approach and predefined, typical placements for PV and wind generators, this study shows the clear advantage of wind energy in Switzerland given the hydropower infrastructure and the water inflows. For high shares of PV, oversized capacities or larger reservoirs do not help. However, large shares of wind energy do not need such measures to keep seasonal imbalances at current levels, and modest oversizing of capacity or reservoirs already leads to a more balanced situation. Under those modeling assumptions, the reaction of the Swiss transmission network to such high shares of PV or wind energy remains an open question. It is also unknown whether spatially distributed hydropower plants can act together to compensate for the distributed fluctuations and to stabilize the grid.

Importance of spatially explicit models

Spatially explicit models of electrical grids are often used to assess how an electrical system reacts, as a whole, under certain distributed loads and generators. These models describe the grid and associated generation with various levels of detail. For Europe, (33) introduce a model of the electrical grid, the generation, and the economics, that maximizes welfare. For Switzerland, (44) simulates the dispatch and load flow through the transmission grid and exchanges with neighboring countries via a linear cost minimization and a detailed representation of the hydropower system. In the same model, (1) integrates a market model and a long-term investment model. The system is optimized to minimize dispatch and investment costs. For more details about modeling tools for energy and electricity systems, the reader is invited to look at the inter-comparison provided in (41). Those Swiss models consider monetary costs as the main drivers for how hydropower plants, among others, are used as dispatchable sources. They supply the generation (or pumping) at any time to perfectly match the demand while minimizing the costs. For hydropower, the costs are defined by the availability of water, and managers try to use it when it is most profitable: at peak demand times when market prices are higher. A free, unregulated market can be seen as on overarching regulating system that generates higher prices when electricity is scarce, thus motivating operators of dispatchable generators to use their resources (water, coal, gas, ...). In Europe, multiple electricity markets that act on different time scales ranging from minutes to years ensure the regulation of the system as a whole. Given the extreme complexity and apparent fragility of the system, it is remarkable that blackouts almost never occur. With increasingly more non-controllable, hard to predict, distributed generation, the grid and associated markets are challenged and new measures will have to be implemented. Only a complex combination of technical, economical and regulatory measures will ensure the safe

operation of the electrical system.

Given the uncertainties about which measures will be implemented, it is important to first identify the dynamics of the system as a function of physically determined variables. Such variables are for example, the solar radiation or kinetic energy from the wind available at any given location and at any particular time. As hydropower can mitigate some of the drawbacks of those energies, we can also look at the theoretical potential for such mitigation given the characteristics of the hydropower infrastructure (turbining / pumping capacities and efficiencies, storage capacity of hydroelectric reservoirs, temporal structure of their water inflows). For Switzerland, a high level of detail with regard to the modeling of the hydropower system is required to capture the potential interplay between the various sources. Part I presents such a modeling effort and shows how the grid and hydropower system react to a particular generation scenario. This scenario reflects the current trend in Switzerland, where the production from nuclear energy is replaced by a large amount of PV panels in populated areas, and by a modest share of wind energy located across the country. This spatially explicit model corroborates the findings (Appendix A) on which some of the hypotheses tested in this thesis are based: Large urban PV installations would increase the seasonal imbalance significantly, but the current grid infrastructure is already sufficient to host the installation of new renewables, and hydropower can be used to accommodate short-term fluctuations.

1.2.3 Synergies between energy sources

The modeling efforts presented in Part I and Appendix A used predetermined, standard placements for PV panels and wind turbines. A synergy between those generators and hydropower can already be observed on several aspects. First, correlations of PV or wind with demand can be exploited to reduce the need for balancing capacities or storage. The complementarity between sources with respect to demand is the subject of many studies (4; 8; 21; 25; 35; 45). Second, storage hydropower can keep its water reserves for times when PV and wind energy do not provide enough to satisfy the demand. Third, overproduction can be absorbed by pumping water to higher elevations. Fourth, hydroelectric reservoirs can act as a buffer on longer time scales, as long as the production profile from PV and wind does not coincide with the water inflow regime, which peaks in June. The research question arising from this is whether these synergies can be amplified even more in order to create a more balanced and robust system.

Strong spatio-temporal variability

Switzerland is characterized by a multitude of microclimates induced by its abrupt topography. In the mountains, the local weather is generated by a combination of synoptic and locally generated circulations. In long valleys, wind is strongly conditioned by thermally driven effects that generate the typical valley winds. When solar radiation on the surrounding slopes is strong, air rises and generates ascending (anabatic) slope flows, which in turn suck the

air from the valley resulting in up-valley winds. At night, the reversed process occurs, with descending (katabatic) slope flows pushing air into the valley, which leads to down-valley winds. Under those effects, wind has a much larger spatial variability in Switzerland than in flatter countries (32). This implies that wind turbines distributed across the country would have generation profiles that are less correlated with each other, which would reduce the peaks of production and the periods of no-production. (32) also showed that measured wind speeds differ between locations with respect to their daily and annual profiles. In long valleys, wind turbines would generate more electricity in summer, especially in the middle of the day, while turbines on ridges or in smaller mountains like the Jura would have an increased winter production. On larger scales, (19) shows that optimized wind turbine capacities in various European countries, under various local weather regimes, can provide a more balanced energy supply, and (2) shows the advantage of interconnecting wind farms in the USA to reduce power fluctuations.

Concerning PV generation, the spatio-temporal variability of solar radiation in Switzerland can also be exploited to influence the production profile. This was investigated in (29), where increased winter production from PV was identified in the Alps. With particularly good weather conditions in winter and the added effects of a thinner atmosphere and of a higher ground reflection from snow, PV panels at high elevation can be installed at steeper angles without losing total (annual) production and can boost the production in winter significantly. This study also uses the model described in Appendix A to evaluate the impact of the location of PV panels on the system as a whole, more specifically on the seasonal mismatch. Alpine PV panels can significantly reduce the deficit of energy in winter, and can consequently reduce the need for supplementary seasonal storage or for import of foreign electricity.

A large space of placement scenarios to explore

The spatio-temporal variability of PV and wind energy is an asset for the Swiss electrical system. Smartly selected and located generators could offer an aggregated production profile that forms the best possible member in the triumvirate composed of demand, storage (pumped) hydropower, and non-dispatchable generation. The optimal synergy between the three, under the constraints imposed by the grid, is explored in Part II. OREES (Optimized Renewable Energy by Evolution Strategy), a novel, nature-inspired algorithm based on evolutionary strategy explores for the first time the space of potential solutions for the installation of PV panels and wind turbines on a national or international level. As mentioned previously, multiple studies focused on finding the optimal generation mix between PV and wind energy for predetermined locations. Other studies focused on the best locations for those generators on a distribution grid, thus on much smaller domains without spatial variability (30). OREES can simultaneously optimize the generation mix and the location of the generators on a high-resolution grid given spatially distributed time series and grid constraints. This can be done on large domains, and dispatchable generation or storage such as storage (pumped) hydropower is used to accommodate the introduction of large shares of fluctuating renewable energy as

much as possible.

For Switzerland, OREES corroborates and refines the dynamics observed in Part I and Appendix A: A large share of wind energy from turbines installed in specific locations is the best solution for a balanced electrical system. As (29) identified, alpine PV installations should also play a significant role. Several questions however remain. First: Is there an economic case for PV panels installed at high elevation, where more difficult accessibility might introduce higher installation costs? Appendix B presents a preliminary answer. Using OREES to find the best locations for PV installation while maximizing their revenues based on the market prices simulated by Swissmod (44; 1), the future of alpine installations looks promising. For PV, optimality from a system perspective seems to be in line with optimality from an economic, owner-based, perspective. Second: Given the complexity of the wind in the Alps, are the current datasets for wind potential assessment accurate enough to identify the locations that are favorable for wind turbines and to understand the impact of this generation on the whole system?

Swiss wind energy: the unpopular

Switzerland currently has 42 wind turbines, while its neighboring countries have seen an exceptional rate of installation in the last decade. The country is, in the common knowledge, not recognized as a hot spot for wind energy. Traditionally, the development of wind turbines and wind energy assessment focused on flat lands, coast lines and offshore, shallow water areas. The relatively high population density in the Northern, flatter part of the country generates a lot of opposition against installing turbines. The wind power potential is also not particularly high. Installations in more complex terrain have to face many difficulties, one being the uncertainty of production in a particular location. For smooth mountain ranges like the Jura in the West, numerical models can quite accurately predict what a turbine would produce. This region currently hosts most of the Swiss wind turbines, and OREES suggests that most installations should be located there. However, more complex terrain like the Alps, despite the increased challenge for potential assessment, are generating increasingly more interest for wind turbine installations (e.g. figure 1.1). Certain long valleys already host a few, very productive wind turbines, and some mountain passes were recently chosen for new installations. As the Jura cannot host all the wind turbines required for the Swiss energy transition, the identification of high potential locations in the Alps is important for the promotion of wind energy.

1.3 Towards better estimates of wind energy potentials in the Alps

1.3.1 Uncertainties in wind potential assessment

Wind in highly complex terrain like the Alps (as depicted in figure 1.2) is shaped by multiple effects on different scales. The wind interacts with topography through orographic effects like

deflection, channeling or ridge acceleration. As mentioned previously, local winds are also generated by thermally driven effects. Estimating the potential for wind energy, and especially obtaining time series of wind speed at the height of the turbine's hub, is a difficult task. In Switzerland, several hundred automatic measurement stations installed in various types of terrain provide wind speed and direction at about 10 meters above ground level (m.a.g.l). To obtain time series at different locations, or gridded data, interpolation schemes are necessary. Unfortunately most of those methods, despite their success on less complex terrain, cannot provide realistic wind fields for the Alps. Numerical Weather Prediction (NWP) models, on the other hand, provide a physically consistent description of the state of the atmosphere on a 3-dimensional grid. The wind fields from such models exhibit the orographic effects and thermally driven flows mentioned above, because the various processes involved in the shaping of the winds are explicitly resolved by the dynamical cores of the models. Despite rapid improvements in computational power, NWP models with domain covering Switzerland and able to generate time series of at least a year have horizontal resolutions greater than a kilometer. For example, the model used operationally by Meteoswiss for the Swiss weather forecast: COSMO-1 (Consortium for Small-scale MOdeling) has a horizontal resolution of 1.1 km, even if it is executed on a super computer (384 graphic processors (GPUs) and 48 conventional CPUs.). In this model, special attention was given to the Alps and underlying interactions with the atmosphere. However, with a 1.1-km resolution, the terrain used in the model is much smoother than the real topography and multiple small valleys and ridges are even not present. Furthermore, for numerical stability, an additional smoothing has to be applied to this terrain to avoid slopes larger than 30 degrees.

When comparing wind fields from COSMO-1 with those from coarser models like COSMO-2 (2.2 km), COSMO-7 (6.6 km) or ECMWF High-RESolution (European Center for Medium Range Weather Forecasts, 9 km), it is clear that a higher-resolution terrain model is key to capturing more realistic wind fields in the Alps. (31) investigates the use of COSMO-1 for wind energy potential assessment in the Swiss Alps and compares its wind fields with measurements from 177 stations (IMIS network (48)). It is found that the modeled wind speeds have no bias on ridges or summits and are reasonably well correlated with the measured ones (Pearson correlation coefficient > 0.5). However, at locations that are sheltered from the main winds, COSMO-1 strongly overestimates the wind speed. A closer look at the terrain used in the model shows that, given its resolution and smoothness, these sheltered sites are seen as locations near or even on (smooth) summits or ridges. COSMO-1 cannot discriminate between two nearby exposed and sheltered stations. (31) also shows the impact of placing turbines in various locations on the whole, aggregated electricity system. It uses the model described in Appendix A, but assumes the power generation from the turbines to be prescribed by what COSMO-1 predicts for every grid point in Switzerland. In doing so, maps of seasonal imbalances can be built and reveal the impact of each location on the system. Long valleys are identified as the worst locations from a system perspective as they provide a lot of wind energy in summer. Exposed ridges and summits on the other hand contribute significantly to the reduction of seasonal imbalance. COSMO-1 can thus show important features of the alpine

wind energy, but its resolution strongly limits the analysis and identification of promising potential locations for new wind turbines. An analysis of the performance of COSMO-2 for wind energy in Switzerland and the possibility of exploiting the various weather regimes to balance the wind variability is provided in (38).

1.3.2 Downscaling methods

To obtain higher-resolution datasets (wind fields for example) from coarser-resolution, available datasets, scientists have developed downscaling methods. Such methods are generally categorized as dynamical or statistical. The former consists in using a physically-based model at high resolution, with boundary conditions and initial conditions prescribed by the coarser dataset. This is often performed in a nested manner, with a cascade of multiple model runs of progressively higher resolutions on smaller inner domains. The Weather Research and Forecasting (WRF) model is an example of such model that is often used to reach resolutions of a few hundred meters (36; 15; 17). Just as for the NWP models described previously, the computational requirements for dynamical downscaling are very high, which implies a trade-off between domain size, resolution and the length of the simulated period. It is currently still impossible to dynamically downscale the entire Swiss Alps at the resolution required for the wind energy assessment ($< \sim$200 m) for long periods (> 1 year). Furthermore, reaching such horizontal resolution remains a difficult task (6).

Statistical downscaling on the other hand is much faster because it does not solve the complex Navier–Stokes equations that govern air flows. Instead, empirical relationships between various predictors (also called explanatory variables) and predictands (the quantity to downscale) are used to generate predictions on higher-resolution grids. For complex topography, the literature offers many methods which often focus on downscaling precipitation. Statistical downscaling of wind, especially in highly complex terrain like the Alps, is less explored. The introduction of Part III provides a review of such methods. In those studies, two different approaches are employed, depending on whether the predictands come from measurements or from high-resolution NWP models. In the first case, point-to-point models (37; 9; 18) are calibrated using wind measurement at some stations and can only give predictions at those stations. Other 2D-to-2D models (34; 27; 24) can replicate higher-resolution wind fields from coarser-resolution atmospheric variables, but only for the domain of calibration. To obtain a model with the ability to give predictions for locations other than the ones used for calibration, one needs to incorporate descriptors of the topography that reflect the wind-topography interactions. Several studies investigated this approach for Switzerland with point-to-point methods that took advantage of the large network of automatic measurement stations. (10; 13) focused on daily maximum wind speed, while (14; 42) focused on mean and monthly values, respectively. Thanks to their topographic descriptors, those studies generated high-resolution maps of the variables investigated.

A further step towards the generation of high spatial resolution time series of wind speed is

provided by (47; 22). The former uses the statistical relationships between the topographic descriptor S_x (46), COSMO-2 and the observed wind speed at 219 stations to generate maps of wind speed with a 25-m resolution. The model performed well for a validation period but was not tested at independent stations, so its generalization capability to new places (between the stations used for calibration) is unknown and it is possible that it overfits (more detail in section 1.3.3) and only performs well at the training stations. (22) adopts a different approach and uses the stations for validation only. The model is trained using a large catalog of simulations from the Advanced Regional Prediction System (ARPS) on synthetic topographies to find the relation between synoptic wind speed and direction, a slope parameter, and local wind speed. When used to downscale COSMO-2, the method gives slightly better performance (compared to a standard interpolation) at exposed sites but is worse at sheltered sites.

Several of the studies mentioned above (37; 9; 18; 24) are based on machine learning techniques and showed the potential to find meaningful statistical relationships between atmospheric conditions on larger scales and local winds. The challenge of a statistical, gridded downscaling method that is effective on highly complex terrain and that maintains good performance at other sites than the calibration ones, remained unsolved. Based on deep learning, Wind-Topo, the new model presented in Part III, is a promising first step that already shows good performance in the Swiss Alps.

1.3.3 A quick introduction to deep learning

Machine learning and its most recent sub-field *deep learning* are showing results that are increasingly better in increasingly more research topics (40; 26). The idea is not new and dates back to the 1960s: a computer algorithm that improves progressively and automatically by using data and feedback about its performance. The recent success and regain of popularity of those methods started with the increased computational power and amount of data available to train the models. This triggered major technical improvements of the models, which now deliver the best results in many applications. Supervised learning is one way to train such models. Some ground truth, also called labeled data or predictand, is required to calculate the errors in the predictions from the model. The errors are computed by a differentiable loss function, for example the mean square error, and the associate gradients with respect to the predicted variable can be successively decomposed using the chain rule to link variation of the model's parameters to reduction of the error. This procedure, called back-propagation (of the error), allows the algorithm to progressively update the model's parameters, which are initialized randomly, in order to minimize the error between predictions and predictands.

Many types of models exist and are based on various building blocks. Probably the most versatile and popular one is the artificial neural network (ANN). It was proven to be able to approximate any type of multivariate function (universal approximation theorem (43)), but it easily suffers from a common drawback of many machine learning algorithms: overfitting. A model that is sufficiently complex and that is trained on a sufficiently large amount of data is

able to replicate its predictands perfectly. This can be seen as a sort of memorization, where the trained model can even predict the noise that is present in its training data. However, such models behave poorly on new data. The common practice is to split the available predictands into at least two sets: one to train the model, and one to evaluate its performance on new data. Many variations of cross-validation exist and are more or less appropriate to each particular situation. A difficult task is to find the best compromise between good performance on the training set and good generalization capability on the validation set. A model that does not perform well on the training set can indicate insufficient complexity, bad architecture, or inadequate training. Whereas a lack of performance on the validation set can indicate excessive complexity, inappropriate predictors, or a lack of regularization.

Deep learning is a sub-field of machine learning that involves more complex models and a lot of data. The most successful deep learning model is the Convolutional Neural Network (CNN), which is broadly used for image processing purposes. As images have hundreds of thousand or millions of pixels, the dimensionality of machine learning models that deal with them is extremely large if each pixel is considered as a unique variable. CNNs circumvent this difficulty by exploiting relations among nearby pixels. The model's parameters are shared among all pixels of the image, thus drastically reducing the number of parameters. This is performed in a way that makes the model learn meaningful patterns and combinations of patterns in the images in order to give a prediction of, for example, the image's content.

The success of deep learning can partially be explained by a relatively recent evolution in the hardware on which the models are trained. The last decade showed a remarkable increase in the computing power provided by Graphical Processing Units (GPUs), which are designed for massively parallelized calculations. They now even possess dedicated cores with an architecture that is optimized for the calculations involved in machine learning. This shift from CPU-based to GPU-based algorithms allowed larger models to be trained with more data, and led to the aforementioned success story.

1.3.4 Wind-Topo: a new downscaling method for highly complex terrain

Wind-Topo, the new downscaling model for near-surface wind fields described in Part III, finds the statistical relationship between the state of the atmosphere surrounding a measurement station, the local topography, and the observed wind speed and direction. Unlike the various downscaling schemes mentioned previously, Wind-Topo adopts a 2D-to-point approach. When trained, the model uses 2D fields of several variables from a NWP model and a high-resolution description of the topography to predict one wind vector. This prediction is for 7 m.a.g.l and is located at the center of those 2D fields. Wind-Topo is trained with two years of measured wind speed and direction from 261 automatic measurement stations in Switzerland. 60 independent stations and a separate year of data are used for validation and show the ability of the model to provide good predictions for new (unseen) locations, given what the NWP model COSMO-1 provides as input data. When trained, Wind-Topo can be used to generate

predictions of wind speed and direction on a high-resolution grid (as fine as 50 m).

The description of the topography provided as input to Wind-Topo is a key element for its performance on highly complex terrain like the Alps. Because of its architecture based on multiple CNNs and because it predicts a wind vector and not only wind speed, new topographic descriptors had to be developed. Wind-Topo is a first step towards a more end-to-end approach, where a deep learning model could learn by itself how to analyze the topography to provide the best possible predictions. As described in Part III, more diverse training data could lead to such a model and to increased performance.

Thanks to its GPU-based, efficient architecture, Wind-Topo can be used, with reasonable computational resources, to obtain long time series of electrical power from potential wind turbines located anywhere in Switzerland. The new data can then be used to refine the findings of Part II: optimal location, optimal generation mix, and impact on the whole electrical system. This is discussed in the chapter Summary, Conclusion and Outlook.

Figure 1.1: Wind turbines and hydropower at Griessee, Switzerland

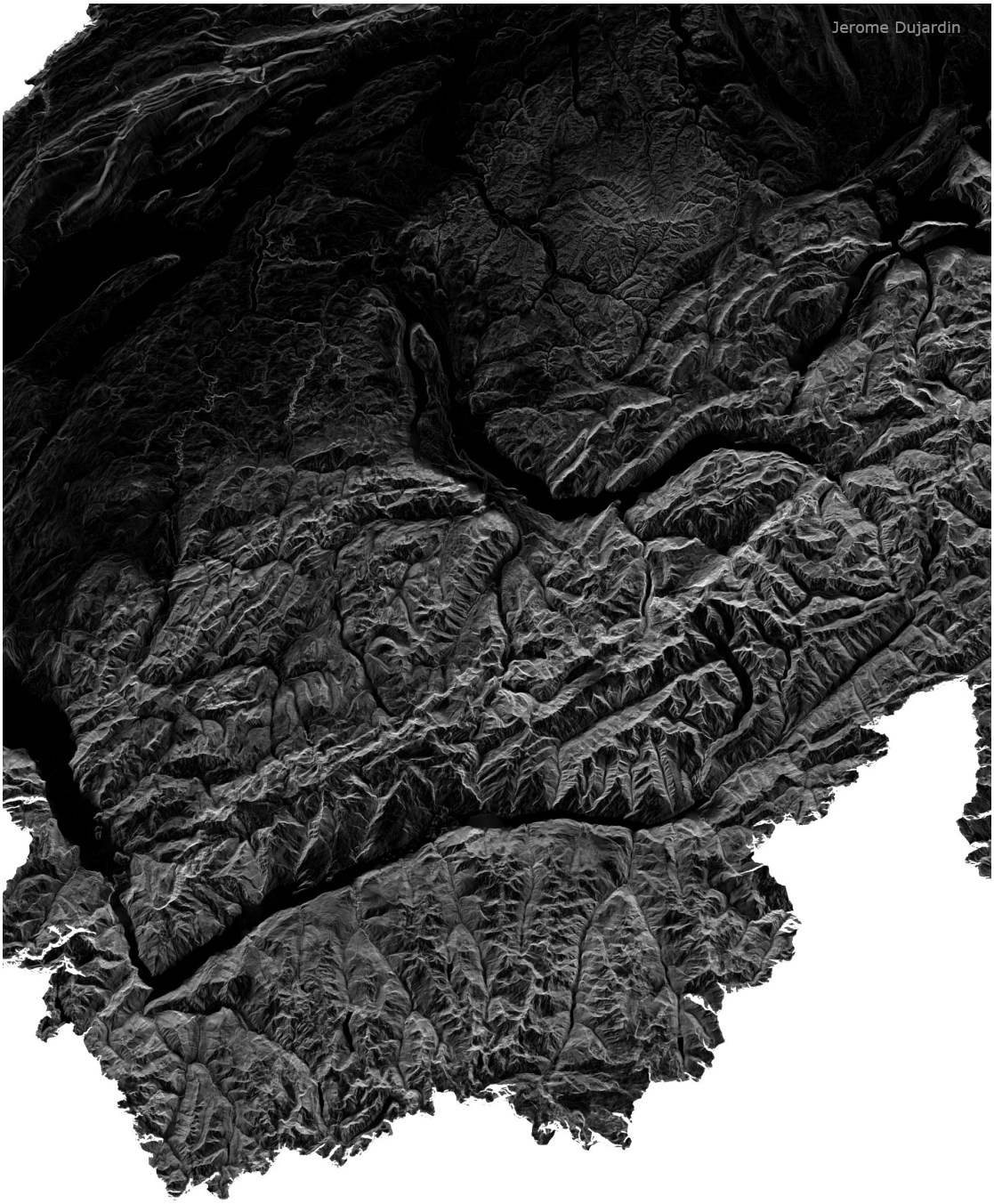

Figure 1.2: The complexity of the Alps

Bibliography

[1] Jan Abrell, Patrick Eser, Jared B. Garrison, Jonas Savelsberg, and Hannes Weigt. Integrating economic and engineering models for future electricity market evaluation: A Swiss case study. *Energy Strategy Reviews*, 25(April 2019):86–106, 2019.

[2] Cristina L. Archer and Mark Z. Jacobson. Supplying baseload power and reducing transmission requirements by interconnecting wind farms. *Journal of Applied Meteorology and Climatology*, 46(11):1701–1717, 2007.

[3] Sarah Becker, Bethany A. Frew, Gorm B. Andresen, Timo Zeyer, Stefan Schramm, Martin Greiner, and Mark Z. Jacobson. Features of a fully renewable US electricity system: Optimized mixes of wind and solar PV and transmission grid extensions. *Energy*, 72:443–458, aug 2014.

[4] Philip E. Bett and Hazel E. Thornton. The climatological relationships between wind and solar energy supply in Britain. *Renewable Energy*, 87:96–110, 2016.

[5] Michael Child, Claudia Kemfert, Dmitrii Bogdanov, and Christian Breyer. Flexible electricity generation, grid exchange and storage for the transition to a 100% renewable energy system in Europe. *Renewable Energy*, 139:80–101, 2019.

[6] Fotini Katopodes Chow, Christoph Schär, Nikolina Ban, Katherine A. Lundquist, Linda Schlemmer, and Xiaoming Shi. Crossing multiple gray zones in the transition from mesoscale to microscale simulation over complex terrain. *Atmosphere*, 10(5), 2019.

[7] Christopher T.M. Clack, Staffan A. Qvist, Jay Apt, Morgan Bazilian, Adam R. Brandt, Ken Caldeira, Steven J. Davis, Victor Diakov, Mark A. Handschy, Paul D.H. Hines, Paulina Jaramillo, Daniel M. Kammen, Jane C.S. Long, M. Granger Morgan, Adam Reed, Varun Sivaram, James Sweeney, George R. Tynan, David G. Victor, John P. Weyant, and Jay F. Whitacre. Evaluation of a proposal for reliable low-cost grid power with 100% wind, water, and solar. *Proceedings of the National Academy of Sciences of the United States of America*, 114(26):6722–6727, 2017.

[8] P. De Jong, A. S. Sánchez, K. Esquerre, R. A. Kalid, and E. A. Torres. Solar and wind energy production in relation to the electricity load curve and hydroelectricity in the northeast region of Brazil. *Renewable and Sustainable Energy Reviews*, 23:526–535, 2013.

[9] Florian Dupuy, Gert Jan Duine, Pierre Durand, Thierry Hedde, Eric Pardyjak, and Pierre Roubin. Valley winds at the local scale: Correcting routine weather forecast using artificial neural networks. *Atmosphere*, 12(2):1–20, 2021.

[10] Christophe Etienne, Anthony Lehmann, Stéphane Goyette, Juan-Ignacio Lopez-Moreno, and Martin Beniston. Spatial Predictions of Extreme Wind Speeds over Switzerland Using Generalized Additive Models. *Journal of Applied Meteorology and Climatology*, 49(9):1956–1970, sep 2010.

[11] European Commission. European Green Deal : Commission proposes transformation of EU economy and society to meet climate ambitions. https://ec.europa.eu/commission/presscorner/detail/en/ip_21_3541, 2021.

[12] Office fédéral de l'énergie (OFEN). Statistique suisse de l'électricité 2019. https://pubdb.bfe.admin.ch/de/publication/download/10112, 2020.

[13] P. Fischer, C. Etienne, J. Tian, and T. Krauß. Prediction of Wind Speeds Based on Digital Elevation Models Using Boosted Regression Trees. *ISPRS - International Archives of the Photogrammetry, Remote Sensing and Spatial Information Sciences*, XL-1-W5:197–202, dec 2015.

[14] Loris Foresti, Devis Tuia, Mikhail Kanevski, and Alexei Pozdnoukhov. Learning wind fields with multiple kernels. *Stochastic Environmental Research and Risk Assessment*, 25(1):51–66, jan 2011.

[15] Franziska Gerber, Nikola Besic, Varun Sharma, Rebecca Mott, Megan Daniels, Marco Gabella, Alexis Berne, Urs Germann, and Michael Lehning. Spatial variability in snow precipitation and accumulation in COSMO – WRF simulations and radar estimations over complex terrain. *The Cryosphere*, 12:3137–3160, 2018.

[16] Dolf Gielen, Francisco Boshell, Deger Saygin, Morgan D. Bazilian, Nicholas Wagner, and Ricardo Gorini. The role of renewable energy in the global energy transformation. *Energy Strategy Reviews*, 24(January):38–50, 2019.

[17] Brigitta Goger, Mathias W. Rotach, Alexander Gohm, Ivana Stiperski, and Oliver Fuhrer. Current challenges for numerical weather prediction in complex terrain: Topography representation and parameterizations. *2016 International Conference on High Performance Computing and Simulation, HPCS 2016*, pages 890–894, 2016.

[18] Naveen Goutham, Bastien Alonzo, Aurore Dupré, Riwal Plougonven, Rebeca Doctors, Lishan Liao, Mathilde Mougeot, Aurélie Fischer, and Philippe Drobinski. Using Machine-Learning Methods to Improve Surface Wind Speed from the Outputs of a Numerical Weather Prediction Model. *Boundary-Layer Meteorology*, 179(1):133–161, 2021.

[19] Christian M. Grams, Remo Beerli, Stefan Pfenninger, Iain Staffell, and Heini Wernli. Balancing Europe's wind-power output through spatial deployment informed by weather regimes. *Nature Climate Change*, 7(8):557–562, jul 2017.

[20] Dominik Heide, Martin Greiner, Lüder von Bremen, and Clemens Hoffmann. Reduced storage and balancing needs in a fully renewable European power system with excess wind and solar power generation. *Renewable Energy*, 36(9):2515–2523, sep 2011.

[21] Dominik Heide, Lueder von Bremen, Martin Greiner, Clemens Hoffmann, Markus Speckmann, and Stefan Bofinger. Seasonal optimal mix of wind and solar power in a future, highly renewable Europe. *Renewable Energy*, 35(11):2483–2489, nov 2010.

[22] N. Helbig, R. Mott, A. Van Herwijnen, A. Winstral, and T. Jonas. Parameterizing surface wind speed over complex topography. *Journal of Geophysical Research*, 122(2):651–667, jan 2017.

[23] Von Hirschhausen. European electricity generation post-2020: Renewable energy not to be underestimated. *DIW Economic Bulletin*, 3(9):16–25, 2013.

[24] Kevin Höhlein, Michael Kern, Timothy Hewson, and Rüdiger Westermann. A comparative study of convolutional neural network models for wind field downscaling. *Meteorological Applications*, 27(6):1–31, 2020.

[25] Christina E. Hoicka and Ian H. Rowlands. Solar and wind resource complementarity: Advancing options for renewable electricity integration in Ontario, Canada. *Renewable Energy*, 36(1):97–107, 2011.

[26] William W. Hsieh. *Machine Learning Methods in the Environmental Sciences: Neural Network and Kernels*. Cambridge University Press, Cambridge, 2009.

[27] Hsin Yuan Huang, Scott B. Capps, Shao Ching Huang, and Alex Hall. Downscaling near-surface wind over complex terrain using a physically-based statistical modeling approach. *Climate Dynamics*, 44(1-2):529–542, 2015.

[28] Mark Z. Jacobson, Mark A. Delucchi, Mary A. Cameron, and Bethany A. Frew. Low-cost solution to the grid reliability problem with 100% penetration of intermittent wind, water, and solar for all purposes. *Proceedings of the National Academy of Sciences of the United States of America*, 112(49):15060–15065, 2015.

[29] Annelen Kahl, Jérôme Dujardin, and Michael Lehning. The bright side of PV production in snow-covered mountains. *Proceedings of the National Academy of Sciences of the United States of America*, 116(4):1162–1167, 2019.

[30] Partha Kayal and C. K. Chanda. Optimal mix of solar and wind distributed generations considering performance improvement of electrical distribution network. *Renewable Energy*, 75:173–186, 2015.

[31] Bert Kruyt, Jérôme Dujardin, and Michael Lehning. Improvement of wind power assessment in complex terrain : The case of COSMO-1 in the Swiss Alps. *Frontiers in Energy Research*, 2018.

[32] Bert Kruyt, Michael Lehning, and Annelen Kahl. Potential contributions of wind power to a stable and highly renewable Swiss power supply. *Applied Energy*, 192:1–11, 2017.

[33] Florian U. Leuthold, Hannes Weigt, and Christian von Hirschhausen. A Large-Scale Spatial Optimization Model of the European Electricity Market. *Networks and Spatial Economics*, 12(1):75–107, 2012.

[34] Alon Manor and Sigalit Berkovic. Bayesian Inference aided analog downscaling for near-surface winds in complex terrain. *Atmospheric Research*, 164-165:27–36, 2015.

[35] F. Monforti, T. Huld, K. Bódis, L. Vitali, M. D'Isidoro, and R. Lacal-Arántegui. Assessing complementarity of wind and solar resources for energy production in Italy. A Monte Carlo approach. *Renewable Energy*, 63(2014):576–586, 2014.

[36] Joseph B. Olson, Jaymes S. Kenyon, Irina Djalalova, Laura Bianco, David D. Turner, Yelena Pichugina, Aditya Choukulkar, Michael D. Toy, John M. Brown, Wayne M. Angevine, Elena Akish, Jian Wen Bao, Pedro Jimenez, Branko Kosovic, Katherine A. Lundquist, Caroline Draxl, Julie K. Lundquist, Jim McCaa, Katherine McCaffrey, Kathy Lantz, Chuck Long, Jim Wilczak, Robert Banta, Melinda Marquis, Stephanie Redfern, Larry K. Berg, Will Shaw, and Joel Cline. Improving wind energy forecasting through numerical weather prediction model development. *Bulletin of the American Meteorological Society*, 100(11):2201–2220, 2019.

[37] Kostas Philippopoulos and Despina Deligiorgi. Application of artificial neural networks for the spatial estimation of wind speed in a coastal region with complex topography. *Renewable Energy*, 38(1):75–82, feb 2012.

[38] Bryn Pickering, Christian M. Grams, and Stefan Pfenninger. Sub-national variability of wind power generation in complex terrain and its correlation with large-scale meteorology. *Environmental Research Letters*, 15(4), 2020.

[39] Morten Grud Rasmussen, Gorm Bruun Andresen, and Martin Greiner. Storage and balancing synergies in a fully or highly renewable pan-European power system. *Energy Policy*, 51:642–651, 2012.

[40] Markus Reichstein, Gustau Camps-Valls, Bjorn Stevens, Martin Jung, Joachim Denzler, Nuno Carvalhais, and Prabhat. Deep learning and process understanding for data-driven Earth system science. *Nature*, 566(7743):195–204, 2019.

[41] Hans Kristian Ringkjøb, Peter M. Haugan, and Ida Marie Solbrekke. A review of modelling tools for energy and electricity systems with large shares of variable renewables. *Renewable and Sustainable Energy Reviews*, 96(April 2017):440–459, 2018.

[42] Sylvain Robert, Loris Foresti, and Mikhail Kanevski. Spatial prediction of monthly wind speeds in complex terrain with adaptive general regression neural networks. *International Journal of Climatology*, 33(7):1793–1804, jun 2013.

[43] Franco Scarselli and Ah Chung Tsoi. Universal approximation using feedforward neural networks: A survey of some existing methods, and some new results. *Neural Networks*, 11(1):15–37, 1998.

[44] Ingmar Schlecht and Hannes Weigt. Swissmod - A Model of the Swiss Electricity Market. *SSRN Electronic Journal*, (June), 2018.

[45] Joakim Widén. Correlations between large-scale solar and wind power in a future scenario for Sweden. *IEEE Transactions on Sustainable Energy*, 2(2):177–184, 2011.

[46] Adam Winstral, Kelly Elder, and Robert E. Davis. Spatial snow modeling of wind-redistributed snow using terrain-based parameters. *Journal of Hydrometeorology*, 3(5):524–538, 2002.

[47] Adam Winstral, Tobias Jonas, and Nora Helbig. Statistical Downscaling of Gridded Wind Speed Data Using Local Topography. *Journal of Hydrometeorology*, 18(2):335–348, feb 2017.

[48] WSL Institute for Snow and Avalanche Research SLF. Automated IMIS stations. https://www.slf.ch/en/avalanche-bulletin-and-snow-situation/measured-values/description-of-automated-stations.html.

[49] Elmar Zozmann, Leonard Göke, Mario Kendziorski, Citlali Rodriguez, Christian Von Hirschhausen, and Johanna Winkler. Distribution and Network Constraints. *Energies*, 14(3):658, 2021.

Part I

Charting the course: A possible route to a fully renewable Swiss power system

2 Main text

Charting the course: A possible route to a fully renewable Swiss power system

Stuart Bartlett[1,2,3], Jérôme Dujardin[1,4], Annelen Kahl[1,4], Bert Kruyt[1,4], Pedro Manso[5] and Michael Lehning[1,4]

[1] Laboratory of Cryospheric Sciences, School of Architecture, Civil and Environmental Engineering, École Polytechnique Fédérale de Lausanne, Lausanne, Switzerland

[2] Division of Geological and Planetary Sciences, California Institute of Technology, Pasadena, United States

[3] Earth Life Science Institute, Tokyo Institute of Technology, Tokyo, Japan

[4] WSL Institute for Snow and Avalanche Research SLF, Davos, Switzerland

[5] Laboratory of Hydraulic Constructions, School of Architecture, Civil and Environmental Engineering, École Polytechnique Fédérale de Lausanne, Lausanne, Switzerland

Abstract

The prospect of a renewable transition seems plausible for many countries, but can be shrouded in risks, costs and challenges. This paper illuminates a path for such a transition with a numerical investigation, aimed at resolving the power dynamics of a country powered only by renewable generators. The focus was Switzerland, with its considerable hydropower infrastructure and plans to phase out nuclear energy. The model uses optimal power flow calculations to compute the transmission of electricity, and also accounts for the movement of water within the hydropower system. Results suggest that the renewable goal is attainable and will not require radical re-building of the country's transmission infrastructure. Under our assumptions, it was found that the transmission grid is placed under slightly lower stress on average, in renewable scenarios. Despite matching supply and demand on average, the fully renewable system required a ~ 107% increase in electrical exchange with neighbouring countries to compensate for seasonal variability, and additional intermittency of electrical supply. Simulation results are described for three scenarios: Current, Intermediate, and Renewable. The bulk power statistics, temporal dynamics, distributions of line use, and spatial patterns are presented, and the implications of the results are discussed.

This chapter was published in the journal *Energy* on November 15^{th} 2018, in the volume 163, pages 942-955.
doi: https://doi.org/10.1016/j.energy.2018.08.018

J.D developed a large part of the model, analyzed the results with S.B, and contributed to the writing of the paper.

2.1 Introduction

The destructive impacts of climate change are being increasingly felt across the world, provoking humanitarian crises and presenting a dire vision of potential futures for our civilisation (12; 18). However, simultaneously, progress in the penetration of renewable energy technologies has been impressive. There are a range of encouraging recent statistics including the achievement of Denmark, where 42% of electrical demand was satisfied by wind energy alone during 2015 (14). Likewise in Germany, 32.5% of electricity consumed was sourced from renewables during the same year (16). More recently, in the UK, offshore wind power is now cheaper than new nuclear installations (19). The costs of solar infrastructure also continue to show an encouraging decline, and new technologies, such as Perovskite solar cells, may accelerate these trends even further (38).

There has also been a vast amount of work on so-called smart systems for renewable resource utilisation. Frontier-level methods from machine learning and optimal control theory have allowed great progress to be made in dealing with the inherent variability of renewable energy (4; 22; 26; 35; 41; 59). Despite the advances in many aspects of renewable power, there remains a need for insight into the dynamics and operational risks of *fully* renewable energy systems at large scales (national and international). Risks in the context of this work include failure to meet demand, both in the short term (e.g., large fluctuations in renewable output that could cause grid level failures) and long term (e.g., large scale production deficits from seasonal differences in renewable output). Other risks of renewable investment include the opposite case, in which significant volumes of renewable production have to be curtailed in order to protect grid integrity. There are further socio-political risks associated with renewable energy. A prime example was the induced seismicity events caused by geothermal drilling operations in Basel in 2006 and 2007 (8; 27; 33).

In the long term, all future power systems will have to be free of non-renewable generators. While this is an ambitious goal, it is appearing more and more attainable with each passing year. There has been a plethora of modelling efforts in this direction, at various levels of resolution and locations including continental Europe (6; 10; 21; 39; 50), the Nordic countries (36), the United States (3; 5; 25; 34), and the entire globe (49; 24; 23; 9). These and other works have provided insights and candidate solutions, including oversizing the generating capacity of the system (20; 11) and moving towards more highly meshed transmission networks (49; 42). Given the inherent risks of investing in new energy infrastructure, there is still a compelling need for guidance on how different future renewable systems could be operated. This was the primary motivation for the current work: to provide detailed insights into the spatio-temporal dynamics of a hypothetical, fully renewable national power system.

Many European countries have the potential to become fully renewable. The United Kingdom has one of the world's largest wind resources, Spain and Italy receive vast amounts of solar energy, and Iceland has more than enough hydropower and geothermal energy to satisfy its electrical and heating requirements. In this work the focus was Switzerland, which presents

a different, but equally viable set of alternatives. The country has long sourced the majority of its electricity from hydroelectric power. At present this accounts for approximately 56% of electricity production (52). The remainder comes almost exclusively from nuclear power and in the long term, these plants will not be replaced after de-commissioning (51). This leaves a considerable deficit which could be alleviated by a range of sources including solar, wind and geothermal energies.

While various calculations have shown that on average, Switzerland can be fully renewable (2; 11) (note also the less optimistic outlook of (40)), there is still a need for ensembles of modelling data concerning exactly how a renewable Switzerland would function. Planning bodies need to know where solar and wind installations should be optimally placed in terms of not only maximising yield, but also minimising the risk of failure to meet local demand, and for assisting with temporal smoothing of other stochastic sources (28). We must explore the scenario space and seek bottlenecks in the transmission grid where upgrades might be required. It is important to investigate how different degrees of climate change might perturb the system in coming decades. Reduced future snow cover (47) will help to close the winter energy gap through earlier snow melt (30), while some authors predicted e.g. glacier loss to have a negative impact on Swiss hydropower (43; 45). The extent to which upgrades to hydropower infrastructure could foster additional flexibility to the system should also be investigated.

There has been work in this direction previously (11; 40; 58), but those investigations were aggregated at the national level and hence could provide no insight into spatial dynamics. Given the considerable spatial heterogeneity of potential renewable energy supplies in Switzerland (2), effective future planning will require an understanding of the spatial flows of electricity within the system.

This paper presents a combined energy and water model that simulates the Swiss power system at the transmission level for extended periods (typically single or multiple years). It uses optimal power flow calculations to find ideal generation portfolios at each time step in the considered period. Reservoir levels are updated based on the output of the hydropower plants and natural inflows. Numerical details of the system's operation can then be analysed.

This paper presents an overview of the results from our first phase of modelling. In the following section, the power system model is described. In section 2.3, the most important findings from the simulations are presented, including bulk power statistics, analysis of transmission line use and exchange volumes, seasonal energy trends, and spatial distributions of power surpluses and deficits. The implications of the results for the future evolution of the Swiss and European power systems are discussed in section 2.4. Conclusions are drawn in section 2.5, and we outline the future directions of our research in section 2.6.

2.2 Model construction

At its heart, our power system model is relatively simple. However there is a certain degree of complexity arising from the processing of input data and initialisation steps. The goal was to predict the medium and short term (periods of years, but resolved to sub-hourly time scales) dynamics of the power flows within Switzerland and with its neighbours. This section will first define the general methodology before moving onto the various power sources and effective costs. Note that the objective was to optimise the technical features and operation of this national power system. Market effects were not considered since this was not the focus of the present work. Once there is a clear and plausible case for a fully renewable Swiss power system, future studies that consider market dynamics can be undertaken.

2.2.1 Overview

The inputs to the model consist of data for electrical demand, solar insolation, wind speeds, river flow rates and reservoir inflows for a given period. This period is discretised into timesteps. The finest resolution timestep is 15 minutes with the current data set, but coarser resolutions can also be chosen for the sake of computational speed. The model is driven by an optimal power flow (OPF) algorithm which, at each timestep, calculates the generating portfolio for satisfying demand at minimum cost. This algorithm consists of a library of functions and routines for power system modelling known as Matpower (63; 62; 61). The OPF within this library uses a primal-dual interior point solver and is run within a Matlab environment. At each timestep, effective cost functions are calculated for all generators, including virtual generators beyond the country's borders, which represent electricity import. There are also dispatchable loads at the same nodes, that allow electricity export to neighbouring countries. The OPF algorithm is supplied with the details of the grid configuration (properties of the transmission lines, transformers, electrical nodes, generators, demand), and carries out its computation of the optimal distribution of power production by the available generators. This procedure is iterated for the entire time period being analysed. Figure 2.1 shows the overall structure of the algorithm that implements the model.

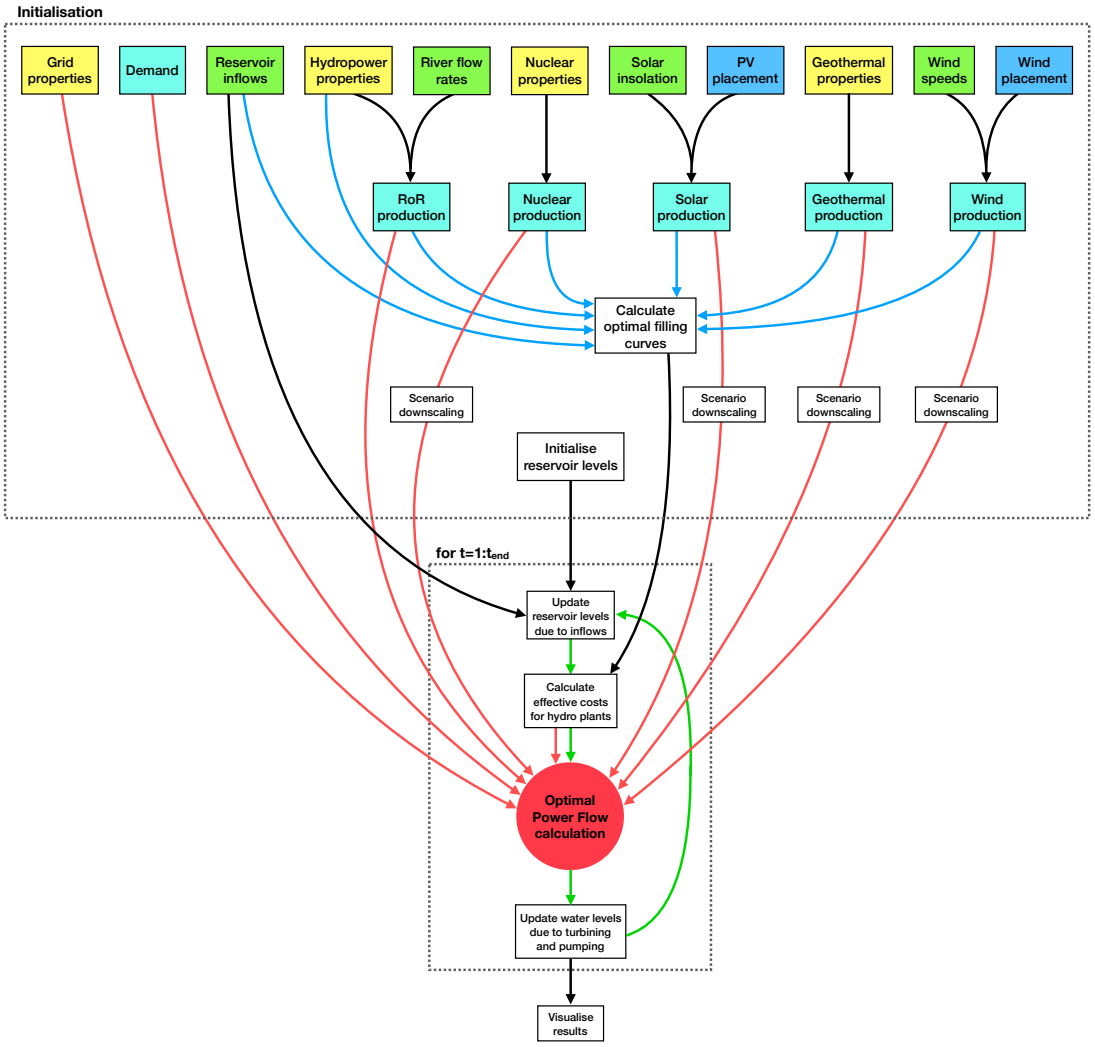

Figure 2.1: Flow diagram showing the primary features of our Swiss power system model. Yellow boxes show static infrastructure properties, cyan boxes represent time series resolved to each grid node, green boxes correspond to energy inputs defined by natural phenomena, and blue boxes are placement strategies. Red lines correspond to the flow of input information to the OPF, blue lines represent the flows of data required to calculate optimal filling fraction curves, green lines show the iterated stages of the main simulation loop, and black lines show the flows of data from initialisation to the main loop, and from the main loop to results analysis.

2.2.2 Hydropower

For many years hydropower has been the most important electricity source in Switzerland, both in terms of volume of produced electricity, and provision of balancing services. Hydropower remains an invaluable component of the power system, and in the year considered in this paper, 2014, hydropower sources provided 39.3 TWh of energy, of which 22.1 TWh came from storage plants and the remaining 17.2 TWh from "run-of-river" (RoR) plants (31).

Since hydropower accounts for ~ 56% of domestic electrical production (in a typical year), it was essential to faithfully represent hydropower infrastructure in the model. Incorporating the system of storage lakes and reservoirs within the country was crucial. These water bodies are often connected via cascades of multiple hydropower plants and connecting tunnels, forming a large and complex fluid exchange system. The largest 67 water bodies were modelled, corresponding to 94% of the total national storage volume and 95% of hydropower production capacity. Including the remaining 6% of small and very small lakes would have entailed a significant increase in computational cost and complexity, since many of the plants operating at such lakes behave akin to a hybrid between RoR plants and true storage hydropower plants. The production from these small reservoirs is estimated such that total production matches relevant data values, and included as a reduction in peak time demand, at those grid nodes which already include storage hydro plants. It is also scaled to follow water inflow trends (higher average production in summer than winter).

The water levels of the modelled reservoirs are adjusted after each OPF calculation using the natural inflow values (interpolated runoff data), and the water consumed via turbining (or added via pumping, for those plants with pumping ability). This is a simple calculation that converts between electrical production and displaced water volume.

The optimal satisfaction of electrical demand at a given time is a function of the marginal costs of all active generators within the network, as well as import and export costs. Given that the model represents the Swiss power system, the most important dispatchable generators are storage hydro plants. Such plants are highly flexible, typically able to adjust their output between zero and full production in a matter of minutes. However, they also seek to ensure such capacity is available year round by carefully managing the water resources of their lakes and reservoirs.

The majority of these reservoirs are artificial, created using dams that block the outward flow of water from one or several river valleys. The highest natural inflows are during the summer months when snow melts. In winter, flows of water are dramatically reduced due to precipitation being immobilised as snow and ice. This seasonal variation has to be carefully tamed by hydropower operators, who strive to ensure that reservoirs never become empty. This normally translates to storage being full by the end of summer, and very low by early spring.

The constraints of these seasonal variations mean that storage hydro plants are reluctant to

generate if it will take them away from the optimal filling curve (approximately sinusoidal with a peak in September and minimum around late March). From the modelling perspective, this reluctance to generate when a reservoir is deviating from its ideal filling curve, translates into a higher generating cost (effective cost, given as input to the OPF algorithm) for the given plant. The ideal filling curve is calculated for each reservoir, and is a function of its inflow characteristics, the demand time series, and the national energy mix (relative contributions of different generating sources), see Figure 2.1 and (11).

Despite having the relevant time series of inputs (solar production, river runoff rates etc.) *a priori*, time dependence (contingency) enters into the system because of temporal feedbacks between when the hydropower plants generate (or pump), and thus how the reservoir levels evolve over time. These feedbacks prevent the system's dynamics from being amenable to simple algebraic calculation. The primary degrees of freedom are the choices of which hydropower plants to utilise at a given timestep, and how to compensate for surpluses and deficits through foreign exchange and pumping. The outputs from renewable generators (solar, RoR, geothermal and wind) are always used fully since it incurs no fuel cost. When there is a domestic surplus from such production (e.g., in summer), the system is forced to consume the surplus through pumping hydropower plants or export.

Approximately half of the hydropower production in the Swiss system comes from RoR plants. With no directly connected lake or reservoir, the electrical outputs of such plants are inextricably tied to the flow rate of the river within which they are embedded. Thus it was assumed that their outputs follow the same time variation as the flow rates of their rivers, and the system is forced to make use of those outputs.

2.2.3 Solar

The most relevant source of new renewable energy for Switzerland is solar photovoltaics (PV). Calculation of the solar resource starts with satellite-derived irradiance data, provided by Meteoswiss. This data consisted of yearly time series of horizontally incoming global shortwave radiation, combined with considerations for clouds and topography shading [see section 2.1.2 of (11) for further details].

It was assumed that a sufficient number of PV panels are installed to cover the annual deficit that remains when the nuclear fleet is removed (or halved, in the Intermediate scenario), and a certain amount of wind and geothermal plants are constructed (in line with national targets (51)). As with RoR plants, the output from PV installations is naturally constrained, in this case by the incoming solar radiation, which varies due to seasonal changes, diurnal variations and short term stochasticity due to cloud cover. The marginal cost of such production is essentially negligible (the real cost is in construction, installation and maintenance), and curtailment was not permitted.

Provision of solar insolation values and surface area of PV panels does not suffice to define

the spatio-temporal distribution of solar production. The PV infrastructure has to be spatially distributed. This constitutes a substantial and complex optimisation problem, which is being addressed in a parallel project. For the simulations used in the present work, PV panel placement was weighted proportionately to population density and electricity production was computed for a panel tilt of 39°, and a range of panel orientations between southeast and southwest [see section 2.1.2 of (11) for full details]. This was motivated by the desire to spatially align production with demand, and the assumption that rooftop PV installations will be most politically feasible and more likely to be exploited first. Figure 2.2 shows the distribution of PV panel density across the country.

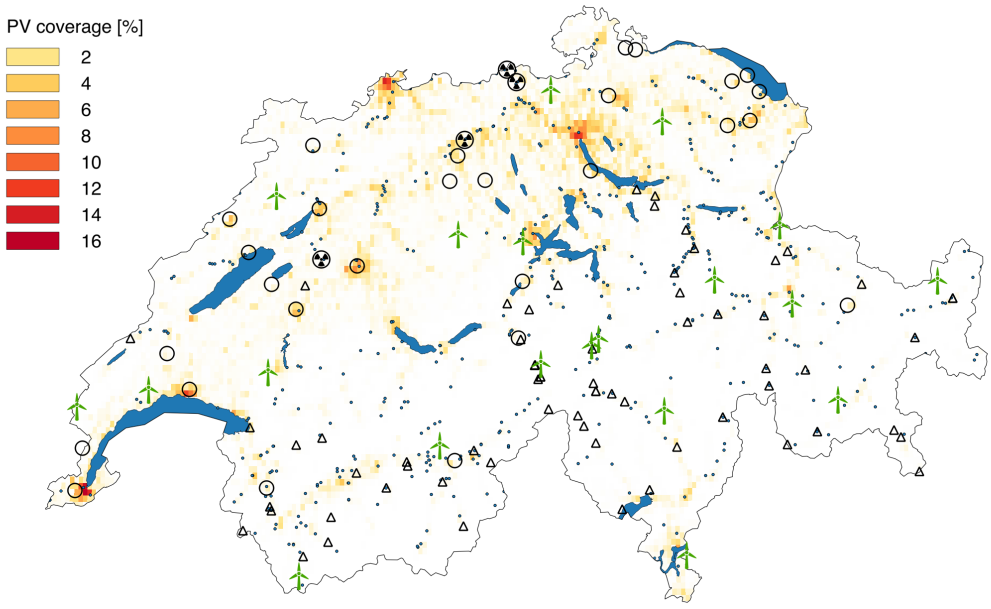

Figure 2.2: Map of Switzerland showing the individual plants making up the modelled power system. Black triangles show storage hydro plants, dark blue dots show RoR plants, radiation symbols show nuclear plants, green turbines show wind plants and open black circles show geothermal plants. Solar PV panel density (in percentage ground coverage) is shown by shade of yellow-red colouring.

Note that at the time of writing, Switzerland had a total installed PV capacity of approximately 1.6 GW, whereas a value of 0 is assumed in the Current scenario (see section 2.3). It was not possible to include this PV contribution in the present work for the following reasons. Firstly, it was not possible to obtain the exact data concerning the placement of this infrastructure. Such data would have to come from many different utilities and organisations, and would in many cases be restricted, commercially or privately sensitive, or incomplete. Furthermore, it is a very small component of Switzerland's current generating portfolio, and thus it is reasonable to represent the present-day portfolio with only hydropower and nuclear sources, allowing us

to properly highlight the transition from hydropower and nuclear, to fully renewable.

2.2.4 Geothermal

It was assumed that geothermal plants are able to provide a constant output that is always fully utilised. Note that there are no geothermal plants in operation at the time of writing, but the Swiss government has ambitious plans to construct such installations. The national Energy Strategy 2050 includes an annual target of 4.4 TWh from geothermal energy (51). Hence a constant, non-dispatchable supply of this magnitude was assumed. The spatial distribution of this input, shown in Figure 2.2, was derived from the current plans for geothermal power plant construction (13). Thus the model employed 28 plants, each producing an average of 17.9 MW.

2.2.5 Wind

Wind power was traditionally seen as a low potential resource in Switzerland due to its alpine topography and low average wind speeds. However, recent results are beginning to show that the true resource may be higher, since average wind speeds mask certain local, high potential locations (e.g., mountain passes at high elevation) (28; 7). The optimal partitioning of required production between wind and solar constitutes another optimisation problem, also being addressed by our group (11). For the present work, an annual wind production of 1 TWh was assumed, since this is a feasible increase over the current output of 0.1 TWh.

As was the case for solar installations, wind plants must be placed in the most suitable locations. This was achieved using a simple algorithm that places turbines in the most ideal locations first until the target production level is reached (28; 11). This translated into the use of 208 Enercon E82 2 MW turbines, situated in 20 different locations, shown in Figure 2.2. Wind speeds were extracted from data produced by 117 measurement stations from the Swiss weather service MeteoSwiss (32), and this was translated into output power series using the power curve of the Enercon E82 turbine, commonly used in Swiss installations.

2.2.6 Nuclear

As well as renewable configurations, simulations with the system as close to its current configuration as possible (with nuclear and a small amount of fossil fuel production working alongside the hydropower fleet) were also conducted. This scenario gave a benchmark from which it was possible to chart the course to a fully renewable Swiss power system, including an Intermediate, mixed scenario.

The nuclear configuration (designated as Current) was also used to compare model results with real data for the year concerned. However such a comparison is inherently limited by the fact that the model does not include the distribution grid or transit flows, and the fact that it

was not possible to acquire exact data on the spatial distribution of foreign exchange flows.

2.2.7 Grid and demand

Detailed data of the Swiss high voltage transmission network were kindly provided by Swissgrid. The Strategic Grid 2025 (54) was used, since this includes all grid expansions that Swissgrid is currently working towards. The data included all 220 kV and 380 kV lines, and some 150 kV lines. The model did not incorporate medium and low voltage lines (the distribution grid). This lower voltage grid was excluded because it comprises a very high number of links and nodes, and each regional network is run by a different utility, preventing straightforward data access.

Figure 2.3 shows the lines included in the model. For this figure the shortest paths, rather than actual line paths are plotted. The real resistivities and other line properties are of course faithfully represented in the model.

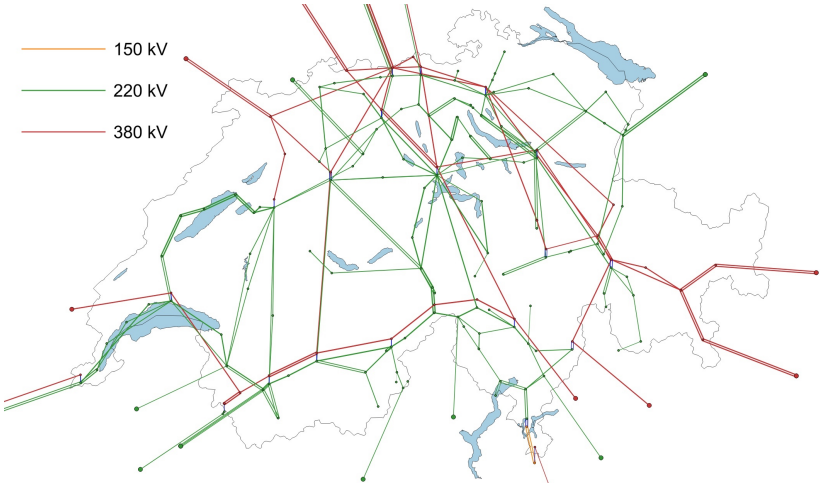

Figure 2.3: The Swiss high voltage transmission grid as used in the power system model.

Inputting the grid data and generator costs at a given time step allows the OPF algorithm to find an optimal specification of the power outputs of all the generators within the system (Figure 2.1). Note that these are only effective costs, not monetary costs. They are calculated at each time step such that hydropower plants adhere as closely as possible to their ideal filling fraction targets. Other generators (RoR, nuclear, PV, geothermal and wind) are assumed to have zero cost and the model is forced to make use of their output.

Electrical consumption data was sourced from the Swissgrid public repository (53). These time series are given at the national level or resolved by canton. It was thus necessary to construct a spatial distribution scheme that partitioned the demand across the transmission grid nodes. In this work, the national time series were used, and population density was assumed as a proxy for fractional demand. There are a small number of industrial regions where this assumption may be less valid, but for the bulk of the demand (urban areas), it is a

reasonable approximation. The population density data had a resolution of 100x100m, and was also sourced from a public repository provided by the Swiss Federal Office of Statistics (15). Fractional population values were calculated for each of the regions served by the nodes of the transmission network, and these fractions were used to calculate the demand values for each grid node. A value of 8% was added to the demand values to account for distribution losses. This was calculated from the difference between the power output from the transmission system and the end-user consumption.

Once the OPF has found the ideal generating portfolio for a given time step, the model uses those outputs to adjust the water levels of the reservoirs and lakes, in addition to natural inflows. Note that combined turbining and pumping stations were also modelled, but they could not be used to alleviate the summer-winter seasonal gap (storing summer solar energy for the winter) because the reservoir system is not sufficiently sized to incorporate large amounts of extra water. The pumping stations were used only to absorb short term excesses in production, that could then be returned to the system by turbining at later times. The consequences of increasing dam heights were addressed in (11) at the national level, and similar analyses with a spatially resolved model are ongoing.

Foreign exchange was constrained by the ampacity limits of the transmission lines connecting Switzerland to neighbouring countries. This placed a limit on the maximum power of foreign exchange, but there was no limit placed upon total exchanged energy. It is clear that technical and financial constraints would place restrictions on total exchanged energy in a real renewable power system. However, the objective in this work was to illustrate a functional example system, and use the results as a guiding perspective on the future evolution of the Swiss system. Even if the necessary exchange energies prove to be unrealistic in practice, they at least place approximate limits on different scenarios, which can allow engineers and state actors to make more informed decisions.

2.3 Results

This work focused upon the year 2014, with three different scenarios: Current, Intermediate and Renewable, described quantitatively in Table 2.1. All scenarios use storage hydro as a dispatchable generator, and have access to the same RoR production.

2.3.1 Summary analysis

The Current scenario utilises storage hydro, RoR, and nuclear power. For the year considered in this paper, there was a net overproduction by the Swiss generating fleet (primarily nuclear), so the nuclear output was downscaled such that total demand for the year was matched by generation. This was motivated by the fact that sizing of renewables was defined by matching annual demand with supply.

Configuration	Current	Intermediate	Renewable
Storage Hydro	21.3 (34.5%)	21.2 (34.4%)	21.0 (34.1%)
RoR	17.3 (27.9%)	17.3 (28.0%)	17.3 (28.1%)
Nuclear	23.2 (37.6%)	11.6 (18.8%)	0
Solar	0	8.93 (14.5%)	17.9 (29.0%)
Geothermal	0	2.20 (3.56%)	4.40 (7.15%)
Wind	0	0.50 (0.81%)	1.00 (1.63%)
Total	61.8	61.7	61.5
Demand	60.9	60.9	60.9
Losses	0.702	0.475	0.471
Net export	0.179	0.321	0.118

Table 2.1: Contributions to the national generating portfolio from the various energy sources, in the three different modelled scenarios. Apart from percentages, all values are in units of TWh per year.

The Intermediate scenario uses all of the different generator types. Nuclear output is halved relative to the Current scenario, and PV, Wind and geothermal sources are introduced but their outputs are halved relative to the Renewable scenario. This represents an exact midpoint between the present-day power system and one that is fully renewable.

The Renewable scenario eliminates nuclear output entirely and uses the full complement of PV, wind and geothermal sources. Solar output is scaled to match the remaining net deficit over the year (after hydropower, wind and geothermal productions are subtracted from the demand).

In all three cases, foreign exchange is used for instantaneous energy balancing and compensating for seasonal surpluses and deficits that cannot be dealt with by storage of water in reservoirs. The storage hydro fleet does have sufficient power capacity to take care of all required balancing services, however such a strategy would prematurely consume the available water (reservoirs would become empty) and prevent year-round availability of production. It is the availability of energy, not power, that is the key seasonality issue in the Swiss power system (11).

Note that the *a priori* calculation (before running the model) of annual power output is not perfectly accurate, since there are feedbacks between generator deployment, line losses, water use and hydropower production, that occur as a time dependent function of the dynamics of the model. Thus while the aim was to match annual supply and demand by scaling the solar or nuclear outputs, by the end of any given simulation there was a small degree of mismatch resulting in a net export (last row of Table 2.1).

There is a significant decrease in total line losses when the system moves to renewable sources (also see Table 2.4 and Figure 2.4). This is related to the more distributed nature of the generating portfolio (see discussion in subsection 2.3.1) when nuclear sources are downscaled. This additional energy was exported in the Intermediate scenario. However, in the Renewable

scenario, the net production from storage hydro was reduced, and the net export was lower than both the Intermediate and Current scenarios.

Net storage hydro production decreased in the Renewable case due to two factors. Firstly, actual production increased with renewable penetration, but consumption by pumping stations increased to a greater extent. The need to store excess solar energy led to this increased requirement for pumping, and this in turn reduced the net storage hydro output.

In all three scenarios, there was a slight water level deficit at the end of the year, and this effect increased with renewable penetration. This appeared to be caused by the model choosing to deviate from filling fraction curves rather than using additional foreign exchange. Improvements that can prevent this subtle effect, such as shifting export incentives within a given model run, are currently underway.

The year chosen for analysis, 2014, had relatively few atypical features. When dealing with a large, complex system such as a national power grid, it is impossible to select a truly representative and typical year from a given dataset, since there is no such thing. The intention was to focus on a single year for this work for the sake of clarity and ease of results interpretation. Multi-year simulations are currently being analysed, as the input dataset expands in size and resolution. This was explored in previous work, but at the nationally aggregated level (11). Apart from the excess nuclear production, the year 2014 was not significantly different from an average annual period, exhibiting representative seasonal trends in reservoir inflows and river flow rates.

Table 2.2 presents the number of installations of each renewable energy type, the capacities of each plant type, and the mean capacity factors. PV panels were assumed to be 15% efficient. The values correspond to the Renewable configuration. In the Intermediate case, the capacities are simply halved, but the capacity factors remain essentially unchanged.

Source	Installations	Capacity	Mean capacity factor
Solar	$84 km^2$	$150 W m^{-2}$ (12.6GW)	16%
Wind	208	$2 MW$ (0.42GW)	27%
Geothermal	28	$17.9 MW$ (0.5GW)	100%

Table 2.2: Summary of renewable infrastructure required for a fully renewable Swiss power system. Total installed capacities are shown in terms of the power of each plant and the national totals in brackets (multiplying this figure by the capacity factor yields the real average output).

Table 2.3 displays the volumes of electricity exchanged with foreign neighbours. It illustrates the principle difficulty of transitioning to a fully renewable power system (after construction of the renewable generators): a significant increase in both import and export. Domestic supply and demand are approximately matched in all cases, but a renewable power system entails just over a doubling of both import and export.

There are also differences in the way that the transmission grid is used between the three scenarios. Table 2.4 summarises the statistical features of line use by the model system. While

Configuration	Current	Intermediate	Renewable
I [TWh]	3.56	4.97	7.50
E [TWh]	3.74	5.29	7.61
ΔI	0	39.6%	111%
ΔE	0	41.5%	104%

Table 2.3: Annual foreign import I and export E for the three power system scenarios. Changes in import and export are shown relative to the Current configuration.

the maximum injected power is highest for the Renewable scenario, a surprising result is that the mean line use and percentile values actually decrease as a function of renewable penetration. The intermittent nature of the solar output and concomitant large import/export flows are the likely sources of the higher maximum line use values. However, the percentile values show a decreasing trend as renewable penetration is increased, implying that for the majority of the time, the transmission grid is actually slightly less stressed in a more renewable-dominated system. These results are illustrated graphically in Figure 2.4, which shows the distributions of line use values.

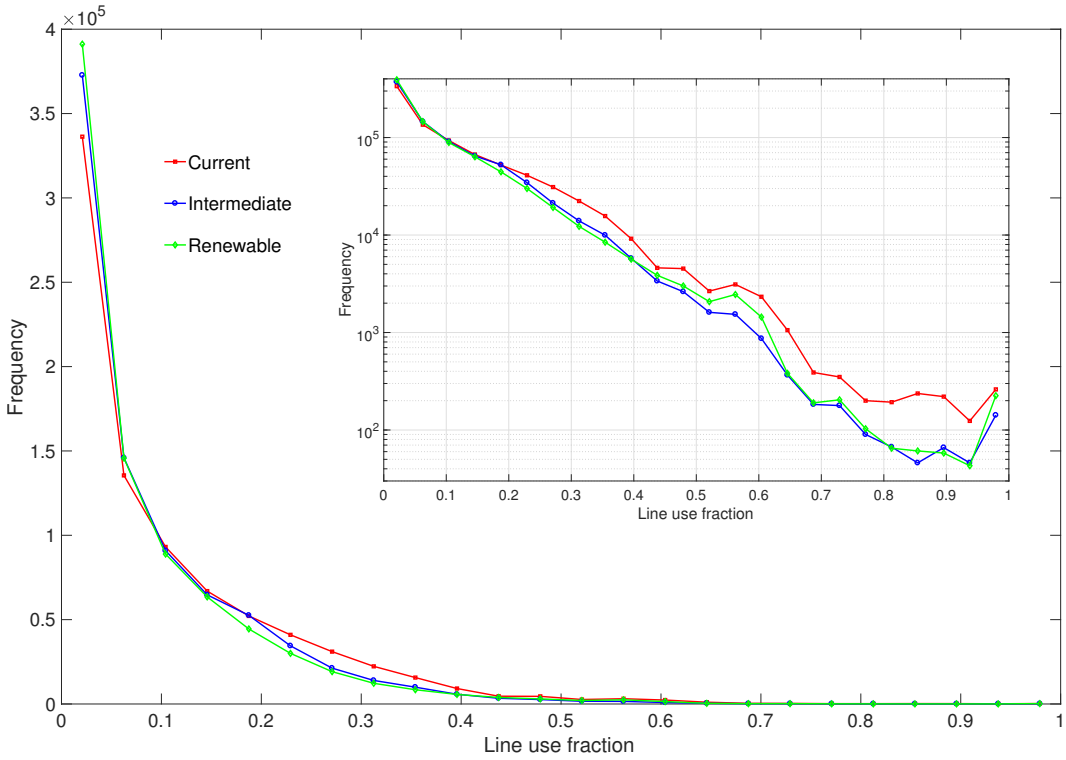

Figure 2.4: Distributions of transmission line use in the three model scenarios. Frequency of occurrence is shown as a function of fraction of line ampacity limit used. The final data points (far right) show that a subset of the lines are frequently used at or very near full capacity. The inset graph shows the same data plotted on logarithmic axes.

Note however that since these statistics are for the entire grid, there is the possibility that some individual lines have become more stressed in the more renewable scenarios. It is therefore possible that grid expansion in some areas would still be required with renewable penetration.

Configuration	Current	Intermediate	Renewable
$\mu\{L\}$	74.9	62.6	60.4
$P_{50}\{L\}$	49.2	41.8	38.0
$P_{95}\{L\}$	234	197	197
$P_{99}\{L\}$	369	310	314
$max\{L\}$	836	800	903

Table 2.4: Statistics of line use L for the three scenarios. All values are apparent powers in MVA. The mean value $\mu\{L\}$ is shown in the first row, the following three rows are the 50^{th}, 95^{th}, and 99^{th} percentile values, respectively, and the final row shows the absolute maximum.

2.3.2 Temporal dynamics

The Swiss power system shows dramatic seasonal variations and a primary objective of the hydropower operation is to retain the ability to generate throughout the year. This requires a carefully planned filling fraction target and prudent use of resources as a function of electricity price and available water. In principle, the storage capacities of the Swiss reservoirs could be used to try to alleviate the reduction in solar output during winter. However, the system currently struggles to even retain the ability to turbine throughout the year (the reservoirs are typically very low by the end of winter). In addition, pumped storage has until recently only been used as a profit-making mechanism, wherein operators pump using low-cost night time electricity and turbine during peak times. This may change in the near future as several large pumped storage facilities come online, and it becomes possible to operate these quasi-closed loop systems over longer timescales.

The model constructs optimal filling fraction curves for each storage hydro plant, based on inflow data and demand, and the system is incentivised against deviations from those ideal curves. The introduction of intermittent and summer-dominated solar inputs creates an extra optimal control challenge. This causes energy mismatches that are typically greater in magnitude and higher in frequency than those of the Current scenario. Thus the system must use foreign exchange to compensate. Note that while total import and total export increase with renewable penetration, they are both of approximately equal magnitude: Domestic supply and demand are balanced in all scenarios, when averaged over the year. These seasonal dynamics are illustrated in Figure 2.5, which shows the daily average outputs of the various generators as a function of time, as well as demand and foreign exchange.

In the Renewable configuration, wind energy provides a relatively minor fraction of the domestic production. Thus wind energy would need a very large amount of investment and development to be a major player in the Swiss power system (the 1 TWh assumption already requires the construction of several hundred new turbines). Geothermal provides a small, but important fraction of the total generation. In such a hypothetical scenario, it is also conceivable that curtailment of geothermal output could be employed to assist with balancing services, if necessary.

The RoR output represents approximately one third of total production and is crucial to the operation of the system, with a relatively slow seasonal variation (though there are regional variabilities that cannot be shown by Figure 2.5). The PV output shows dramatic variability, sometimes dropping to very low values (even when averaged over a 24h period), before returning to high levels of output within short time scales. The average summer production is also greater than that in winter. The storage hydro plants are utilised to mitigate against these variations but exchange with foreign neighbours is used throughout the year for a large fraction of the balancing. PV and storage hydro both need to produce in summer, at a time when, unfortunately, demand is low compared to winter.

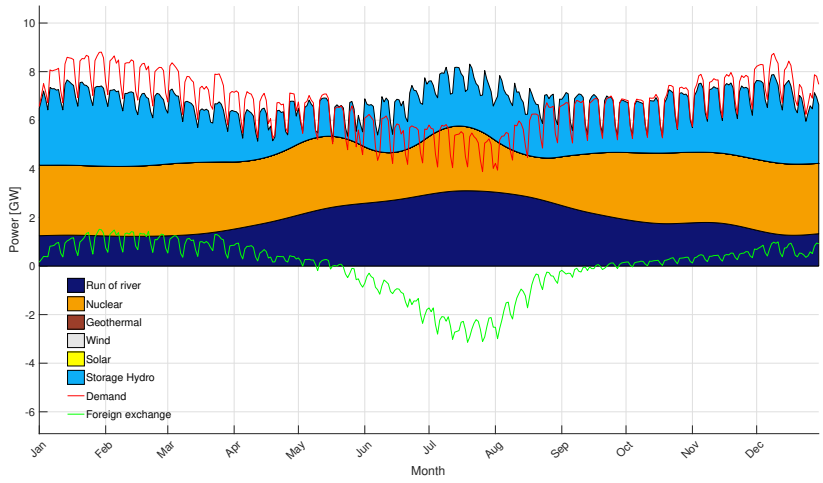

(a) Current

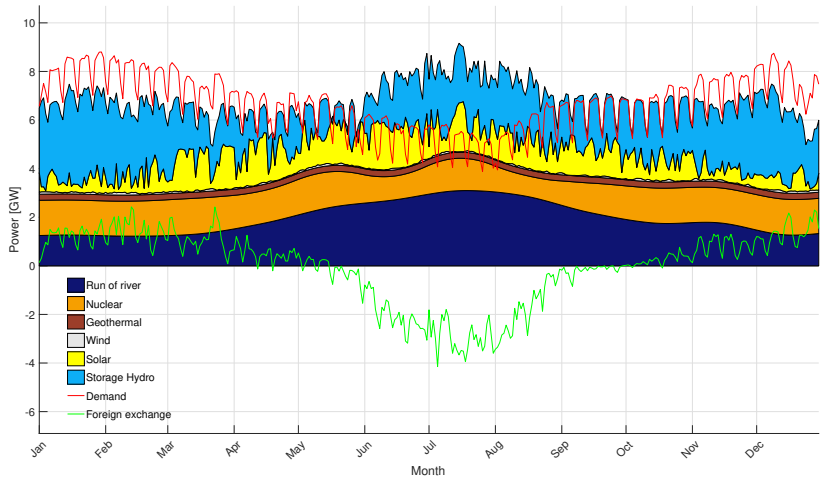

(b) Intermediate

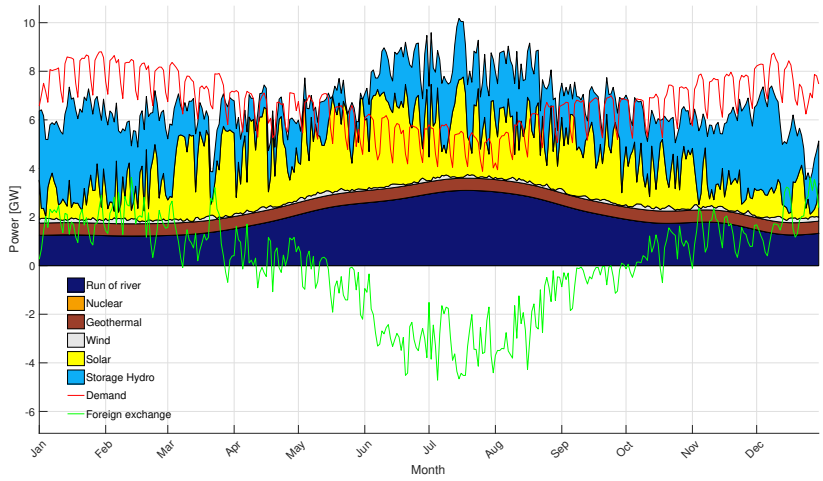

(c) Renewable

Figure 2.5: Time evolution of the various generating sources as well as demand and foreign exchange, for the three power system configurations. Note that import corresponds to negative foreign exchange and vice versa. Values are daily averages.

2.3.3 Spatial dynamics

The Swiss landscape is varied in its topography, with a relatively flat northern region, accompanied by one of the most mountainous and rugged areas in Europe in its southern half. This alpine region provides the gradients that are responsible for the country's massive hydropower resource. However, such elevation also provides an advantage with respect to solar insolation, with higher regions receiving sunlight that has passed through a thinner cross-section of atmosphere. Furthermore, fog and cloud cover are reduced in the winter, producing a smaller summer/winter production difference than lower altitude regions.

Alpine terrain induces habitation difficulties, which is why the majority of the Swiss population, and hence the electrical demand, are located in the less mountainous northern half of the country. Hence on the largest scales, the Swiss transmission system must convey power from the productive high Alps in the south, to the more consumption-dominated regions in the north. The exceptions to this general trend are the four nuclear stations currently operating (absent in the Renewable configuration) and several large RoR stations that are also located in the north.

In order to visualise these trends and observe how they vary as a function of renewable penetration, Figure 2.6 displays regional surplus production (total production minus demand), averaged over the year simulated, as well as line use (displayed as 99^{th} percentile values normalised by the relevant line capacity). Note that a very small number of lines experienced 99^{th} percentile values that were greater than the figure upper limit of 0.5. However, if the entire range $[0,1]$ was shown, there would be very little colour distinction, since the majority of lines are used at relatively low fractional values for most of the time (see Figure 2.4).

Careful inspection of these figures reveals how the average line stress is slightly reduced as renewable penetration increases. In Figure 2.6a, the general divide of the largely productive south and consumption-dominated north can be discerned. However there are four regions of average excess production, with three corresponding to the locations of nuclear plants (see Figure 2.2 for nuclear plant locations), and the fourth corresponding to a fairly large RoR plant. As the transition to renewable generators takes place, these three production hotspots disappear and in the Renewable scenario (Figure 2.6c), three of these regions become neutral in terms of production and consumption. The figure also shows that the intensity of the average deficit in the north reduces with renewable penetration. The solar output, which is dispersed across the demand-dominated regions, reduces the net average production deficit of this area. Note that this masks short term variability: while on average the PV production reduces local production deficits, its variations must be constantly balanced by other sources or sinks.The final significant trend illustrated in Figure 2.6, is the spatial shifts and reductions of line stress with renewable penetration. Several lines that connect Switzerland with neighbouring countries become more stressed in the Renewable case, due to the increased balancing and exchange from those countries. However several domestic lines show lower stress in the Renewable case.

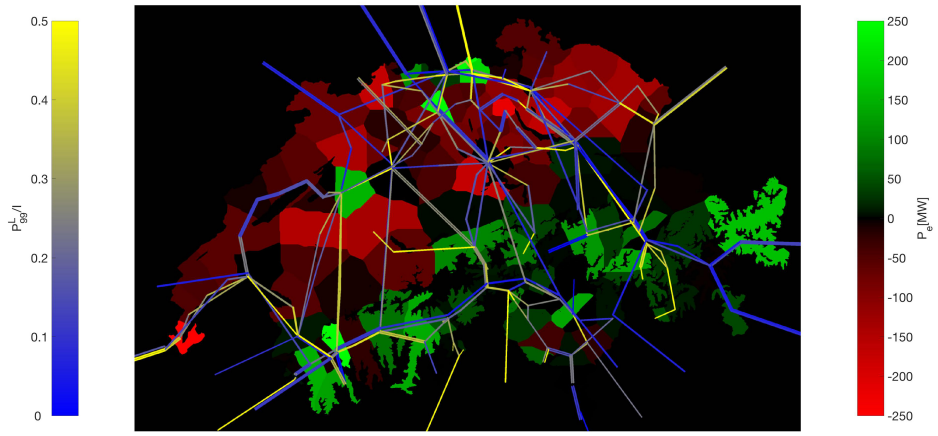

(a) Current

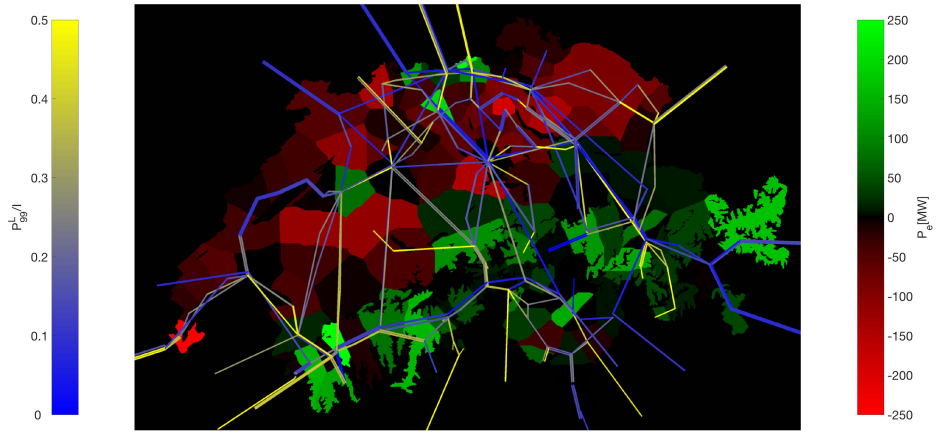

(b) Intermediate

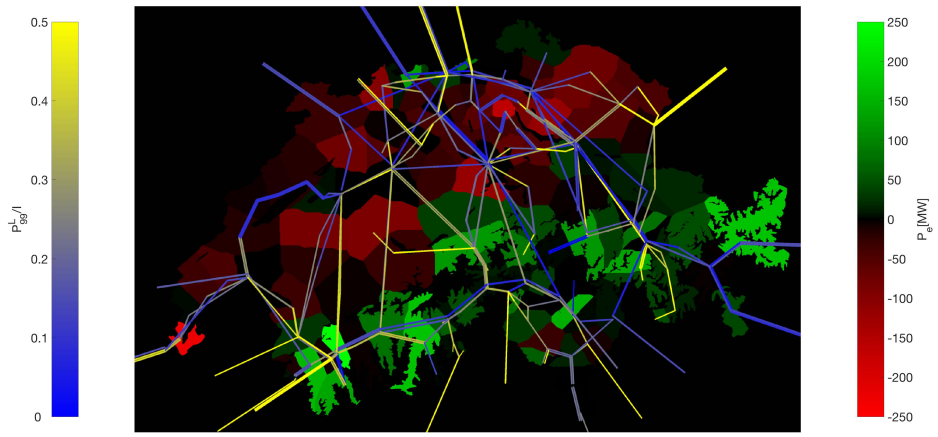

(c) Renewable

Figure 2.6: Spatial distribution of average surplus production and line use. The shade of green (red) corresponds to average surplus (deficit) production from all sources, with demand subtracted, for the area served by each transmission grid node. Line colour corresponds to the 99^{th} percentile values for line use normalised by line ampacity limit (e.g. yellow implies that a line was used at 50% of its capacity or less, for 99% of the time).

2.4 Discussion

The first conclusion of this work is that Switzerland can indeed satisfy all of its electrical demand with renewable sources. This work used a solar-dominated portfolio, with a small but steady contribution from geothermal, and additional production from wind energy. Previous work showed that there are many alternatives to such a combination, such as higher shares of wind (11). The political and social barriers to large numbers of wind turbines in Switzerland are significant, and identifying favourable locations in regions with relatively low mean wind speeds (at the coarse-grained level) is a matter of ongoing research (28).

Despite the relative feasibility of the Renewable scenario, it comes with challenges. Installing approximately 84 km^2 of solar panels is a formidable, but achievable target, given the continued decline in PV costs, coupled with advances in insolation monitoring and prediction, which reduce the operational burden to utilities (1; 48; 55; 60). In this work, PV installations were spread relatively diffusely across the country, weighted by population density, such that demand and supply were well-matched spatially. Detailed investigations of optimal solar placement and alignment configurations are currently in progress for Switzerland, and it is likely that placing solar farms in high alpine regions will also be a favourable option. This is due to the high altitude and low latitude (compared to the population centres in the north), but there are also alignment options (choice of tilt and azimuth angles) that can assist with smoothing the average daily demand curve. Intermittency is always an inevitable feature of solar energy, but the Swiss hydropower fleet is well-positioned to deal with the majority of this balancing (11).

The construction of approximately 28 geothermal plants is also a challenging, but manageable task. Deep drilling operations in Switzerland were marred by the induced seismicity event that occurred in Basel in late 2006 and early 2007 (8; 27; 33; 57; 56). Since that time, intense research efforts have been exploring a range of risk mitigation strategies that can enable deep drilling with minimal danger of induced seismicity (44). With these continued efforts, it should be possible for the geothermal production target to be met in the long term (51).

At present, there is a small, but growing wind power fleet in Switzerland. Land use is heavily regulated due to a variety of factors including the objective of retaining natural beauty and promoting tourism. Assuming that the planning process and bureaucratic barriers can be successfully navigated, there is ample scope for the construction of new wind turbines, including in alpine locations, which can have higher than expected wind speeds (28; 7).

In conclusion, there are no fundamental impediments to the construction of the renewable infrastructure outlined in this paper. The main challenges will be cost and planning. Given the relatively high GDP per capita and political will for a renewable transition, it should be possible to find the required investment for this new infrastructure. Whether the planning and land access aspect of the problem can be solved is more complex. Political will is insufficient if public opinion is too strongly opposed to new energy projects.

A further result presented in this paper is the slight reduction in line stress as a function of renewable penetration. Figure 2.4 shows that on average, the frequency of very high line use events decreases in the Intermediate and Renewable scenarios, compared to the Current scenario. In fact the probability of using between 75 and 95% of a line's capacity is reduced by a factor of ~ 2.5 with renewable generators.

The main reason for this line stress reduction is the fact that the country's nuclear output is concentrated at only three grid nodes (two plants share a node, the other two have a node each). This large and relatively steady output must be distributed across the country to consumers that may be in a distant location. In contrast, when a similar volume of electrical output is dispersed geographically, as in the case of large amounts of solar production, there is a reduced probability that a small subset of lines have to carry large volumes of power.

This effect seems to imply the possibility of a certain degree of electrical decentralisation in Switzerland. However the irreplaceable auxiliary and balancing services of the large hydropower plants in the south of the country will be essential for the near future and beyond. Intra and inter-day variations in solar output will have to be alleviated by a combination of dispatchable sources, primarily storage hydro and foreign exchange. Only with very high solar penetration and grid level intra-annual storage, would real microgridding in the north of the country become feasible. There have been investigations of microgridding in rural regions of the country, with mixed results (17; 37).

In contrast to co-locating PV installations with demand centres, a more optimal solution could be to place solar farms in the alpine southern regions. As mentioned above, these regions are particularly favourable from a resource perspective, and a careful selection of sites e.g. in ski areas, on avalanche defense structures, or co-located with dam installations, would limit any impact on the landscape. In addition, they could take advantage of the high voltage, high capacity transmission lines that are currently used by the storage hydro plants. This would not place such lines under additional stress because PV output would simply take the place of a certain fraction of the hydropower output, allowing those plants to turbine a lower volume of water. Thus a future renewable energy vision for Switzerland could be one in which the mountains provide not only the topographic gradients required for storage hydro, but also the altitude for significant solar production, and even favourable alpine wind conditions (28; 7).

Transit flows are an important and significant aspect of the Swiss transmission system. Large volumes of electricity are exchanged between Switzerland's four neighbours: Italy, Germany, France and Austria (46). France commonly exports power due to its large nuclear fleet and hydropower resources. Italy has traditionally been an importer of electricity, but this may change in the near future if there is significant investment in PV, for which there are favourable conditions across much of the country. Germany has undergone its own energy transition in recent years and often exports surplus production, particularly to Italy and other European nations. Austria is also undergoing changes in its energy system, with ambitious plans for wind and solar infrastructure. There is no doubt that the energy exchange relationships within

Europe will become more complex in the coming decades, as markets are opened, and the diversity of generating sources increases (10; 20; 29).

The current model did not include transit flows, since sufficiently resolved data for this aspect of the power system was not available. However, this component will be added in future work. Since these flows were not included in any of the three scenarios, and the conclusions are based on the comparisons between those scenarios, the lack of transit flows should not have a significant impact on the results.

Arguably the most prohibitive aspect of the Renewable scenario is the massive increase in import and export (~ 107%, see Table 2.3), an inevitable consequence of the seasonal anti-correlation between demand and solar output. This augments the formidable challenge faced by storage hydro operators: retaining the ability to generate throughout the year in spite of a highly seasonal runoff pattern. These reservoir inflows generally peak in the middle of the year (early Summer, caused by melting of alpine snow and ice), and reach a minimum towards the end of the year (mid Winter, when most precipitation is frozen or becomes frozen).

The large volumes of additional exchange energy represent the largest technical bottleneck of our hypothetical system. This result can now be used to motivate future modelling studies into further means to alleviate seasonal energy mismatches. Indeed an ongoing project within our group aims to explore the influence of modifications to the Swiss hydropower infrastructure in highly renewable scenarios (11).

Adding market dynamics has thus far been avoided, since it is a highly complex endeavour with large uncertainties. The objective of this work was to assess the technical characteristics of a fully renewable Swiss power system. However it is still possible to speculate as to the potential market features of these systems. The work of (40) also considered data from the year 2014, and used a different power system model to assess the feasibility of 2035 and 2050 targets (51). They concluded that Switzerland will be unable to satisfy its domestic demand with domestic production, in scenarios with high shares of renewables (their analysis also included a small but significant share of fossil fuel production). The spatial flows of electricity were not modelled and their solar and wind placement and proportions were different from those of the present work. They allocated a 19% and 7% share of production to solar and wind, respectively, for the year 2050 (compared to 34% and 1.6% in the present work). Despite the differences in modelling details and assumptions between the work of (40) and the present paper, the gross conclusions were similar: a renewable Swiss power system will require large, additional volumes of foreign exchange in order to maintain stability. The most plausible alternatives to this prospect are oversizing the renewable supply, and increasing dam heights (see section 2.6 and (11)).

At present, the Swiss hydropower fleet does have a high degree of flexibility, in the sense that it can turbine and generate when prices are high, and to an increasing extent, pump water to higher reservoirs when prices are low. Until now, most pumped storage facilities have been used to generate revenue, taking advantage of intra-day and intra-week price variations and

foreign exchange to make optimal use (in financial terms) of the available water. In the future, with an increased pumped storage capacity, a larger number of non-dispatchable, renewable generators, and an even more open market, the situation will potentially be very different, and almost certainly more complex. However, it may be possible that the large increases in foreign exchange that are necessary for a fully renewable system, may not induce massive increases in costs. In principle, with a sophisticated management strategy of pumped storage facilities, it may be possible to leverage all available resources to make sufficient revenue from peak time solar and storage hydro production, to cover the costs of large amounts of import in winter. If solar farms are constructed in alpine regions, the differences in solar yield between summer and winter might also be reduced.

In this work, it was assumed that foreign exchange was a constantly available source or sink of power. In a highly renewable future Europe this assumption would likely be less valid. If most European nations become powered by large numbers of non-dispatchable generators, the sustained availability of balancing services from foreign neighbours cannot necessarily be guaranteed. Our previous work showed that in principle, a ~ 50% increase of reservoir capacity in Switzerland would allow the country to be almost entirely self-sufficient, in terms of electrical energy (11). This target is not achievable in practice, but at least provides a quantitative limiting case.

2.5 Conclusions

This paper presented a set of numerical modelling analyses, aimed at elucidating the feasibility of renewable Swiss power systems. Three hypothetical scenarios were assessed: Current, Intermediate, and Renewable. The Current scenario was representative of the present-day configuration, the Intermediate scenario entailed a halving of the Swiss nuclear capacity, with the deficit replaced by solar, geothermal and wind sources, and the Renewable scenario made use of only hydropower, solar, geothermal and wind sources.

It was found that $84 km^2$ of 15% efficient solar panels, 208 $2MW$ wind turbines and 28 $17.9MW$ geothermal plants would be required to transition the country to a fully renewable power system. This radical change in generating infrastructure entailed a large increase in energy exchange with foreign neighbours, due to short term stochasticity of wind and solar inputs, and longer term, seasonal variations. However, it was found that the frequency of high line stress events actually decreased slightly as a function of renewable penetration. This suggests that large amounts of grid expansion may not be required, beyond those already planned by Swissgrid (54), which were included in this study.

The results suggest that Switzerland is well placed to shift away from nuclear and fossil fuel energy sources, and could become one of the first central European nations to become fully renewable.

2.6 Further work

The present work presents a compelling case for Switzerland and its renewable energy transition. Many key details were included in the model, but inevitably, simplifying assumptions had to be introduced. Future work could include more accurate price variations on intra-daily and intra-annual time scales. More realistic constraints on import/export flows would also improve the realism of the model. Ideally, the grid representation would be expanded to include lower voltage grids and more highly resolved demand data. Finally, the national hydropower system, a highly complex system in its own right, can always be more accurately represented, in particular the thousands of tunnels and smaller infrastructure, which generally have a small impact, but are relevant to the system's operation nonetheless.

Aside from accuracy improvements, which are an ongoing, long term endeavour, the model framework can also be used to ask different questions about future energy systems. In particular, it would be insightful to quantitatively explore the effect of increasing reservoir capacities. The Swiss hydropower fleet is rarely limited by its total power output, but rather constrained by intra-annual energy storage capacity (11). Furthermore, there is a non-linear relationship between dam height and reservoir water storage volume (imagine an inverted triangular prism growing vertically), meaning that small increases in dam height can yield disproportionately large increases in storage capacity. Thus a very important result to establish is the relation between reduction of import/export requirements, as a function of increased dam heights for the largest and most important reservoirs.

One of our main current endeavours is exploring the optimal placement of solar and wind infrastructure across Switzerland. This is a complex, multi-objective optimisation problem wherein the ideal solution has not only high yield, but also minimal intermittency, minimal disturbance of natural environments, and low cost. A hybrid optimisation procedure driven by a genetic algorithm has been employed, coupled with the power flow model presented here.

While this paper focused on a single year represented by real data, it would be beneficial to not only use multi-year datasets, but also to go further and generate ensembles of synthetic time series for wind speeds, solar insolation, river flow rates, reservoir inflows, and electrical demand. Such artificial test data would have to adhere to realistic constraints and the statistical properties of the equivalent real data. This would create a robust testing procedure for any power system control strategy. In fact, novel national control strategies could be developed through iterative learning processes, wherein a subset of the synthetic data is used as training sets.

Taking this idea further, it would also be valuable to carry out tests using extreme weather scenarios (from both real and synthetic data). The occurrence of extreme weather events will only increase in future, and the volume of water supplied to storage reservoirs will also change as a result of glacier melt and changes in annual precipitation (43; 45). Understanding and preparing for such situations will be essential for future risk mitigation.

Acknowledgements

Main funding from the Swiss Competence Centre for Energy Research, Supply of Electricity (SCCER-SOE) as part of Innosuisse. Important funding from the Swiss National Science Foundation, mainly NFP 70. We generously thank Swissgrid for providing the necessary grid data. We also thank Meteoswiss for the provision of solar insolation and wind speed data.

Bibliography

[1] S. Alessandrini, L. Delle Monache, S. Sperati, and G. Cervone. An analog ensemble for short-term probabilistic solar power forecast. *Applied Energy*, 157:95 – 110, 2015.

[2] Stuart John Bartlett, Bert Kruyt, Annelen Kahl, and Michael Lehning. Risks and reliability in a fully renewable switzerland. In *European Safety and Reliability Conference 2015*, 2015.

[3] Sarah Becker, Bethany A. Frew, Gorm B. Andresen, Timo Zeyer, Stefan Schramm, Martin Greiner, and Mark Z. Jacobson. Features of a fully renewable US electricity system: Optimized mixes of wind and solar PV and transmission grid extensions. *Energy*, 72(0):443 – 458, 2014.

[4] Andrey Bernstein, Lorenzo Reyes-Chamorro, Jean-Yves Le Boudec, and Mario Paolone. A composable method for real-time control of active distribution networks with explicit power setpoints. part i: Framework. *Electric Power Systems Research*, 125:254 – 264, 2015.

[5] Cory Budischak, DeAnna Sewell, Heather Thomson, Leon Mach, Dana E. Veron, and Willett Kempton. Cost-minimized combinations of wind power, solar power and electrochemical storage, powering the grid up to 99.9% of the time. *Journal of Power Sources*, 225(Supplement C):60 – 74, 2013.

[6] Christian Bussar, Melchior Moos, Ricardo Alvarez, Philipp Wolf, Tjark Thien, Hengsi Chen, Zhuang Cai, Matthias Leuthold, Dirk Uwe Sauer, and Albert Moser. Optimal allocation and capacity of energy storage systems in a future european power system with 100% renewable energy generation. *Energy Procedia*, 46(Supplement C):40 – 47, 2014. 8th International Renewable Energy Storage Conference and Exhibition (IRES 2013).

[7] A. Clifton, M. H. Daniels, and M. Lehning. Effect of winds in a mountain pass on turbine performance. *Wind Energy*, 17(10):1543–1562, 2014.

[8] Nicholas Deichmann and Jacques Ernst. Earthquake focal mechanisms of the induced seismicity in 2006 and 2007 below basel (switzerland). *Swiss Journal of Geosciences*, 102(3):457, Nov 2009.

[9] Mark A. Delucchi and Mark Z. Jacobson. Providing all global energy with wind, water, and solar power, part II: Reliability, system and transmission costs, and policies. *Energy Policy*, 39(3):1170 – 1190, 2011.

[10] Dominik Heide and Lüder von Bremen and Martin Greiner and Clemens Hoffmann and Markus Speckmann and Stefan Bofinger. Seasonal optimal mix of wind and solar power in a future, highly renewable europe. *Renewable Energy*, 35(11):2483 – 2489, 2010.

[11] Jérôme Dujardin, Annelen Kahl, Bert Kruyt, Stuart Bartlett, and Michael Lehning. Interplay between photovoltaic, wind energy and storage hydropower in a fully renewable switzerland. *Energy*, 135:513 – 525, 2017.

[12] Kerry Emanuel. Assessing the present and future probability of Hurricane Harvey's rainfall. *Proceedings of the National Academy of Sciences*, 114(48):12681–12684, 2017.

[13] Energie Schweiz. Projektlandkarte tiefengeothermie. http://www.geothermie.ch/index.php?p=deep_geothermal_projects, 2014.

[14] Energinet.dk. New record-breaking year for danish wind power. http://energinet.dk/EN/El/Nyheder/Sider/Dansk-vindstroem-slaar-igen-rekord-42-procent.aspx, 2016.

[15] Swiss Federal Office for Statistics. https://www.bfs.admin.ch/bfs/de/home.html, 2018.

[16] Patrick Graichen, Mara Marthe Kleiner, and Christoph Podewils. The energy transition in the power sector: State of affairs 2015. https://www.agora-energiewende.de/fileadmin/Projekte/2016/Jahresauswertung_2016/Agora_Jahresauswertung_2015_Slides_web_EN.pdf, 2016.

[17] Morgane Le Guen, Lucas Mosca, A.T.D. Perera, Silvia Coccolo, Nahid Mohajeri, and Jean-Louis Scartezzini. Achieving energy sustainability in future neighborhoods through building refurbishment and energy hub concept: a case study in hemberg-switzerland. *Energy Procedia*, 122(Supplement C):265 – 270, 2017.

[18] James Hansen, Makiko Sato, Paul Hearty, Reto Ruedy, Maxwell Kelley, Valerie Masson-Delmotte, Gary Russell, George Tselioudis, Junji Cao, Eric Rignot, et al. Ice melt, sea level rise and superstorms: evidence from paleoclimate data, climate modeling, and modern observations that 2 c global warming could be dangerous. *Atmospheric Chemistry and Physics*, 16(6):3761–3812, 2016.

[19] R. Harrabin. Offshore wind power cheaper than new nuclear. http://www.bbc.com/news/business-41220948, Sep 2017.

[20] Dominik Heide, Martin Greiner, Lüder von Bremen, and Clemens Hoffmann. Reduced storage and balancing needs in a fully renewable european power system with excess wind and solar power generation. *Renewable Energy*, 36(9):2515 – 2523, 2011.

[21] K. Heussen, S. Koch, A. Ulbig, and G. Andersson. Unified system-level modeling of intermittent renewable energy sources and energy storage for power system operation. *IEEE Systems Journal*, 6(1):140–151, March 2012.

[22] M. Iqbal, M. Azam, M. Naeem, A.S. Khwaja, and A. Anpalagan. Optimization classification, algorithms and tools for renewable energy: A review. *Renewable and Sustainable Energy Reviews*, 39(Supplement C):640 – 654, 2014.

[23] Mark Z. Jacobson. Roadmaps to transition countries to 100% clean, renewable energy for all purposes to curtail global warming, air pollution, and energy risk. *Earth's Future*, 5(10):948–952, 2017.

[24] Mark Z. Jacobson and Mark A. Delucchi. Providing all global energy with wind, water, and solar power, part I: Technologies, energy resources, quantities and areas of infrastructure, and materials. *Energy Policy*, 39(3):1154 – 1169, 2011.

[25] Mark Z. Jacobson, Mark A. Delucchi, Mary A. Cameron, and Bethany A. Frew. Low-cost solution to the grid reliability problem with 100% penetration of intermittent wind, water, and solar for all purposes. *Proceedings of the National Academy of Sciences*, 112(49):15060–15065, 2015.

[26] Sunil Kr. Jha, Jasmin Bilalovic, Anju Jha, Nilesh Patel, and Han Zhang. Renewable energy: Present research and future scope of artificial intelligence. *Renewable and Sustainable Energy Reviews*, 77(Supplement C):297 – 317, 2017.

[27] Theresa A. K. Knoblauch, Michael Stauffacher, and Evelina Trutnevyte. Communicating low-probability high-consequence risk, uncertainty and expert confidence: Induced seismicity of deep geothermal energy and shale gas. *Risk Analysis*, 2017.

[28] Bert Kruyt, Michael Lehning, and Annelen Kahl. Potential contributions of wind power to a stable and highly renewable swiss power supply. *Applied Energy*, 192:1 – 11, 2017.

[29] Florian U. Leuthold, Hannes Weigt, and Christian von Hirschhausen. A large-scale spatial optimization model of the european electricity market. *Networks and Spatial Economics*, 12(1):75–107, 2012.

[30] M. Bavay and T. Grünewald and M. Lehning. Response of snow cover and runoff to climate change in high alpine catchments of eastern switzerland. *Advances in Water Resources*, 55:4 – 16, 2013.

[31] Pedro Manso, Bettina Schaefli, and AJ Schleiss. Adaptation of swiss hydropower infrastructure to meet future electricity needs. In *Hydro 2015*, 2015.

[32] MeteoSchweiz. Automatisches messnetz, 2016.

[33] A Mignan, D Landtwing, P Kästli, B Mena, and S Wiemer. Induced seismicity risk analysis of the 2006 basel, switzerland, enhanced geothermal system project: Influence of uncertainties on risk mitigation. *Geothermics*, 53:133–146, 2015.

[34] James Nelson, Josiah Johnston, Ana Mileva, Matthias Fripp, Ian Hoffman, Autumn Petros-Good, Christian Blanco, and Daniel M. Kammen. High-resolution modeling of the western north american power system demonstrates low-cost and low-carbon futures. *Energy Policy*, 43:436 – 447, 2012.

[35] Lanre Olatomiwa, Saad Mekhilef, M.S. Ismail, and M. Moghavvemi. Energy management strategies in hybrid renewable energy systems: A review. *Renewable and Sustainable Energy Reviews*, 62(Supplement C):821 – 835, 2016.

[36] Jon Olauson, Mohd Nasir Ayob, Mikael Bergkvist, Nicole Carpman, Valeria Castellucci, Anders Goude, David Lingfors, Rafael Waters, and Joakim Widén. Net load variability in nordic countries with a highly or fully renewable power system. *Nature Energy*, 1:16175 EP –, 11 2016.

[37] Kristina Orehounig, Georgios Mavromatidis, Ralph Evins, Viktor Dorer, and Jan Carmeliet. Towards an energy sustainable community: An energy system analysis for a village in switzerland. *Energy and Buildings*, 84(Supplement C):277 – 286, 2014.

[38] Nam-Gyu Park, Michael Grätzel, Tsutomu Miyasaka, Kai Zhu, and Keith Emery. Towards stable and commercially available perovskite solar cells. *Nature Energy*, 1:16152, 2016.

[39] Morten Grud Rasmussen, Gorm Bruun Andresen, and Martin Greiner. Storage and balancing synergies in a fully or highly renewable pan-european power system. *Energy Policy*, 51(0):642 – 651, 2012.

[40] Paula Diaz Redondo and Oscar van Vliet. Modelling the energy future of switzerland after the phase out of nuclear power plants. *Energy Procedia*, 76:49 – 58, 2015.

[41] Lorenzo Reyes-Chamorro, Andrey Bernstein, Jean-Yves Le Boudec, and Mario Paolone. A composable method for real-time control of active distribution networks with explicit power setpoints. part ii: Implementation and validation. *Electric Power Systems Research*, 125:265 – 280, 2015.

[42] Rolando A. Rodriguez, Sarah Becker, Gorm B. Andresen, Dominik Heide, and Martin Greiner. Transmission needs across a fully renewable european power system. *Renewable Energy*, 63:467 – 476, 2014.

[43] Jonas Savelsberg, Moritz Schillinger, Ingmar Schlecht, and Hannes Weigt. The impact of climate change on swiss hydropower. *Sustainability*, 10(7), 2018.

[44] SCCER-SoE. SCCER-SoE Science Report. http://www.sccer-soe.ch/export/sites/sccersoe/publications/.galleries/dwn_sciencereport2017/SCCER-SoE_Science-Report-2017_fin_web.pdf, 2017.

[45] B. Schäfli, B. Hingray, and A. Musy. Climate change and hydropower production in the Swiss Alps: quantification of potential impacts and related modelling uncertainties. *Hydrology and Earth System Sciences Discussions*, 11(3):1191–1205, 2007.

[46] Ingmar Schlecht and Hannes Weigt. Linking Europe: The Role of the Swiss Electricity Transmission Grid until 2050. *Swiss Society of Economics and Statistics*, 151(2):125–165, 2015.

[47] Edgar Schmucki, Christoph Marty, Charles Fierz, and Michael Lehning. Simulations of 21st century snow response to climate change in switzerland from a set of rcms. *International Journal of Climatology*, 35(11):3262–3273, 2015.

[48] Enrica Scolari, Fabrizio Sossan, and Mario Paolone. Irradiance prediction intervals for pv stochastic generation in microgrid applications. *Solar Energy*, 139(Supplement C):116 – 129, 2016.

[49] Spyros Chatzivasileiadis and Damien Ernst and Göran Andersson. The global grid. *Renewable Energy*, 57(Supplement C):372 – 383, 2013.

[50] Florian Steinke, Philipp Wolfrum, and Clemens Hoffmann. Grid vs. storage in a 100% renewable europe. *Renewable Energy*, 50(Supplement C):826 – 832, 2013.

[51] Swiss Federal Office of Energy. Energy strategy 2050. http://www.bfe.admin.ch/themen/00526/00527/index.html?lang=en&dossier_id=05024, 2013.

[52] Swiss Federal Office of Energy. Hydropower in switzerland. http://www.bfe.admin.ch/themen/00490/00491/index.html?lang=en, 2014.

[53] Swissgrid. Grid Data. https://www.swissgrid.ch/en/home/operation/grid-data.html, 2018.

[54] Swissgrid. Strategic Grid 2025. https://www.swissgrid.ch/swissgrid/en/home/grid/strategic_grid_2025.html, 2018.

[55] D. Torregrossa, J.-Y. Le Boudec, and M. Paolone. Model-free computation of ultra-short-term prediction intervals of solar irradiance. *Solar Energy*, 124(Supplement C):57 – 67, 2016.

[56] Evelina Trutnevyte and Olivier Ejderyan. Managing geoenergy-induced seismicity with society. *Journal of Risk Research*, 0(0):1–8, 2017.

[57] Evelina Trutnevyte and Stefan Wiemer. Tailor-made risk governance for induced seismicity of geothermal energy projects: An application to switzerland. *Geothermics*, 65:295 – 312, 2017.

[58] Nicolas Weidmann, Ramachandran Kannan, and Hal Turton. Swiss climate change and nuclear policy: A comparative analysis using an energy system approach and a sectoral electricity model. *Swiss Journal of Economics and Statistics (SJES)*, 148(II):275–316, 2012.

[59] Trevor Williams, Dan Wang, Curran Crawford, and Ned Djilali. Integrating renewable energy using a smart distribution system: Potential of self-regulating demand response. *Renewable Energy*, 52:46 – 56, 2013.

[60] C. Yang, A. A. Thatte, and L. Xie. Multitime-scale data-driven spatio-temporal forecast of photovoltaic generation. *IEEE Transactions on Sustainable Energy*, 6(1):104–112, Jan 2015.

[61] R. D. Zimmerman and C. E. Murillo-Sanchez. *Matpower 6.0 User's Manual*, 2016.

[62] R. D. Zimmerman, C. E. Murillo-Sanchez, and R. J. Thomas. Matpower's extensible optimal power flow architecture. In *2009 IEEE Power Energy Society General Meeting*, pages 1–7, 2009.

[63] R. D. Zimmerman, C. E. Murillo-Sanchez, and R. J. Thomas. Matpower: Steady-state operations, planning, and analysis tools for power systems research and education. *IEEE Transactions on Power Systems*, 26(1):12–19, Feb 2011.

Part II

Synergistic optimization of renewable energy installations through evolution strategy

3 Main text

Synergistic optimization of renewable energy installations through evolution strategy

Jérôme Dujardin[1,2], Annelen Kahl[1,2] and Michael Lehning[1,2]

[1] School of Architecture, Civil and Environmental Engineering, Swiss Federal Institute of Technology in Lausanne (EPFL), Lausanne 1015, Switzerland

[2] Institute for Snow and Avalanche Research (SLF), Swiss Federal Institute for Forest, Snow and Landscape Research (WSL), Davos 7260, Switzerland

Abstract

With large parts of the world moving toward renewable energies, there is an urgent need to organize this large-scale transition effectively. This paper presents a new methodology to guide the planning and siting of renewable electricity generation for countries or larger geographical regions. Its flexible approach accounts for the specific boundary conditions, constraints and available resources of the region of interest and enables solutions that optimize the interplay between the various types of generation. Evolution strategy permits a simultaneous optimization of the placement and the share of renewable electricity generation technologies that are to be added to a system, while most efficiently combining the new with the existing electricity generation and respecting the constraints of the electrical grid. Using Switzerland as case study, we demonstrate the method's ability to devise national installation scenarios that are efficient, realistic with respect to land use and grid infrastructure and reduce significantly the need for seasonal storage. We show how the spatio-temporal variability of weather-driven electricity generation can be exploited to benefit the electrical system as a whole.

Keywords: renewable energy, evolution strategy, optimization, energy planning, photovoltaic, wind energy, pumped-storage hydropower

This chapter was published in the journal *Environmental Research Letters* on May 20^{th} 2021, in the volume 16, number 6.
doi: https://doi.org/10.1088/1748-9326/abfc75

J.D developed the idea and the model, performed the simulations, analyzed the results, and wrote most of the paper.

3.1 Introduction

Many countries are currently on their path to more renewable energy and scientists are trying to aid this endeavor to their best ability (5; 10; 14; 31). But every place has its own unique environmental potential and is constrained by specific boundary conditions. Instead of following an organic growth, renewable installations could be planned under the consideration of the system as a whole. A major challenge in replacing conventional by renewable electricity generation is to manage a typically much more volatile generation profile. Depending on the country, this might pose a problem on short time scales only, but particularly in the mid-latitudes, seasonal energy deficits and overproduction emerge, which cannot be alleviated with existing storage technologies. The spatio-temporal variability of wind, solar and hydro is an asset that can be used to better align electricity generation and consumption and reduce the need for storage. We propose a new optimization scheme that can devise realistic installation scenarios at high spatial resolution for renewable electricity generation. Our method is particularly suited for geographical regions that exhibit high spatial heterogeneity in the weather that drives the renewable generators. As in our test case: Switzerland, such regions can be rather small but can nevertheless show high variability across short distances. This variability is also found in much larger geographical regions like Europe or North America, which are affected simultaneously by various synoptic weather systems. The high resolution (number of grid cells in the considered territory) admitted by our method allows to truly capture and optimize the electricity generation profiles from solar, wind and hydro sources.

Energy modeling is an active research field that tackles many facets of the energy or electricity sectors. The optimization of the generation mix can be addressed in multiple manners, each one targeting certain features of the system and neglecting others. In Europe, (13) optimized the photovoltaic (PV) and wind turbine capacities in each country to reduce the need for storage given the load curve. The effect of excess generation was then investigated in (12). (22) adopted a similar approach but aggregated at the European level. (8) presents a comparable work for Switzerland, with a detailed representation of the hydropower system. Those studies used predetermined locations for PV panels and wind turbines and considered unrestricted power transmission (copper-plate assumption). In those non-economic approaches, the optimization was performed by computing the effect of all possible generation mixes. (4) did a similar work for the USA but included a simplified electrical grid and used a combination of least-cost optimization and simulated annealing for the optimization of the Levelized Cost of Electricity. (15; 5) present a cost-optimized model of a fully-renewable USA without explicit power flow but considering transmission. (17) uses particle swarm optimization, a heuristic method, to find the best integration of PV panels and wind turbines on a distribution grid and offers a detailed review of similar work based on heuristics. Another line of research focuses more on the effect of renewable electricity generation on the transmission grid and the electricity market. (19) introduce a European model of the grid, generation and economics that maximizes social welfare through non-linear optimization. In Switzerland, (24) simulates the dispatch and load flow via a linear cost minimization and a detailed representation of

the hydropower system. (3) shows with the same level of detail the impact of large shares of PV panels in Switzerland, but without economic considerations. Another detailed electricity model for Switzerland is presented in (1). It integrates a dispatch model on the transmission grid, a market model and a long-term investment model. The system, formulated as a quadratic problem, is optimized to minimize dispatch and investments costs. A detailed review of modeling tools for energy and electricity systems can be found in (23).

The complementarity between diverse renewable generators installed at various locations is a key component of a reliable electricity system with large share of renewables. This is shown in (11) , where optimized wind power capacities across Europe, under the local weather regimes, can deliver a more balanced generation. To our knowledge, there has been no work optimizing simultaneously the generation mix and location of renewable power plants while considering a detailed grid and the spatio-temporal variability of renewable electricity generation, instead of predetermined locations.

We present a novel approach which optimizes simultaneously the generation mix and location of renewable generators at high spatial and temporal resolution and the management of storage hydropower plants (SHP) and pumped-storage hydropower plants (PSHP) while considering the electrical grid. The optimization considers the spatio-temporal demand, the existing generators, the electrical grid, the weather variability in space and time and the land availability. We adopted a hybrid approach that combines evolution strategy, a heuristic optimization that mimics the biological evolution of a population as its individuals get fitter with respect to a certain objective function, and a reduction of the problem complexity by regionally ranking the best locations. Because of its heuristic nature, there is no restriction in the problem formulation and the objective function can be freely defined to target any of the important aspects of the system.

Intermittent renewable electricity generation is never a perfect substitute for dispatchable generation. Within a geographical region, overproduction needs to be stored, exported or curtailed, underproduction needs to be compensated by dispatchable generation or import. In our Swiss test case, we want to show how a smart planning of renewable installations can better align generation and consumption by efficiently combining the various generators given the spatio-temporal variability of the weather that drives them. We applied our method in a new model called OREES: Optimized Renewable Energy by Evolution Strategy. This model finds the optimal configuration of PV panels and wind turbines in Switzerland in order to replace the currently operational but soon decommissioned nuclear reactors, while minimizing the mismatch between electricity generation and consumption. This Swiss-specific combination of PV panels and wind turbines is not necessarily the economic optimum, especially when considering the Pan-European electricity market. Instead, we show how weather variability can realistically be exploited to reduce some drawbacks of solar and wind energy, namely the need for large storage and the grid congestion.

3.2 Data and Methods

3.2.1 Test scenario

As case study we selected Switzerland because of its ambitious plan to phase out nuclear energy by 2035, replacing it by the largest possible share of renewables. However, because of its high flexibility, our methodology can be applied to other countries or bigger geographical regions with different boundary conditions or objective functions. The initial setup is based on the year 2016, given its spatially distributed time series of modeled wind speeds, measured solar irradiance, estimated water inflows into the reservoirs (equivalent to 17.1 TWh), actual electricity production from run-of-river (16.6 TWh) and real electricity consumption (62.5 TWh). We use the transmission network as projected by Swissgrid for 2025 (26) (Figure 3.1). If nuclear and conventional thermal plants would be removed from the generation mix in 2016, a net domestic production deficit of 29 TWh would result. It is this gap, mostly occurring from November to April (referred to as winter in the following) that we aim to fill with new PV and wind energy. We focused on those two technologies as hydropower is already almost fully developed. While the deployment of such a large capacity will take several years or decades, we consider a completed installation, i.e. the total installed capacity does not change throughout the year. The analysis is repeated for 2017 and 2018 and yields very similar results which are presented in the supplementary information (SI).

This modeling effort is rooted in detailed simulations of the Swiss hydropower system and its interplay with PV and wind (8) through the electrical grid (3) by means of a least-cost dispatch model. A summary of those models is provided in section 3.2.4 and from now on, as in those studies and in section 3.2.2, we will use the term “import” as a placeholder defining any supplementary electricity storage or dispatch needed to balance the system after SHP and PSHP have been invoked. We compute hourly, spatially explicit electricity generation from PV panels and wind turbines using the SUNWELL model (16) on a 1.6 x 2.3 km grid and the wind fields from the Numerical Weather Prediction model COSMO-1 (21) on a 1.1 km grid (see section 3.2.5). The location-specific tilt and azimuth of each PV panel is chosen to maximize its winter production.

3.2.2 Constraints and objective function

In Switzerland, the capacity factor (i.e. the fraction of the nominal power that is reached on average) and the cost per installed capacity, are roughly equivalent for PV panels and wind turbines, respectively. If we consider similar lifespans and maintenance costs, and similar sales values (EUR/MWh) for both technologies, their equivalent annual costs and revenues are also similar. Under those assumptions, we can exchange one unit of installed capacity of one type of generator with the other, without changing the associated costs and revenues. To equitably compare every scenario of installation our optimization explores, their combined installed capacity remains constant between each optimization step. Given an expected capacity factor

of 18.5% in the optimized locations (as achieved in Figure 3.6), 17.85 GW of installed capacity is needed to reach the aforementioned 29 TWh of generation in 2016. A constant capacity implies that the total generation from PV and wind varies at each optimization step, which is compatible with the objective of reducing the total required import.

(8) used a quantity termed "required import" as an overall metric for the synergy between the various renewable energies and their interplay with SHP and PSHP. This quantity corresponds to the amount of supplementary electricity needed to balance the grid after all domestic generation and storage has been used. As described in 3.2.4, our dispatch model is set to minimize the exchanges with neighboring countries. If the PSHP would be large enough (installed capacity and energy storage), the dispatch model would not need to activate those exchanges and hydropower would compensate for the fluctuations of solar and wind. However, given its limited size, the current hydropower infrastructure cannot compensate for all those fluctuations. This results in e.g. export of excess solar energy in summer and import of electricity in winter. In this context, the total amount of (required) import is the quantity we aim to reduce, by aligning production and demand as much as possible and by concurrently optimizing the operation of the hydropower system.

3.2.3 Genetically encoded generation mix and installation locations

As detailed in SI, our optimization is split into two sub-problems: i) How many PV panels and wind turbines should be connected to each node of the electricity network; ii) where within the territory surrounding the node should those installations be located. The first is treated by the evolution strategy algorithm and the second is treated by a deterministic ranking of the locations given their winter production potential.

Following the previously used, biological metaphor, a candidate solution to our problem is represented by one individual which can propagate its genetic information to its descendants. We start with a pool of 12 random individuals, each one being close to a uniform distribution of placement and having a random generation mix from PV and wind. Progressively, as the best individuals are selected, their breeding and mutations lead to an evolution toward better solutions until the optimum is reached. Except for very small values, the size of the population pool did not influence the optimal solution. Larger pools converge after fewer optimization steps because more diversity exists simultaneously but require more computation per step. The total number of individuals evaluated before convergence, and thus the total computational time, was minimal for a pool of 12 individuals.

3.2.4 Power and energy balance models and objective function

At the heart of our optimization scheme lays the nationally aggregated power and energy balance model described in (8) and the spatially distributed optimal power flow model described in (3). They use hourly time series of electricity consumption, non-dispatchable generation

from run-of-river plants and water inflows into the hydropower reservoirs. The total effective storage capacity of the reservoirs amounts to 6.3 TWh and the pumping capacity amounts to 3.5 GW. As depicted in Figure 3.1, we discretize the country into 129 clusters surrounding 169 indigenous grid nodes (several nodes are collocated) and aggregate generation and consumption inside each cluster to then distribute it across its nodes. Those two models share the same goal: to balance electricity supply and demand at any time while minimizing the amount of import and export with the neighboring countries. Their behavior can be described in 3 steps: i) The non-dispatchable generation (run-of-river, PV, wind) is subtracted from the demand at each node; ii) the dispatchable SHP and PSHP are invoked to decrease the overproduction or underproduction within its capabilities while adhering to a long-term water management strategy; iii) import and export are used to guarantee that total generation equals total consumption at any time.

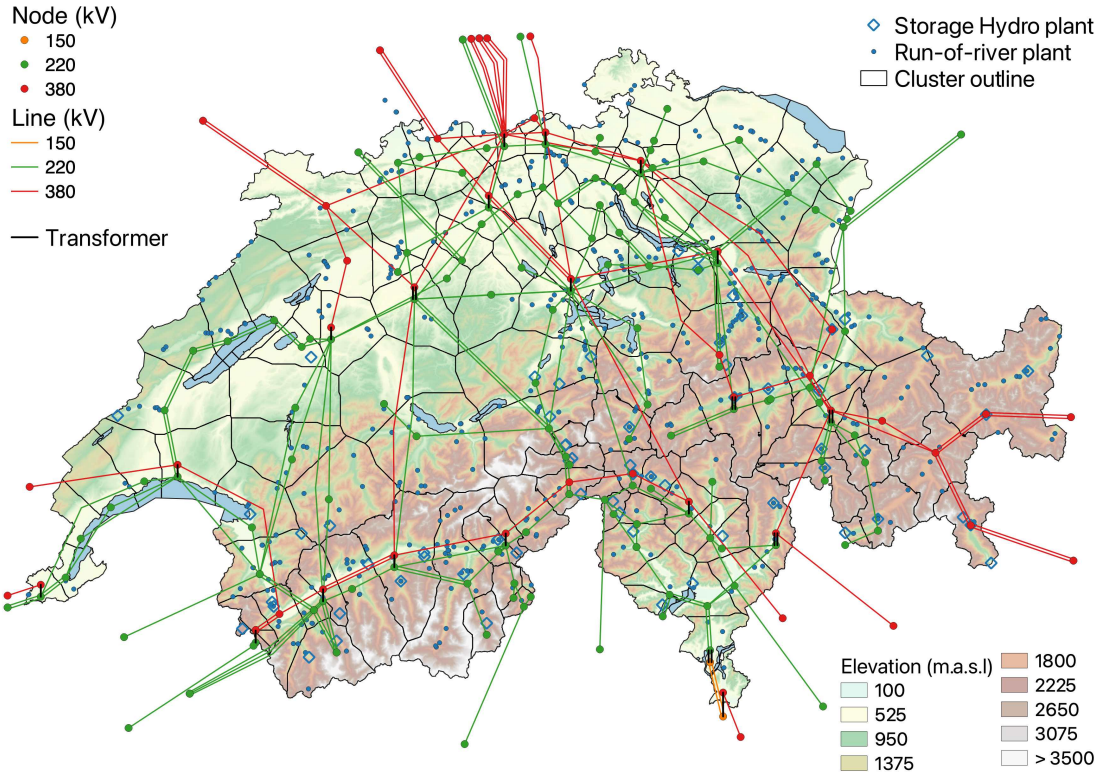

Figure 3.1: High voltage electric network, outline of the node-centered clusters and hydropower plants considered in our spatially distributed power flow model. The background color shows the elevation

The aggregated model computes the theoretical lower limit of required import, and determines how SHP and PSHP should be used in coordination with the other generators. The spatially explicit model combines a simulation and water management strategy of the largest 67 Swiss hydroelectric reservoirs and 69 associated SHP and PSHP with a dispatch model on 169 Swiss electric nodes and 37 foreign ones. Given the (non-monetary) generation costs of each domestic and foreign generator, the DC optimal load flow from the MATPOWER library (30) ensures that generation and demand match at any given time for the least total generation

cost. This dispatch respects the grid constraints (node voltages and current rating of lines and transformers). In our setup, electricity import occurs only when necessary. This is realized by using a constant cost for foreign electricity generation, which is higher than the average costs of domestic generation. The domestic costs fluctuate given the water availability and long-term water management strategy. The results from this setup (when aggregated spatially) are similar to the results from the aggregated model. In OREES, we use the aggregated model as a first filter to exclude candidate solutions that do not achieve a decrease in import, because of its low computational cost. We apply the spatially distributed model to each of the remaining solutions in order to eliminate those that are not compatible with the grid.

3.2.5 Electricity generation from PV panels and wind turbines

PV generation is computed with the SUNWELL model, which uses Meteosat Second Generation (MSG) data. The model is described in (16). Based on hourly satellite-derived radiation and albedo maps (25) on a 1.6 km x 2.3 km grid, SUNWELL computes the potential production as function of the panel's tilt and orientation. Based on a nominal power of 150 W/m^2 at 20°C, the panel efficiency is adjusted for environmental conditions (air temperature and wind speed). The model is conceived to capture the complex irradiance conditions in alpine areas; it accounts for topographic shading, cloud cover and the highly variable reflectance from the ground as the snow cover varies throughout the year.

Hourly time series of wind power are computed using the curve of the coefficient of performance from the Enercon E-82 E4 wind turbine (common model in Switzerland), which has a nominal power of 3.02 MW, a hub height of 84 m and a diameter of 82 m (18), (9). The calculation involves the wind speed at 90 meters above ground level from COSMO-1 analysis dataset and a correction for the local air density which varies strongly given the wide range of elevations investigated in this study. Details for this calculation are given in SI. Figure 3.2 shows the capacity factor of PV panels (upper panel) and wind turbines (lower panel) calculated in their respective grid cells.

3.2.6 GIS analysis for installation potential

Since the geographic placement strongly influences the electricity generation from PV panels and wind turbines, we used a Geographical Information System (GIS) analysis to determine their feasible installation areas on a 50 m grid, accounting for accessibility and social acceptance. Based on high-resolution datasets (27; 28), we exclude for both installations grid cells which are: i) on slopes steeper than 30 degrees, or within 150 m from them; ii) at elevations greater than 2700 m; iii) farther than 500 m from a motorable road; iv) within the National Park. The Corine Land Cover inventory (CLC) (6) is used to exclude glaciers and areas of persistent snow cover. It is further used only for PV installations to exclude all surface cover types except for: urban fabric, industrial or commercial units, non-irrigated arable land, permanently irrigated land, pasture, heterogeneous agriculture areas, natural grasslands, bare rocks and

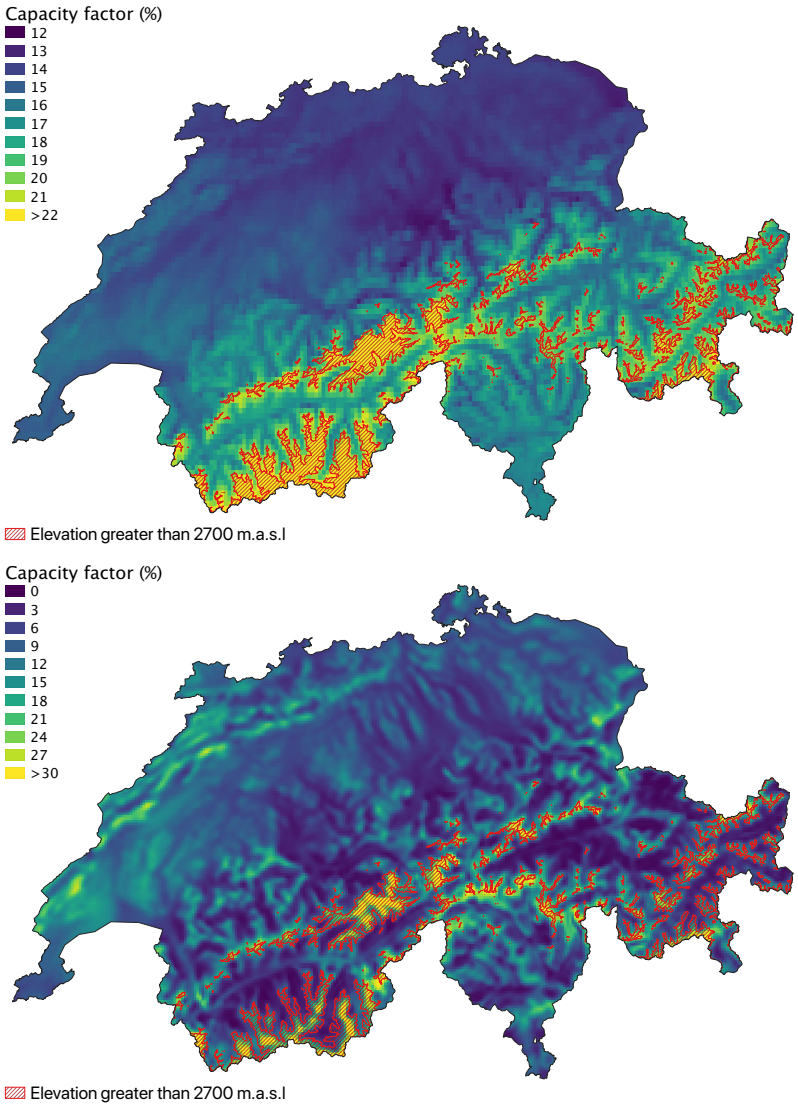

Figure 3.2: Capacity factors of potential PV (upper panel) and wind power (lower panel) installations in each grid cell. To enhance the contrast, we saturated the representation to the maximum values encountered at elevations smaller than 2700 m. Elevation larger than this limit (red hatch) are not considered as potential location.

sparsely vegetated areas. For wind turbines only, we exclude areas within a radius of 500 m from houses. Additionally, we exclude northern orientations ($slope \times cos(0.5 \times aspect) > 10°$) for PV. This procedure generates binary maps at 50 m resolution indicating the possibility of installation. For PV, we allow a maximum of 5% coverage for the selected areas. In the 2552 km^2 of constructed areas, 5% approximates the 150 km^2 of roof area suitable for PV installation (29). For non-urban territories, 5% corresponds to one PV farm with a footprint of 1 km^2 (500000 m^2 of panels) in an area of 10 km^2. We enforce a minimum distance of 500 m between wind turbines, which limits the density of installations in each contiguous potential area. Aggregating those maps on the grids of the respective time series (Figure 3.3), yields 9148 MSG pixels for potential PV and 22269 COSMO-1 pixels for potential wind installations.

This rather conservative analysis reveals that Switzerland could accommodate 605.77 km^2 of PV panels and 50398 wind turbines. This potential is large in comparison to the aforementioned installed capacity required to reach our production target. Our optimization will thus have the freedom to place these installations in various configurations.

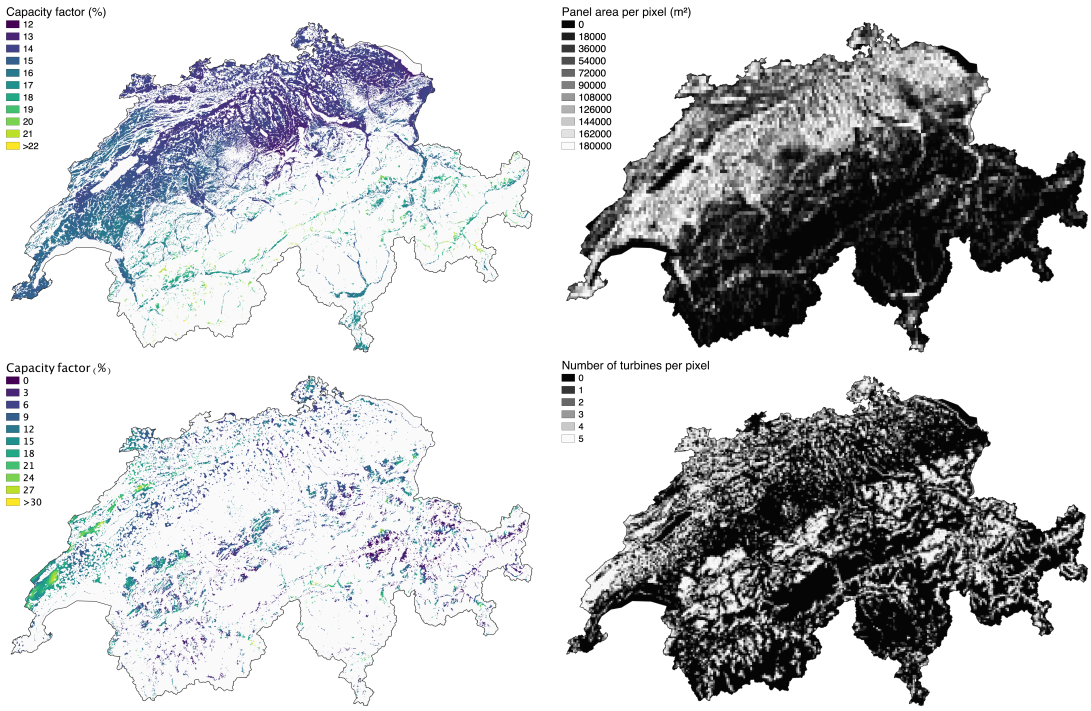

Figure 3.3: Potential locations for PV installations (upper panels) and wind turbines (lower panels). The left panels show in color the capacity factors in the potential locations at high resolution (50 m). The areas in white are not considered potential locations. The right panels show the aggregated potential installations on the coarser input data grids (MSG for PV and COSMO-1 for wind).

3.2.7 Evolution Strategy

As represented schematically in Figure 3.4, the optimization algorithm surrounds our power and energy models to supply them with changing times series of PV and wind power produc-

tion that progressively lead to lower values of required import. Each individual in the pool of candidate solutions is a vector representation of how much installed capacity of PV panels and wind turbines is connected to each grid node.

This vector thus has 338 (2 times 169) entries. For each vector entry we compute the corresponding time series of power generation using the previously mentioned ranking algorithm within each cluster. A pre-filtering step checks if newly-created individuals lead to import values lower than the highest value obtained in the previous optimization step. In other words, children should be better than the worst parent. Individuals not fulfilling this condition are discarded and new individuals are created until 6 viable children are generated from the 6 parents. This reproduction is based on a random selection of 2 out of 6 parents, on their breeding (linear combination of their vectors with random weights) and on 4 mutations within the child (exchange of a random value between two randomly chosen vector entries). The aforementioned random values are generated within controlled boundaries such that the vector entries of the child are always within a range of values which are coherent with the installation potential on each grid node. SI describes how we define the solution space in such a way and how we generate those random but controlled values. The 6 children are then filtered by the power flow model to guarantee that the grid can handle the corresponding configurations of PV panels and wind turbines. Individuals who fail are discarded. Finally, we select the 6 individuals with the lowest amount of import among the 6 parents and the remaining children. They become the parents of the next pool. The first iteration is atypical as we generate random individuals until we can form a pool of 12 solutions that pass the power flow test. This guarantees that our initial solutions are all compatible with the grid and won't propagate wrong configurations of PV and wind to their children. The next pool is based on the 6 solutions that have the lowest import and is created through the described procedure. A sensitivity analysis showed that population size, survival rate and mutation rate only affect the speed of convergence, but not the final solution of the optimization. SI provides a description of the reasons that guided the architecture of our optimization scheme and the required computation to reach the optimal solution.

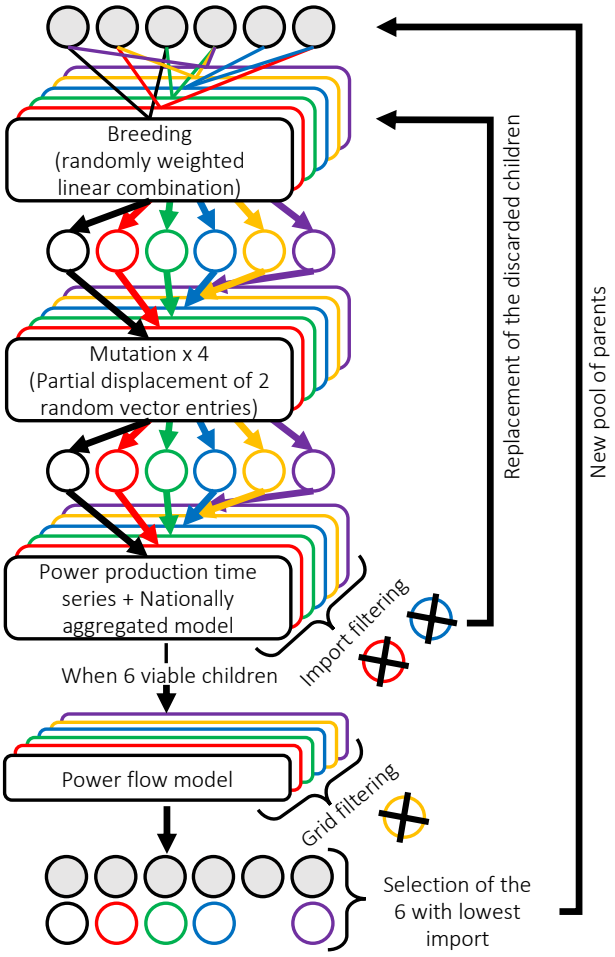

Figure 3.4: Methodology employed for the evolution of the pool of candidate solutions.

3.3 Results

In our test case, the optimal solution of PV panel and wind turbine installations has the following characteristics: a high share of wind turbine capacity, and placements in mountainous areas with high wind speeds and high solar radiation in winter. Moreover, this solution is compatible with the electrical grid and the SHP and PSHP are optimized to work concurrently. For Switzerland, installing 29.63 km^2 (4.44 GW) of PV panels and 4438 wind turbines (13.40 GW) in the specific locations identified by our model reduces the mismatch between generation and demand, via the optimized support from hydroprower, to the lowest possible amount. This better alignment with demand and complementarity between PV, wind and hydropower reduce the requirements for supplementary seasonal storage and the reliance on foreign exchanges at times when many neighboring countries will face similar challenges of overproduction and deficits.

3.3.1 Wind dominated evolution

Starting with 12 random individuals, the pool of candidate solutions evolved toward an optimal configuration where 75.1 % of the capacity is from wind turbines and 24.9% is from PV panels. Figure 3.5 shows how import changes during this evolution. This change is computed with respect to the averaged import value (7.09 TWh) associated to the initial 12 candidate solutions. The green curve, reflecting our objective function, indicates the change of import associated to the best solution in the pool at each optimization step.

We must first identify the origin of this reduction of import. Our evolution strategy has the control over two variables: the generation mix of PV panels and wind turbines and their locations. We can further decompose the effect coming from the latter into two parts: the change in yield (total annual production, red band) because of higher radiation or wind speed in certain locations, and the change in the temporal pattern of the production because of the local weather characteristics (blue band). At each optimization step, we generated three fictitious solutions that demonstrate the effect of generation mix, yield and timeliness of production. This decomposition, described in SI, is quite accurate, as the sum of the change of import from the three factors almost equals the change of import from the real solution.

The thumbnail in Figure 3.5, a normalized version of this figure, helps to identify the relative importance of each contribution. Initially the optimization could achieve the highest improvements through changes in the generation mix. Subsequently, changes in installation location, more specifically the associated increase in yield and better synchronization with the demand, contributed more to the reduction in import.

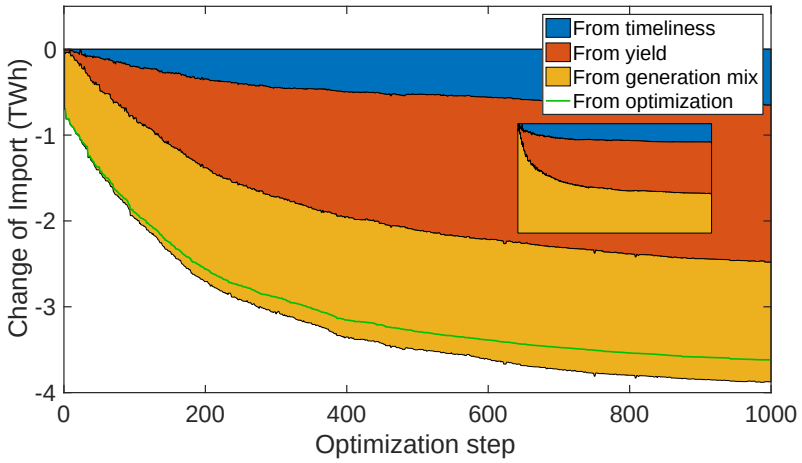

Figure 3.5: Change of import throughout the optimization. The green curve represents the best candidate solution in the pool at each optimization step. The three colored bands represent the contribution of three main factors responsible for this change of import. The thumbnail is a normalized copy of this figure that shows the relative contribution of each factor.

Our optimization scheme reduces the required import from an initial 7.09 TWh to a final 3.47 TWh: a reduction by 51%. We can put this achievement into perspective: in a conventional

base load scenario, a constant production leading to our 29 TWh target would require 5.9 TWh of import. Furthermore, compared to the business as usual scenario described below, which requires 17.48 TWh of import despite its higher capacity of 21.7 GW, the reduction amounts to 80%. It is thus possible to achieve a lower dependence on import with renewable than with a conventional base load. But this is only possible if these renewable generators are smartly selected and located.

3.3.2 A solution for the benefit of all

One might wonder where this high level of performance comes from. Figure 3.6 shows how PV panels and wind turbines perform as our algorithm optimizes them. It depicts the evolution of the generation mix and the capacity factors of PV panels and wind turbines calculated for the entire year and for the winter period only. As comparison, we also show values for a Business As Usual scenario (BAU) with a more standard setup where only 4 TWh (as targeted by the Swiss Energy Strategy 2050) come from 679 wind turbines located in productive areas and the remaining 25 TWh are produced by 131 km^2 of rooftop PV panels in urban areas, as described in SI. The first important element that we can observe is the continuous increase of the capacity factors as the system gets optimized. The optimization does not just reduce the import, which is beneficial for the system as a whole, but also boosts the yields which is beneficial for the owner of such installations. Unsurprisingly for Switzerland, winter electricity generation from wind turbines is always higher than from PV panels. Their relative improvement however is similar. Even if the BAU scenario has a yearly PV capacity factor close to the initial one of our optimization, it performs poorly in winter with values as low as 5%. In comparison, the optimization covers winter values ranging from 13.1% for homogeneously distributed locations to 17.6% as they are displaced toward the mountains: A value that is 3.5 times higher than in the BAU scenario.

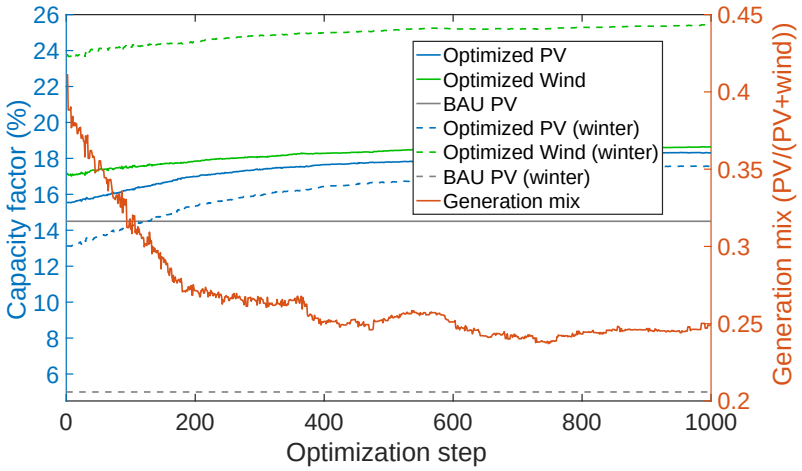

Figure 3.6: Evolution of the capacity factors of PV panels and wind turbines (left vertical axis) and evolution of the mix of their installed capacities (right vertical axis, 0 corresponding to 100% wind and 1 to 100% PV). Plain lines are used for capacity factors computed on the entire year while dash lines are used for those computed on the winter period. The capacity factors for the BAU scenario are constant because they are not optimized by our model.

We can summarize these findings with two short statements: i) Many locations offer high winter production from wind turbines, which favors a high share of wind in the system; ii) Winter PV production is mediocre in many areas but mountains offer some exceptionally favorable locations.

The efficiency of those two renewable generation technologies in the system does not stand on its own: SHP and PSHP play a major role. In Switzerland, most of the solar and wind fluctuations can be compensated by the flexibility of the hydropower system. Underproduction can be covered by turbining water from the reservoirs and overproduction can be absorbed by pumping water to fill them. This interplay is described in (8) and is fully represented in our model. The optimization exploits this capability to its limits. Interestingly, as the optimization progresses, so does the use of the PSHP. Its initial utilization rate of 13.8% increases to 17.8% at the end of the optimization. Thus, by improving the system as a whole, the optimization turns the PSHP into a more profitable generator. This however implies a change in its operation, with more occurrences of ramp-ups and ramp-downs to accommodate the fluctuations in the new power generation profile. This has impacts on the equipment and on the water discharges, which are the objects of multiple studies (7; 20).

3.3.3 Grid constraints

As described in sections 3.2.4 and 3.2.7, each candidate solution undergoes a power flow test ensuring that the entire grid can satisfy the overall balance between generation and consumption. Figure 3.1 depicts the characteristics of the Swiss transmission network: Multiple high capacity lines connect the mountains in the south and the urban centers in the north. Those lines currently transport electricity from dispatchable alpine SHP. They could also transport electricity from alpine PV panels or wind turbines when they are active and hydro-electricity otherwise. Moreover, when there is too much solar or wind energy for the system to consume or even to transport, the pumps which are located nearby, can absorb and store the overproduction.

To visualize the constraints imposed by the grid, we perform a parallel optimization run which leaves out the power flow model, but keeps the upper limits of installed capacities on each node. As described in SI, the solution space, hence the theoretical potential for installation on each node, is bounded by the installation potentials from the GIS analysis and by the capacities of the lines connected to the node. In this alternative scenario, we keep the line-imposed limits in order to prevent unrealistic concentration of installations is certain locations. The results from our two scenarios show the impact of grid congestion on the optimal solution and on its performance. Figure 3.7 shows the differences in location of PV installations (upper panel) and wind turbines (lower panel) between the optimal solutions of the two scenarios described above. Areas depicted in blue did not show any change while the red areas lost some installations (relocated in the green areas) because of the limitations imposed by the grid. In grey, we show the location of PV panels used in the BAU scenario. The change of installed

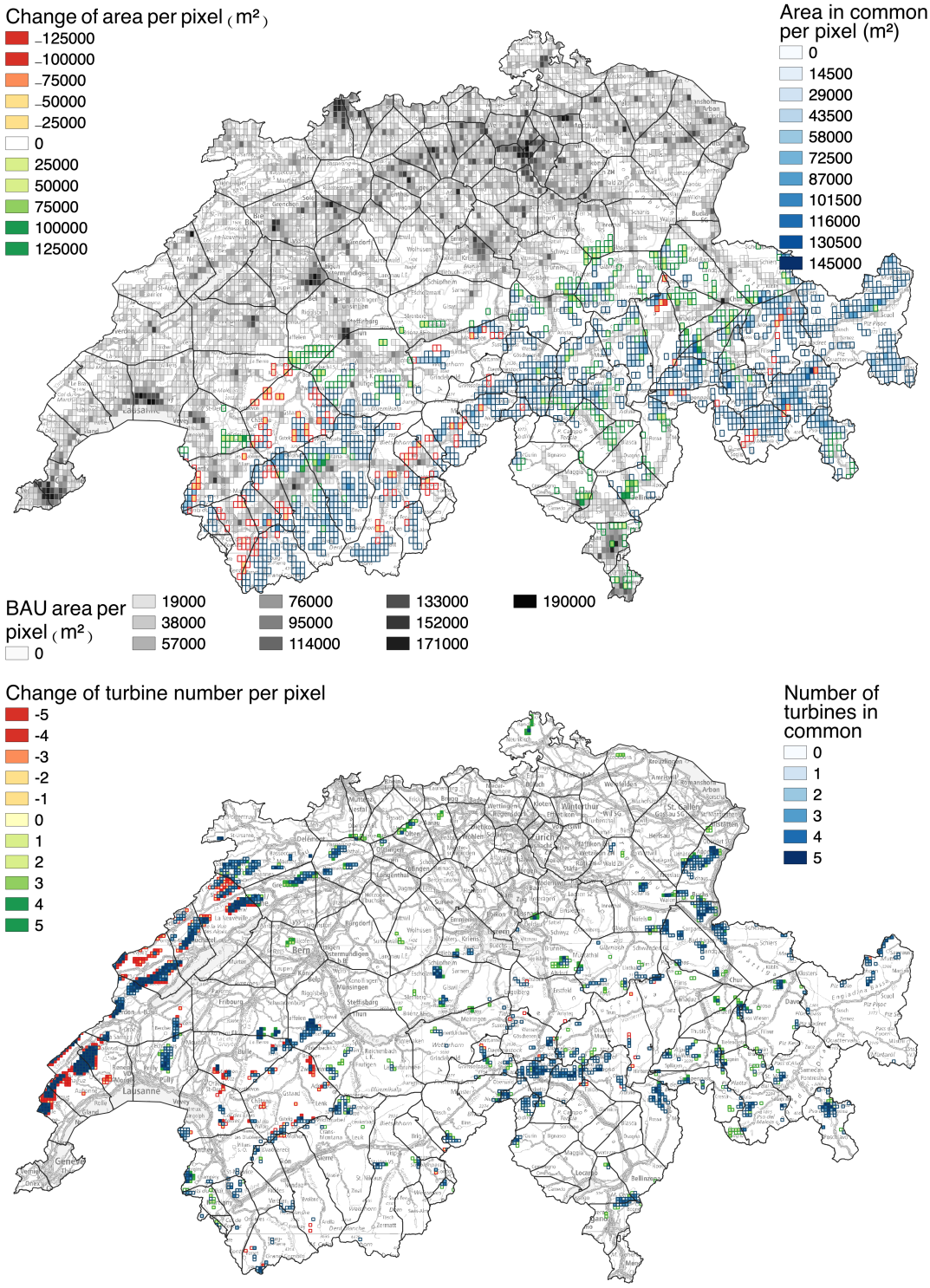

Figure 3.7: Installed PV panel area (upper panel) and installed wind turbines (lower panel) in each grid cell as a result of the optimization for the two scenarios: with and without power flow. The blue colors indicate areas with identical installation in the two scenarios. The red colors indicate the reduction in the installation due to grid congestion. The green colors indicate where those installations are relocated. The upper panel also shows in grey the PV installations used in the BAU scenario.

capacity can also be observed in the lower panels of Figure 3.8, in a cluster-wise aggregated way. The upper panels depict the installed capacities in each cluster for our initial scenario (with power flow).

Concerning PV installations, one large cluster located in the northwestern part on the Alps shows the strongest reduction (90 MW) of its installed capacity, which is almost half of what was installed in the no-powerflow scenario. From the 3.9 GW of total PV capacity in this scenario, 1.06 GW have to be removed from which 0.56 GW have been relocated due to grid congestions. The remaining 0.5 GW are replaced by turbine capacity because of the change in generation mix between the scenarios (see below). This relocation mostly happens in: i) The northern part of the Alps which is directly connected to the northern urban centers; ii) around two nodes with strong grid infrastructure in the southwestern Alps; iii) in Ticino in the South, which is well connected to Italy.

For wind turbine installations, the Jura mountain range in the West holds almost 40% of the total installed capacity because of its strong winter winds and numerous potential installation sites. However, due to the congestion of the lines, large relocations were needed, which populated the pre-Alps and the Alps. In total, 3.15 GW of the initial 13.9 GW of turbine capacity in the no-powerflow scenario where displaced.

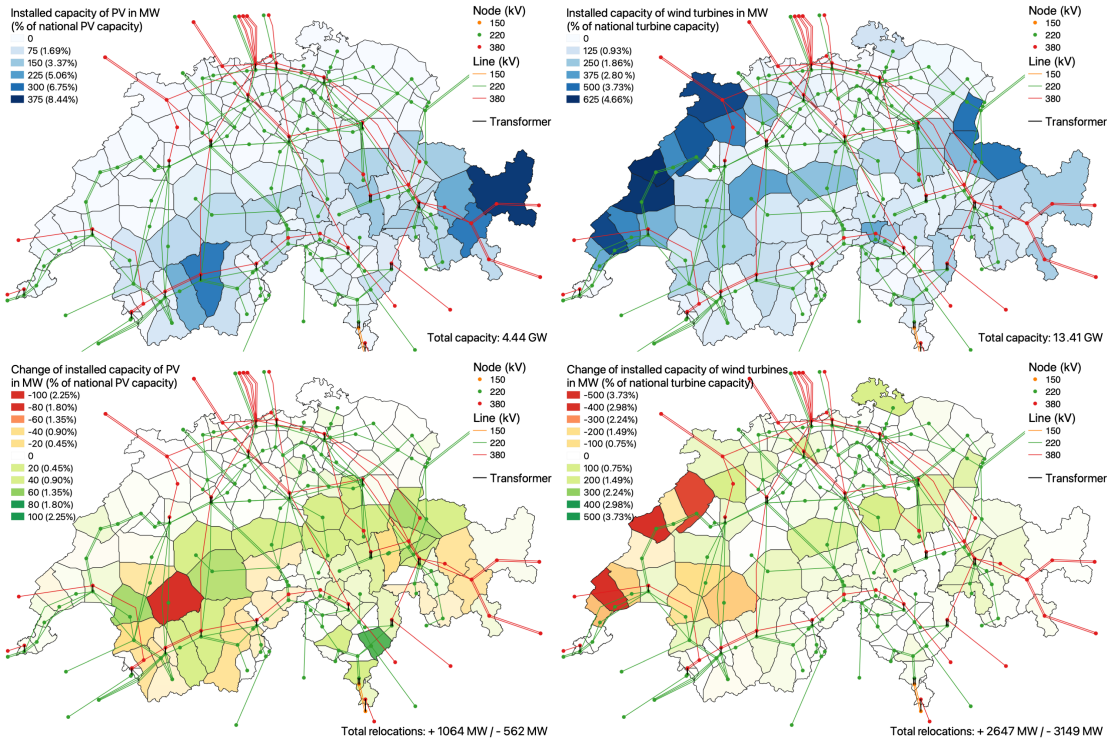

Figure 3.8: The upper panels show the installed capacity in MW of PV panels (left) and wind turbines (right) in each geographical cluster for the optimal scenario with power flow. The share of the total installed capacities are given in brackets. The lower panels show the change in installed capacities from the scenario without power flow to the scenario using it. Regions in red lost capacities while regions in green gained some. The relative changes are given in brackets.

Remarkably, the performance of the two scenarios is quite similar, with required import values of 3.47 TWh with power flow and 3.14 TWh without it. Even if the grid forces the relocation of certain installations, they are placed in locations that are almost as good. The optimal generation mix is also not strongly affected by the grid, with shares of PV equal to 24.9% and 22.1% respectively. Figure 1 in SI depicts how the winter electricity generation from PV and wind varies from place to place and how it correlates with the electricity consumption. Our optimization takes advantage of this spatial variability while respecting the grid constraints.

3.4 Conclusion and discussion

Our methodology matches weather-driven electricity generation with electricity consumption given the available storage and grid infrastructure. It devises placement scenarios for renewable installations, determines how hydropower should be used and displays the associated system dynamics. For our test case, we showed that Switzerland has a wind energy resource that should be exploited in coordination with the existing hydropower system. PV installations should also play a significant role, especially if located in alpine terrain which offers high winter insolation. If the optimal configuration of electricity generation is employed, winter production from PV panels can be increased threefold and dependence on import or supplementary electricity storage can be reduced by 80%, while reducing by 18% the capacity needed to reach the desired total generation. Such methodology can be applied to different geographical regions, with different scales and boundary conditions, in order to discover the optimal interplay between the various renewable electricity generators.

Given the complexity of the socio-politico-economic conditions determining where renewable installations will be built, our conservative assumptions aimed at reaching a midway between extreme restriction and improbable freedom while ensuring opportunities for harvesting energy in favorable places. This work did not aim to provide a turnkey solution to the future Swiss electricity supply but aimed to reveal the weather-driven optimality in electricity generation that can be used to secure the supply of electricity. Being free from economic considerations, our model can show how combining the various sources smartly can positively impact the system as a whole. It reveals the highest level of complementarity between those sources that can be achieved given the spatio-temporal heterogeneity of the weather. In this work, we did not consider curtailment of renewable electricity generation nor demand side response. Those features would certainly alter the optimal solution. However, as for the relatively small change observed between our two scenarios involving the grid or not, it is expected that curtailment or demand-side response, if they have a relatively small magnitude, would not influence strongly the observed dynamics.

We hope this work will inspire scientists, energy planners and policy makers to orient their investigations and decisions toward more encompassing approaches based on the environmental conditions and on the behavior of the system as a whole. Optimization models as the one presented in this article have the ability to associate the various renewable energies

together in a synergistic manner while considering physical, social and economic constraints. The current work should also motivate the modeling of similarly detailed but larger systems like the European, North American, Chinese or Indian electrical grids where neighboring states or countries will have to rely on each other to guarantee their interoperability. Smartly complementing and coordinating renewable energies over large regions can smooth intermittencies by reducing correlations among generators and among consumers (11; 2). Seasonal deficits can be alleviated through the wider range of weather patterns that drive the generation in distant places.

Data availability statement

The data that support the findings of this study are available upon reasonable request from the authors.

Acknowledgment

We thank Massimiliano Zappa (WSL) for the hydrological inputs of our models generated from the model PREVAH. This work was funded by Innosuisse through the Swiss Competence Center for Energy Research, Supply of Electricity.

Bibliography

[1] Jan Abrell, Patrick Eser, Jared B. Garrison, Jonas Savelsberg, and Hannes Weigt. Integrating economic and engineering models for future electricity market evaluation: A Swiss case study. *Energy Strategy Reviews*, 25(June 2019):86–106, 2019.

[2] Cristina L. Archer and Mark Z. Jacobson. Supplying baseload power and reducing transmission requirements by interconnecting wind farms. *Journal of Applied Meteorology and Climatology*, 46(11):1701–1717, 2007.

[3] Stuart Bartlett, Jérôme Dujardin, Annelen Kahl, Bert Kruyt, Pedro Manso, and Michael Lehning. Charting the course : A possible route to a fully renewable Swiss power system. *Energy*, 2018.

[4] Sarah Becker, Bethany A. Frew, Gorm B. Andresen, Timo Zeyer, Stefan Schramm, Martin Greiner, and Mark Z. Jacobson. Features of a fully renewable US electricity system: Optimized mixes of wind and solar PV and transmission grid extensions. *Energy*, 72:443–458, aug 2014.

[5] Christopher T.M. Clack, Staffan A. Qvist, Jay Apt, Morgan Bazilian, Adam R. Brandt, Ken Caldeira, Steven J. Davis, Victor Diakov, Mark A. Handschy, Paul D.H. Hines, Paulina Jaramillo, Daniel M. Kammen, Jane C.S. Long, M. Granger Morgan, Adam Reed, Varun Sivaram, James Sweeney, George R. Tynan, David G. Victor, John P. Weyant, and Jay F. Whitacre. Evaluation of a proposal for reliable low-cost grid power with 100% wind, water, and solar. *Proceedings of the National Academy of Sciences of the United States of America*, 114(26):6722–6727, 2017.

[6] Copernicus European Earth Monitoring. Corine Land Cover inventory. *https://land.copernicus.eu/pan-european/corine-land-cover/clc2018*, 2018.

[7] J. Decaix, V. Hasmatuchi, M. Titzschkau, L. Rapillard, and C. Münch-Alligné. Hydrostructural stability investigation of a 100 MW Francis turbine based on experimental tests and numerical simulations. *IOP Conference Series: Earth and Environmental Science*, 405(1), 2019.

[8] Jérôme Dujardin, Annelen Kahl, Bert Kruyt, Stuart Bartlett, and Michael Lehning. Interplay between photovoltaic, wind energy and storage hydropower in a fully renewable Switzerland. *Energy*, 135:513–525, sep 2017.

[9] Enercon. Specification sheet. *https://www.enercon.de/fileadmin/Redakteur/Medien-Portal/broschueren/pdf/en/ENERCON_Produkt_en_06_2015.pdf*, page 18, 2015.

[10] Dolf Gielen, Francisco Boshell, Deger Saygin, Morgan D. Bazilian, Nicholas Wagner, and Ricardo Gorini. The role of renewable energy in the global energy transformation. *Energy Strategy Reviews*, 24(January):38–50, 2019.

[11] Christian M. Grams, Remo Beerli, Stefan Pfenninger, Iain Staffell, and Heini Wernli. Balancing Europe's wind-power output through spatial deployment informed by weather regimes. *Nature Climate Change*, 7(8):557–562, jul 2017.

[12] Dominik Heide, Martin Greiner, Lüder von Bremen, and Clemens Hoffmann. Reduced storage and balancing needs in a fully renewable European power system with excess wind and solar power generation. *Renewable Energy*, 36(9):2515–2523, 2011.

[13] Dominik Heide, Lueder von Bremen, Martin Greiner, Clemens Hoffmann, Markus Speckmann, and Stefan Bofinger. Seasonal optimal mix of wind and solar power in a future, highly renewable Europe. *Renewable Energy*, 35(11):2483–2489, nov 2010.

[14] Von Hirschhausen. European electricity generation post-2020: Renewable energy not to be underestimated. *DIW Economic Bulletin*, 3(9):16–25, 2013.

[15] Mark Z. Jacobson, Mark A. Delucchi, Mary A. Cameron, and Bethany A. Frew. Low-cost solution to the grid reliability problem with 100% penetration of intermittent wind, water, and solar for all purposes. *Proceedings of the National Academy of Sciences of the United States of America*, 112(49):15060–15065, 2015.

[16] Annelen Kahl, Jérôme Dujardin, and Michael Lehning. The bright side of PV production in snow-covered mountains. *Proceedings of the National Academy of Sciences of the United States of America*, 116(4):1162–1167, 2019.

[17] Partha Kayal and C. K. Chanda. Optimal mix of solar and wind distributed generations considering performance improvement of electrical distribution network. *Renewable Energy*, 75:173–186, 2015.

[18] Bert Kruyt, Jérôme Dujardin, and Michael Lehning. Improvement of wind power assessment in complex terrain : The case of COSMO-1 in the Swiss Alps. *Frontiers in Energy Research*, 2018.

[19] Florian U. Leuthold, Hannes Weigt, and Christian von Hirschhausen. A Large-Scale Spatial Optimization Model of the European Electricity Market. *Networks and Spatial Economics*, 12(1):75–107, 2012.

[20] P Meier, P Manso, M Bieri, A J Schleiss, S Schweizer, A U Fankhauser, and B Schwegler. Hydro-peaking mitigation measures: Performance of a complex compensation basin considering future system extensions. *Hydro*, (December), 2016.

[21] Federal Office of Meteorology and Climatology MeteoSwiss. COSMO forescasting system. *https://www.meteoswiss.admin.ch/home/measurement-and-forecasting-systems/warning-and-forecasting-systems/cosmo-forecasting-system.html*.

[22] Morten Grud Rasmussen, Gorm Bruun Andresen, and Martin Greiner. Storage and balancing synergies in a fully or highly renewable pan-European power system. *Energy Policy*, 51:642–651, 2012.

[23] Hans Kristian Ringkjøb, Peter M. Haugan, and Ida Marie Solbrekke. A review of modelling tools for energy and electricity systems with large shares of variable renewables. *Renewable and Sustainable Energy Reviews*, 96(April 2017):440–459, 2018.

[24] Ingmar Schlecht and Hannes Weigt. Swissmod - A Model of the Swiss Electricity Market. *SSRN Electronic Journal*, (June), 2018.

[25] Reto Stoeckli. The HelioMont surface solar radiation processing 2017 update. *Scientific Report MeteoSwiss*, (93):122 pp, 2013.

[26] Swissgrid. Strategic grid 2025. *https://www.swissgrid.ch/en/home/projects/strategic-grid.html*, 2017.

[27] Federal Office of Topography Swisstopo. swissAlti3D. *https://www.swisstopo.admin.ch/en/geodata/height/alti3d.html*, 2019.

[28] Federal Office of Topography Swisstopo. swissTLM3D. *https://www.swisstopo.admin.ch/en/geodata/landscape/tlm3d.html*, 2019.

[29] Alina Walch, Roberto Castello, Nahid Mohajeri, and Jean Louis Scartezzini. Big data mining for the estimation of hourly rooftop photovoltaic potential and its uncertainty. *Applied Energy*, 262(December 2019):114404, 2020.

[30] Ray D. Zimmerman, Carlos E. Murillo-Sánchez, and Robert J. Thomas. MATPOWER's extensible optimal power flow architecture. *2009 IEEE Power and Energy Society General Meeting, PES '09*, (2):1–7, 2009.

[31] Elmar Zozmann, Leonard Göke, Mario Kendziorski, Citlali Rodriguez del Angel, Christian Von Hirschhausen, and Johanna Winkler. 100% Renewable Energy Scenarios for North America - Spatial Distribution and Network Constraints. *Energies*, 14, 2021.

4 Supplementary Information

Synergistic optimization of renewable energy installations through evolution strategy
Supplementary Information

Jérôme Dujardin, Annelen Kahl and Michael Lehning

This material was provided to the journal *Environmental Research Letters* and is available with the main article at:
https://doi.org/10.1088/1748-9326/abfc75

Results for 2016, 2017 and 2018

The main text presents the detailed boundary conditions for the year 2016: demand, existing production and characteristics of the hydropower system, deficit to cover with new PV and wind installations and total installed capacity that the evolution strategy distributes in Switzerland. In addition to 2016, we optimized the allocation of PV panels and wind turbines for the years 2017 and 2018 under the constraint of keeping a total installed capacity of 17.85 GW. Table 4.1 shows the results of this optimization for the three years and shows how the optimal placement scenario for 2016 performs in 2017 and 2018. We can first see that the deficit in production (demand minus production form hydropower) varies slightly from year to year, as does the total production from the optimized 17.85 GW of PV and wind capacity. The optimal placement scenarios for 2017 and 2018 are almost identical to the one of 2016 and are thus not depicted. The optimal generation mix for each year is between 24% and 28% PV. Compared to the balanced 2016, there is an overall deficit of production equal to 0.38 TWh in 2017 and this leads to 0.57 TWh of supplementary import. In 2018, the situation is reversed, with an overall overproduction of 1.62 TWh leading to an optimized import value 1.54 TWh lower than for 2016. For all years, the optimization reduces the required import by more than 3 TWh as compared to the initial solutions. Finally, we can observe that the optimal solution for 2016 performs almost as well in 2017 and 2018 than their own optimal solutions, with only 0.16 and 0.3 TWh of supplementary import. We can conclude that the generation mix and placement of PV panels and wind turbines defined by our optimization are robust to inter-annual variations in wind speed, solar radiation, water availability in the hydropower system, and demand profile. We can also see that oversizing the generation, as in 2018, leads to even lower import values.

Year	Deficit (TWh)	PV+wind production (TWh)	Initial import (TWh)	Optimal generation mix (%)	Optimized import (TWh)	Import with 2016 placement (TWh)
2016	28.92	28.95	7.09	24.9	3.47	3.47
2017	30.40	30.02	7.11	28.0	4.04	4.20
2018	27.31	28.93	5.79	24.3	1.93	2.23

Table 4.1: Comparison of the main quantities of interest for 2016, 2017 and 2018

Spatial variability in electricity generation from PV panels and wind turbines

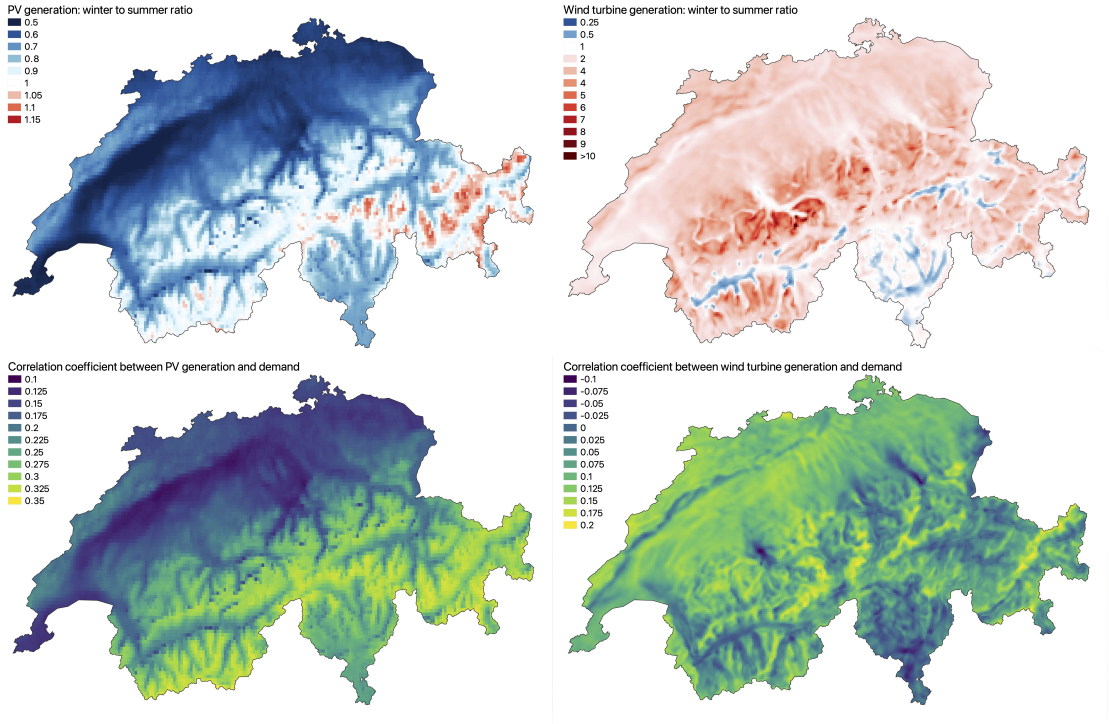

Figure 4.1: The upper panels show the ratio between the electricity generation during the winter months and during the summer months from PV panels (left) and wind turbines (right). Red areas depict regions where the winter production is higher than the summer one. The lower panels show the Pearson correlation coefficient between local electricity generation and national electricity consumption. All data are for the year 2016.

Separation of the optimization problem into 2 sub-problems

Our optimization aims at finding how much PV panel area and how many wind turbines should be built in each pixel of the respective environmental datasets (9148 MSG pixels for PV and 22269 COSMO1 pixels for wind) in order to minimize the amount of required import. The total installed capacity should equal 17.85 GW and the electric grid should be able to

carry electricity from where it is produced to where it is consumed. We can approximate the number of solutions to such a problem by discretizing the 17.85 GW into 10 MW generators and allowing only one of them in each pixel. This problem of allocation, which is a strong simplification of our real problem, leads to the binomial coefficient $\binom{9148+22269}{1785}$ solutions: an incalculable number. Furthermore, each candidate solution needs to be tested through the spatially aggregated model and the distributed power flow model which require about 5 minutes of computation. It is clear that we need to reduce the solution space significantly if we want to reach a global optimum. To do so, we divide our problem in two sub-problems.

Grid nodes

The first sub-problem consists in optimizing the amount of installed capacity connected to each grid node instead of the amount in each pixel. As we have 169 electric nodes and 2 types of generators, the number of possibilities is reduced to $\binom{2\times169}{179}$ if we consider discrete generators of 100 MW. Despite this coarse discretization, there is still a 100-digits-number of solutions. Nevertheless, our evolution strategy explores this vast space of solutions very quickly and does so in a continuous way.

Cluster-wise ranking

The second sub-problem is fairly simple and consists in filling first the best locations within each cluster surrounding the electric nodes in order to reach the installed capacity prescribed by the evolution strategy method. This sub-problem is deterministic and can be solved once and for all by ranking the pixels in each cluster given an objective function that mimics the import reduction that we aim for. As shown in (2), the increase of winter production is an excellent proxy for the decrease of import. Thus, we chose to rank the pixels given their winter production potential (decreasing order).

Generation of fictitious solutions to determine the origin of import reduction

To determine the origin of the reduction of required import at each optimization step, we create 3 fictitious solutions to our problem. Those solutions are time series of power production from PV and wind installations connected to each grid node. In the following, we describe how we generate those time series. We first compute the generation mix, total annual production from PV and wind, and corresponding time series for the average solution of the first 12 individuals of the first optimization step. Then, at each time step, we compute the same elements for the current best candidate solution in the pool.

Generation mix

To identify the effect of generation mix alone, at each optimization step we use the initial solution and change its generation mix to equal the one of the current best candidate solution. Thus, the yield (total annual production) and timeliness (normalized time series) are identical to the ones of the initial solution. For this fictitious solution, power generation from PV and wind can thus be respectively calculated by the following equations:

$$\begin{cases} P_{fict}^{pv} = P_{init}^{pv} \times \dfrac{\alpha_{cur}}{\alpha_{init}} \\ P_{fict}^{wind} = P_{init}^{wind} \times \dfrac{1-\alpha_{cur}}{1-\alpha_{init}} \end{cases} \tag{4.1}$$

where P stands for power production (time series), subscripts *fict*, *init*, *current* indicate the fictitious, initial and current solutions respectively, and α is the generation mix defined as the annual production from PV divided by the annual production from PV and wind.

Yield

The effect coming from the yield alone is identified by using the initial solution and scaling it to obtain a total production that is equal to the current one. The associated power generation time series are computed as:

$$\begin{cases} P_{fict}^{pv} = P_{init}^{pv} \times \dfrac{P_{cur}^{tot}}{P_{init}^{tot}} \\ P_{fict}^{wind} = P_{init}^{wind} \times \dfrac{P_{cur}^{tot}}{P_{init}^{tot}} \end{cases} \tag{4.2}$$

where P^{tot} is the total annual production from the considered scenario.

Timeliness

The effect of timeliness alone can be measured by using the power time series of the current solution and changing its generation mix to equal the one of the initial solution, and then scaling its magnitude to reach the same total annual production as the initial solution. These

two steps are performed as follows:

$$\begin{cases} P^{pv}_{temp} = P^{pv}_{cur} \times \dfrac{\alpha_{init}}{\alpha_{cur}} \\ P^{wind}_{temp} = P^{wind}_{cur} \times \dfrac{1-\alpha_{init}}{1-\alpha_{cur}} \\ P^{pv}_{fict} = P^{pv}_{temp} \times \dfrac{P^{tot}_{init}}{P^{pv}_{temp} + P^{wind}_{temp}} \\ P^{wind}_{fict} = P^{wind}_{temp} \times \dfrac{P^{tot}_{init}}{P^{pv}_{temp} + P^{wind}_{temp}} \end{cases} \tag{4.3}$$

where subscript *temp* indicates the result from the first step that adapts the generation mix of the current solution.

Business As Usual scenario

As baseline we defined a Business As Usual scenario (BAU) that reflects the current strategy for the energy transition in Switzerland. As the country wishes to keep its dependence on foreign electricity as low as possible after the nuclear phaseout and as most of the potential for hydropower has already been exploited, the gap will have to be filled, for the most part, by PV and wind energy. Given the current political and social barriers wind energy is facing in Switzerland, it is expected that only 4 TWh per year could come from this source and the rest would come from solar energy. Similar barriers prevent the development of PV farms, leading to a strategy based on rooftop PV panels.

PV

In our BAU scenario of PV installations we use the Corine Land Cover inventory (CLC) (1) to extract the areas classified as urban fabric and industrial or commercial territories at a 50-meter resolution. These areas include any constructed zones ranging from the biggest cities to the smallest villages and cover 2555 km^2. To match the 150 km^2 of suitable roof area (4) available in the country, we consider that each urban pixel can hold 5% of 50x50 meters, thus 125 m^2. We aggregate the map of PV potential at 50 m-resolution to the coarser MSG grid (1.6x2.3 km) of our PV potential production dataset. The time series of potential power production in each MSG pixel are computed by the model SUNWELL using a conventional rooftop installation geometry (23° of tilt, south-facing). Finally, we distribute the total PV panel area required to produce 25 TWh in 2016 proportionally to the potential area in each MSG pixel.

Wind

For the installation of wind turbines, a BAU scenario is more difficult to define. We want to generate 4 TWh in 2016 and have a potential location map defined by our GIS analysis. Given the current installation strategy consisting in exploiting the most productive locations first, we distribute the turbines required to reach the annual target on all sites which have a capacity factor higher than 20%. As the total production from wind turbines in the BAU scenario represents only 6.4% of the Swiss electricity production, even strong variations from this placement strategy did not show significant changes in the amount of required import.

Power generation from COSMO-1 wind fields

Switzerland displays a wide range of elevations, with valleys as low as 195 meters above sea level (m.a.s.l) and summits as high as 4634 m.a.s.l. In our study, we consider elevations up to 2700 m.a.s.l. where the air density is only about 77% of the standard sea level value ($\rho_0 = 1.225\ kg.m^{-3}$). The power output of a wind turbine can be computed with the following formula:

$$P = \frac{1}{2} \cdot \rho \cdot U^3 \cdot A \cdot C_p(U), \tag{4.4}$$

where ρ is the air density in $kg.m^{-3}$, U is the average velocity of the flow entering the swept area in $m.s^{-1}$, A is the swept area in m^2, and C_p is the coefficient of performance of the wind turbine (efficiency of power extraction for a given velocity U).

Standard coefficient of performance C_p

The wind turbine manufacturer provides the values of C_p for the range of velocities for which the turbine is operational and for an installation at sea level ($\rho = \rho_0$). Below the cut-in velocity and above the cut-out velocity, the turbine does not produce anything, hence $C_p = 0$. In between those two values, C_p ranges from 0 to a maximum value that is always smaller than the theoretical upper limit: the Betz limit (16/27). The shape of the $C_p(U)$ curve depends on the design of the wind turbine and is meant to maximize the overall power production in the environment that the turbine experiences.

Air density

To compute the power production at high altitude, it is clear that we need to use Equation 4.4 with the local air density values. If we directly apply $C_p(U)$ as provided by the turbine manufacturer, the computed values would never allow to reach the nominal power of the turbine. For example, at 2700 m.a.s.l, with $\rho = 0.77\rho_0$, the selected 3 MW Enercon E82 E4 would at most reach $0.77 \times 3 = 2.31$ MW. The control of the wind turbine is in fact adapted to the local air density, which allows to reach the nominal power output. For low air densities, this will be reached at higher wind speeds than at sea level.

Adapted C_p

For a given velocity U and air density ρ, it is possible to incorporate the aforementioned change in control strategy by using the value $C_p(U \cdot (\frac{\rho}{\rho_0})^{\frac{1}{3}})$ instead of $C_p(U)$. This is equivalent to the standard procedure described in (3), which consists in using the power curve with a normalized wind speed $V_N = V \cdot (\frac{\rho}{\rho_0})^{\frac{1}{3}}$ instead of V. The COSMO1 dataset provides us with hourly velocity, temperature and pressure at 90 meters above ground level (m.a.g.l). We compute the air density at any location and any time with the ideal gas law:

$$\rho = \frac{M \cdot p}{R \cdot T} \tag{4.5}$$

where M is the molar mass of dry air equal to 0.02896 $kg.mol^{-1}$, p is the pressure in Pa, R is the ideal gas constant equal to 8.31447 $m^3.Pa.K^{-1}.mol^{-1}$ and T is the temperature in K. Power production is thus calculated as:

$$P = \frac{1}{2} \cdot \rho \cdot U^3 \cdot \frac{\pi D^2}{4} \cdot C_p(U \cdot (\frac{\rho}{\rho_0})^{\frac{1}{3}}), \tag{4.6}$$

where D is the diameter of the swept area and $C_p(v)$ is the coefficient of performance at sea level for the velocity v.

Boundaries of the solution space and generation of new candidate solutions

Solution space

Our solution space is a subspace of $[0,1]^{338}$. It is however possible to reduce it considerably by taking into account the limitation imposed by the grid infrastructure and the total potential for installed capacity in each cluster surrounding the grid nodes. If we consider a solution $\mathbf{x} = (x_1, x_2, ..., x_{338})$, the first 169 components represent the fraction of the total installed capacity that is connected to each grid node in the form of PV installation. The remaining 169 are the equivalent for wind installations. Thus, $\sum_{i=1}^{338} x_i = 1$. For the i^{th} grid node ($i \in [1,169]$), we can define the upper boundaries for x_i and x_{i+169} by computing how much installed capacity can be located in the i^{th} cluster given the maps of potential installations generated by our GIS analysis. This simple analysis gives us the values m_i^{pot} which already limit our solution space: $x_i \in [0, m_i^{pot}], \forall i \in [0,338]$. Furthermore, for each grid node we can compute the total power transmission capacity of all the lines that are connected to it. We then aggregate all the non-dispatchable power consumption (demand) and production (run-of-river), and the pumping capacity, connected to this node and subtract it from the computed total line capacity. This gives us the residual line capacity at any time which is available to transport any supplementary power generation (from PV and wind) outside the cluster. This does not consider the bottleneck effects occurring when several adjacent nodes will have to get rid of some power in the same direction in the grid. However, any local power production that is

higher than this computed limit will certainly exceed the grid capacity.

Given this upper limit on maximum power production from PV or wind within each cluster we can compute the maximum installed capacity for those 2 sources that can be connected to the grid node: m_i^{grid}. Finally, our solution space is defined as:

$$(x_1, x_2, ..., x_{338}), x_i \in [0, m_i], \forall i \in [0,338], \; with \begin{cases} \sum_{i=1}^{338} x_i = 1 \\ m_i = min(m_i^{pot}, m_i^{grid}) \\ m_i^{pot} \in [0,1] \\ m_i^{grid} \in [0,1] \end{cases} \tag{4.7}$$

In our optimization for 2016, this procedure gives us:

$$\max_{i \in [1,169]} min(m_i^{pot}, m_i^{grid}) = 0.1243 \tag{4.8}$$

$$\max_{i \in [170,338]} min(m_i^{pot}, m_i^{grid}) = 0.1762 \tag{4.9}$$

$$\sum_{i=1}^{169} min(m_i^{pot}, m_i^{grid}) = 3.2816 \tag{4.10}$$

$$\sum_{i=170}^{338} min(m_i^{pot}, m_i^{grid}) = 2.7233 \tag{4.11}$$

$$\tag{4.12}$$

The cluster with the biggest potential for PV installation can hold 12.43% of the 17.85 GW of total installed capacity and the cluster with the biggest potential for wind installation can accommodate 17.62%. The total installation potentials amount to 328.16% for PV and 272.33% for wind. We can thus observe that the initial solution space of $[0,1]^{338}$ has been considerably reduced.

Generation of the first 12 candidate solutions

It is essential to start the optimization with a pool of candidate solutions that is diverse and balanced between PV and wind capacities and that is viable with respect to grid constraints. Random individuals are generated iteratively and tested with the optimal power flow model until such a population is created. We create each initial candidate solution by generating two individuals, one with only PV installations and the other with only wind installations. Then, a random generation mix is chosen between 0.4 and 0.6 and the corresponding linear combination of the pair of solutions forms our individual. The 2 solutions in the pair are generated from a random variation in the range ± 25% around a homogeneously distributed

solution (constant fraction of m_i). Thus, the solution with only PV installation is:

$$\begin{aligned}&(x_1, x_2, ..., x_{169}, 0, ..., 0),\\ &\textit{where } x_i = \frac{m_i}{3.2816} \cdot \epsilon_i \textit{ and } \epsilon_i \textit{ are uniformely distributed numbers in } [0.75, 1.25].\end{aligned} \tag{4.13}$$

And the solution with only wind installation is:

$$\begin{aligned}&(0, 0, ..., y_{170}, ..., y_{338}),\\ &\textit{where } y_i = \frac{m_i}{2.7233} \cdot \epsilon_i \textit{ and } \epsilon_i \textit{ are uniformely distributed numbers in } [0.75, 1.25].\end{aligned} \tag{4.14}$$

Our initial solution formed from this pair is:

$$(z_1, z_2, ..., z_{338}), \textit{where } z_i = \alpha \cdot \frac{x_i}{\sum_{i=1}^{338} x_i} + (1-\alpha) \cdot \frac{y_i}{\sum_{i=1}^{338} y_i}, \textit{ with } \alpha \in U[0.25, 0.75]. \tag{4.15}$$

Breeding

Creating a new candidate solution **z** from 2 parents **x** and **y** is performed by a linear combination of **x** and **y** with a random weight β. Thus, the new solution is given by:

$$\mathbf{z} = \beta \cdot \mathbf{x} + (1-\beta) \cdot \mathbf{y} \textit{ , which garantees that: } \sum_{i=1}^{338} z_i = 1. \tag{4.16}$$

β must be generated in a way ensuring that $z_i \in [0, m_i]$, $\forall i \in [1, 338]$:

$$\beta = \beta_{min} + (\beta_{max} - \beta_{min}) \cdot \epsilon, \textit{ with } \epsilon \in U[0,1] \tag{4.17}$$

$$\beta_{min} = \max\left(\max_{i \in [0,338]} \left(\frac{0 - y_i^+}{x_i^+ - y_i^+} \right), \min_{i \in [0,338]} \left(\frac{m_i^- - y_i^-}{x_i^- - y_i^-} \right) \right) \tag{4.18}$$

$$\beta_{max} = \min\left(\min_{i \in [0,338]} \left(\frac{0 - y_i^-}{x_i^- - y_i^-} \right), \max_{i \in [0,338]} \left(\frac{m_i^+ - y_i^+}{x_i^+ - y_i^+} \right) \right), \tag{4.19}$$

$$\textit{where } v_i^+ = max(v_i, 0) \textit{ and } v_i^- = min(v_i, 0) \textit{ , } v \textit{ representing } x, y \textit{ or } m. \tag{4.20}$$

Mutation within a solution

When a new candidate solution **z** is generated by breeding as described above, we successively apply 4 random mutations. A mutation is an exchange of a random value γ between two randomly chosen components (indexes p, q) of the solution. The following procedure ensures that the modified vector components remain within the acceptable boundaries:

$$z_p = z_p - \gamma, \textit{ where } p \in U_{\mathbb{N}}[1, 338] \tag{4.21}$$

$$z_q = z_q + \gamma, \textit{ where } q \in U_{\mathbb{N}}[1, 338] \textit{ and } q \neq p \tag{4.22}$$

$$\gamma = \eta \cdot \min(z_p - 0, m_p - z_p), \textit{ where } \eta \in U[0,1] \tag{4.23}$$

Architecture of the optimization scheme

Power and energy models

At each optimization step, the 6 new candidate solutions in the pool must be tested by the optimal power flow (OPF) model which consists in a primal-dual interior point solver that minimizes the effective cost of generation while assuring power transmission within the grid capabilities. This solver is part of the library MATPOWER (5) and runs in a MATLAB environment. On a Intel(R) Xeon(R) CPU E5-2630 v3 2.40GHz, the OPF (in DC mode) requires about 5 minutes of computation for a year of hourly data and our Swiss grid composed of 169 nodes, 37 foreign nodes, 309 lines and 106 dispatchable generators or loads.

Optimized architecture

The OPF represents about 90% of the computation required in one optimization step. It is thus necessary to invoke this OPF only for candidate solutions that are potentially better than the parent generation. Consequently, at the beginning of each optimization step, the much faster nationally aggregated power and energy balance model is used to eliminate the newly generated candidate solutions that lead to higher required import values than the parent generation. Only when 6 promising candidate solutions could be generated we invoke the OPF to test them. This is done in parallel, one core computing the OPF for one candidate solution.

Computational requirements

Our evolution strategy has a few parameters that affect the speed of convergence toward the global optimum. The population size, survival rate and mutation rate have been manually tuned to accelerate the convergence. About 1000 optimization steps are then required to reach a solution that is close enough to the global optimum. With the aforementioned CPU, the optimization requires about 1000 x 5 minutes / 0.9: 4 days.

Bibliography

[1] Copernicus European Earth Monitoring. Corine Land Cover inventory. *https://land.copernicus.eu/pan-european/corine-land-cover/clc2018*, 2018.

[2] Jérôme Dujardin, Annelen Kahl, Bert Kruyt, Stuart Bartlett, and Michael Lehning. Interplay between photovoltaic, wind energy and storage hydropower in a fully renewable Switzerland. *Energy*, 135:513–525, sep 2017.

[3] IEC. Iec 61400-12-1. *International Electrotechnical Commission*, 2005:179, 2005.

[4] Alina Walch, Roberto Castello, Nahid Mohajeri, and Jean Louis Scartezzini. Big data mining for the estimation of hourly rooftop photovoltaic potential and its uncertainty. *Applied Energy*, 262(December 2019):114404, 2020.

[5] Ray D. Zimmerman, Carlos E. Murillo-Sánchez, and Robert J. Thomas. MATPOWER's extensible optimal power flow architecture. *2009 IEEE Power and Energy Society General Meeting, PES '09*, (2):1–7, 2009.

Part III

Wind-Topo: Downscaling near-surface wind fields to high-resolution topography in highly complex terrain with deep learning

5 Main text

Wind-Topo: Downscaling near-surface wind fields to high-resolution topography in highly complex terrain with deep learning

Jérôme Dujardin[1,2] and Michael Lehning[1,2]

[1]School of Architecture, Civil and Environmental Engineering, Swiss Federal Institute of Technology in Lausanne (EPFL), Lausanne 1015, Switzerland

[2] Institute for Snow and Avalanche Research (SLF), Swiss Federal Institute for Forest, Snow and Landscape Research (WSL), Davos 7260, Switzerland

Abstract

Predicting wind flow in highly complex terrain like the Alps is a challenge for all models. When physical processes need to be resolved in a spatially explicit manner, grids with high horizontal resolutions of a few hundred meters are often required and drastically limit, in many cases, the extent and duration of the simulations. Many surface process models, like the simulation of heterogeneous snow covers across a season, however, need long time series on large domains as inputs. Statistical downscaling can provide the required data but no model can effectively reach the desired resolutions and provide temporally-resolved wind speed and direction on highly complex topography. The assessment of the potential for wind energy in the Alps, a promising player in the energy transition, is an example where the current shortcomings cause strong limitations. We present "Wind-Topo", a novel approach based on Deep Learning that discovers the interactions between high-resolution topography and coarser-resolution states of the atmosphere to generate near-surface wind fields with a 50-meter resolution. In our test case, we use a large number of measurement stations in Switzerland to train the model and an operational weather prediction model (COSMO-1) as predictor. Wind-Topo employs a custom architecture that analyses the state of the atmosphere at various scales and associates it with high-resolution topography. A dedicated loss function leads to good scoring metrics as well as accurate wind speed distributions at 60 independent stations used for a thorough validation. 50-meter resolution wind fields are efficiently generated and exhibit the expected orographic effects. Furthermore, the bias and mean absolute error from COSMO-1 at the alpine validation stations, being 0.72 m/s and 1.77 m/s respectively, are reduced to -0.07 and 1.21 m/s.

Keywords: downscaling, deep learning, wind, complex terrain, orographic effect

This chapter was submitted to the *Quarterly Journal of the Royal Meteorological Society*

J.D developed the idea and the model, collected the data, analyzed the results, and wrote the paper.

5.1 Introduction

In complex terrain, synoptic wind flows are transformed by their interaction with the topography and by near-surface processes generating local winds. Numerical Weather Prediction (NWP) models are increasingly more capable of reproducing such effects, thanks to the constant improvement of their resolution, dynamical cores and parametrizations. In highly complex terrain like the Alps, fine scale models are required to correctly resolve the terrain and obtain flows that are close to observations. Despite the improvements in NWP models, there still exists a trade-off between the extent of the simulation's domain, its resolution, and the modeled period. In highly complex terrain, given the required resolution, large domains cannot be modeled for long periods. The modeling of many surface processes like snow preferential deposition and transport, however, requires long time series of high-resolution wind fields on large domains (29; 20). This is also true for wind energy potential assessment in such type of terrain where spatial variability is high.

A solution to the limitation in computational resource is to use NWP models at coarser resolution succeeded by a statistical downscaling model. The former describes the state of the atmosphere on a coarse topography and the latter uses empirical relationships between this data and another source of information that describes the true nature of the wind. This ground-truth information can have various origins, but it may represent the best yet partial description of the wind flow in the real terrain. Statistical downscaling is employed in many fields and on many types of data. In complex terrain, wind and precipitation are the prime examples because of their high spatial variability and importance in surface process modeling. A vast repertoire of techniques is also available. Machine Learning is gaining importance in environmental sciences (15) and its extension Deep Learning begins to offer state-of-the-art results (25).

For downscaling wind in complex terrain, two different approaches are employed, depending on whether the ground truth comes from measurements or from high-resolution NWP models. (23) trained an Artificial Neural Network (ANN) to predict the hourly wind speed at a certain station given the measurements from other stations in Greece. (1) also used ANN to estimate hourly wind speed at a French station but from the values predicted by the Weather Research and Forecasting (WRF) model with a 3-kilometer resolution. Similarly, (10) used analyses from the European Center for Medium Range Weather Forecasts (ECMWF, 9 km resolution) as predictor for random forest or gradient boosting models to predict wind speed at 171 French stations. Those studies calibrated (trained) point-to-point models that were only capable of predicting wind speed at specific locations. To obtain spatially distributed predictions, (19) developed a Bayesian-aided selection within a catalog of 0.5-km resolution WRF simulations for northern Israel. The model replicates this high-resolution near-surface wind speed and direction from a coarser 4.5-km WRF dataset. For California, (16) trained a linear model calibrated with WRF at 3 km to downscale the North American Regional Reanalysis (NARR, 32 km, 3-hourly). Deep Learning super-resolution Convolutional Neural Network (CNN) was employed by (14) to recreate ECMWF High-RESolution (HRES, 9 km) from ECMWF ERA5

(30 km) for southern France. Those 2D-to-2D methods are constrained to the domain on which they are calibrated because they do not incorporate descriptors of the topography. Furthermore, their targeted resolutions are not sufficient for highly complex topographies like the Alps. Other types of models like WindNinja (30; 13; 26) and TopoSCALE (6) are based on physical descriptions of wind-topography interactions and are not bound to the domain of calibration. WindNinja is used frequently for wild fire propagation but was used recently by (29) to model snowdrift. However, given their generic nature, those methods do not benefit from the valuable information of measurements or high-resolution simulations and might thus not perform well in particular terrain under particular conditions.

An interesting line of research took advantage of the vast network of measurement stations in Switzerland to develop point-to-point methods that can generate spatially distributed predictions in the highly complex Swiss Alps. All of them use descriptors of the topography to predict wind speed at the location of the measurement stations. When calibrated, the models can be used at other locations and generate maps of wind speed. (2) employed General Additive Models (GAM) for daily maximum wind speed using landform categories and (7) employed Gradient Boosted Regression Trees and the topographic exposure for the same purpose. (8), and (27) respectively used Support Vector Regression on mean wind speed and GAM on monthly values, with various terrain descriptors (slope, difference of Gaussians and directional derivative). Those methods only use topographic descriptors as explanatory variables and are thus limited to temporally-static predictions. Using the Consortium for Small-scale Modeling at 2-km and 7-km resolutions (COSMO-2, COSMO-7) (3) and the directional-dependent terrain parameter Sx (31), (32) trained a linear model to generate maps of wind speed at 25-meter resolution. As all stations were used for calibration, the model's validation did not reflect the performance at other locations. The results at the stations were however promising and showed the importance of considering the distribution of wind speed and not only aggregated metrics. From COSMO-2 and a slope parameter, (11) proposed a downscaling method that is calibrated from a large catalog of simulations from the Advanced Regional Prediction System (ARPS) run at a 30-meter resolution. Using stations for validation only, the method slightly outperforms COSMO-2 at exposed sites but is worse at sheltered ones. Those two methods offered the resolution and efficiency required for the generation of the long time series on large domains mentioned previously. However, they do not consider the change in wind direction when going from coarse to fine resolution and were either not validated spatially or ineffective on leesides.

We present a novel 2D-to-point statistical downscaling model: Wind-Topo, first of its kind and based on deep learning, that uses kilometric-resolution NWP model outputs and high-resolution topography to predict near-surface wind speed and direction in highly complex terrain. 261 Swiss measurement stations are used for calibration (training) and 60 different stations are used for validation. In our test case, the 1.1-km resolution COSMO-1 is used as predictor and near-surface wind fields can be downscaled to a 50-meter resolution. The custom architecture that relies on multiple CNNs as well as the custom loss function extract meaningful statistical relationships between the low-resolution atmospheric state surrounding

the point of interest, wind measurement and high-resolution topography. The universal wind-topography interactions discovered by the model are successfully applied at the validation stations and to a high-resolution grid that exhibit most of the expected orographic effects.

5.2 Methods

5.2.1 General approach

As ground truth, we use wind speed and direction from 321 measurement stations spread across Switzerland from the IMIS and SwissMetNet networks (33; 4), at 7 and 10 meters above ground level (m.a.g.l.) respectively (Figure 5.1). From IMIS, 69 "exposed" stations are installed on summits or ridges and 86 "sheltered" stations are in locations that are protected from the main winds (18). The remaining 166 ("other") stations are uncategorized and are installed in diverse terrain. As we want the model to predict wind speed and direction, and given the non-continuity of the direction, we use u and v the horizontal components of the wind vector. We use hourly data from October 1^{st} 2015 to October 1^{st} 2018. For the same times, the COSMO-1 analysis dataset describes the local state of the atmosphere surrounding each station, based on the coarse resolution and smoothed topography (slope < 30°) of the model (background of Figure 5.1). Wind-Topo combines this information with a high-resolution Digital Elevation Model (DEM) to predict the station measurements u and v. In Wind-Topo, "local" means an area of about 21 x 21 km (19 x 19 COSMO-1 pixels) surrounding each station, as depicted in Figure 5.1. The model's training consists in optimizing the model's parameters such that the predictions $\hat{u}$ and $\hat{v}$ are as close as possible to u and v, using only COSMO-1 and topographic inputs. For training, we use the first and last year of the mentioned period and a selection of 261 stations. The remaining 60 stations and/or the middle year are used to test the model, more precisely its temporal and spatial generalization capabilities.

5.2.2 Model inputs

The model's predictors come from either COSMO-1, with the aforementioned spatial extent and resolution, and from the high-resolution DEM. For the later, we combined a 2-meter DEM from Swisstopo (5) inside Switzerland and a 1-arcsec DEM (about 36 meters) (21) outside the country. We resampled them such that each COSMO-1 pixel contains exactly 21 x 21 DEM pixels [1]. As COSMO-1 (on a 0.01x0.0146 lat/lon grid) has a resolution in our whole Swiss domain of 1113 meters in latitude and 1113+/-22 meters in longitude, the high-resolution topographic inputs have a resolution of 53 x 53+/-1 meters. Accordingly, our input topographic patches, covering 21.147 x 21.147+/-0.418 km, have a resolution of 399 x 399 pixels. The exact same extent is covered by 19 x 19 COSMO-1 pixels. The two upper left panels of Figure 5.2 show an example of such input data from COSMO-1 and DEM.

[1] This number of pixels (21 x 21) is coincidentally the same as the size of the COSMO-1 input domains. There is no link between them.

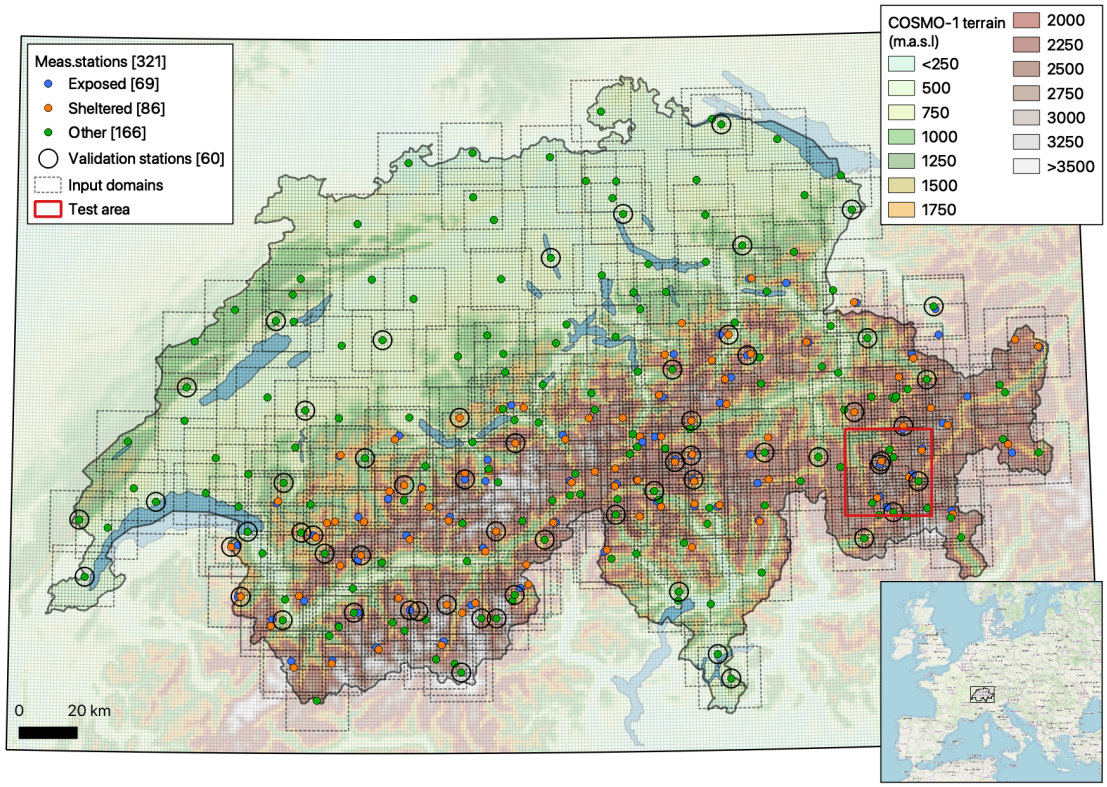

Figure 5.1: Location of the measurement stations used to train or validate Wind-Topo. The background shows the topography used in COSMO-1 and the squares around each station represent the extent of the data used by Wind-Topo to predict the wind at the location of the stations.

From COSMO-1, we select 2D fields of horizontal components of the wind vector u_c and v_c (subscript c standing for cosmo) for 5 vertical layers of the model (terrain following coordinates) which have average heights of 10, 89, 293, 589, 1164 m.a.g.l. We also use the perpendicular deviation of the wind vector from the layer surfaces, denoted w', which indicates on the 5 layers where the flow follows the terrain ($w' = 0$), or separates upwards ($w' > 0$), or converges towards the ground ($w' < 0$). w' also indicates areas of convection or subsidence. The atmospheric stability is considered via the vertical gradient of potential temperature between the 5 layers: $\Delta\theta/\Delta h$. The last inputs are the ground surface sensible heat flux q_s and the elevation of the model's terrain z_{cosmo}. Concerning the high-resolution topographic descriptors, elevation z_{topo} and the associated $slope$ and $aspect$ are employed.

5.2.3 New topographic descriptors

Ideally, deep learning could allow an end-to-end approach where the model learns by itself the operations to apply to the DEM (z_{topo}). However, the rather small variability in topographic inputs (only 321 unique z_{topo} images, one for each local patch) is far from sufficient for obtaining an end-to-end model with good spatial generalization. Such model could only generate smooth wind fields, lacking small-scale features, and only increased u_c and v_c around

ridges and summits. We thus had to use other topographic inputs that show more directly the wind-topography interactions. Two such descriptors that are well-known were initially employed: TPI indicating the relative height of a location with respect to its neighborhood and S_x (31) indicating how exposed or sheltered a place is given a specific wind direction. Both of them share one important parameter: the radius considered for the neighborhood (typically 500 to 4000 m). Trained with them, Wind-Topo obtains scores that are almost as good as the ones presented in section 5.3. However, the predicted wind fields exhibit a strong dependency on the radius parameter and look like copies of the descriptors, even if several descriptors with various radii are provided. To avoid this problem, we created a set of new topographic descriptors, which are free of such parameters, and let Wind-Topo decide how to process them. Given its CNN-based nature, Wind-Topo can decide how to integrate them spatially, thus creating an internally-controlled and dynamic radius parameter.

Figure 5.2 shows the variables z_{cosmo}, z_{topo}, $slope$ and $aspect$ for the input patch centered around the station ELA-1 (section 5.3). From $slope$, $aspect$ and the values of u_c, v_c at the center of the patch we generate 6 topographic descriptors. First, we compute E_+ and E_- respectively representing how much a location is exposed to or sheltered from the wind given its direction as follows:

$$\begin{gathered}\begin{cases} E_+ = max(sin(\alpha), 0) \\ E_- = min(sin(\alpha), 0) \end{cases}, \text{where } \alpha \text{ is defined as:} \\ \alpha = arctan(tan(slope)cos(\delta)), \text{with} \\ \delta = arctan2(-v_c, -u_c) - aspect. \end{gathered} \tag{5.1}$$

The best results were obtained when this direction is computed from the second layer above ground in the COSMO-1 inputs (89 m.a.g.l). Contrary to S_x, E_+ and E_- do not incorporate a search distance and are purely local. Splitting this exposure/sheltering into two allows the model to find specific rules for each of them independently. When summed together (as in Figure 5.2) and integrated over a certain radius, the result resembles S_x. As a CNN cannot directly multiply some of its inputs together, and because our model showed difficulties in learning it, we provide $E_+ u_c$, $E_+ v_c$, $E_- u_c$ and $E_- v_c$ to the model. The two remaining descriptors address the challenge of wind deflection: how to change u_c and v_c to obtain a flow that turns when facing a steep slope. We provide the model with the offsets for u_c and v_c: Δu_{tan} and Δv_{tan} needed to obtain such effect. They are computed as follows:

$$\begin{gathered}\begin{cases} \Delta u_{tan} = (cos(\beta) - 1)u_c - sin(\beta)v_c \\ \Delta v_{tan} = sin(\beta)u_c + (cos(\beta) - 1)v_c \end{cases}, where\ \beta = (\frac{\pi}{2} - |\,\delta\,|)sign(\delta)sin(slope), \\ \text{with the constraint that } \delta \in]-\pi, \pi] \text{ (δ from Equation 5.1).} \end{gathered} \tag{5.2}$$

Equation 5.2 shows that the steeper the slope, the more the flow will have to follow the

topographic contours (be tangential), based on the angle between the aspect and the wind direction. Using information about the state of the atmosphere, Wind-Topo can scale this effect in a dynamic way.

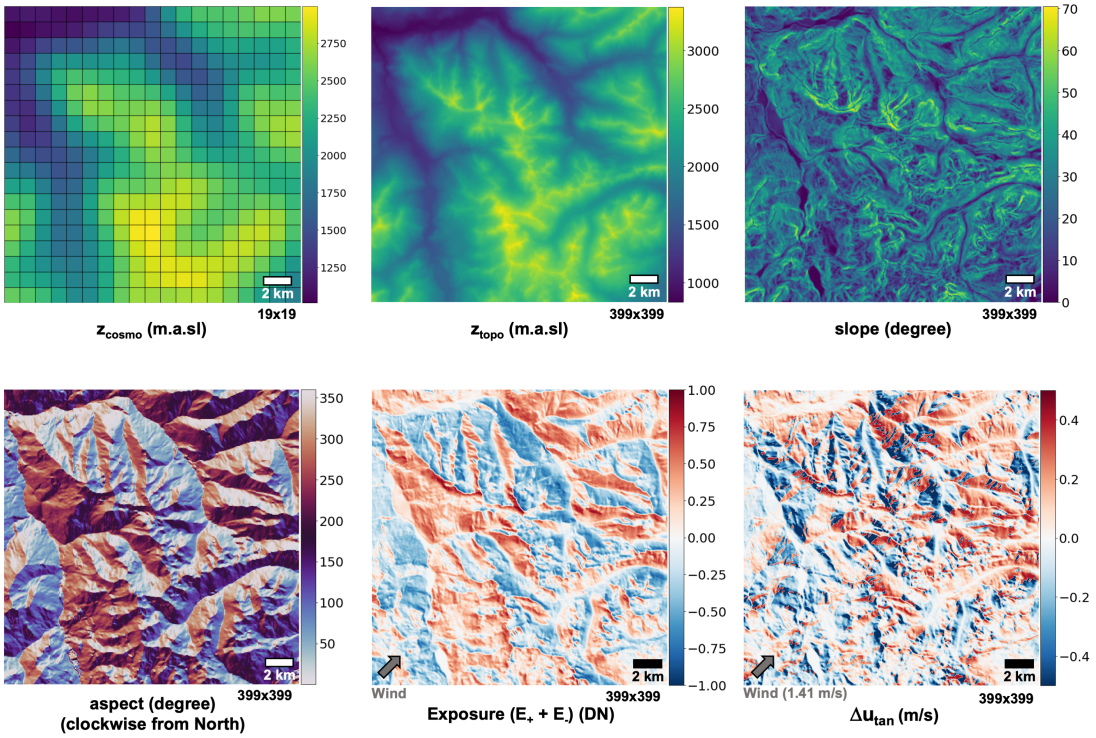

Figure 5.2: Example of topographic inputs for a particular training station (ELA-1). z_{cosmo} is the topography used in COSMO-1 and z_{topo} is a 53-meter resolution Digital Elevation Model with the same extent. $slope$ and $aspect$ are computed from z_{topo}. $(E_+ + E_-)$ reflects places exposed to the wind (red) or sheltered from it (blue). Δu_{tan} shows the offset to apply to u to obtain a flow that is progressively tangential to the terrain as the slope increases, given the wind speed and direction.

5.2.4 Data flow

Given the large amount of training data (261 stations x 17520 timesteps x n variables), treating the 399 x 399 inputs is an enormous task (3 TB of data). As Wind-Topo predicts the wind at the center of the input patch, the more relevant information is located close to the center, while the edges of the patch should provide only coarser information. To significantly decrease the amount of information (by a factor 13) and to help the model focus on high-resolution information towards the center and on progressively coarser information at a distance, we apply two consecutive operations to all topographic inputs (Figure 5.3). First, each input is split into two: The full-extent input is on the one hand resized to a resolution of 77 x 77 pixels, and on the other hand a crop of the central 77 x 77 pixels (a zoom) is extracted. Second, we apply a foveal blur (see bottom right of Figure 5.3) which smooths the information as we move away from the center. For consistency in the model's architecture, which is described below,

the same splitting is applied to the COSMO-1 inputs.

As presented in Figure 5.3, we have low-resolution COSMO-1 data (full and zoom patches), high-resolution topographic data (full and zoom patches), and values for all those descriptors at the exact location of the station. Time-of-the-day and day-of-the-year are also provided as pointwise information via a cosine-sine transformation for continuity. Wind-Topo has two branches: one that predicts u and one that predicts v. Both are independent when making a prediction but they are trained jointly via a common loss function (section 5.2.6) that optimizes their parameters simultaneously. This double architecture gave the best results and allows the model to consider u and v jointly.

A wide spread technique in machine learning is to artificially augment the amount and diversity of the training data. For image processing purposes, e.g. with CNNs, it is common to randomly rotate, flip, crop, offset and rescale the images. In our situation, as we only have 261 different input topographies, this augmentation is crucial. Randomly rotating the 2D data and transforming all values related to u, v, u_c, v_c and $aspect$ in a consistent manner that artificially rotates topography and wind together was very effective. To stay consistent with wind-topography interactions like preferential deflection to the right due to Coriolis, flip, crop and rescale were avoided and proved to be ineffective when tried. Offsets of elevation were investigated but did not help. The data augmentation by rotations was also central in obtaining a model with a good rotational-invariance (similar predictions when the inputs are rotated by an angle and the prediction is then rotated oppositely).

5.2.5 Deep learning architecture

Figure 5.4 shows the constitutive blocks of the model, the data dimensions, and how the various types of data are associated to predict u and v. Each input variable is pretreated by a dedicated CNN (one CNN for u_c, one for v_c, ...) to generate a tensor. Tensors with similar spatial extent (full or zoom) are concatenated and treated by another type of CNN. As seen in Figure 5.4 and Figure 5.5, those latter CNNs and the ones pretreating the high-resolution topographic descriptors generate an additional vector that contains values at the exact center of the patch. This procedure retains important high-resolution information at multiple stages of the CNNs. Classically, the outputs of the CNNs on the concatenated tensors are fed into fully connected neural networks (FCNN) to generate two 128-entry vectors. Finally, all vector data are concatenated and treated by a FCNN having a unique output which is $\hat{u}$ or $\hat{v}$ depending on the model's branch.

Figure 5.5 details the building blocks of the various CNNs and FCNNs. The CNNs have a classical alternation of convolution layers and pooling layers in order to extract increasingly larger and higher-level features from each input data and from the concatenated data. Special attention was given to the size of the inputs and kernels, as well as to the strides, to avoid padding on the edges and lateral shifts of information. As Wind-Topo gives a prediction for the exact patch's center, it is essential that each operation leads to an odd number of rows and

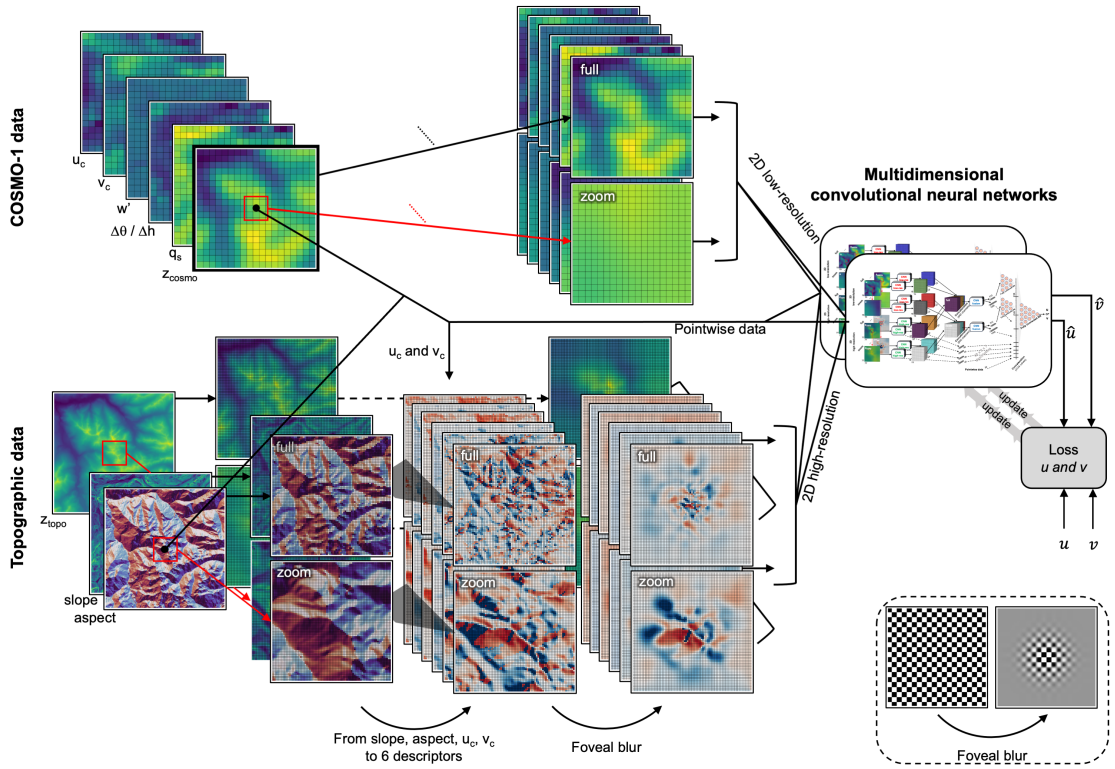

Figure 5.3: Chain of operations to obtain the predicted $\hat{u}$ and $\hat{v}$ at the center of the patch of input data.

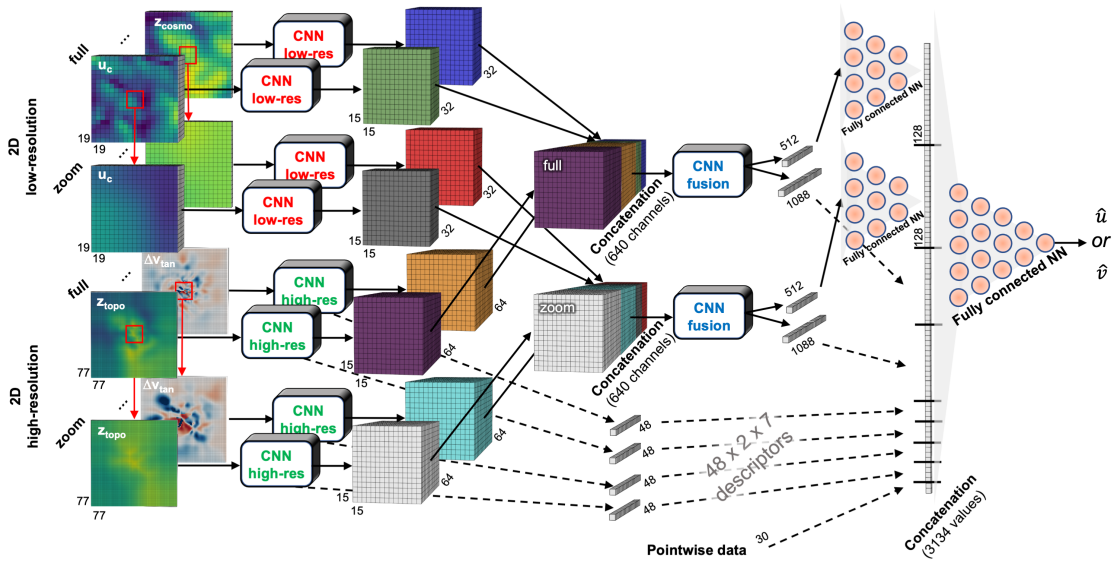

Figure 5.4: Deep learning architecture of Wind-Topo. Each "CNN low-res" and "CNN high-res" is unique to each input variable. The two distinct "CNN fusion" blocks treat the concatenated tensors with full or zoom extent respectively.

columns and that the kernels fall centered on the central pixel. The Sigmoid Linear Unit (SiLU) function ($silu(x) = x\sigma(x)$, where $\sigma(x) = 1/(1+e^{-x})$ is the logistic sigmoid) (12) was the best

activation function, slightly outperforming the standard ReLU function, most likely because of its continuity (important for a regression problem). A particularity of the CNNs treating the high-resolution topographic data is the addition of a directional mask after the first activation. This mask, which sets to zero the area that is downwind from the patch's center, has two advantages: i. It helps the model understand the notion of wind direction and how to deal with windward and leeward information; ii. It augments the number of distinct topographic inputs. As mentioned previously, central values (red) are extracted before each pooling layer and before several convolution layers in order the retain low-level high-resolution information about the center of the patch.

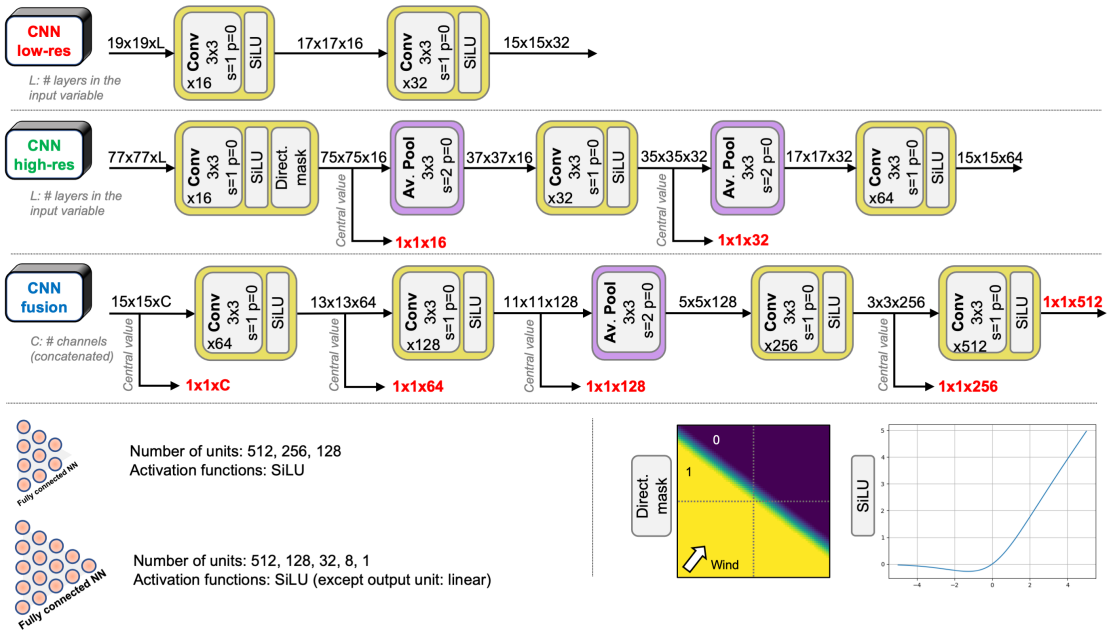

Figure 5.5: Deep-learning constitutive blocks of Wind-Topo. The convolution blocks (yellow) indicate the kernel size (3x3), the stride s, the padding size p and the number of filters (x16 e.g.). The average-pooling blocks (purple) depict the same information. Vectors of central information (red) are extracted at various places. The first convolution layer of "CNN high-res" has an additional directional mask based on the wind direction from COSMO-1 (e.g. mask in lower right corner). The two types of fully connected neural networks are detailed in the lower left corner.

Training the model consists in optimizing the values of the model's parameters (e.g., weights and biases of the neurons in an ANN or values of the convolutional kernels in a CNN). One needs to adopt a strategy to do so, in order to reach the best performance on the training and validation sets. The various elements that compose this strategy are generally referred to as the hyperparameters of the model. For Wind-Topo, an iterative procedure led to the hyperparameters presented in Table 5.1.

Parameter	Value
Optimizer	ADAM (17)
Initialization	Xavier, uniform, gain=1 (9)
Learning rate	5.10^{-6}
Weight decay	0
Early stopping	10^{th} epoch
Batch size	128

Table 5.1: Hyperparameters used to train the model.

5.2.6 Loss function

The design of an appropriate loss function was critical to obtain the current performance of Wind-Topo. Using any standard loss function like mean square or absolute error (MSE, MAE) led to distributions of $\hat{u}$, $\hat{v}$ and of the associated horizontal wind speed $\hat{vel}$ that were too narrow. The model chose to decrease the range of its predictions, favoring values near the mean value. This is a well-known problem in statistical downscaling (32). The countermeasure was to compose the loss function $\mathscr{L}$:

$$\begin{aligned} \mathscr{L} &= \frac{1}{N}\sum_{i=1}^{N} \tau_i[(\hat{u}_i - \beta_i u_i)^2 + (\hat{v}_i - \beta_i v_i)^2], \text{ where} \\ \beta_i &= \frac{\epsilon + vel_i}{\epsilon + \hat{vel}_i} \quad \text{and } \tau_i = \begin{cases} \tau & if \quad \hat{vel}_i \geq vel_i \\ 1-\tau & if \quad \hat{vel}_i < vel_i \end{cases} \end{aligned} \tag{5.3}$$

This loss function is essentially a MSE over a batch of training data of size N, with a scaling by β_i of the target values u_i and v_i based on the overestimation or underestimation of the predicted velocities $\hat{vel}_i$. Additionally, the term τ_i, inspired by the pinball loss function (28), allowed to remove the consistent negative mean bias error (MBE) of $\hat{vel}$. ϵ, controlling the strength of the scaling, and τ were tuned iteratively to their respective optimal values of 4 and 0.425. A lower value of ϵ led to an unstable behavior and incorrect distributions, while larger values led to squeezed distributions. The current value of τ allowed to obtain an unbiased model on the test set. The quality of the distributions of predicted wind speed is essential for many applications of high-resolution wind fields. This loss function is the result of an intense effort to find a differentiable function that efficiently guides the gradient-descent algorithm of the model's optimization towards distributions that closely match the measured ones, while obtaining very low MAE and MBE and high Pearson Correlation Coefficients between predictions and measurements. Those three scoring metrics reflect important qualities of the predictions. A low MBE guarantees no bias between predictions and observations, while a simultaneous low MAE and high correlation indicate that the model is accurate for a large range of observations. The development of Wind-Topo was guided by those three scoring metrics on the validation set, and section 5.3 focuses on them.

5.2.7 Making predictions

Wind-Topo was trained to make a point-prediction from centered patches of COSMO-1 data and of high-resolution DEM covering exactly 21.147 km. Thus, when Wind-Topo is used to generate a wind field on e.g., a 100-meter grid, this is performed in a point-by-point manner. Each predicted grid point is an independent output of the model, to which we provide the centered patches of data. In this 100-meter case, COSMO-1 needs to be resampled every 100 m to avoid that 11 consecutive grid points receive the same COSMO-1 inputs, which would lead to a chessboard-like pattern in the resulting high-resolution wind field. This sub-pixel resampling is performed efficiently using convolutions with Lanczos kernels. If the same method is applied to the topographic data as well, it is possible to generate wind fields at a higher resolution than the 53-meter DEM input data. However, as the model was trained on this particular DEM, higher resolutions lead to smooth outputs, with no additional information. In our case, wind fields generated at a 50 to 100-meter resolution contain the highest level of detail.

The complex pipeline needed to obtain all the required input data for every grid point can be performed by the CPU, in parallel to the predictions performed by the GPU. In our case, for Wind-Topo coded with Pytorch (22; 24), it is possible for any domain size to obtain a perfect parallelization of those two tasks, without noticeable overhead and with a GPU running constantly at full capacity. As the model is pointwise and time-independent, it is easily parallelizable on multiple GPUs and/or machines with e.g., one GPU computing one part of the domain or a sub-period, and another GPU computing the rest. On a NVIDIA RTX2080Ti GPU, one prediction takes 0.6 milliseconds and a 300 x 300 domain requires 54 seconds. This is 30% faster than on a previous-generation GTX1080Ti, which indicates that Wind-Topo would be even faster on the latest-generation high-performance GPUs.

5.3 Results

After training Wind-Topo on 261 stations and years 1 and 3, we tested it on separate datasets to assess its performance at new locations and/or over a new time period: test set 1 (60 stations, years 1 and 3), test set 2 (261 stations, year 2), and test set 3 (60 stations, year 2) being the most informative because reflecting the spatio-temporal generalization. In this section, we will first evaluate Wind-Topo quantitatively, and then qualitatively by discussing some predicted wind fields. From now, when COSMO-1 is mentioned, it should be understood that a bicubic interpolation was applied at the desired locations. Importantly, the 60 test stations were selected by an algorithm that ensures an equitable evaluation. First, all stations were tagged with an 8-dimensional vector of: 1. Mean measured wind speed; 2. MAE (of COSMO-1 with respect to measurement), 3. MBE; 4. Correlation; 5. Normalized MAE (MAE at a station divided by its average measured wind speed); 6. Elevation; 7. Latitude; 8. Longitude. Then, the algorithm semi-randomly split the stations into training and test sets to have in both a good representation of this 8-dimensional space and a similar performance of COSMO-1.

Concerning the separation of training and test times, our investigation showed that a random split cannot reflect the temporal generalization: It is easy for a model trained on hour h and $h+2$ to predict hour $h+1$. Consequently, we kept the complete intermediate year for validation. In this section, we employ the same colors as in Figure 5.1 for stations that are exposed (blue), sheltered (orange) and uncategorized ("other", green).

Station ($\overline{vel}$)	Model	Corr. (DN)	MBE (m/s)	MAE (m/s)	nMAE (DN)	MAEdir (deg)
Exposed	C	0.51	-0.25	1.83	0.56	41.3
(3.43 m/s)	WT	0.66	-0.05	1.49	0.45	32.5
Sheltered	C	0.42	1.90	2.27	1.43	67.0
(1.67 m/s)	WT	0.45	-0.04	1.03	0.63	58.1
Other	C	0.59	0.18	1.34	0.61	50.5
(2.46 m/s)	WT	0.64	-0.16	1.16	0.51	47.5
Alps	C	0.50	0.72	1.77	0.90	56.4
(2.35 m/s)	WT	0.55	-0.07	1.21	0.56	50.1

Table 5.2: Performance of COSMO-1 (C) and Wind-Topo (WT), with respect to measurement. Each value is the average of the scores at each test station, computed on the test period. The left column gives the average measured wind speed of the three station categories. Corr. is the Pearson correlation coefficient. MBE is the Mean Bias Error. MAE is the Mean Absolute Error. nMAE is the normalized MAE (MAE at a station divided by its average measured wind speed). MAEdir is the MAE of the wind direction.

5.3.1 Aggregated scores

Table 5.2 shows various scoring metrics for COSMO-1 and Wind-Topo on test set 3. Each score is the average of the scores at the stations belonging to the category. This is more meaningful than computing the scores on all the data as e.g., correlations computed on all the data are significantly higher but are potentially misleading. We can observe the importance of the station's classification in the left column: The average wind speed at exposed sites is more than twice that of sheltered sites. Given its resolution, COSMO-1 cannot discriminate them and has a large positive bias (1.9 m/s) at sheltered sites. Surprisingly, the highest wind speeds are predicted there. Nevertheless, its performance is quite high at exposed locations and in the flat lands and large valleys (a considerable part of the "other" stations). Wind-Topo significantly improves COSMO-1, for all metrics and at all station types. The correlation is improved the most at exposed and other sites, while the large bias at sheltered sites is completely removed, leading to a much lower MAE. The normalized MAE (nMAE) allows the comparison of all types of stations and shows again the lack of performance of COSMO-1 at sheltered sites and the capability of Wind-Topo to correct it. Finally, Wind-Topo also corrects wind directions, as expressed by the MAE of wind direction (MAEdir), computed from events with a wind speed greater than 1 m/s. As Wind-Topo was designed for complex terrain, the lower line in Table 5.2 provides overall scores for the 44 test stations located in the Alps.

The scores for Wind-Topo were obtained from predictions of the trained model. Figure 5.6

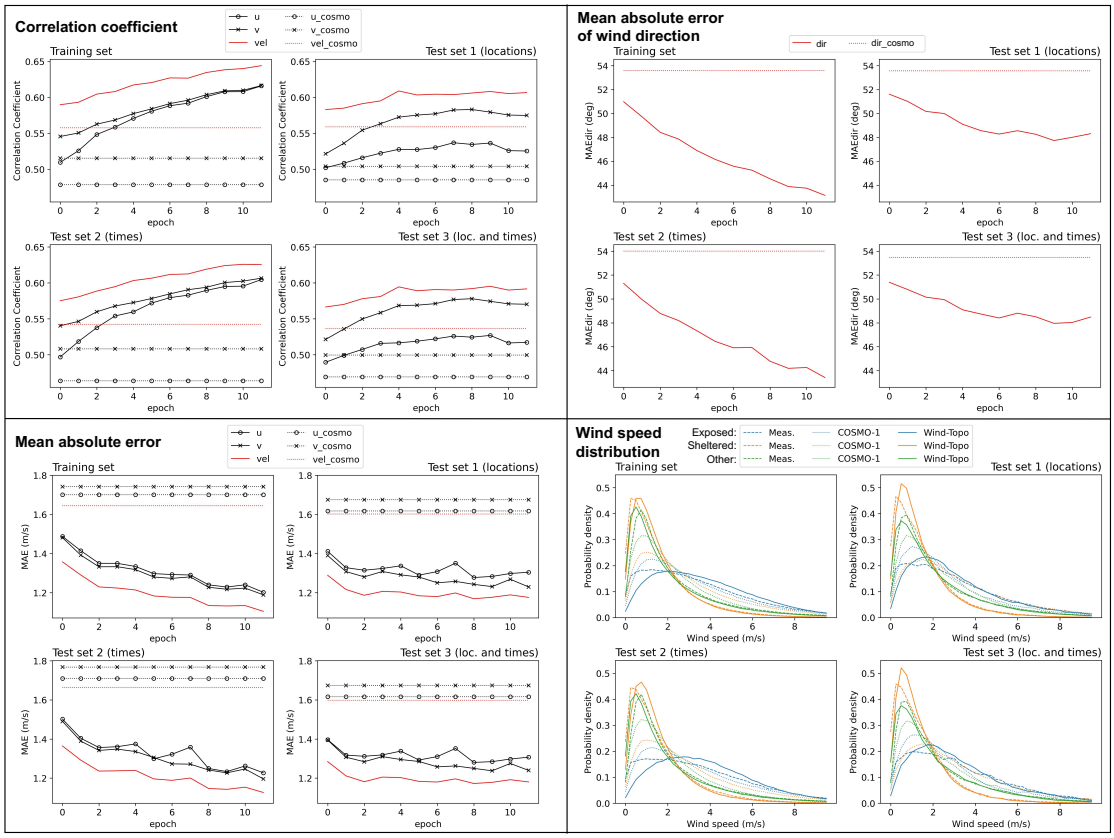

Figure 5.6: Quality of the predictions of Wind-Topo compared to COSMO-1 throughout the training phase (1 epoch is 1 pass through the entire training set). For each quality assessment, the upper left panel corresponds to the behavior of Wind-Topo on the training set while the right panels correspond to the test stations and the lower panels to the test period. Scores for wind speed (vel) and direction (dir) are computed from u and v and are depicted in red. The lower right figure shows with various colors the distributions of wind speed for the three station categories. Various lines styles are used to depict those distributions from measurement, COSMO-1 and Wind-Topo.

depicts some of them during the training. After each epoch (pass through the training set), we evaluated the model on the four datasets. Correlation, MAE and MAEdir improved progressively until epoch 9, whose model's state was used for all predictions in this work. Later on, a typical overfitting is observed, where the spatial generalization decreases. Interestingly, there is no overfitting with respect to the temporal generalization. When training the model further (not shown), the scores on test set 2 keep improving (MAE < 1 m/s, correlation > 0.8). Temporal generalization was easily obtained: many (simpler) models can give accurate predictions on test set 2. In other words, the corrections to COSMO-1 can be easily learned on a certain period and successfully applied to new periods. Furthermore, a small amount of timesteps is required. All presented results are based on Wind-Topo trained with only half the training times, and no improvement was observed using all times. The strong temporal generalization offers a different application: If a short measurement campaign of surface wind is performed somewhere, the collected data can be used to train a model like Wind-Topo, which can generate longer "synthetic" time series covering the same period as the NWP model. The lower right

panel of Figure 5.6 shows the distributions of measured and predicted wind speeds for the three station types. We again observe the lack of discrimination of COSMO-1 between exposed and sheltered sites. It is however clear in the measurement, and Wind-Topo can reproduce it well. The distributions of predicted wind speed match accurately the observed ones for all station types and for the four datasets.

The "early stopping" procedure presented above, in association with the chosen learning rate, provides the best scores and distributions. Other regularization techniques like Weight Decay did not show any supplementary advantage. On a RTX2080Ti GPU, the 12 epochs of Figure 5.6 required 43 hours.

5.3.2 Disaggregated scores

We can further assess Wind-Topo by looking at the scores at each station. Figure 5.7 shows such a disaggregated view for the MAE. The Supplementary Information (SI) provides similar plots for correlation, MBE, nMAE and MAEdir. Each segment represents a station, with its extremities being the scores on training and test periods. The test stations are circled in black and are the ones we should focus on. Any point located below the black curve indicates that Wind-Topo has a lower MAE than COSMO-1. This is the case for all exposed and sheltered stations. Wind-Topo is however slightly worse at some "other" stations and significantly worse at one. The clustering of the station categories is remarkable. Wind-Topo strongly reduces the MAE at the sheltered sites with high COSMO-1 MAE. This is also the case at exposed sites, albeit less pronounced. The reduced performance at the "other" stations is due to the already good performance of COSMO-1. The orientation of the segments indicates how the MAE in COSMO-1 changes from one period to another and how Wind-Topo reacts to it. An orientation parallel to $y = x$ reflects that Wind-Topo follows the variation of score in COSMO-1. An upward deviation from this orientation (triangle to circle) shows that Wind-Topo suffers from a lack of temporal generalization and becomes (relatively) worse on the test period. This is almost never the case and the opposite behavior dominates.

The "outlier" mentioned above in an interesting test station located on the smooth ridge of a hill (700 m above the plains). Its topography is well represented in COSMO-1, which performs well with almost no MBE (0.2 m/s) and a low MAE (1.2 m/s). Wind-Topo overestimates the wind speed there (MBE of 1.2 m/s), which leads to a higher MAE (1.5 m/s). Surprisingly, at another (training) station located 11 km from there and 450 m higher on the ridge, COSMO-1 behaves very differently. It underestimates the wind speed (4.6 m/s) compared to measurement (7.7 m/s). This large bias is almost entirely corrected by Wind-Topo (MBE of -0.9 m/s). Being in the training set, this performance does not necessarily reflect appropriate corrections. However, it seems that the learned corrections of COSMO-1's underestimation in this type of topography is applied to our nearby "outlier". Such topographies are not common in our dataset and Wind-Topo would certainly benefit from more training stations, located in more diverse terrain.

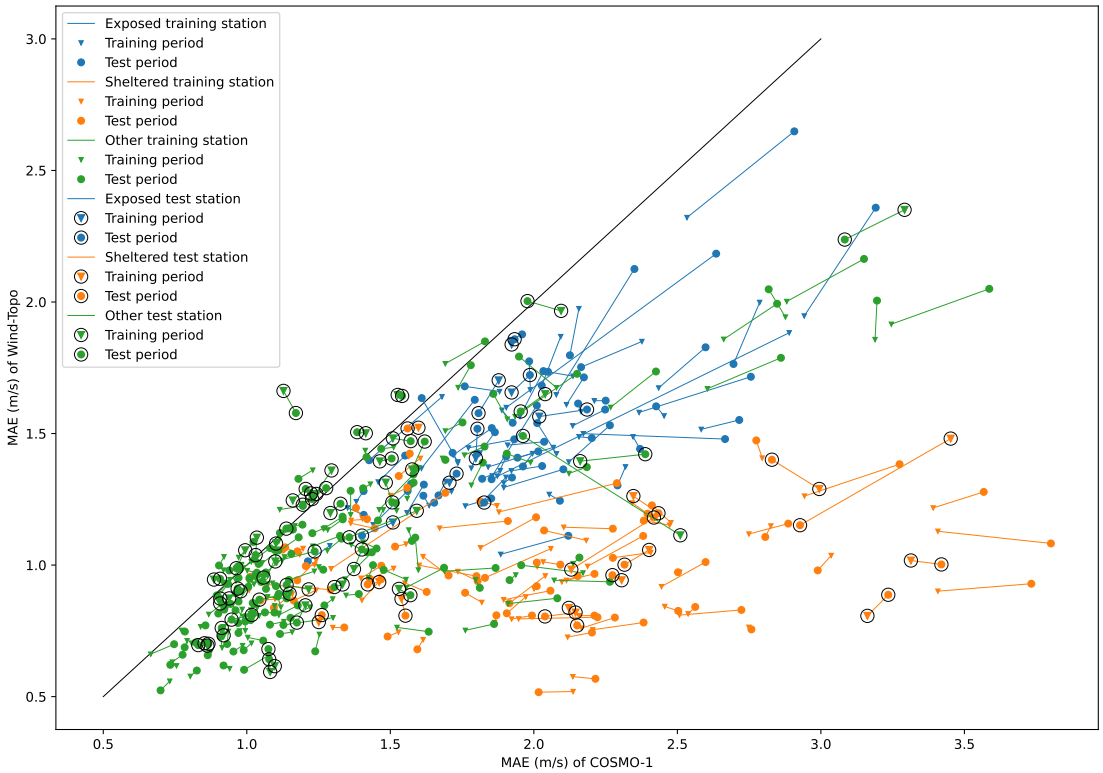

Figure 5.7: Mean Absolute Error of Wind-Topo at all 321 stations compared to COSMO-1. Each segment corresponds to one station. The color indicates the category of the station. The extremities of each segment show the MAE computed on the training period (triangles) and the test period (circles). The 60 test stations are circled in black. Any point below the black line is a station where Wind-Topo has a lower error than COSMO-1.

Figure 5.8 provides a temporal disaggregation of the scores for each month of the test period. The 0.25, 0.5 and 0.75 quantiles, computed for the 60 test stations, are represented in bright colors for Wind-Topo and faint colors for COSMO-1. The upper panel shows that the winter period is the windiest and that COSMO-1 predicts similar wind speeds at exposed and sheltered sites. This large positive bias (MBE panel) is always corrected by Wind-Topo. The negative bias occurring at exposed sites in winter is also corrected, as well as the slight positive bias at the "other" stations in summer. The panel on correlation shows the significant improvement from Wind-Topo at exposed sites, especially in early summer when thermally-driven flows become active. At the "other" stations, Wind-Topo closely follows but slightly surpasses COSMO-1. The same happens at sheltered sites, except in July to September when the correlation is slightly decreased in Wind-Topo, despite a low MAE. We should note the low average wind speed for this period (1.2 m/s) and the corresponding large MAEdir from COSMO-1 (68°). Wind-Topo can lower it to 60°, but at a cost of a lower correlation. Finally, the MAE of wind speed and direction are systematically lower with Wind-Topo. This is true for the 0.5 quantile and almost always true for the other quantiles, showing that the downscaling performs well at almost all stations and for all seasons.

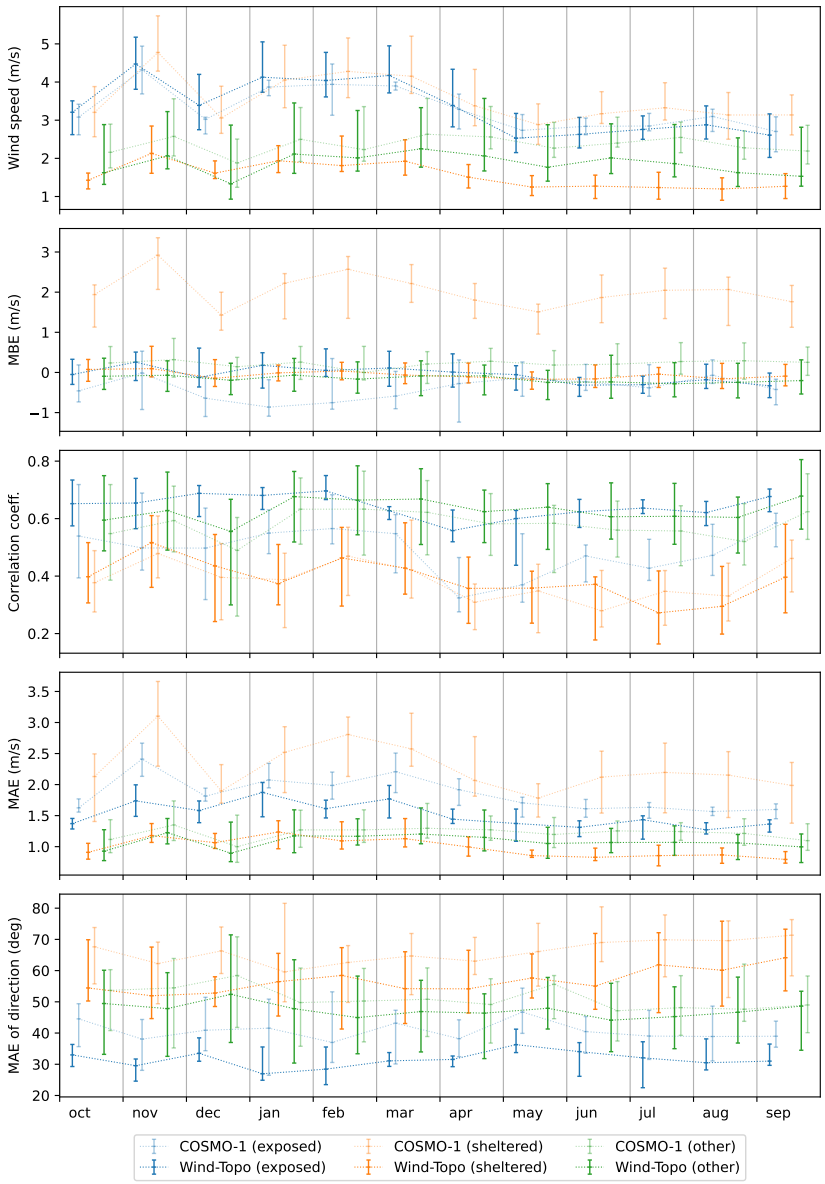

Figure 5.8: Each panel shows monthly average values for the three types of test stations (colors). Those values are the 0.25 quantiles (lower extremities of the vertical segments), 0.5 quantiles (marks within the segments) and 0.75 quantiles (upper extremities) of the monthly values for each station. Values for Wind-Topo are depicted with bright colors while values for COSMO-1 are fainter. MBE stands for Mean Bias Error and MAE for Mean Absolute Error (with respect to measurement).

5.3.3 Selected stations

For a last quantitative analysis, we selected three test stations in the test area of Figure 5.1: ELA-1, ELA-2 and SAM-0. Indices 1, 2, 0 stand for exposed, sheltered and other, respectively. Their locations are depicted in Figure 5.10. We can first look at scatter plots of predicted wind speed versus measurement for Wind-Topo and COSMO-1 (Figure 5.9). As expected, COSMO-1 shows no particular bias at ELA-1 and SAM-0, but a strong overestimation at ELA-2.

Wind-Topo is capable of reducing the scatter at ELA-1 and of removing the bias at ELA-2 completely. For this station, the scatter however persists. As COSMO-1 already captures well the topography surrounding SAM-0, Wind-Topo cannot improve the wind prediction and does not alter what COSMO-1 predicts.

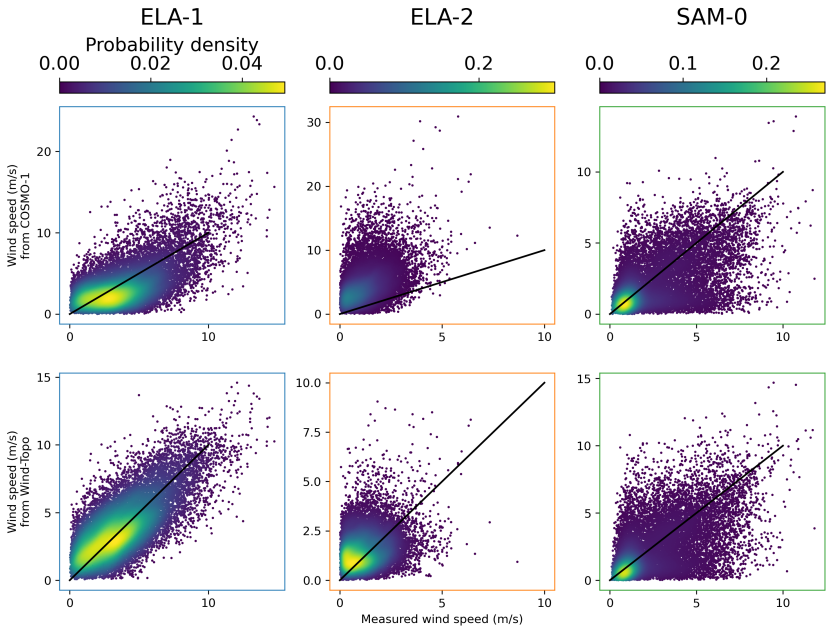

Figure 5.9: Scatter plots of all available wind speeds during the test period for three test stations. ELA-1 is exposed, ELA-2 is sheltered and SAM-0 is uncategorized (other). The x-axis is the measured wind speed while the y-axis is the predicted wind speed from COSMO-1 (upper panels) and from Wind-Topo (lower panels). Each data point is colored according to the probability density (Gaussian kernel-density estimate). A narrow scatter around the black line indicates accurate predictions.

Figure 5.10 details the predictions of the two models at the three stations throughout the test year and for each hour of the day. The histograms of wind speed for the whole year reflect the typical behavior of COSMO-1 at two nearby exposed and sheltered stations (ELA-1, ELA-2): The two stations have similar distributions in the model, which does not correspond to the measurements. This is again corrected by Wind-Topo. The daily patterns of wind speed are quite different from site to site and for different times of the year. SAM-0 has typical mid-afternoon thermally-driven flows, stronger in summer. COSMO-1 captures them very well and Wind-Topo replicates it. The measurements at ELA-1 show peculiar wind patterns: Wind is steadier and stronger in winter, and is significantly reduced in the middle of the day in summer due to complex boundary layer - free atmosphere interactions. COSMO-1 predicts the opposite, with an increase of wind speed in the middle of the day in summer. It is remarkable that Wind-Topo can reproduce the observed patterns and does not simply copy COSMO-1 at this exposed station which is located on a type of terrain where COSMO-1 normally performs quite well.

To complement the analysis on wind speeds, we can look at wind rose diagrams to evaluate the models with respect to wind direction. We can see in Figure 5.11 that the wind direction

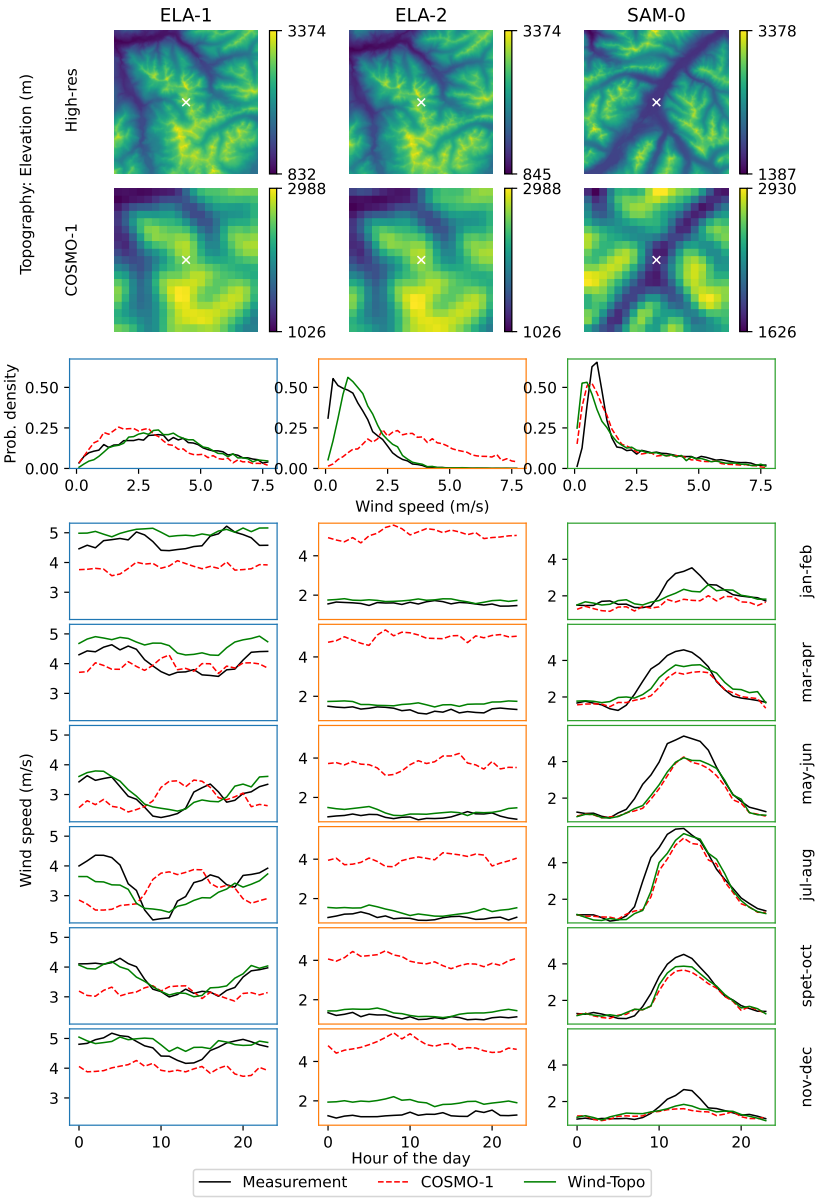

Figure 5.10: Topography used by Wind-Topo (upper panels) and COSMO-1 (below) for the three selected test stations. Below the topographies are the distributions of wind speed for the test period from measurement (black), COSMO-1 (red) and Wind-Topo (green). With the same colors, the lower panels show, for each pair of months (in the test period), the average wind speed (y-axis) for each hour of the day (x-axis).

in Wind-Topo is strongly influenced by COSMO-1. This is especially the case at ELA-1 where Wind-Topo can only partially correct the westerly winds from COSMO-1. At SAM-0, the situation is reversed, with COSMO-1 direction being accurate while Wind-Topo rotates it slightly. This can be explained by the peculiar location of this station (intersection of several valleys) and it reflects a weakness of Wind-Topo. The correction at ELA-2 is however impressive.

This quantitative analysis displayed many strengths of Wind-Topo, which can: i. Accurately

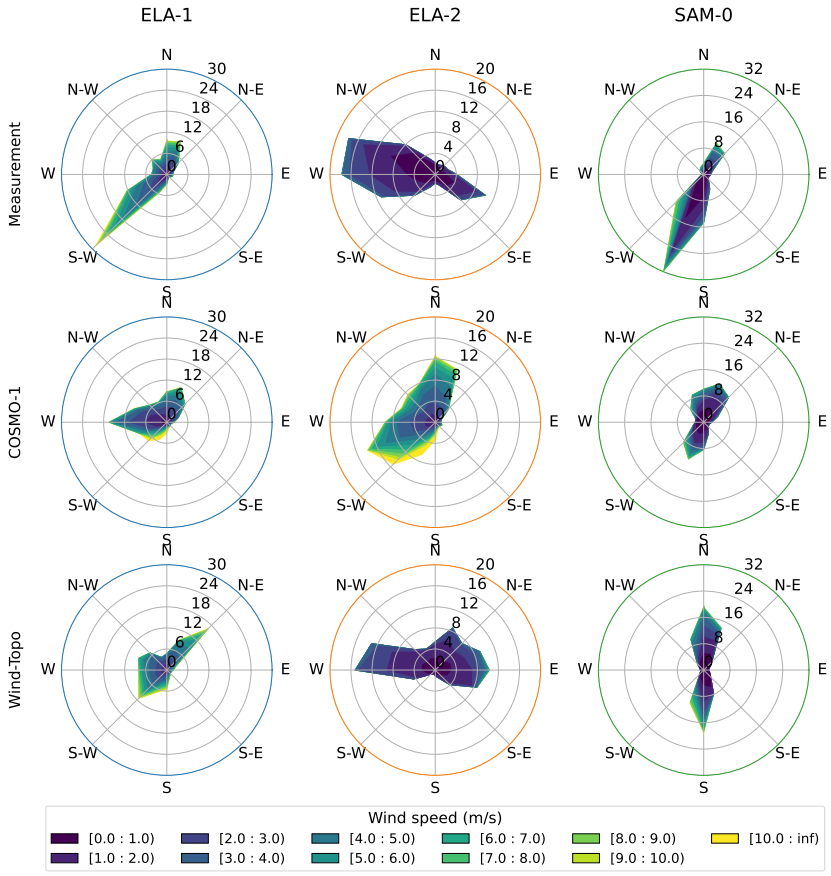

Figure 5.11: Wind rose diagrams for the three selected test stations during the test period from measurement, COSMO-1 and Wind-Topo. The color indicates the wind speed of the events while the distance from the center indicates the probability in percent that the wind comes from one of 16 directions. To help compare the models, the radial-axis has the same extent for the three data sources.

distinguish exposed and sheltered locations and reduce the biases resulting from a simple interpolation of COSMO-1 to a higher resolution. ii. Generate better wind distributions in complex terrain. iii. Capture complex small-scale wind-topography interactions. The model is not perfect and can introduce errors in locations where COSMO-1 is performing well. Given the current level of performance, based on only 261 training stations, we are confident that more diverse training data (ground truth at other locations) would strongly benefit Wind-Topo.

5.3.4 Generated wind fields

We can finally look at some examples of generated wind fields for the test area in Figure 5.1. COSMO-1 was downscaled for all hours of the test year to a 100-meter grid covering this 30 x 30 km domain, with a bicubic interpolation and with Wind-Topo. The latter required 5.5 days on a RTX2080Ti GPU. Panel a) of Figure 5.12 shows an example of interpolated COSMO-1 wind field and the underlying (interpolated) model's terrain. Panel b) is the 100-meter DEM, and panel c) shows the prediction from Wind-Topo with wind speed enhanced on ridges and

exposed slopes, and reduced on sheltered slopes. It is not a pale copy of COSMO-1 with a simple scaling by elevation or exposition. A careful observation (full-size panels available in SI) indicates the presence of flow deflection and recirculation areas on some leesides. COSMO-1 shows such effects on a much larger scale. Wind-Topo can even remove them in some areas, before introducing them in others. We should also note the continuity in wind speed in the generated field, despite the point-by-point method. This is caused by the large overlap of input data between neighboring points. To better visualize the flow deflection and continuity of wind direction, panel d) depicts the wind azimuth with a cyclic colorscale, and associated streamlines.

Panel e) and f) provide an insight into the entire downscaled dataset. The former shows the average wind speed and the latter depicts the distributions at every grid point. A Weibull distribution is fitted to the histogram of wind speed at each grid point, and the corresponding parameters are used to determine the color. The scale parameter (resembling the average wind speed) defines the brightness, while the shape parameter defines the hue. Blue areas have a shape parameter close to 1, meaning broad distributions, while red areas show narrower distributions which are more centered around the average. Here, we also observe a good spatial continuity in the fitted distributions. The large valleys all have a low scale parameter, which increases towards the summits and ridges. However, in many locations the highest values are not found there, but slightly below them. Also, the concave areas on slopes exhibit higher scale parameters than their surroundings. A similar plot for COSMO-1 is provided in SI and shows the same increase in concave areas on larger scales. This local increase can be explained by the channeling that occurs in such places and that generates many situations with relatively high wind speed but few occurrences of very large one. Wind-Topo is able to reproduce such effect on smaller scales.

One might wonder about the physical consistency of the generated wind fields. As Wind-Topo only predicts a near surface wind field, we cannot compute a 3D divergence to assess the mass conservation. We can nevertheless estimate the ground-perpendicular motion caused by the divergence of the 2D field. SI describes this analysis along with figures, which we summarize here. The large majority of such motions at 7 m.a.g.l are between -0.04 and 0.04 m/s (negative for motions towards the ground). Rarely, it can reach 10 times those values. When averaged for the entire year, we obtain values between -0.06 and 0.05 m/s. Furthermore, if we apply a spatial averaging to coarse-grain those maps to the scales resolved by COSMO-1, we obtain patterns that are very similar to those of COSMO-1 in terms of magnitude (-0.01 to 0.006 m/s) and location.

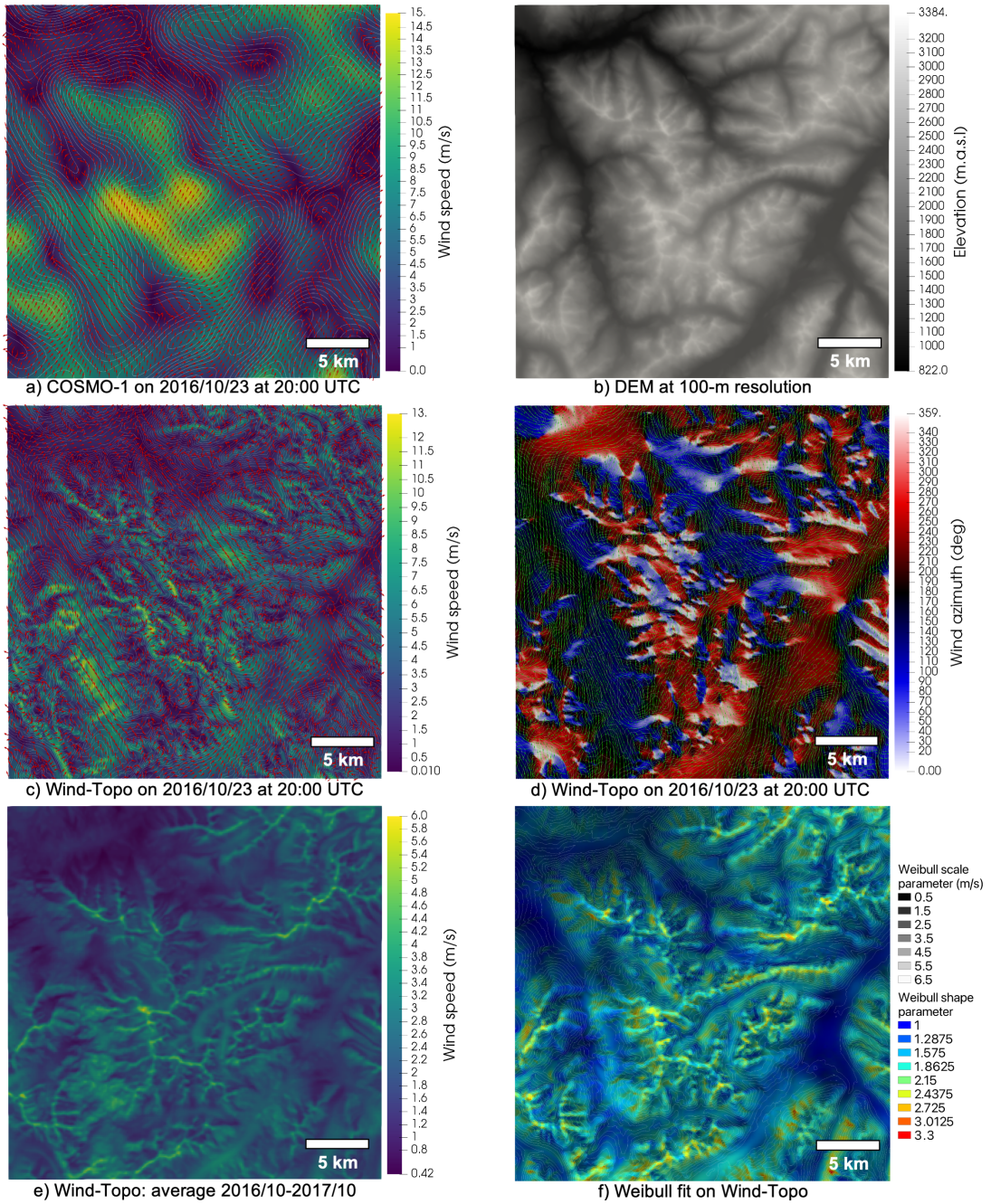

Figure 5.12: a) Wind field from COSMO-1, interpolated (bicubic) on a 100-meter grid, for a specific time. Background color indicates the wind speed and red arrows indicate the wind direction every 500 m. Grey lines show the 100-meter contours of the associated topography. b) 100-meter Digital Elevation Model used by Wind-Topo covering the same domain. c) 100-meter wind field generated by Wind-Topo for the same time. Grey lines show the underlying topography (100-meter contours). d) Associated wind direction (clockwise from North) with a cyclic colorscale. The green lines are the stream lines of the wind field with arrows indicating the flow direction. e) Average wind speed from Wind-Topo over the test period. f) Weibull parameters of the distribution fitted in each pixel. The brightness indicates the scale parameter and the color indicates the shape parameter. 100-meter contours in grey show the underlying topography.

5.4 Conclusion

A high spatial resolution in complex terrain is essential to capture effects like sheltering, ridge acceleration or deflection, and those effects are the main drivers of phenomena like snow preferential deposition or transport. Even state-of-the-art operational models like COSMO-1 running on supercomputers cannot provide the required resolution for topographies like the Alps. Wind-Topo offers the possibility to extract the most information from such models and to correct the near surface wind fields to closely match observations. The systematic biases observed on different types of terrain and at different times of the year and times of the day are strongly reduced. The downscaled wind fields exhibit many of the expected orographic effects, and Wind-Topo does not alter the predictions from the low-resolution input model in areas where it already performs well. At 44 measurement stations located in diverse topographies in the Alps and put aside for validation, Wind-Topo offers an average correlation of 0.55, a low bias of -0.07 m/s and a MAE of 1.21 m/s. This should be compared to the values obtained by a simple interpolation of COSMO-1: correlation of 0.50, bias of 0.72 m/s and MAE of 1.77 m/s.

With its novel architecture, Wind-Topo downscales not only the wind speed to higher resolutions but also incorporates local orographic deflections. Its current level of performance is already remarkable and further improvements are expected, in particular if more diverse locations with observed or modeled "ground truth" can be used for training. Given the rapid evolution of the research on deep learning, we believe that its architecture will also be improved in the near future.

The point-by-point nature of Wind-Topo can be seen as a strength or as a weakness. Using point observations as predictands avoids the introduction of inaccuracies or biases that other (modeled) data sources would have. The pointwise prediction also simplifies the parallelization of the downscaling scheme. It however prevents the introduction of physical constraints during the training and the predictions that would guarantee the generation of physically consistent flows. Ideally, Wind-Topo should be further developed to incorporate high-resolution 2D or 3D modeled data as well, which could help identify wind-topography interactions not yet discovered by the model. This new data source could also provide physical constraints needed when generating wind fields.

Wind-Topo is already quite fast and can be optimized further. In our Swiss case study, it can downscale COSMO-1 (1110 m) to 6 million grid points in one hour on one standard GPU. It is thus possible to operationally (hourly) downscale the Swiss Alps (about 29 000 km^2) to a 50-meter grid with a 2-GPU machine. As the computation requirements scale linearly with the number of desired grid points, Wind-Topo can be applied to much larger domains at this resolution with reasonable resources.

We hope this work will pave the way to new methods based on deep learning that will downscale not only the wind, but other atmospheric variables to higher resolutions in complex terrain. Such methods will be able to efficiently combine state-of-the-art high-resolution NWP models, observations and operational models.

Acknowledgments

We thank Mathieu Schaer for his contribution to the initial investigation on the architecture of Wind-Topo during his master's project and Quentin Fisch for his help on the parallelization of the code. This work was funded by Innosuisse through the Swiss Competence Center for Energy Research, Supply of Electricity.

Bibliography

[1] Florian Dupuy, Gert Jan Duine, Pierre Durand, Thierry Hedde, Eric Pardyjak, and Pierre Roubin. Valley winds at the local scale: Correcting routine weather forecast using artificial neural networks. *Atmosphere*, 12(2):1–20, 2021.

[2] Christophe Etienne, Anthony Lehmann, Stéphane Goyette, Juan-Ignacio Lopez-Moreno, and Martin Beniston. Spatial Predictions of Extreme Wind Speeds over Switzerland Using Generalized Additive Models. *Journal of Applied Meteorology and Climatology*, 49(9):1956–1970, sep 2010.

[3] Federal Office of Meteorology and Climatology MeteoSwiss. COSMO forescasting system. https://www.meteoswiss.admin.ch/home/measurement-and-forecasting-systems/warning-and-forecasting-systems/cosmo-forecasting-system.html.

[4] Federal Office of Meteorology and Climatology MeteoSwiss. SwissMetNet. https://www.meteoswiss.admin.ch/home/measurement-and-forecasting-systems/land-based-stations/automatisches-messnetz.html.

[5] Federal Office of Topography swisstopo. swissALTI3D. https://www.swisstopo.admin.ch/en/geodata/height/alti3d.html.

[6] J. Fiddes and S. Gruber. TopoSCALE v.1.0: Downscaling gridded climate data in complex terrain. *Geoscientific Model Development*, 7(1):387–405, 2014.

[7] P. Fischer, C. Etienne, J. Tian, and T. Krauß. Prediction of Wind Speeds Based on Digital Elevation Models Using Boosted Regression Trees. *ISPRS - International Archives of the Photogrammetry, Remote Sensing and Spatial Information Sciences*, XL-1-W5:197–202, dec 2015.

[8] Loris Foresti, Devis Tuia, Mikhail Kanevski, and Alexei Pozdnoukhov. Learning wind fields with multiple kernels. *Stochastic Environmental Research and Risk Assessment*, 25(1):51–66, jan 2011.

[9] Xavier Glorot and Yoshua Bengio. Understanding the difficulty of training deep feedforward neural networks. In *Proceedings of the Thirteenth International Conference on Artificial Intelligence and Statistics*, volume 9, pages 249—-256. PMLR, 2010.

[10] Naveen Goutham, Bastien Alonzo, Aurore Dupré, Riwal Plougonven, Rebeca Doctors, Lishan Liao, Mathilde Mougeot, Aurélie Fischer, and Philippe Drobinski. Using Machine-Learning Methods to Improve Surface Wind Speed from the Outputs of a Numerical Weather Prediction Model. *Boundary-Layer Meteorology*, 179(1):133–161, 2021.

[11] N. Helbig, R. Mott, A. Van Herwijnen, A. Winstral, and T. Jonas. Parameterizing surface wind speed over complex topography. *Journal of Geophysical Research*, 122(2):651–667, jan 2017.

[12] Dan Hendrycks and Kevin Gimpel. Gaussian Error Linear Units (GELUs). pages 1–9, 2016.

[13] James Hilton and Nikhil Garg. Rapid wind-terrain correction for wildfire simulations. *International Journal of Wildland Fire*, 30(6):410–427, 2021.

[14] Kevin Höhlein, Michael Kern, Timothy Hewson, and Rüdiger Westermann. A comparative study of convolutional neural network models for wind field downscaling. *Meteorological Applications*, 27(6):1–31, 2020.

[15] William W. Hsieh. *Machine Learning Methods in the Environmental Sciences: Neural Network and Kernels*. Cambridge University Press, Cambridge, 2009.

[16] Hsin Yuan Huang, Scott B. Capps, Shao Ching Huang, and Alex Hall. Downscaling near-surface wind over complex terrain using a physically-based statistical modeling approach. *Climate Dynamics*, 44(1-2):529–542, 2015.

[17] Diederik P. Kingma and Jimmy Lei Ba. Adam: A method for stochastic optimization. *3rd International Conference on Learning Representations, ICLR 2015 - Conference Track Proceedings*, pages 1–15, 2015.

[18] Michael Lehning, Perry Bartelt, Bob Brown, Tom Russi, Urs Stöckli, and Martin Zimmerli. SNOWPACK model calculations for avalanche warning based upon a new network of weather and snow stations. *Cold Regions Science and Technology*, 30(1-3):145–157, 1999.

[19] Alon Manor and Sigalit Berkovic. Bayesian Inference aided analog downscaling for near-surface winds in complex terrain. *Atmospheric Research*, 164-165:27–36, 2015.

[20] R. Mott, M. Schirmer, M. Bavay, T. Grünewald, and M. Lehning. Understanding snow-transport processes shaping the mountain snow-cover. *Cryosphere*, 4(4):545–559, 2010.

[21] NASA and NGA. https://doi.org/10.5066/f7pr7tft.

[22] Adam Paszke, Sam Gross, Soumith Chintala, Gregory Chanan, Edward Yang, Zachary DeVito, Zeming Lin, Alban Desmaison, Luca Antiga, and Adam Lerer. Automatic differentiation in PyTorch. In *31st Conference on Neural Information Processing Systems (NIPS 2017),*, 2017.

[23] Kostas Philippopoulos and Despina Deligiorgi. Application of artificial neural networks for the spatial estimation of wind speed in a coastal region with complex topography. *Renewable Energy*, 38(1):75–82, feb 2012.

[24] Pytorch. Pytorch. https://github.com/pytorch/pytorch/tree/v1.8.1.

[25] Markus Reichstein, Gustau Camps-Valls, Bjorn Stevens, Martin Jung, Joachim Denzler, Nuno Carvalhais, and Prabhat. Deep learning and process understanding for data-driven Earth system science. *Nature*, 566(7743):195–204, 2019.

[26] O. Rios, W. Jahn, E. Pastor, M. M. Valero, and E. Planas. Interpolation framework to speed up near-surface wind simulations for data-driven wildfire applications. *International Journal of Wildland Fire*, 27(4):257–270, 2018.

[27] Sylvain Robert, Loris Foresti, and Mikhail Kanevski. Spatial prediction of monthly wind speeds in complex terrain with adaptive general regression neural networks. *International Journal of Climatology*, 33(7):1793–1804, jun 2013.

[28] Ichiro Takeuchi, Quoc V.Le, Tim Sears, and Alexander Smola. Nonparametric Quantile Regression. *Journal of Machine Learning Research*, 2005.

[29] Vincent Vionnet, Christopher B. Marsh, Brian Menounos, Simon Gascoin, Nicholas E. Wayand, Joseph Shea, Kriti Mukherjee, and John W. Pomeroy. Multi-scale snowdrift-permitting modelling of mountain snowpack. *Cryosphere*, 15(2):743–769, 2021.

[30] Natalie S. Wagenbrenner, Jason M. Forthofer, Brian K. Lamb, Kyle S. Shannon, and Bret W. Butler. Downscaling surface wind predictions from numerical weather prediction models in complex terrain with WindNinja. *Atmospheric Chemistry and Physics*, 16(8):5229–5241, 2016.

[31] Adam Winstral, Kelly Elder, and Robert E. Davis. Spatial snow modeling of wind-redistributed snow using terrain-based parameters. *Journal of Hydrometeorology*, 3(5):524–538, 2002.

[32] Adam Winstral, Tobias Jonas, and Nora Helbig. Statistical Downscaling of Gridded Wind Speed Data Using Local Topography. *Journal of Hydrometeorology*, 18(2):335–348, feb 2017.

[33] WSL Institute for Snow and Avalanche Research SLF. Automated IMIS stations. https://www.slf.ch/en/avalanche-bulletin-and-snow-situation/measured-values/description-of-automated-stations.html.

6 Supplementary Information

Wind-Topo: Downscaling near-surface wind fields to high-resolution topography in highly complex terrain with deep learning
Supplementary Information

Jérôme Dujardin and Michael Lehning

This material was provided to the *Quarterly Journal of the Royal Meteorological Society* to accompany the main article.

Additional scatter plots of scoring metrics comparing COSMO-1 and Wind-Topo (complement Figure 7 of main text)

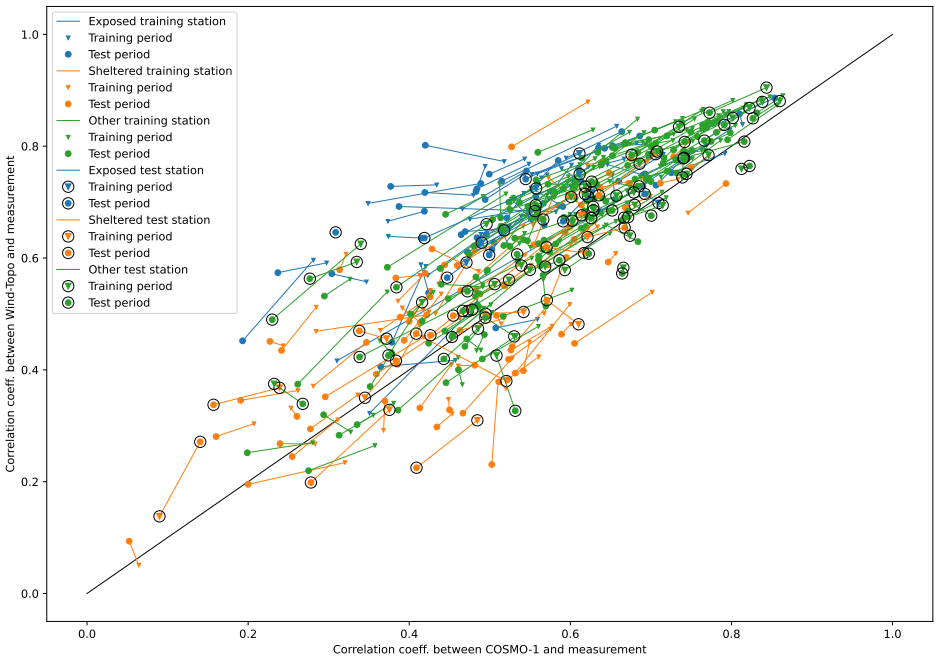

Figure 6.1: Pearson Correlation Coefficient of Wind-Topo at all 321 stations compared to COSMO-1. Each segment corresponds to one station. The color indicates the category of the station. The extremities of each segment show the correlation computed on the training period (triangles) and the test period (circles). The 60 test stations are circled in black. Any point above the black line is a station where Wind-Topo has a higher correlation with measurement than COSMO-1.

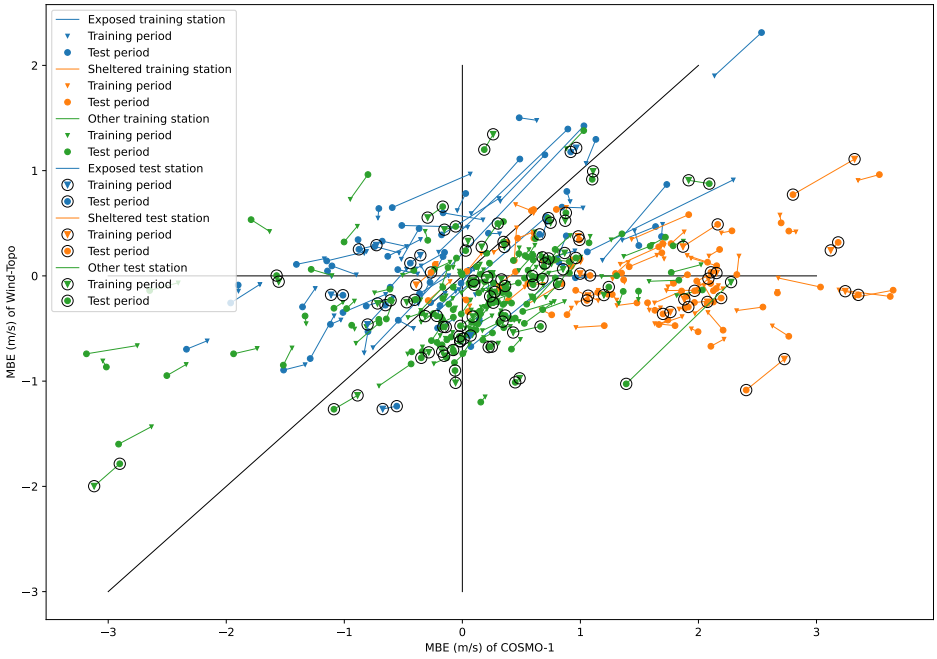

Figure 6.2: Similar plot as Figure 6.1 for the Mean Bias Error. The closer the point to the x-axis the better Wind-Topo corrects the bias coming from COSMO-1.

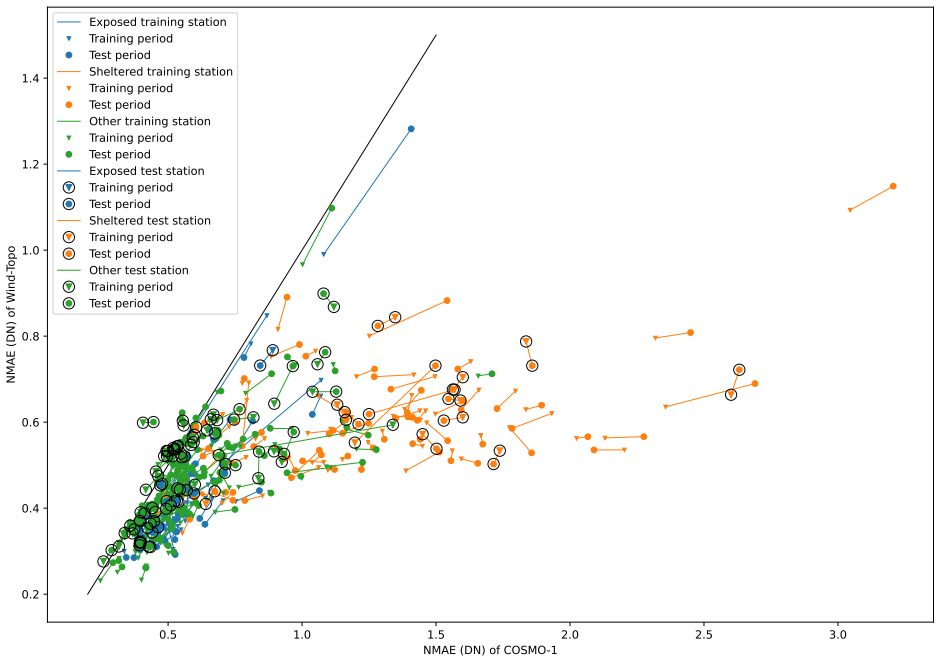

Figure 6.3: Similar plot as Figure 6.1 for the Normalized Mean Absolute Error. Any point below the black line is a station where Wind-Topo has a lower error than COSMO-1.

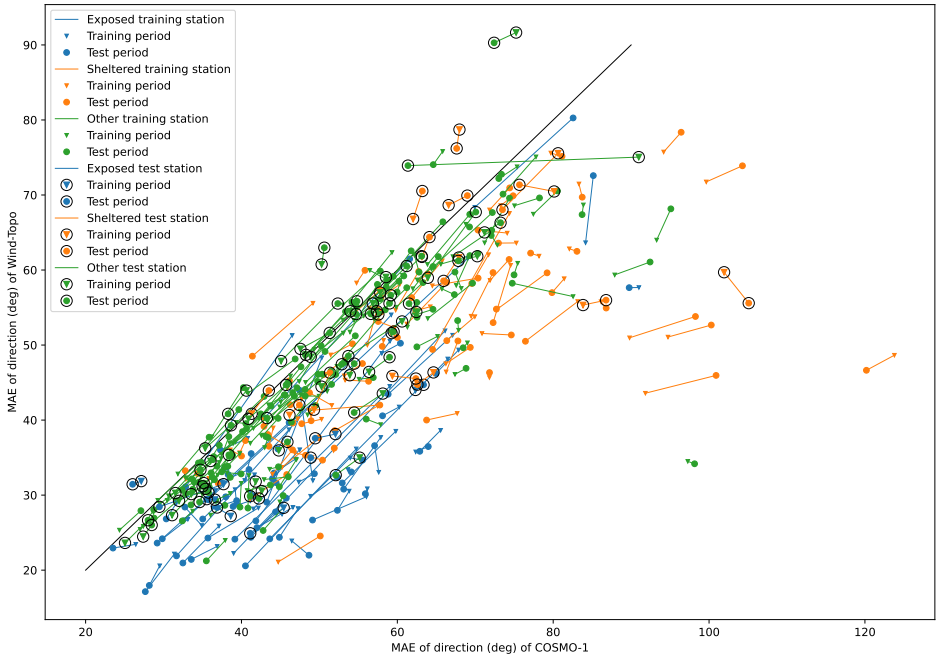

Figure 6.4: Similar plot as Figure 6.1 for the Mean Absolute Error of wind direction. Only events with a wind speed greater than 1 m/s are considered. Any point below the black line is a station where Wind-Topo has a lower error than COSMO-1.

Additional figures: Scoring metrics as function of wind speed

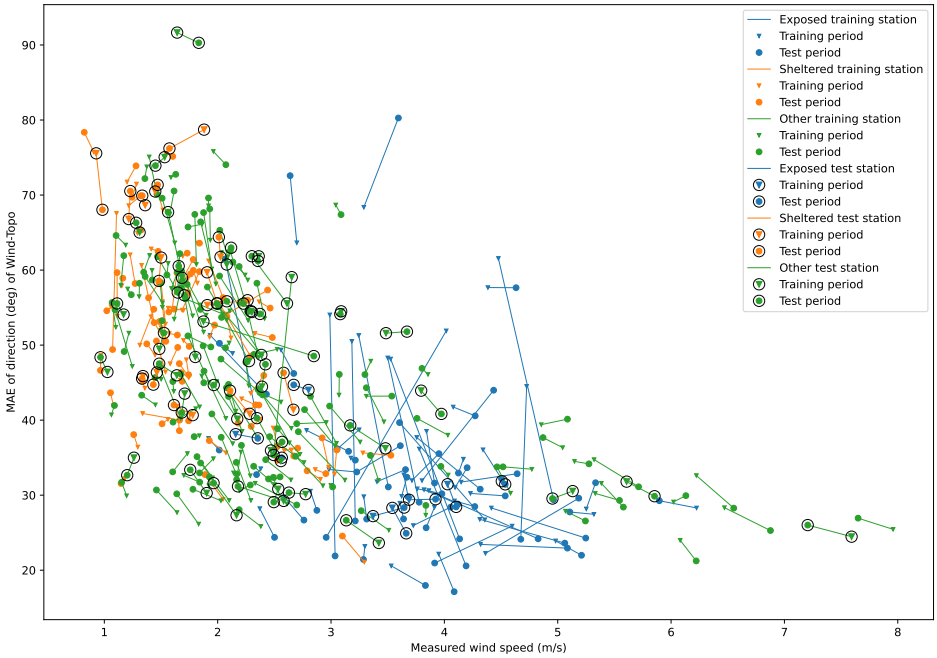

Figure 6.5: Mean Absolute Error of wind direction of Wind-Topo at all 321 stations as function of average measured wind speed. Same codes as Figure 6.1

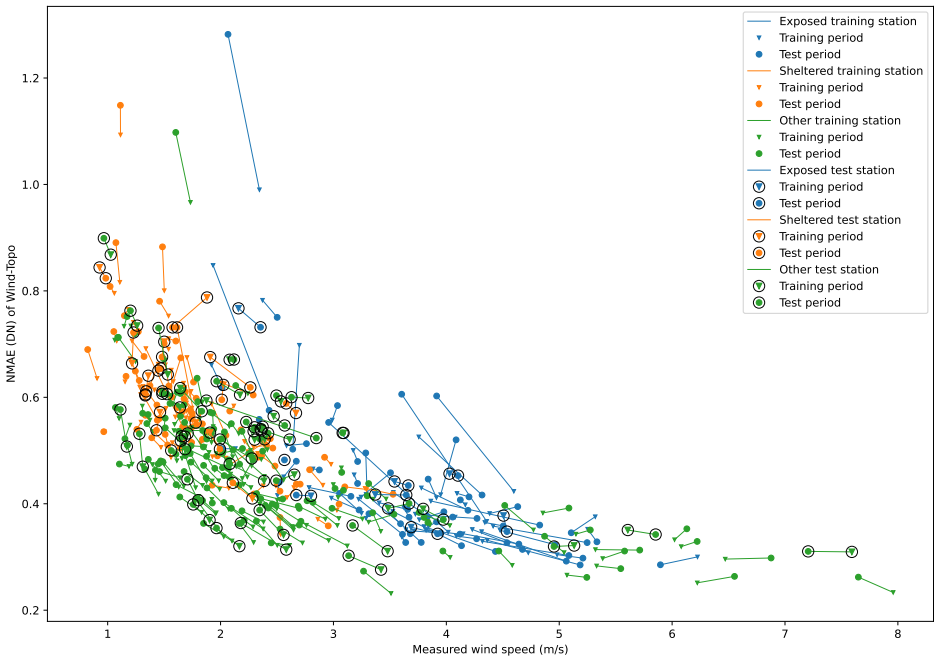

Figure 6.6: Normalized Mean Absolute Error of Wind-Topo at all 321 stations as function of average measured wind speed. Same codes as in Figure 6.1.

Full-resolution panels of Figure 12 (main text)

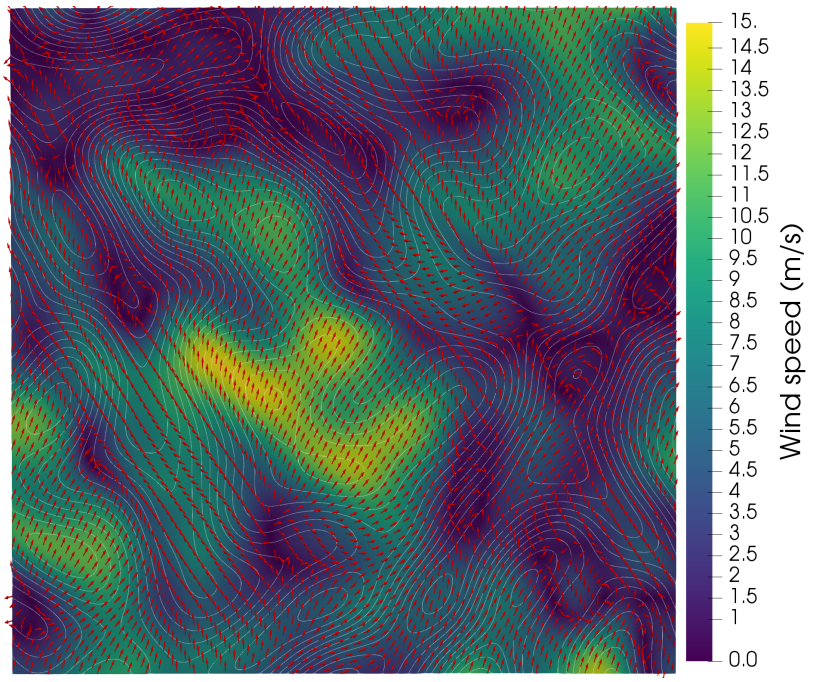

Figure 6.7: Wind field from COSMO-1, interpolated (bicubic) on a 100-meter grid, for a specific time. Background color indicates the wind speed and red arrows indicate the wind direction every 500 m. Grey lines show the 100-meter contours of the associated topography.

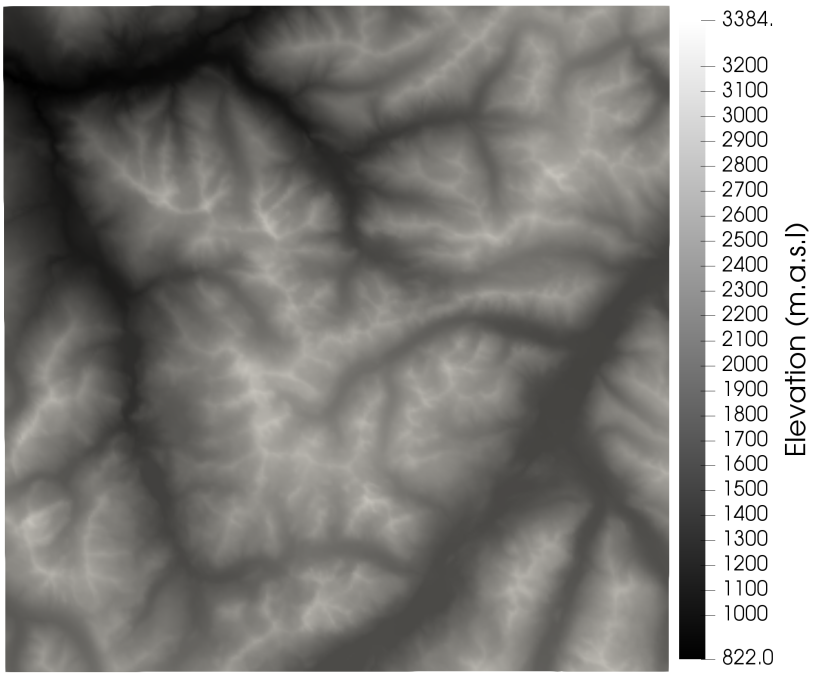

Figure 6.8: 100-meter Digital Elevation Model used by Wind-Topo covering the same domain.

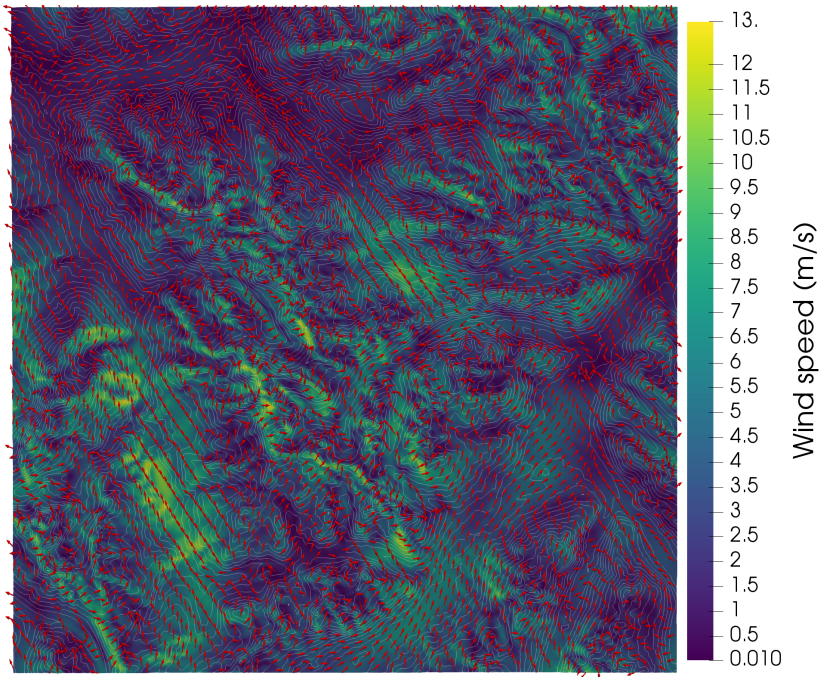

Figure 6.9: 100-meter wind field generated by Wind-Topo for the same time. Grey lines show the underlying topography (100-meter contours).

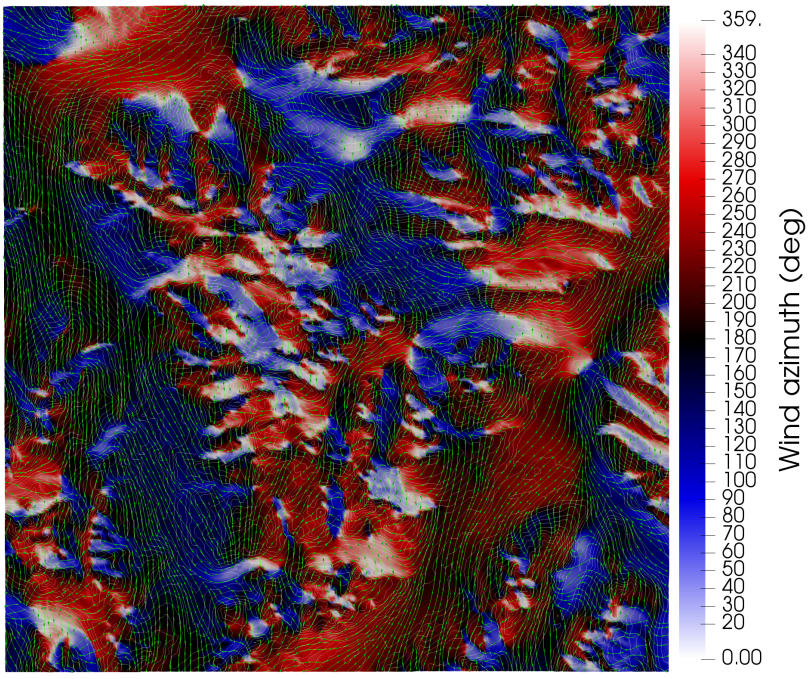

Figure 6.10: Associated wind direction (clockwise from North) with a cyclic colorscale. The green lines are the stream lines of the wind field with arrows indicating the flow direction.

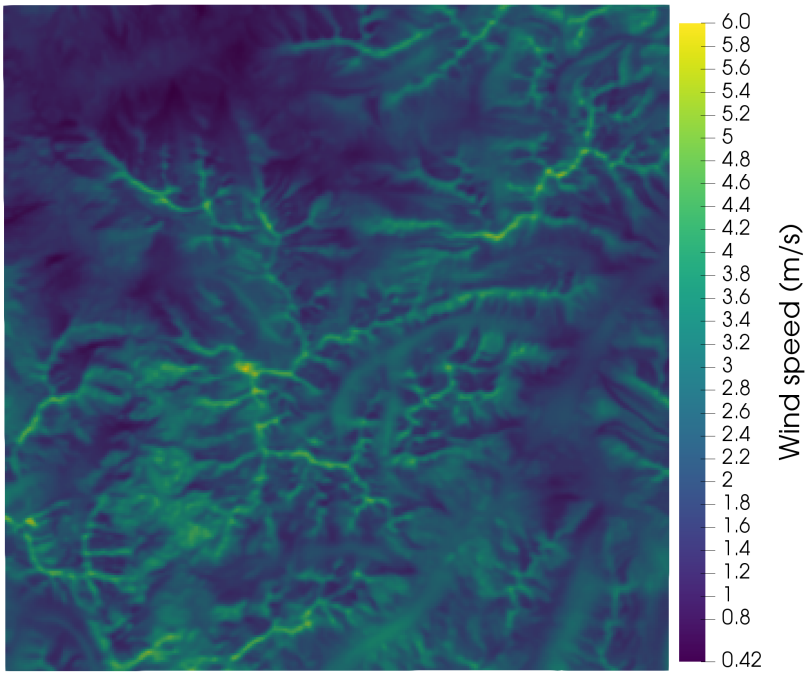

Figure 6.11: Average wind speed from Wind-Topo over the test period.

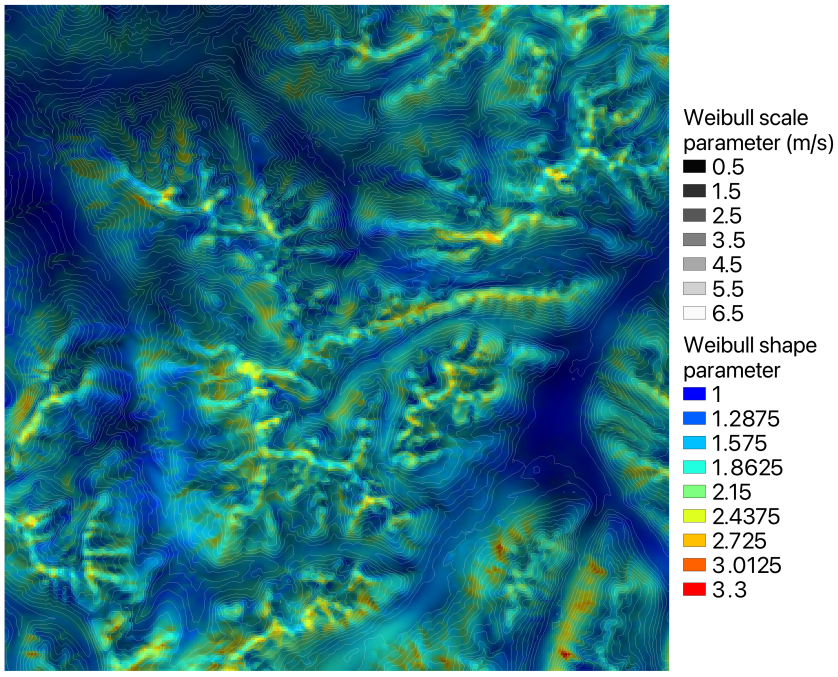

Figure 6.12: Weibull parameters of the distribution fitted on the Wind-Topo data in each pixel. The brightness indicates the scale parameter and the color indicates the shape parameter. 100-meter contours in grey show the underlying topography.

Additional panel: Fitted Weibull distributions on COSMO-1 data

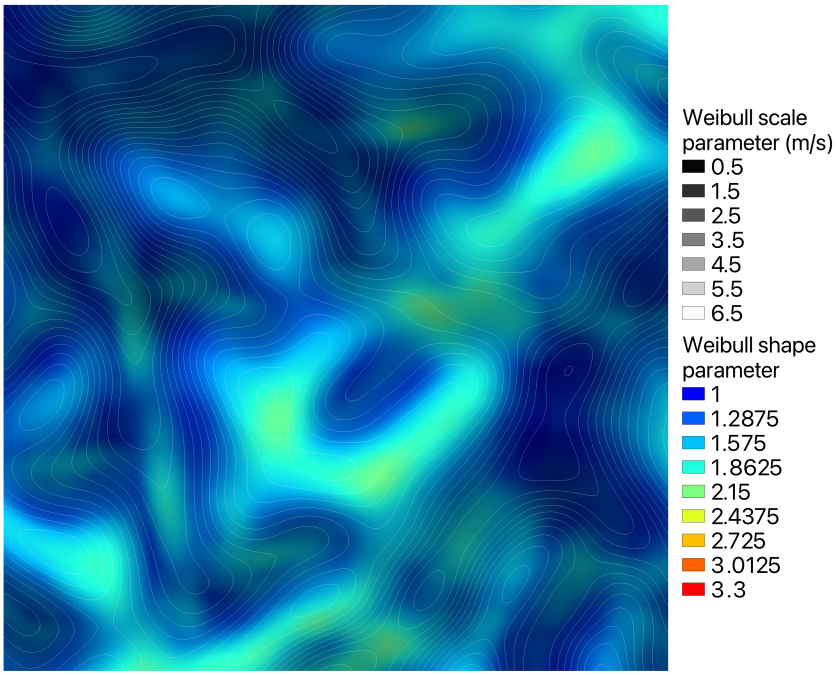

Figure 6.13: Weibull parameters of the distribution fitted on the COSMO-1 data in each pixel. The brightness indicates the scale parameter and the color indicates the shape parameter. 100-meter contours in grey show the underlying topography. To ease the comparison, the ranges are the same as in Figure 6.12

Ground-perpendicular velocity induced by the divergence of u and v fields from Wind-Topo

Wind-Topo generated the 2-dimensional wind fields depicted in Figures 6.9-6.12 for all hours of the period October 1^{st} 2016 to October 1^{st} 2017. As the wind fields are not 3-dimensional, we cannot check the mass conservation. However, we can estimate the velocity perpendicular to the ground induced by the divergence in the terrain-following field. A few assumptions are required:
i. As Wind-Topo predicts u and v at 7 meters above ground level (m.a.g.l), we assume that the flow is locally parallel to the ground, which causes a w component, with
$w = \sqrt{u^2+v^2}(-tan(slope)cos(aspect-\Theta))$, with $\Theta = atan2(v,u)$
ii. We consider a terrain following coordinate system in which the flow is described with only 2 components: $u_p = vel_p cos(\Theta)$ and $v_p = vel_p sin(\Theta)$, where $vel_p = \sqrt{u^2+v^2+w^2}$
iii. In this coordinate system, the partial derivative along x_p and y_p can be discretized using the resolutions along latitude res_y and longitude res_x and the variation in elevation between the grid cells Δz as expressed in Equation 6.1.
iv. We assume that u_p and v_p are 0 on the ground and vary linearly with height between ground and $h = 7$ m.a.g.l. This leads to the approximation of the integral in Equation 6.1.

The ground-perpendicular velocity w_p is computed as follow:

$$
\begin{aligned}
& w_p = \int_{z_p=0}^{z_p=h} \frac{\partial w_p}{\partial z_p} dz_p \quad \textit{is approximated by} \quad \frac{h}{2} \frac{\partial w_p}{\partial z_p}|_{z_p=h} \\
& \textit{where} \quad \frac{\partial w_p}{\partial z_p} = -\frac{\partial u_p}{\partial x_p} - \frac{\partial v_p}{\partial y_p} \quad \textit{is computed as:} \quad \begin{cases} \frac{\partial u_p}{\partial x_p} = \frac{\Delta u_p}{\Delta x_p} = \frac{\Delta u_p}{\sqrt{res_x^2 + (\Delta z)^2}} \\ \frac{\partial v_p}{\partial y_p} = \frac{\Delta v_p}{\Delta y_p} = \frac{\Delta v_p}{\sqrt{res_y^2 + (\Delta z)^2}} \end{cases} \\
& \qquad \textit{with the follwing quantities:} \\
& \qquad \begin{cases} u_p = vel_p cos(\Theta) \\ v_p = vel_p sin(\Theta) \end{cases} \\
& \qquad \begin{cases} \Theta = atan2(v,u) \\ vel_p = \sqrt{u^2 + v^2 + w^2} \\ w = \sqrt{u^2 + v^2}(-tan(slope)cos(aspect - \Theta)) \end{cases}
\end{aligned}
\tag{6.1}
$$

w_p was computed for each grid cell and every hour. The (temporally) averaged values are depicted in Figure6.14. The same procedure was applied to the COSMO-1 interpolated data (Figure6.15). The dominant winds are North-Westerly. As expected, the slopes exposed to such wind direction and the summits have negative average w_p values. In the terrain following coordinate system, this indicates a (lateral) divergence of the flow, compensated by a movement of air towards the ground. The opposite can be observed on the leesides. Both Wind-Topo and COSMO-1 show this behavior, but with different magnitudes. Wind-Topo exhibits small-scale higher-intensities divergence and convergence.

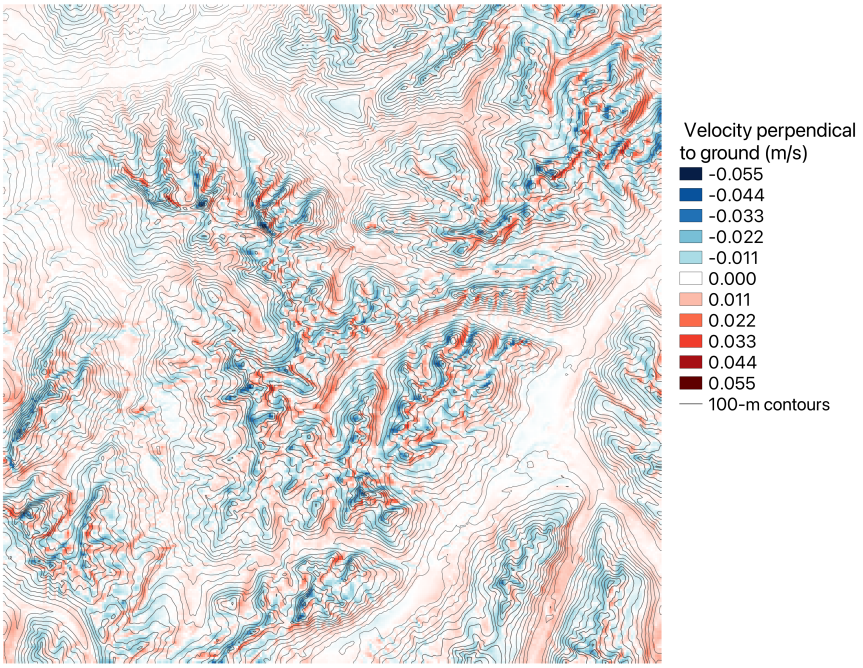

Figure 6.14: Annual average of wind velocity perpendicular to the ground w_p from Wind-Topo. Negative values indicate a motion towards the ground. 100-meter contours show the topography used in Wind-Topo.

To assess if the magnitude of w_p from Wind-Topo, which is about 5.5 times that of COSMO-1, is realistic, we applied a spatial averaging on the maps of w_p from Wind-Topo. As COSMO-1 has a resolution (before interpolation) of 1113 m, an averaging by this diameter should be applied to Wind-Topo (which has a resolution of 100 m). Using a convolution with a binary disk kernel of 11 x 11 pixels, the resulting w_p still presented features with scales smaller than the ones of COSMO-1. In fact, applying this convolution to the DEM of Wind-Topo showed that the topography used in COSMO-1 is significantly smoother than a high-resolution DEM down-scaled to 1113 m. For numerical stability, COSMO-1 uses an additional smoothing of the low-resolution topography to avoid slopes larger than 30 °. To obtain a topography that resembles the one of COSMO-1 from the DEM of Wind-Topo, a kernel of 23 x 23 is necessary. Figure6.16 was obtained by applying such kernel on w_p from Wind-Topo, and the contours show the associated topography. We can observe that the magnitudes and patterns of w_p are comparable between COSMO-1 and the spatially-averaged Wind-Topo. This analysis reveals that the divergence and convergence areas in the fields generated by Wind-Topo are realistic, in terms of magnitude and location.

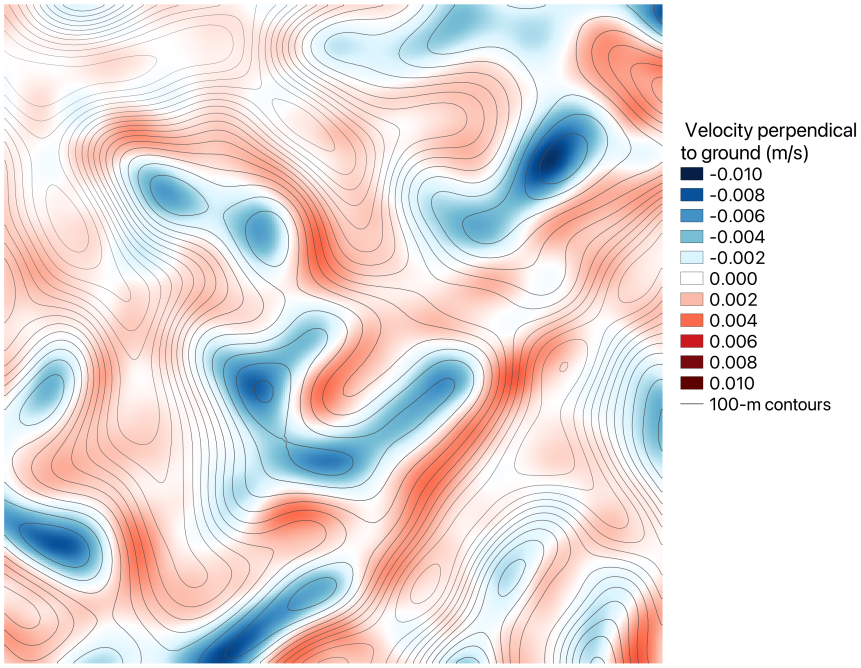

Figure 6.15: Annual average of wind velocity perpendicular to the ground w_p from COSMO-1. Negative values indicate a motion towards the ground. 100-meter contours show the topography of COSMO-1.

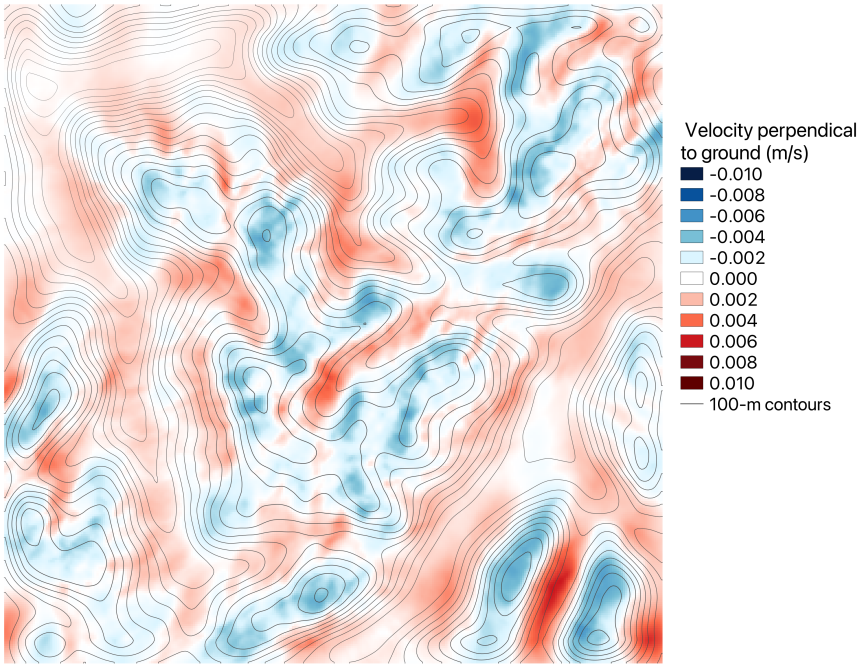

Figure 6.16: w_p from Wind-Topo after a convolution with a binary disk kernel of 23 x 23 pixels. Negative values indicate a motion towards the ground. 100-meter contours show the topography used in Wind-Topo after the same convolution.

Summary, Conclusion and Outlook

Summary and conclusions

Synergy between renewable sources

The first two parts of this thesis investigate the behavior of the Swiss electrical system under various scenarios for the replacement of the five Swiss nuclear reactors by renewable energy. If Switzerland maintains the decision to phase out nuclear energy while being carbon neutral by 2050 without largely relying on the neighboring countries for its electricity supply, the required installation of photovoltaic (PV) panels or wind turbines will be a prodigious endeavor. Even if only the best locations for such generators are used, more than 100 km^2 of PV panels or more than 5000 wind turbines will be needed. Those nature-driven generators bring multiple complications into the electrical system which have to be addressed to ensure a secure supply of electricity. The complex topography of Switzerland is responsible for a strong variability of the renewable sources across comparably short distances. This variability imposes the use of spatially distributed models with a high resolution, but can also offer some complementarity between the sources.

As a first step, with the hypothesis that the electrical grid does not strongly influence the dynamics of the whole system, the results presented in Appendix A show that wind energy provides a better complementarity with the storage hydropower system and can contribute to a much lower seasonal imbalance between electricity production and consumption. Part I and Part II describe how this hypothesis is tested with the electrical grid, and show that an optimized generation mix and placement scenario can lead to a more balanced system. If Switzerland continues its organic growth of PV installations in urban centers, the seasonal imbalance will increase drastically compared to current levels. In Part I, PV panels are installed in urban areas with a geometry (tilt) optimized for maximum annual production (39°), and this leads to a doubling of the seasonal imbalance. In Part II, a more constraining assumption is used for the urban panels: As currently required by the law, except for flat roofs, the panels must be installed with the same inclination as the roof, which is on average 23° in Switzerland. In this case, a scenario where nuclear is replaced by such panels causes the seasonal imbalance to increase five-fold because of the extremely low productivity of such installations in winter.

Regardless of the chosen scenario, this imbalance will have to be compensated with large amounts of imports in winter and large exports or curtailment in summer because no currently available storage technology can provide seasonal storage at that scale. However, an optimized generation mix from PV panels and wind turbines located in specific places can greatly change this dynamic. Part II shows that a mix of 75% wind and 25% PV located in the mountains is ideal to work in synergy with storage hydropower in order to limit the cross-border exchanges. The optimization scheme takes advantage of the spatial variability in solar and wind energy and considers the electrical grid and the land use. The result is promising as it keeps the seasonal imbalance to the current nuclear-based level, thus preventing the five-fold increase mentioned previously.

Concerning the electrical grid, it is remarkable to see that the current transmission grid is already well suited for a large deployment of renewable generators. In Part I, it is found that the frequency of high line stress events is slightly decreased in the fully renewable (urban PV) scenario than in the nuclear scenario. This is however different in Part II, as the optimization model tries to place as much generation from PV and wind as possible in specific areas that have a high yield in winter. The model pushes the grid to its limits. Compared to an optimization where the grid limitations are removed, a large amount of wind turbines in Jura (3 GW) cannot be installed because of grid congestion and have to be relocated. Despite this limitation, the current grid can accommodate 40% of the 4400 suggested wind turbines in the Jura mountains. With multiple high-capacity lines connecting storage hydropower to urban centers, the Alps could host a large number of new renewable installations. When the sun shines or the wind blows, those lines could transport solar and wind energy while hydropower saves its water for other less productive times.

Alpine PV installations have a bright future because they offer multiple advantages compared to conventional urban installations. From a system perspective, PV panels installed at steeper angles at high elevation can provide an advantageous production profile that is enhanced in winter while losing no or only little annual production. Appendix B shows that such installations are also potentially very profitable, with up to 33% more revenue than urban installations. For wind energy, high elevation is also desirable as winds are on average stronger. Given the weather regimes in Switzerland, winds on mountain ridges are also stronger in winter. The high share of wind energy and mountain placements discovered in Part II are based on the numerical model COSMO-1 used by the Swiss weather forecast which, as shown in Part III, provides accurate estimates on mountain tops and not too complex topographies. Consequently, the dynamics of the whole system with the suggested large installations of wind turbines in the smooth Jura mountain range and in the pre-Alps are expected to be quite accurate. The wind energy potential in the Alps is more uncertain but could nevertheless be of high value for the energy transition. If high shares of wind energy have to be installed in Switzerland, social acceptance, especially in areas like the Jura, will be critical. Shifting a large part of the suggested wind turbines to more remote alpine areas could be a solution to a more

socially acceptable scenario. Such placements cannot, however, be accurately identified with COSMO-1.

Towards better estimates of alpine wind energy

Part III introduces a new method to downscale near surface wind fields from a relatively coarse resolution model (COSMO-1 in the Swiss test case). This downscaling is capable of generating gridded wind speed and direction with a 50-meter resolution. The main idea consists in finding the statistical relationships between: the state of the atmosphere as described by COSMO-1 around measurement stations, the topography at high-resolution, and the observed wind speed and direction. A deep learning approach was chosen, and the model is trained on 261 stations located in Switzerland. This new model, called Wind-Topo, adopts a 2D-to-point approach, where the predictors are 2D fields of several variables from the input model (COSMO-1). Using multiple convolutional neural networks that can treat the multiple input variables at various scales and resolutions, Wind-Topo predicts the horizontal wind vector at the center of the input domain. The high-resolution topography is provided to the model through several descriptors that were specifically developed to allow the prediction of a wind vector on highly complex terrain. To obtain good scoring metrics and accurate distributions of wind speed, a custom loss function was developed. Wind-Topo is validated at 60 stations that were not used during training, and shows good agreements with respect to observations. Compared to a standard bicubic interpolation of COSMO-1 at the validation sites located in the Alps, Wind-Topo reduces the bias from 0.72 m/s to -0.07 m/s, while reducing the mean absolute error from 1.77 m/s to 1.21 m/s. Even more importantly for an application in wind energy potential assessment, the distributions of the wind speeds predicted by Wind-Topo are very close to the measured ones. The model improves the prediction of wind speed and direction at almost all stations and for all times of the year. The generated wind fields also exhibit realistic orographic effects like deflection, sheltering, and ridge acceleration. So far, this new model has not been used to compute wind energy potentials but its efficiency already allows us to generate long time series of near surface wind speed and direction (2 years, hourly) for 350 000 locations in about three weeks on a standard 2-GPU machine. This number of locations approximately corresponds to all the areas identified, in the geographical analysis of Part II, as potential locations for wind turbines in the pre-Alps and in the Alps with a 100-meter granularity.

Limitations and Outlook

The modeling of a system as complex as the electrical grid and power generation for an entire country entails many simplifications and is often constrained by the availability of data. The spatially distributed model described in Part I has several such limitations. From a grid perspective, only the transmission lines (voltage > 150 kV) are represented because an homogeneous and comprehensive dataset describing the smaller distribution lines is currently

not available. This lack of information has two major consequences. First, several nodes in our transmission grid model are in reality linked by additional lower voltage (distribution) lines that we don't model. They alter the flow of current through the whole grid, compared to what our model predicts. Second, we considered that all power generation can be injected into the transmission grid without further restriction than what this grid imposes. Many small renewable generators would in fact be connected to the distribution grid, which would inject the production into the transmission grid. Thus, within each region surrounding our (transmission) grid nodes, we used a copper plate assumption, where electrical power can be transferred without any restriction. This assumption is used for the auto-consumption within these areas and for connection to the transmission grid. The characteristics of the distribution grid would certainly impose some strong limitations to the scenarios explored in Part I, and Part II. For those scenarios to be realistic from a electrical perspective, the distribution grid would probably have to be upgraded in some locations.

As various results of this thesis suggest, storage hydropower (and pumping) has a central role to play if large shares of PV and wind energy have to be installed. How it is operated will have major consequences on the integration of new renewables in the electrical system. In our case, hydropower was used as a facilitator to this new power generation. The buffering capacity of the hydroelectric reservoirs was used to decrease the seasonal imbalance as much as possible, and turbining / pumping was performed to reduce the fluctuations in solar and wind energy. In reality, the electricity market (and some regulations) dictates how those power plants are operated. Consequently, models that integrate this market can be considered more reliable. To be accurate, such models have to simulate the entire market, and thus the entire European grid in our case. This, in turn, implies multiple simplifications that can also lead to inaccuracies. Furthermore, as markets are strongly influenced by political decisions like subsidies and carbon tax, it is very difficult to predict what the electricity market will look like in a few decades. Both approaches that include the market or not reveal important dynamics of the system and should be used jointly to guide the political agenda.

As mentioned previously, Wind-Topo predicts wind speed and direction close to the ground. Those predictions thus need to be converted to power generation from wind turbines. The wind speed at 7 meters above ground needs to be converted to a vertical profile of wind speed that covers the swept area of the turbine. This is particularly challenging in complex terrain, where the standard log-law is not always valid, even under neutral atmospheric conditions. For turbines located in the Alps, many other atmospheric disturbances like turbulence or icing will also have a strong impact on the power generation. As a first next step, the outputs of Wind-Topo will be converted to wind speed at the height of the wind turbine's hub using information about the state of the atmosphere in COSMO-1. Electrical power will be obtained from the turbine's characteristics. This will be performed for a large number of potential locations in Switzerland, which will be used by OREES (Part II) to optimize the number of turbines and their locations. The updated results will be compared to what was obtained with

COSMO-1 and will show to which degree the system is impacted by the quality of the wind power data. Various models of turbine will then be used by OREES, first manually and them optimized for each location.

This thesis focused on wind energy as a key player in the energy transition in Switzerland. Despite its advantages, many challenges remain to be addressed such as social acceptance, economic competitiveness, land use, and landscape protection. All the simulations were based on current electricity consumption, and it is important to keep in mind that electricity represents only a quarter of the energy used in Switzerland. Two competing factors will strongly influence the evolution of electricity consumption. On the one hand, electrification of many sectors like transportation and heating will significantly increase the consumption. On the other hand, improvements in building insulation, industrial processes, and the use of more efficient appliances can counterbalance, or at least can moderate this increase. New technologies for energy storage and for synthetic fuels, and biomass are also expected to provide solutions for the energy transition.

A Interplay between photovoltaic, wind energy and storage hydropower in a fully renewable Switzerland

Interplay between photovoltaic, wind energy and storage hydropower in a fully renewable Switzerland

Jérôme Dujardin[1], Annelen Kahl[1], Bert Kruyt[1,2], Stuart Bartlett[1,3] and Michael Lehning[1,2]

[1] School of Architecture, Civil and Environmental Engineering, École Polytechnique Fédérale de Lausanne, Lausanne, Switzerland

[2] WSL Institute for Snow and Avalanche Research SLF, Davos, Switzerland

[3] Earth Life Science Institute, Tokyo Institute of Technology, Tokyo, Japan

Abstract

As part of its ambitious long term energy strategy, Switzerland plans to phase out nuclear power production and replace most or all of its significant share of national electricity production (40%) by renewables, in particular by photovoltaics (PV) and wind energy. The existing large fraction of hydropower and significant pumped-storage hydro capacity in the mountainous regions of the country will potentially provide valuable balancing and ancillary services for the management of intermittent production from PV and wind. We present a set of calculations based on data from the current Swiss electricity system, which investigate the effect of different PV-wind mixing ratio scenarios on required import and export from foreign neighbors. It is shown that the current hydropower is a good basis to deal with intermittent energy sources and to keep import rates of electricity at current levels in a fully renewable Switzerland as long as the PV-wind ratio is small. For higher PV-shares, forced export and import will increase but appear acceptable if PV-contribution stays below 0.6. Enlargement of reservoir capacity or oversizing of intermittent renewables can further reduce required import effectively. These findings are quantitatively specific for Switzerland but qualitatively transferable to similar mountainous environments with abundant hydropower resources.

Keywords: renewable energy, photovoltaic, wind, hydropower, balancing, intermittency

This chapter was published in the journal *Energy* on September 15^{th} 2017, in the volume 135, pages 513-525.
doi: http://dx.doi.org/10.1016/j.energy.2017.06.092

J.D developed the idea and the model, performed the simulations, analyzed the results, and wrote the paper with A.K.

A.1 Introduction

Renewable generation of electricity is one of the major milestones in Switzerland's roadmap towards their 2050 Energy Strategy. By that time all existing nuclear power plants will have been decommissioned and the targeted 60% reduction in the country's CO_2 emissions will limit the installation of fossil fuel plants (25). With a large share of variable power generation from renewable sources such as wind and solar, it becomes increasingly important to carefully proportion the energy mix in order to maintain efficient and reliable production (1; 23). While on an annual average scale the production potential from renewables may be sufficient, even well-adapted designs will not be able to perfectly match the demand at every instant. The remaining mismatch has to be compensated for by dispatchable power generation and storage, or by import and export with neighboring countries. An oversized generating capacity can also help alleviate the problem (9).

It is a highly non-trivial optimization problem to discern which combination of these measures will be the most advantageous. Hence it is our goal in this paper to systematically analyze the interplay between mixing ratio, oversizing of wind and photovoltaic (PV) generation, sizing of storage, and the resulting required import and export. This investigation was conducted in the spirit of similar work performed for other nations (2; 10). Similar to these studies we consider Switzerland in the present work as a copper plate with unconstrained transmission capacity and without any power engineering limitations. Hence all generation, consumption and storage is aggregated, which of course is a simplification. But, given the dense infrastructure that is already in place, not a completely unrealistic one. Our next paper will address the potential limitations in the electrical system that might be encountered as a result of development of PV and wind energy in Switzerland. The choice not to integrate the electrical constraints in this study allows us to solely focus on the natural resources, which should be done in isolation. Electrical constraints are soft constraints that could be adjusted, while the natural resources are hard constraints, which represent the absolute limits of what is available and possible.

The results of our analysis will inform decision-making for the future mix of renewable electricity production for Switzerland with its unique set of boundary conditions. This country is in the privileged position of already having more than half of its electricity needs provided by renewable hydropower. In mostly or fully renewable future energy scenarios, this would provide an essential balancing capacity, when timed and distributed in accordance with the intermittent production from wind and solar power. Our analysis may be generalized to other countries with similar boundary conditions such as Austria, or smaller countries in other mountain ranges such as the Himalayas or the Andes.

A.1.1 Mixing ratios of wind and solar

Currently about 40% of Switzerland's electricity demand is covered by nuclear and fossil fuel production and this is the portion that will have to be replaced by newly installed renewables. The combination of solar and wind energies has been studied for other countries (4; 3; 11; 19;

30). Depending on the characteristics of the available renewable resources and on seasonal trends in demand, the optimal mix of a renewable portfolio can vary strongly from country to country. In countries with a high use of air conditioning (e.g. Brazil, parts of the U.S.), PV is an ideal source of electricity because its production correlates in time with demand (in the middle of the day and in summer) (4). If cold temperatures lead to peak energy consumption, then wind production profiles are more aligned with demand (30). However, both wind and solar have a high level of variability and solar is of course completely absent during the night.

The two sources also display pronounced spatial correlation patterns (8; 6), presenting both risks and opportunities in terms of management. Spatial decorrelation can be exploited to produce a more stable supply (14). In general however, the variability of intermittent renewable resources does not correlate with demand, resulting in mismatches that require efficient mitigation. Previous studies have found that a mix of different production types and a wide spatial distribution can provide a certain degree of smoothing (11; 30). The present work investigates in detail how the proportions of wind and solar in future Swiss energy mixes affect the resulting required import and export. We also explored the role of storage hydropower in power and energy balancing. Currently the installed capacity of wind and solar power production generates only 0.11 TWh and 1.12 TWh per year (2015) respectively, which accounts for 0.18% and 1.79% of the country's demand. In fully renewable configurations, these values will have to go up drastically to cover approximately one third of the country's electricity consumption. It is therefore essential to understand which combination of generators would generate the most advantageous production profile. A similar question has been addressed by (23; 9; 10), but at a European scale.

A.1.2 Import/export

To set the stage for this analysis we must first define the term "required" import and export. For 2014 Swissgrid reported an annual total import of 28.12 TWh and a total export of 32.46 TWh. These numbers include the large volumes of electricity that traverse Switzerland, highlighting its important role as a central European transit country. The total transit energy in 2014 was 25.03 TWh. Subtracting it from the annual import and export yields a net import of 3.09 TWh and a net export of 7.43 TWh (see section A.2.1.1).

Those values are themselves a combination of a) the required and b) the economically driven import/export. The economically driven import/export is a result of electricity prices varying over short time scales. Due to the large proportion of storage hydropower, which acts as a buffer, Switzerland has the leisure to delay import to moments when it is least costly. Correspondingly it can overproduce and export at times when electricity prices are high. This advantage is not only used to compensate for overproduction and power deficits, but also to generate profit. However, modeling and predicting this market behavior is beyond the scope of the present work. Since we are trying to capture the available resources and their temporal behavior, we consider only the volume of import and export that is necessary to balance

the Swiss internal production with demand. We will refer to those quantities as “required import” and “required export”. With about 25 TWh for 2014, the described transit represents a considerable portion of the total energy transmitted by the electrical network. This amount includes the electricity that traverses Switzerland from producing to consuming countries and represents the balancing role that Switzerland plays within the European market. As renewable - and thus intermittent - energy production increases, this balancing role will become even more crucial, and the portion of the transmission line capacity dedicated to it will have to grow. With this perspective, the self-sufficiency of the Swiss electricity system, i.e. keeping required import low, is of great importance. We will discuss the potential impacts of the European electrical system on our results in section A.4.

A.1.3 Selected scenario

In 2015, 2 nuclear reactors from the Beznau Swiss power plant were shut down for the entire second semester. In addition, precipitation was particularly low during fall. Those two events resulted in an abnormally low water level in the reservoirs at the end of the year and a storage hydropower annual production that was above average. Thus, we decided to use the year 2014 in our investigation, which shows more typical values for demand and production. During that year, the total demand was 61.79 TWh, the run-of-river (RoR) hydropower plants generated 17.24 TWh, storage hydropower plants generated 19.71 TWh (in addition to 0.24 TWh of surplus in the reservoirs at the end of the year) and the nuclear and fossil fuel power plants generated 30.33 TWh (26). For that particular year, the total production exceeded demand by 5.49 TWh which equals the annual surplus of export. In addition to the detailed analysis of 2014, we also describe the inter annual variability for the time period 2009-2015 in section A.3.4.

For the present work, focused on 2014, we replace the electricity production from nuclear and fossil fuel by a combination of PV, wind and geothermal energy, which must produce 24.59 TWh. With this production level, the annual production would equal the annual demand and there would not be any surplus of export. The Swiss Energy Strategy 2050 targets an annual geothermal production of 4.4 TWh. Assuming this or any other kind of base load leaves 20.19 TWh of production to PV and wind.

A.1.4 Outline

In this paper we intend to answer the following question: Given the optimal use of available balancing capacity from hydropower, how does required import and export of electricity change as a function of the ratio between solar and wind power generation in a hypothetical, fully renewable Swiss power system? And secondly: How does the addition of storage or oversizing the generating capacity alter this functional dependence?

The paper consists of the following sections: in section A.2 we outline the numerical methods used to carry out our energy computations. We then present our main results in section A.3

including graphical illustrations of storage energies and import/export requirements as a function of the key parameters of the system. In the final section we conclude that, within the framework of our study, a fully renewable Swiss power system is indeed highly feasible. What remains to be decided is the exact combination of oversizing renewable capacity, increasing storage capacity, or increased imports, to ensure a constant and reliable electricity supply.

A.2 Methods

A.2.1 Data

A.2.1.1 Electricity demand, import and export

We use a 15-minute time series of electricity demand (annual total of 61.79 TWh) as a time reference and compute all other datasets at exactly those time steps. This means that all hourly and monthly time series described from hereon are interpolated to generate 15-minute time series matching the one of the demand. The 2014 data for demand, import, export and transit were sourced from the Swissgrid website (28). As mentioned above, the net annual import and export amount to 3.09 TWh and 7.43 TWh.

Figure A.1 displays the net exchange at every time step (export minus import) in blue and the cumulative net exchange in red throughout the year in question. The cumulative exchange shows an increasing deficit that peaks around the end of March, followed by a surplus peak centered in mid-December. The deficit represents the import-dominated exchange in winter, when local production is low and demand is high, while the surplus results from export-dominated exchange during summer when the hydropower production is high and demand is low.

The accumulated energy deficit during the period from January 1st to the deficit peak and from the excess peak to the end of the year corresponds to the amount of import that is required to balance the energy deficit of 2014. It amounts to 2.2 TWh.

When we combine the import and export into a single time series (blue curve of Figure A.1), we can subtract the mean value and shift the data such that total import is made equal to total export. This results in a total of 5.07 TWh for both import and export, similar in effect to a reduction (about 500 MW or 14%) of the steady base load provided by nuclear and fossil fuel plants. In this situation the required import represents 3.5 TWh. This value agrees with the one computed in section A.3.3.1. The time series of import and export also show us that the peak power of import plus export reaches a value of 12 GW. Hence we conclude that the combined capacity of all transmission lines between Switzerland and the neighboring countries amounts to at least this value, and is likely higher.

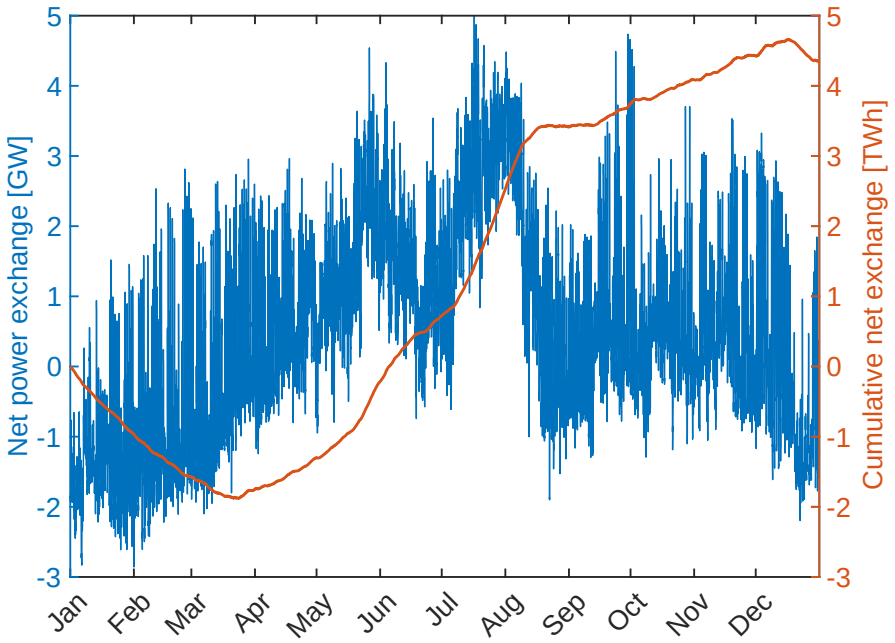

Figure A.1: Net electricity exchange (export minus import) at a 15-min time step from Switzerland to neighboring countries in 2014 (blue line). The red line shows the cumulative sum of the net exchange, which is positive at the end of the year implying an overall electricity surplus for that year.

A.2.1.2 Electricity production from solar power

The electricity production from PV that we use in this work was calculated from satellite-derived irradiance data provided by MeteoSwiss. The imagery is captured by the spinning enhanced visual and infrared imager (SEVIRI), which is installed on MeteoSat satellites and has been operational since 2004. Based on hourly reflectance data, a cloud cover factor is derived and applied in radiative transfer calculations to estimate the amount of shortwave radiation that reaches the surface of the earth. The spatial resolution is 1 arc second which corresponds to approximately 1.6km x 2.3km over Switzerland.

Considerations of local topography account for shading and reflection, and special attention is given to potential misclassification of snow as clouds. (17) describes the processing steps in more detail. To convert the irradiance data into power production, we need to assume a spatial distribution of PV installations throughout the country, as well as their installation geometry. As a simple first approach we scale and distribute the total surface area of PV panels in line with population density (data sourced from (27)), and place enough PV panels to generate the desired annual target. This approach assumes that panels will be primarily placed on rooftops and it thus attempts to spatially associate electricity production with demand centers. Given the high population density and the land protection in Switzerland, this siting scenario seems to be the most probable, at least under current legislation. Moreover, Swiss law requires

PV panels to be mounted directly onto the roof and thus prohibits any solar tracking or tilt adjustments during the year. Our current research shows that siting, geometry and addition of tracking or tilt adjustments can partially alleviate the seasonal mismatch. This will be the subject of our next publication that will also incorporate the limitations imposed by the transmission grid.

Hourly global irradiance is calculated for 6 different panel orientations from southwest to southeast at an optimal tilt angle (39°) for Swiss latitudes. We assume equal panel area for each of the orientations and scale the surface area to generate 1000 time series with a national annual production target between 0.02 and 20.19 TWh. In the conversion from W/m^2 of solar irradiance to electricity we assume an efficiency of 15%.

To verify whether the installed surface area stays within reasonable bounds, we plotted the Swiss-wide percent coverage for the case of maximum installed PV capacity. A handful of spatially isolated pixels would require unrealistically high coverage. But since there was enough surface available in the immediate surroundings and since spatial correlation of solar energy is much higher than the pixel-size (30), we assume that minor dispersion around the over-charged pixels will not result in detectable changes in electricity production.

This siting scenario, generating 20.19 TWh in 2014, would require a total PV surface of 95.06 km^2, which corresponds to an installed capacity of 14.26 GW (assuming 15% efficiency at 1000 W/m^2 of irradiance). With an average installation cost in Europe of $1.41 per Wpeak (see p.83 of (29)) the 100% PV scenario would need an investment of $20.11 billion. In the following paragraph, we will compare this value with the equivalent investment for a 100% wind scenario.

A.2.1.3 Electricity production from wind power

To compute potential wind power time series for Switzerland we use wind speed data from 117 measurement stations from the Swiss weather service MeteoSwiss (18). We select stations that are below 2500 m.a.s.l. and have sufficient data for the year 2014. Switzerland has a high fraction of mountainous terrain, which influences meteorological parameters (and especially wind speeds) to such an extent that coarse resolution weather model data is thought to be inaccurate for wind power assessment (13). Other statistical methods such as the recently updated Swiss wind atlas use statistical interpolation of measurement data combined with CFD modeling to estimate mean wind speeds (24). However, as our method requires time series, we used measurement data, which, although lacking the spatial coverage of modelled data, has the advantage of capturing the terrain induced variability such as valley winds and katabatic flows.

Missing data is filled in using data from other years, using the software package Amelia (12). Power is calculated based on the power curve of an Enercon E82 2-MW turbine, which is common in current Swiss installations. We correct for reduced yield at altitude due to lower air

density, and transform the measured wind speeds at 10m up to the hub height of 80m using a simple power law. Although the wind shear coefficient is acknowledged to vary significantly and thus influence the power yield (15; 5), for lack of better parametrization, we used the common rule of thumb value of 0.14.

As a result, 1000 composite wind power time series were calculated for each annual national production target between 0.020 and 20.19 TWh of wind power. The number of locations used to satisfy each target scales linearly from 15 in the first step to 117 in the last. The relative contribution of each station to the national series is weighted by the station's relative potential, meaning better locations contribute more. Then the selected locations' capacities are scaled to meet the desired annual target. This methodology is designed to mimic the dynamics of wind farm siting where the most productive locations are used first and less productive locations are gradually included as penetration of wind power increases.

A notable shortcoming of this method is the fact that at high penetration rates, certain locations may see more installed capacity than is feasible. However, as assumed for PV placements, it can be argued that similar locations exist close by and the estimates are reasonable. For higher penetration rates (especially those approaching 20.19 TWh of annual production) the spatial dispersion is likely underestimated. In view of current potential estimates (4.2 TWh in 2050 (22)), these results at the upper end of the wind power production scenarios should be interpreted as conceptual in nature rather than as viable expansion scenarios. Reliable calculation of the actual wind power resource of Switzerland is an ongoing line of research that is beyond the scope of the present work.

A sensitivity analysis was performed by running a second wind siting scenario, where the total capacity was distributed equally over the included locations for each series. Although this resulted in a slightly higher variability in the national wind series due to the less stably producing locations contributing more, the effect on the overall result, albeit visible, was marginal.

The 100% wind scenario, generating 20.19 TWh in 2014, would require the installation of 6536 wind turbines of the 2-MW model cited previously. This amounts to a total installed capacity of 13.07 GW, for a total cost of $20.26 billion, given the current cost of $1.55 per Wpeak (see p.81 of (29)). Even if the estimation of this cost, as well as the one of the 100% PV scenario, is in reality a much more complex task which is beyond the scope of this paper, it appears that both of the 100%-scenarios would require a similar investment for a similar lifespan of 20 to 30 years. Thus, all intermediate scenarios will also cost about $20 billion. It is important to put this amount into perspective with the current technology used in Switzerland: the nuclear energy. The new generation of nuclear reactors installed in Europe (which could replace a considerable part of the current nuclear fleet) is the EPR reactor from AREVA. It generates an electrical power of 1650 MW and has a capacity factor of 90%, which means an annual production of 13 TWh. Our 20.19 TWh scenario would thus require 1.55 times the production of an EPR reactor. Given its current construction cost of $9.6 billion, this would

scale up to $14.88 billion for our production target. For several reasons this price is not directly comparable to the $20 billion of our renewable PV and wind fleet. Firstly, the nuclear reactor has a lifespan of more than 60 years, while the PV and wind infrastructures would only last between 20 and 30 years. Secondly, the nuclear energy requires a combustible that is not freely available. And lastly, nuclear power plants do not just generate electricity, but also heat, which is not the case for PV and wind. It is still interesting to see that the installation costs for the fully renewable scenario outlined in our paper are not much higher than for the nuclear technology it is supposed to replace.

A.2.1.4 Electricity from run-of-river and geothermal energy

To constrain the number of variables of our investigation, we consider the power generation from run-of-river (RoR) power plants and geothermal energy to be non-dispatchable, even though they do offer some balancing capacity. For most plants, the RoR generated power shows strong intra-annual variation because of seasonal trends in precipitation and snowmelt. We use the 2014 monthly electricity production values of Switzerland's RoR power plants (sourced from (26)) that we interpolate to get a data series matching the timesteps of the demand. This time series is depicted in green in Figure A.2. The annual production amounts to 17.24 TWh.

The power production from geothermal energy is considered as a constant base load of 502.28 MW (annual total of 4.4 TWh), which corresponds to about 7% of the annual national production, in line with the targets of the Swiss 2050 Energy Strategy (25).

A.2.1.5 Electricity production from storage hydropower

Switzerland has a large and complex storage hydropower system, composed of 125 power plants with a power above 300 kW (capable of turbining, pumping, or both) (21). This results in a combined capacity of 10.42 GW. If we include the capacity of the Nant de Drance and Limmern power plants that are currently under construction (see section A.2.1.6), the maximum capacity rises to 12.32 GW. The power plants are connected to over 200 reservoirs and lakes via a complex network of tunnels. In this work, we consider the storage hydropower system as a single, lumped, dispatchable generator connected to a single reservoir with an available capacity of 6.29 TWh. This value was derived from the difference between the minimum and maximum energy stored in the reservoirs in 2014 (20).

The storage hydropower system receives energy from the precipitation that reaches the reservoirs by gravity or pumping. In this paper we separate those two such that the energy generated by our lumped hydropower plant comes only from the energy inflow into our single reservoir that does not require pumping. The pumping part is described in section A.2.1.6. The inflow to the reservoir is computed from the monthly time series of net production of national storage hydropower (after subtracting consumption from pumping) (26) and from the weekly time

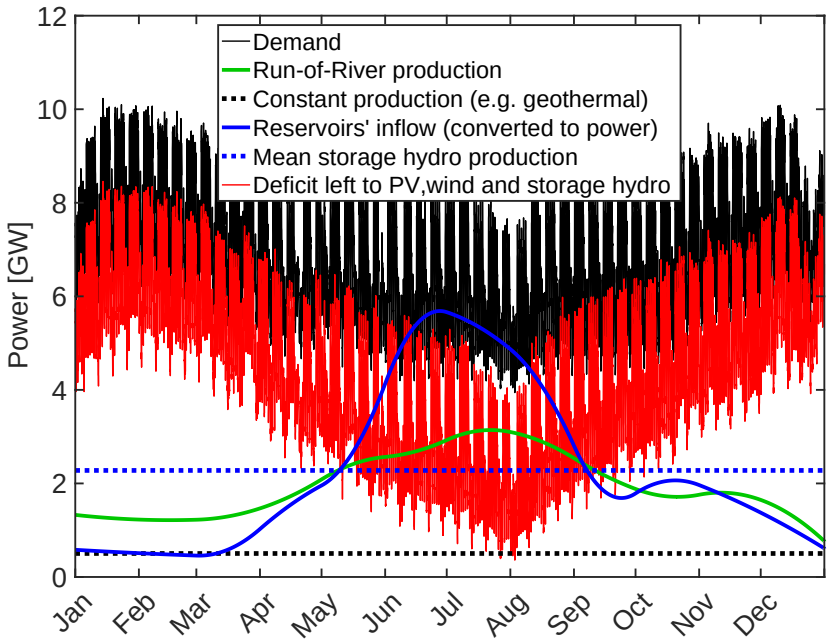

Figure A.2: Time series of all relevant variables shaping our analysis for the year 2014.

series of the national energy stored in the reservoirs (20). We interpolated these to generate a 15-minute time series of power inflow into the reservoir (blue curve in Figure A.2). The annual sum amounts to 19.95 TWh, which is equal to the annual production from storage hydropower used in our investigation.

A.2.1.6 Electricity storage from pumped-storage hydropower

Switzerland already has several pumped-storage (PS) installations, and 2 major plants (Limmern and Nant de Drance) that are still under construction, due to be commissioned in 2017 and 2019, respectively. Their pumping powers of 1 GW and 0.9 GW, respectively, will more than double the existing capacity to a total of 3.56 GW (21). Since we aim to provide a window on a future renewable Switzerland, we include them in our analysis.

Each PS plant is connected to an upper and a lower reservoir and the volume of energy that can be stored is limited by the water available in the lower reservoir and by the free volume in the upper reservoir. If we consider each PS unit to be a closed system, we can estimate the stored energy capacity from the elevation difference and the volume of the reservoirs. The total energy that can be stored before the upper reservoir is full or the lower reservoir is empty amounts to approximately 440 GWh. This value only describes what could be stored if we were dealing with a completely closed system. In reality the reservoirs receive external water from precipitation and snowmelt, that provides energy on the one hand, but also occupies

some of the storage space. Hence it is difficult to assign an exact number.

A more realistic and useful value is the amount of energy that PS plants can accumulate and deliver in a daily cycle. We will show that this could compensate for the majority of the mismatch between demand and intermittent production from PV and wind (see section A.2.2.2). If we consider an efficiency of 88% for both pumping and turbining, the round trip efficiency of this storage system is 77.5% (as an average of existing facilities, (16; 7)). Given this value and the assumption that pumping and turbining powers are equal, we can compute that it takes 13.52 hours of pumping and 10.48 hours of turbining to transfer equal amounts of water between the reservoirs during one daily cycle.

Comparing the volume of water that a plant can pump per hour with the volume of its two reservoirs yields the number of hours of consecutive pumping that this plant can sustain. For all Swiss PS units this value lies above 13.52 hours. Hence size is not a limiting factor for any of the reservoirs in the estimate of maximum energy accumulated per day. Consequently, the amount of energy that can be stored during a daily cycle is only a function of the pumping power and the amount of pumping time. The Swiss fleet of PS installations can absorb 48.13 GWh of energy in a daily cycle, which corresponds to 42.35 GWh of storage capacity, given the pumping efficiency.

So we can summarize the key elements of PS plants that will be used in this paper:

1. Pumping power capacity: 3.56 GW
2. Daily storage energy capacity: 42.35 GWh
3. Round trip efficiency of charging and discharging: 77.5%
4. Total storage capacity of approximately 440 GWh.

A.2.2 Strategy for balancing supply and demand as a function of PV-wind mixing ratio

A.2.2.1 Mismatch between non-dispatchable generation and demand

The main goal of this work was to capture the dynamics of a hypothetical renewable Swiss power system while varying the PV-wind mixing ratio. A binding constraint is that the demand must always be satisfied by production or import, and that excess production must be pumped or exported. As we can see in Figure A.2, the Swiss demand varies between approximately 5 and 10 GW, following daily, weekly and seasonal patterns. To compute the fraction of demand that must be met by PV, wind and storage hydropower, we subtract the production of geothermal and RoR. The result has an even stronger seasonal behavior, because RoR output is highest during the summer season (due to snowmelt), when demand is relatively low.

Figure A.3 shows the normalized national PV and wind production based on the time series

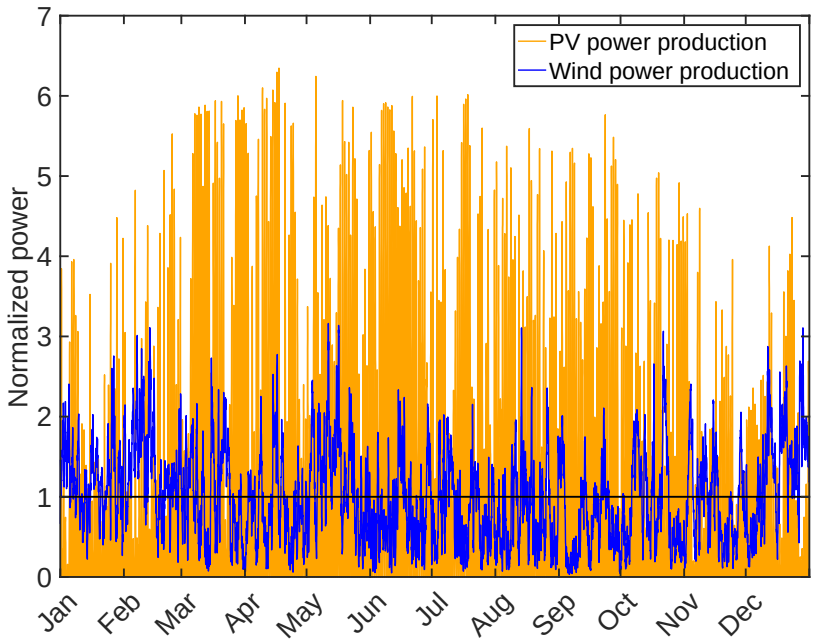

Figure A.3: Variability of wind and solar power production throughout the year, normalized by their respective annual mean values.

described in section A.2.1.2 and section A.2.1.3. PV output is high in summer, low in winter and peaks daily around noon. Production from wind shows a highly stochastic behavior, with slightly higher values in winter. Comparing these trends with the residual demand (red curve in Figure A.2), we can already foresee that storage hydropower, PS, and exchange with neighboring countries will have to provide a large amount of balancing power to satisfy demand at all times, especially for high PV ratios.

By removing the PV and wind production from the red curve in Figure A.2, we are left with the mismatch that must be balanced by storage hydropower, PS and import/export. Instead of looking at the time series of this mismatch, we can compute its statistical distribution. The calculation of the mismatch time series and its statistical distribution was performed for each PV-wind mixing ratio and allowed us to generate the top panel of Figure A.4.

This image should be read like a histogram along the vertical axis, with each cross-section representing the distribution of power mismatch for one specific mixing ratio between wind and solar production over one year. The color shows how frequently different mismatches between the sum of all non-dispatchable production and demand occur. The brighter the color, the more often the mismatch falls into the corresponding 50 MW interval. The distributions are not centered on zero, because the contribution from storage hydropower is not included in the mismatch calculations. The mean storage hydropower production (2.28 GW, computed

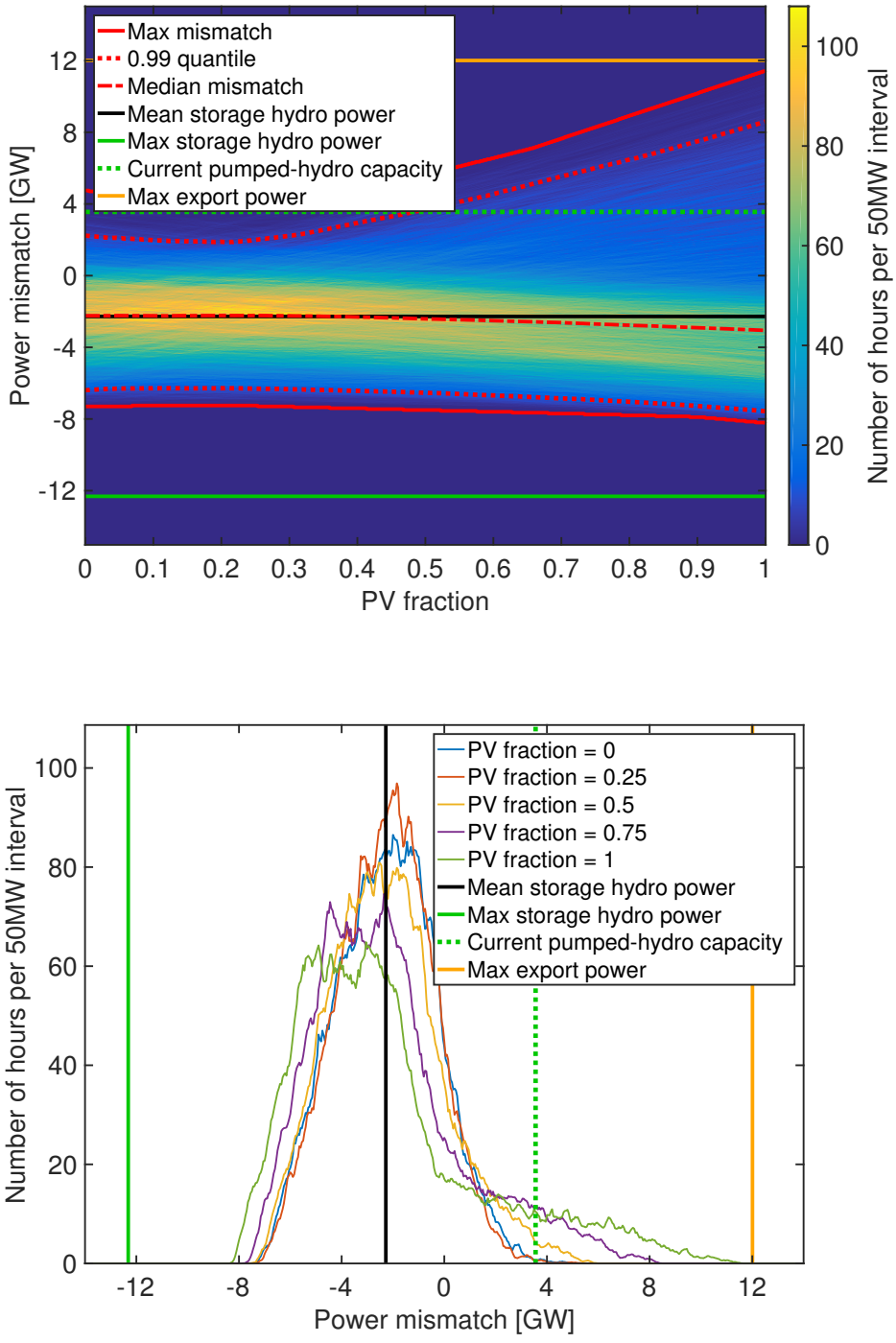

Figure A.4: Top: Distribution of instantaneous power mismatch resulting when the annual total deficit is generated from different combinations of PV and wind. The color change along each vertical cross section represents a histogram of mismatches for the corresponding PV-wind mixing ratio indicated on the x-axis. Bottom: Five examples of such histograms for PV fractions of 0, 0.25, 0.5, 0.75, 1.

from the 19.95 GWh of annual production) is indicated by the black line and the distribution of mismatch is centered upon it. This figure presents a number of important findings that are key to our subsequent analysis; hence we include a short discussion here to justify further steps.

Important insights can be deduced from the various horizontal lines that span the entire range of PV fractions. The distribution of mismatches is completely contained between the orange line at the top and the green line at the bottom. This means:

1. There is no power deficit exceeding the total installed turbining capacity of the national fleet of storage hydropower plants (12.32 GW, see section A.2.1.5).
2. There is no overproduction exceeding the maximum export power of the country's transmission lines to its neighbors (12 GW, see section A.2.1.1).

So if export is the most favorable solution when excess production occurs, then there is no power mismatch that cannot be taken care of. However, if we exclude export as a means of balancing, we have to rely on storage to compensate for any excess power or we have to curtail the production from non-dispatchable sources.

We consider that excess production is first handled through PS up to its limits, and then exported. The estimated capacity of currently available PS (3.56 GW, see section A.2.1.6) is depicted by the dotted green line in Figure A.4 and we can see that for all PV ratios there are instances when the mismatch exceeds the available pumping power. Those events happen more often and with a higher intensity for PV ratios above 0.5.

A.2.2.2 Use of short-term storage to compensate for excess production

In this work, short-term energy storage is characterized by two variables, both of which could limit the system's performance. The first is the total amount of energy that can be stored and the second is the maximum charging and discharging power. We apply our model of short-term storage to the 15-minute power mismatch time series introduced in section A.2.2.1. Charging and discharging power are limited to maximum values $P_{max_{ch}}$ and $P_{max_{disch}}$, which we assume to be equal and in the following we will refer to them as storage power.

The storage energy capacity of the model is intentionally unrestricted, such that we can observe how much energy storage is needed for given values of storage power. Charging occurs when there is a positive mismatch (excess production) and discharging occurs when there is a negative mismatch (power deficit). The charging power always equals the positive mismatch but is limited to $P_{max_{ch}}$. For the discharging power we use two different methods that represent the envelope of what future management strategies might look like:

(a) Fix the power to $P_{max_{disch}}$ to empty the storage as fast as possible and to free up space

that can absorb any upcoming overproduction. In this case, discharging might exceed the power deficit and cause forced export

(b) Flexibly adjust the power (but with an upper limit of $P_{max_{disch}}$) such that the storage exactly compensates the instantaneous power deficit.

Realistic discharging behavior will probably lie somewhere in between these two cases. Even when no electricity is needed and export prices are low, it can be economically advantageous to force discharging, because the flexibility gained through available space in the reservoir might outweigh the low profitability of the situation.

The resulting storage level $S(t)$ is calculated at 15 min timesteps $t \in [1, N]$ with the following update rule:

$$S(t) = S(t-1) + \begin{cases} \eta_{ch} \cdot \min(\Delta(t), P_{max_{ch}}) \cdot \tau & \text{if } \Delta(t) \geq 0 \\ \begin{cases} \text{a: } -\frac{1}{\eta_{disch}} \cdot \min(P_{max_{disch}}, \frac{\eta_{disch} S(t-1)}{\tau}) \cdot \tau \\ \text{b: } -\frac{1}{\eta_{disch}} \cdot \min(-\Delta(t), P_{max_{disch}}, \frac{\eta_{disch} S(t-1)}{\tau}) \cdot \tau \end{cases} & \text{if } \Delta(t) < 0 \end{cases}$$

$\Delta(t)$ is the power mismatch, η_{ch} and η_{disch} are the charging and discharging efficiencies, which we assume to be equal to those of the pumped-storage hydropower plants (88%, see section A.2.1.6), τ is the duration of a timestep (15 minutes in our case).

After storage has been invoked, a final mismatch $\Delta_2(t)$ remains:

$$\Delta_2(t) = \Delta(t) - \begin{cases} \frac{1}{\eta_{ch}}(S(t) - S(t-1)) & \text{if } \Delta(t) \geq 0 \\ \eta_{disch}(S(t) - S(t-1)) & \text{if } \Delta(t) < 0 \end{cases} \tag{A.1}$$

We run the storage model over a range of storage power values and over the entire spectrum of PV-wind ratios. For each value pair we extract the maximum storage energy level as a measure of required storage capacity for the given conditions. The results for the two different discharging methods are shown in Figure A.5 and Figure A.6.

The analysis of these 2 figures (section A.3) reveals that in the current PS system of Switzerland, the storage power influences the dynamics of the system more than the storage energy. Any storage capacity higher than the current one will not change how the short-term mismatches (below a multi-day time scale) are handled. Thus, in the following we will focus on storage power and its impact on the energy and power balance in Switzerland.

A.2.2.3 Energy balance throughout the year using short-term storage, storage hydro, import and export

The remaining power mismatch $\Delta_2(t)$ after applying short-term storage has to be covered by storage hydropower, import and export. It is important to note that storage hydropower can only compensate for negative, but not for positive mismatch. In other words, it can supply

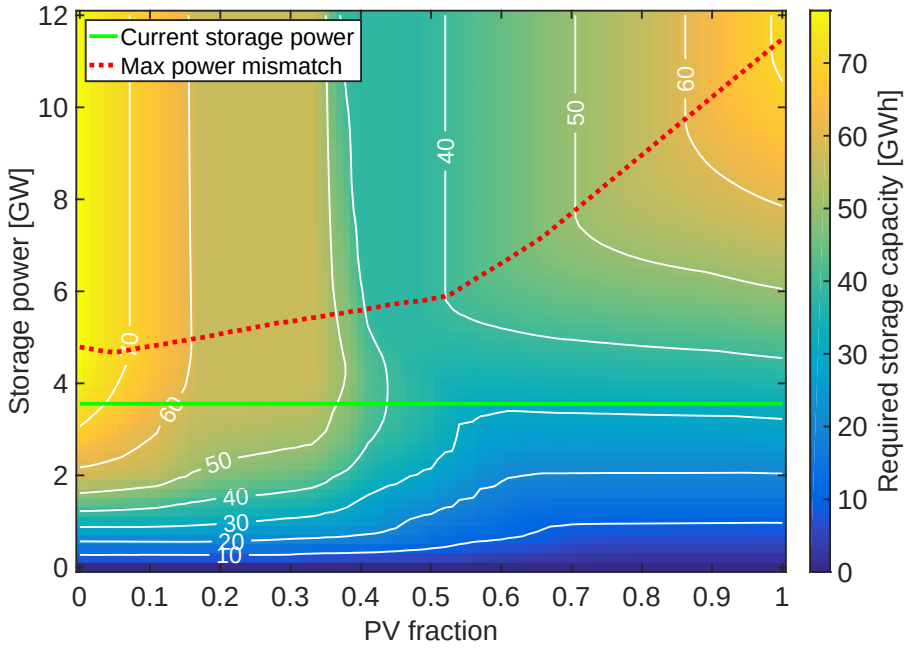

Figure A.5: Required storage capacity as a function of PV fraction and storage power for method (a), where storage is emptied as fast as possible during a power deficit.

power, when needed, but it cannot absorb excess production (unlike PS). Hence any positive mismatch requires immediate export. Summed over the year, we refer to this quantity as "forced export" E_1:

$$E_1 = \sum_{t=1}^{N} \frac{\Delta_2(t) + |\Delta_2(t)|}{2} \tag{A.2}$$

E_1 varies as a function of PV ratio and storage power (Figure A.7).

As shown in section A.2.1.5, the Swiss fleet has the necessary capacity to compensate for any conceivable power deficit. Even though the annual sum of energy inflow into the reservoir is equal to the annual total energy deficit, it is not guaranteed that balancing is possible at all times. The reservoir size is finite, the inflow has a strong seasonal variability (blue curve in Figure A.2) and during extended periods of power deficit the available water might not suffice to compensate the immediate mismatch Δ_2. The reservoir size is thus a critical parameter that drives the import and export throughout the year.

To account for this cumulative effect of repeated power deficit that storage hydropower has to balance and for the temporal behavior of the energy inflow into the reservoirs, we compute the cumulative energy level $L(t)$ at time step t, as a result of the energy balance of all previous steps. $L(t)$ is equal to the cumulative sum of the negative remaining mismatch and the energy

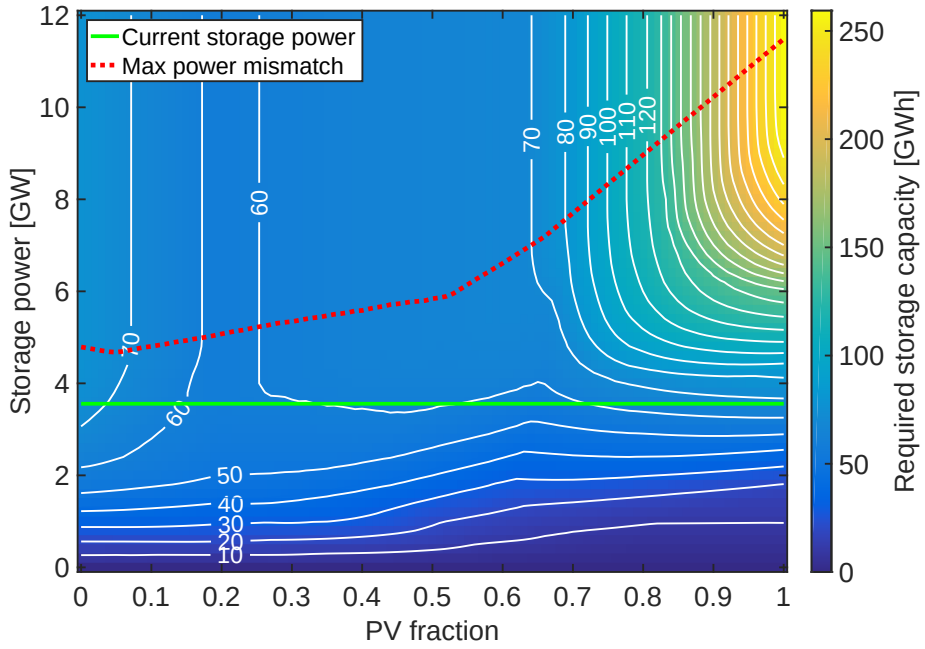

Figure A.6: Required storage capacity as a function of PV fraction and storage power for method (b), where storage is used to exactly compensate for any power deficit.

inflow F throughout the year and is computed as follows:

$$L(t) = \sum_{i=1}^{t} \frac{\Delta_2(i) - |\Delta_2(i)|}{2} + F(i), \quad \forall\, t \in [1, N]. \tag{A.3}$$

$L(t)$ is an indirect function of PV fraction and storage power, but the general behavior is well represented by Figure A.8, which shows the results for a PV fraction of 0.5 and a storage power of 3.56 GW.

From January to April the cumulative energy budget is increasingly negative, due to low inflow and high demand. Excess production during the summer months lifts the energy level back into the positive, until at the beginning of September inflow drops below the negative mismatch and a second descent begins until the end of the year. The final value is negative and represents the "losses in the system" that are due to forced export and to losses in short-term storage cycles (with a round-trip efficiency < 1). The two inflection points of the curve indicate the times of the year at which the reservoir should reach its minimum and maximum filling levels.

At the beginning of the year, there is some energy R_0 available in the reservoir. This energy should be used by storage hydropower in addition to the inflow between the beginning of the year and the moment the reservoir should be empty. The deficit peak in spring is thus reduced

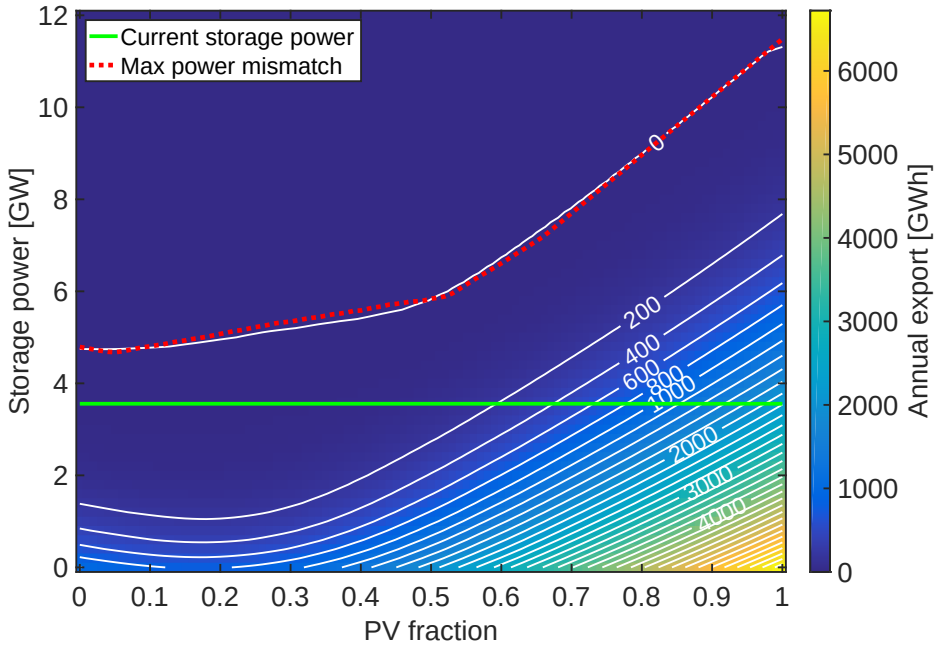

Figure A.7: Annual forced export as a function of PV fraction and storage power.

by the value R_0, and the excess peak increased by the same value.

Similarly, during the period when the reservoir should be filled, the total reservoir capacity R has to removed from $L(t)$, resulting in a reduction of the excess peak by a value R. During that period, there is an excess of energy that has to be exported. This amounts to the value E_2, which is simply the amplitude of $L(t)$ minus R (Equation A.4). We can see that the amount of energy available in the reservoir at the beginning of the year, R_0 does not affect the value of E_2:

$$E_2 = \max(L(t)) - \min(L(t)) - R \qquad \forall\, t \in [1, N] \tag{A.4}$$

The import I required to balance the system throughout the year is equal to E_2 plus the "losses", which correspond to the energy deficit at the end of the year, $-L(N)$. The values of $I = E_2 - L(N)$ for all value pairs of PV fraction and storage power are shown in Figure A.9.

The overall export E required to balance the system is composed of E_1, due to power excess generation on which there is no timing control, and E_2, due to the lack of storage capacity in the reservoir, for which there is some flexibility in the timing ($E = E_1 + E_2$).

Furthermore, as will be shown and discussed in section A.3.3, this methodology was repeated for different values of R to explore the effect of increasing the current reservoir capacity, and also for oversized PV and wind capacities.

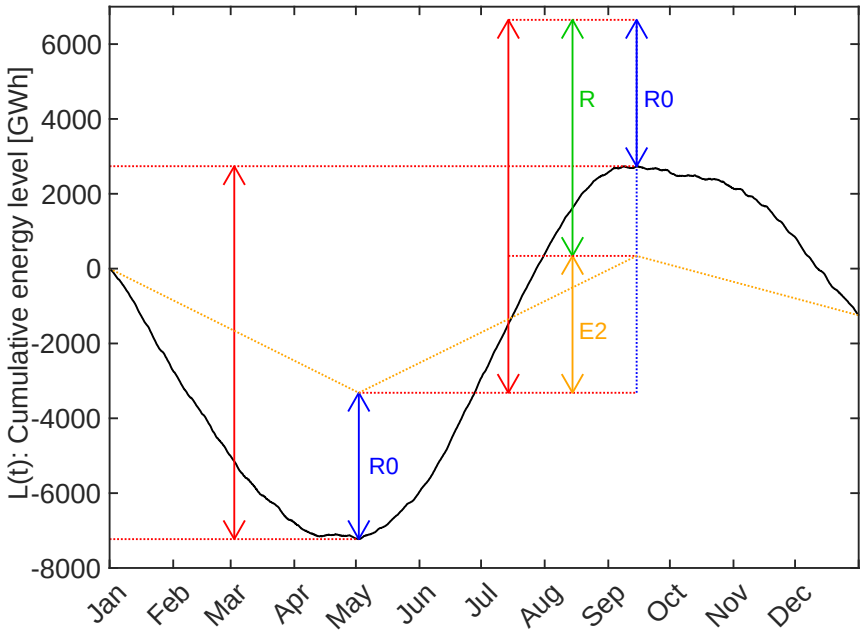

Figure A.8: Cumulative energy level $L(t)$ in Switzerland without invoking the storage capacity of the reservoirs and without import and export. R_0: Initial energy in the reservoir, R: Reservoir storage capacity, E_2: Required export because of the lack of water storage.

A.3 Results

A.3.1 Short-term storage capacity required to compensate for excess production

The required storage capacity, which we define as the highest amount of energy encountered in the storage system, is a function of the charging and discharging rate, i.e. the storage power. It also depends on the production patterns of all other generators in the system, which means it depends on the PV fraction. Figure A.5 and Figure A.6 visualize this value space for the two different discharging scenarios that we consider in this paper. As a reminder from section A.2.1.6: For the currently installed storage power of PS hydro (3.56 GW), the daily storage capacity amounts to 42.35 GWh.

If storage is forced to empty at the maximum discharging speed (Figure A.5), Switzerland has enough storage energy capacity under current conditions, as long as the PV fraction stays above 0.4. If the storage power is increased up to 12 GW, the required storage capacity will increase by 50% for the highest PV shares.

If storage is discharged only to cover power deficits (Figure A.6), following method (b), the overall functional trends for required storage capacity are similar, but the values are slightly higher especially for high PV shares.

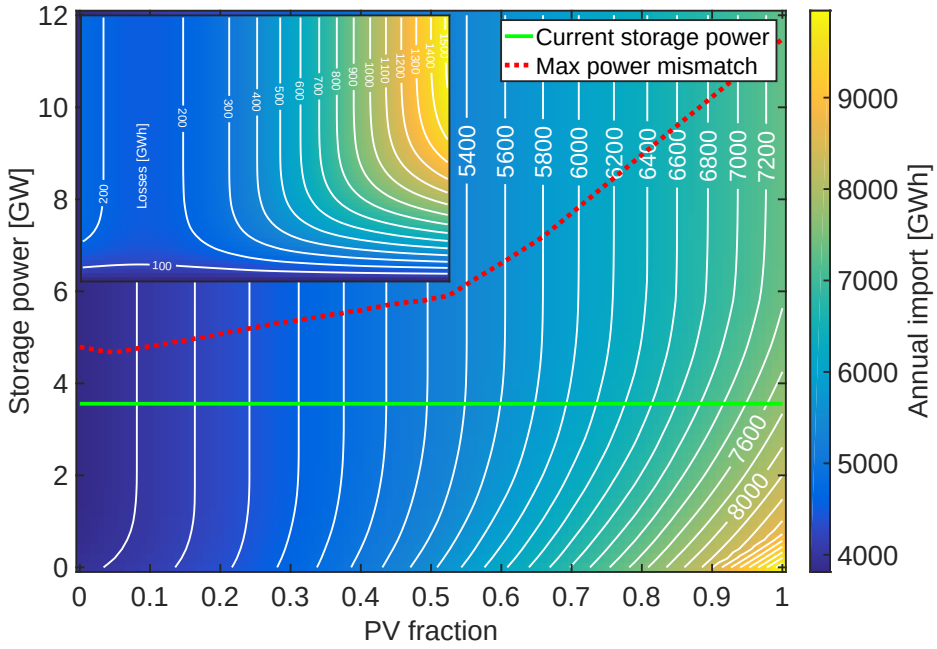

Figure A.9: Required annual import as a function of PV fraction and storage power. The thumbnail shows the corresponding energy lost due to charge/discharge cycles of short-term storage.

In this scenario the daily storage capacity at current storage power is not sufficient for any PV fraction, i.e. along the green line the required storage capacity is always above 42.5 GWh. This means that some of the excess production cannot be stored because there is not enough space. Nevertheless, storage capacity is not the limiting factor here. We need to keep in mind that the total storage capacity of PS hydro amounts to 440 GWh (section A.2.1.6). Hence the storage space is already in place, but the currently installed pumps and turbines are not powerful enough to empty and fill this space in daily cycles. If more turbines were to be installed (which means increasing the storage power), more energy could be stored daily, even in the current reservoirs. For PV fractions above 0.6 and storage powers above 4 GW, there is a strong accumulation effect of overproduction in summer, when there is not enough discharging before the next charging cycle. But even the highest value of 250 GWh for a PV fraction of 1 lies below the 440 GWh of currently available total storage capacity. Thus, we consider that the current short-term storage capacity is already sufficient to deal with the power mismatch for the entire range of PV-wind mixing ratios and storage power values. Consequently, we do not restrict the short-term storage energy capacity and only focus on the impact of storage power on the system.

From Figure A.5 and Figure A.6 alone it may seem as if a low storage power is desirable, because it requires low storage capacity. However, it is important to keep in mind that the term "required storage capacity" in this context denotes the amount of storage which is necessary

to accommodate the energy that can be absorbed by a specific storage system applied to a specific power mismatch time series. It does not however, represent the storage capacity that would be necessary to entirely compensate for the excess production. When storage power is higher than the largest excess generation encountered in the year (above the red line for each PV fraction), then the computed required storage capacity represents what is necessary to always accommodate excess production. An increase of storage power beyond the red line does not change how the storage performs since any excess generation is taken care of. The required storage capacity is thus constant above this line for each PV fraction. The smaller the storage power, the smaller the buffering effect of short-term storage, and the bigger the amount of remaining mismatch that will have to be taken care of by storage hydropower and through exchange with neighboring countries. While power deficits could potentially be alleviated with the help of storage hydropower, there is no measure that could balance overproduction beyond the limits of short-term storage. Excess production will have to be exported on the spot. Thus, the lower the storage power, the higher the forced export. Figure A.7 shows these dynamics.

We see that for high PV fractions especially, the forced export reaches considerably high values. However, already for the current storage power (green line), the forced export is very small, as long as the PV fraction stays below 0.6. Beyond 0.6 the storage power would have to increase substantially in order to keep forced export low.

A.3.2 Annual required import and export

As described in the introduction, PV and wind energy production are sized so that they can bridge the gap between demand and the other electricity sources on a yearly basis. Import and export only function as balancing measures to match instantaneous demand with production. Consequently net exchange have to be zero. The losses from charging and discharging of short-term storage also need to be included in this equilibrium; annual total import is equal to annual total export plus the losses. But the losses are comparably small as shown in the thumbnail of Figure A.9. The strong variability in PV production causes extensive cycling of the short-term storage, which inevitably increases the associated losses. Hence the increase of loss with storage power.

The slight bend in the lower part of Figure A.9 is a result of a shortage in storage power. When its value drops below the red line, not all positive mismatches can be absorbed, causing forced export, as we have seen in Figure A.7. Since any export translates into import eventually, we see an increase in import with decreasing storage power. Above the green line in Figure A.9, an increase in storage power barely affects the amount of annual import. This means that given the current level of storage power the forced export is small compared to the total required export.

The increase of import for higher PV fractions is due to the strong seasonal trend of PV production. Even if the short-term storage can deal with the excess PV production in summer,

storage hydropower is not able to keep all the water for the next winter because of the limited reservoir capacity. The excess water in the reservoir thus has to be either spilled (wasted) or turbined and the extra electricity exported.

A.3.3 Solutions to limit the annual required import

Previously we imposed the limitation that annual total production needs to be equal to the demand. As our analysis shows, the time series of demand and production cannot be aligned at all instances and a certain amount of import and export is required to compensate for the mismatch. In the following, we show the impact of two different measures that aim to reduce this required exchange.

A.3.3.1 Increasing the reservoir capacity

With more volume in the reservoir, part of the seasonal mismatch could be alleviated and less import would be necessary. Figure A.10 shows how the import varies with reservoir size and as a function of PV fraction. All values are calculated assuming the current power level of short-term storage (3.56 GW). As a reference, we also show the import that would be required under current conditions (3.5 TWh per year). It is calculated following the methodology described in section A.2.2.3, replacing the sum of PV, wind and geothermal production by the scaled production from nuclear and fossil fuel sources of 2014 (interpolation of the monthly production values, sourced for (26)).

For a high share of wind, the import values are very similar to the current one, without any change in reservoir volume. A 60% increase in capacity would bring the import close to zero. With more PV in the mix, however, reservoir capacity needs to increase to maintain the current import. In a PV-only scenario, 65% more storage volume would be required to reach current import and beyond that almost no improvements are possible. The abrupt kinks in lines of constant annual import indicate that the buffering effect of the reservoirs is fully exploited; all available water can be stored until it is needed and additional space would be futile. The remaining import beyond this transition corresponds to losses from short-term storage as well as from overproduction that could not be absorbed by short-term storage and thus exported. As we already saw in Figure A.7 and the thumbnail of Figure A.9, these values are higher for high PV fractions.

A.3.3.2 Oversizing PV and wind generation to reduce import

Instead of increasing the reservoir capacity, another option would be to oversize the installed capacity of PV and wind power. Figure A.11 illustrates that for this scenario, the PV fraction becomes even more critical.

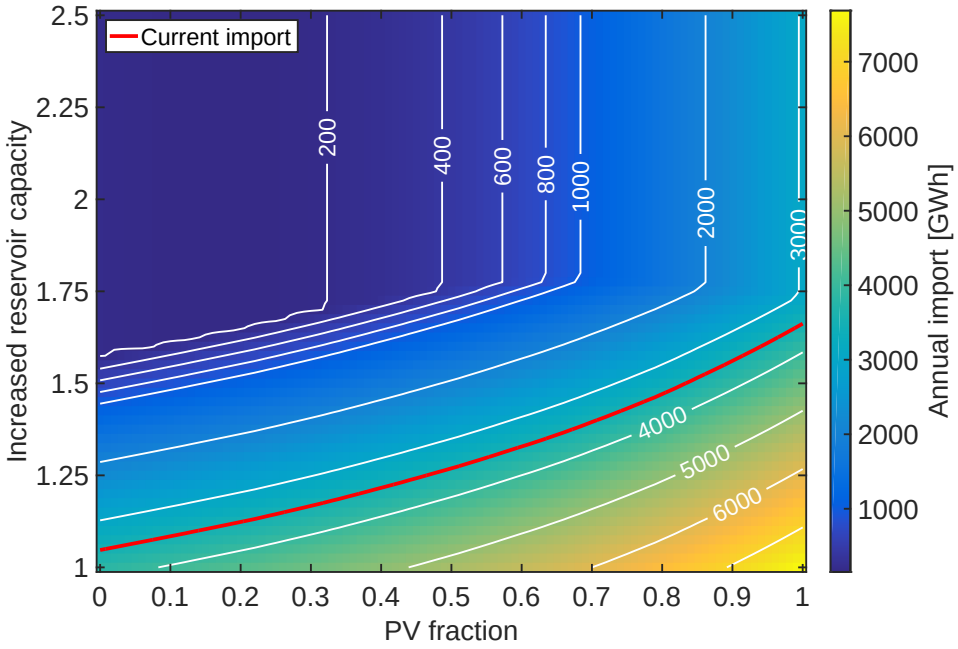

Figure A.10: Annual required import as a function of PV fraction and size increase factor of reservoir capacity, computed with a short-term storage power of 3.56 GW (current installed capacity).

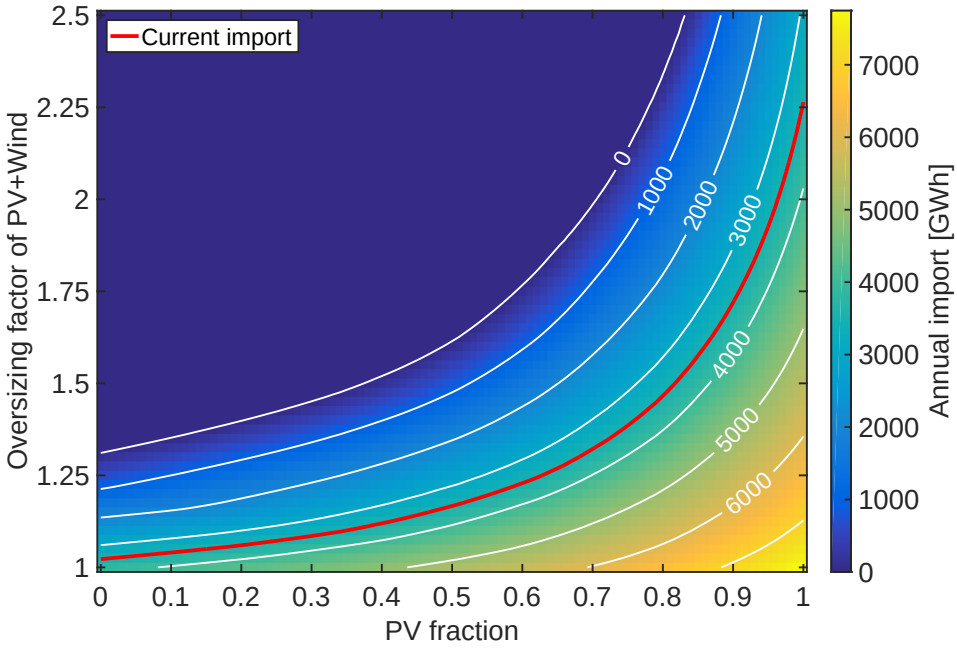

Figure A.11: Annual required import as a function of PV fraction and oversizing factor of installed capacity of PV and wind generation, computed with a short-term storage power of 3.56 GW (current installed capacity).

For high shares of wind, no oversizing is required to preserve the current import level and already a moderate oversizing of 30% removes any need for import. However as soon as the PV fraction exceeds 0.7, the amount of oversizing needed to keep the current import level rises dramatically and reaches 125% for a PV fraction of 1. The problem with oversizing a renewable mix with a high contribution of PV is the pertinent overproduction in summer that is intensified even further. Much of the additional production occurs at times when there is already sufficient energy and the reservoirs are full. Consequently most of it needs to be exported or is lost; while at the same time little relief is provided for times of deficit in winter and import remains high.

So we need to keep in mind that oversizing can decrease the import, but will also increase the forced export. How those two effects relate to each other, strongly depends on the PV fraction of the mix (Figure A.12).

For high PV fractions and high oversizing values, the forced export becomes very large and represents a large fraction of the extra production. For high shares of wind, an oversizing of 25 to 50% eliminates the need for import and does not generate large amounts of forced export.

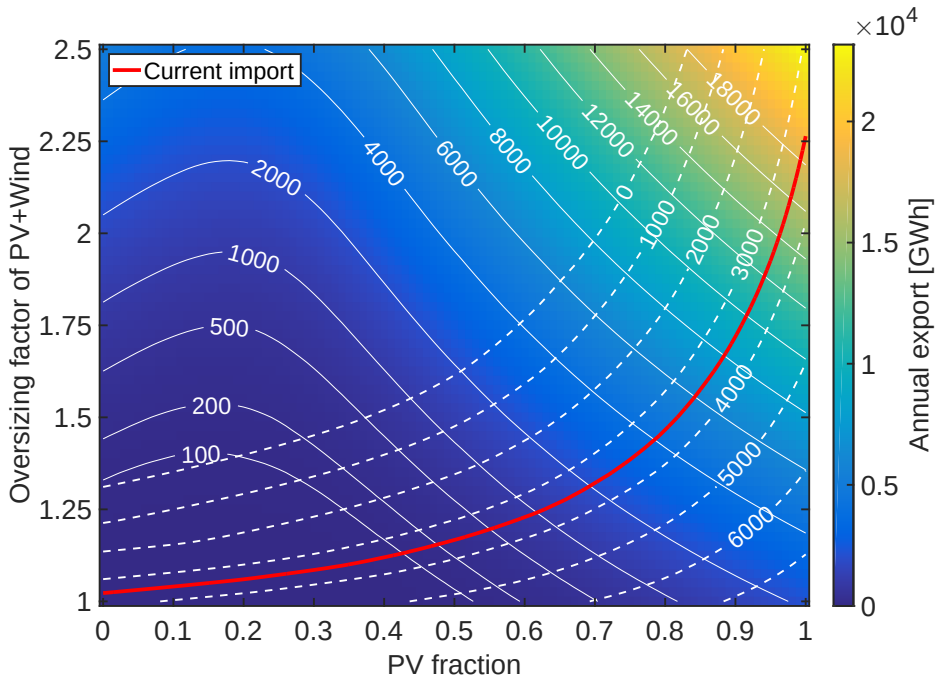

Figure A.12: Annual forced export as a function of PV fraction and oversizing factor of installed capacity of PV and wind generation, computed with a short-term storage power of 3.56 GW (current installed capacity). The corresponding import values are represented by the dashed lines.

A.3.4 Results for the years 2009-2015

For an interannual comparison we used time series of electricity consumption, production from run-of-river and storage hydropower, reservoir level and solar irradiance for the years 2009 to 2015 from the same sources as described in section A.2.1. Wind speed data were only available for 2012 to 2015, thus we filled in the data from our reference year 2014 for the years 2009 to 2011. We kept the same amount of wind turbines and PV surface as in 2014 with the goal to analyze the interannual variation of required import, export and storage capacity. Consequently, the total annual production from wind and PV deviates from the 20.19 TWh in 2014, and is not scaled to match the gap between demand and the other production sources. Figure A.13 displays the variation in demand and various generations as percent deviation from the corresponding quantities in 2014. Moreover, it shows the mismatch as percentage of the demand. As expected, 2014 is balanced, but all other years, except for 2012, have a production deficit; especially 2010 and 2011 due to a particularly low hydropower production. Given the production deficit for those years, it is expected that the corresponding required imports will be higher as well.

The methodology described in section A.2 was applied to each year, and would allow to generate all the figures and results presented previously. For the sake of brevity, we cannot show these plots for all years, and instead summarize the important points below. Despite

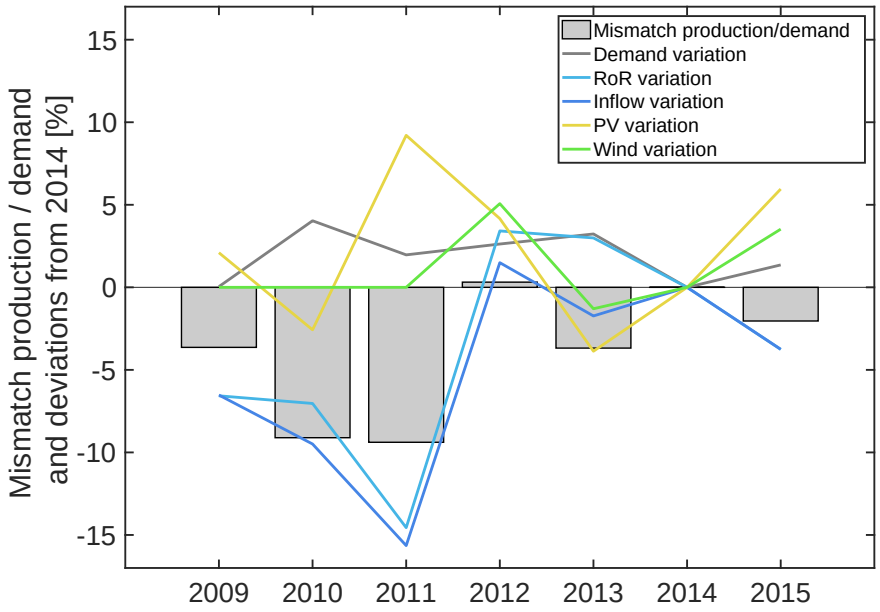

Figure A.13: Percent deviation of demand and production from 2014, and resulting mismatch as percentage of the yearly demand.

the fact that annual production does not equal the annual demand outside of 2014, the methodology remains valid because the deficit at the end of the year $L(N)$ is incorporated in the calculation of the import.

The results remain very similar for all years: the graphs depicting the variation of required storage capacity, import/export, effect of increased reservoir capacity and oversized generation as function of both, PV fraction and storage power (corresponding to Figure A.5 - Figure A.12) show the same trends as in 2014.

- For a storage power equal to the current pumping capacity, the lowest value for required storage capacity always lies between PV fractions of 0.4 and 0.6, and equals about 40 GWh.

- When analyzing the impact of increased reservoir capacity, we observe the effect of saturation at higher values (2.15-fold increase) during years of spiky summer inflow, such as 2009, while years like 2011 with low total inflow reach saturation at values as low as 1.4-fold increase.

- Oversizing the production from PV and wind has always the same effect and is efficient in reducing the import as long as PV fraction stays below 0.6.

- Import variation across PV fraction and storage power follows the same pattern, increasing quasi-linearly with PV fraction. Nevertheless, there is an import offset on the entire range from year to year.

The calculation of required import is of great importance for the energy supply of the country and is thus at the core of our study. As a reminder, the required import value computed for 2014, with a PV fraction of 0.5 and a storage power equal to the current pumping capacity is 5.2 TWh (see Figure A.9).

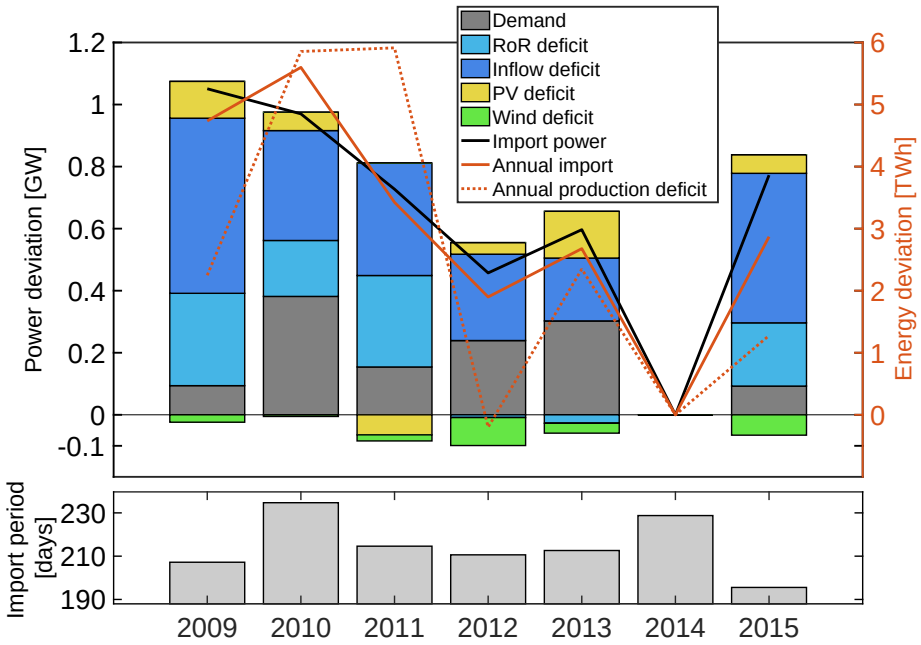

Figure A.14: Left axis (bars and black curve): Deviation (from 2014) of demand, production and import power in winter. Right axis (red curves): Deviation (from 2014) of annual import and production deficit.

The red line in Figure A.14 shows its interannual variation, as deviation from this reference year. The dashed red line represents the annual production deficit with respect to 2014. To identify the origins of the import variation, we also show each year's deviation in the demand and in the production of all generating sources during the import period. This period is defined by the two points in time when the storage hydro reservoir should be full and when it should be empty, as described in section A.2.2.3. Its length is represented by the bar graph at the bottom of Figure A.14, and since it varies from year to year, we chose to represent the variation of demand and production during this period through their deviation in average power. The resulting deviation in average import power is depicted by the black curve.

Figure A.14 reveals some important information:

- As expected, the import power deviation is equal to the sum of demand surplus and production deficit.
- The correlation between the winter deficit of the energy sources and their annual deficit is not very strong.
- Import is strongly correlated with the winter deficit of the energy sources but also with the winter length.
- Hydropower has the strongest winter variability and thus influences import the most.
- The winter production of PV and wind is more stable than the rest, and hence stabilizes the import.
- The timing between demand and availability of the energy sources plays a critical role, as it influences the length of the import period.

To understand the behavior of import, it is important to look at the combination of production and consumption and their relative dynamics throughout the winter period. Despite the existence of substantial short-term storage, the temporal behaviour of demand and energy sources, especially the shortage of running water for hydropower during the winter, strongly increases the amount of required import.

A.4 Conclusion

In this work, we studied the impact of wind-solar mixing ratio on the electricity exchange with neighboring countries that is needed to balance supply and demand within hypothetical, fully renewable Swiss power systems. In addition to the mixing ratio of PV and wind, there are other factors that also affect import and export, including:

- Use and sizing of short-term storage (pumped-storage hydropower, characterized by storage capacity and storage power)
- Oversizing of production from PV and wind energy
- Increase of reservoir size

To tease apart the effects of these factors, we completed a 3-step analysis that progressed logically through the electricity production process:

1. Computation of immediate mismatch Δ_1 between demand and the sum of non-dispatchable sources (PV, wind, RoR and geothermal). The results show that a high share of wind is advantageous, due to better correlation with demand in winter, smaller variability, and 24h-availability.

2. Application of short-term storage as a first measure to compensate for Δ_1, leaving the remaining mismatch Δ_2. Depending on the discharging strategy, a different amount of storage capacity is required. Discharging as fast as possible will entail high flexibility, but also increase the forced export, while discharging proportionately with negative deficits requires more storage capacity. Any realistic use of short-term storage will probably evolve between these two cases and will furthermore have to account for the fact that most pumped-storage hydro facilities are not closed systems. Independent of the exact realization, storage power is the limiting factor in the current pumped-storage hydro installations.

   We find that PV fractions between 0.2 and 0.6 require the smallest amount of storage capacity for any installed storage power at or above the current level.

3. Involvement of storage hydropower and import/export to balance out Δ_2. We introduce a methodology for the storage hydropower that accounts for the temporal behavior of the water inflow into the reservoirs and their size, and computed how this stored energy should be used in the most efficient way throughout the year. Finally, we computed the required import and export as the remainder of all balancing efforts. Both increase monotonically with PV fraction, but the higher the contribution of PV, the steeper the increase. We analyzed two approaches to reduce annual import: increasing the storage volume of the reservoirs and oversizing the production of PV and wind. Both measures decrease import, but the latter also increases forced export and losses, particularly for high shares of PV.

Combining the results of our analysis we conclude that the ideal range of PV fraction lies between 0.3 and 0.6. Previous studies have reported similar proportions, but they were carried out in different geographic regions and they used different methods, objective functions and boundary conditions:

- (10) analyzed 100% renewable scenarios for all of Europe, solely based on wind and solar and found the best mixture to be composed of 55% wind and 45% solar. If however, contributions from fossil fuel and nuclear sources are allowed, the ratio shifts towards more wind.
- (3) and (30) both find a PV fraction of 0.3 to have the lowest variability in production. This ratio only looks at temporal variability of the joint production and considers neither demand nor balancing power from storage and hydropower production.

Overall it is difficult to find a study that is completely comparable, but the general trend seems to indicate that a higher share of wind is preferable. Our investigation does not only look at wind and solar production as isolated entities, but rather sets their contributions into the bigger context of a country-wide, renewable electricity system. Particular attention was given to a detailed representation of the temporal behavior and limitations of the storage and

pumped-storage hydropower system, because they would play a central role in balancing the intermittent renewable sources in Switzerland.

The goal of this paper was to show the technical feasibility of such a fully renewable generating fleet. In terms of hydropower capacities, all estimates in the paper work with the currently available resources, but under the assumption that they are being used in conjunction with the new renewable sources to best compensate the inevitable mismatches and not to optimize the economic benefits of individual generating sources. Nevertheless, it is to be expected that these two interests align, because electricity prices are correlated with demand to a first approximation.

We acknowledge that considering Switzerland as an independent electrical system strongly simplifies its behavior. As part of the European electricity market, the Swiss production covers not only the national, but also international demand, especially during peak hours. This means that some overproduction from renewables could be used by other countries instead of being pumped, and water from the reservoirs could be turbined not only to cover the national but also part of the foreign consumption. This would require additional import at other times to counterbalance this export. Furthermore, the Swiss pumps could be used to absorb some of the international overproduction. Being part of an international network brings some advantages, e.g. spatial smoothening of the intermittent energies and the demand, but might also occupy part of the transmission line capacity, of the storage and of the balancing capacity. Despite those limitations, our study shows what the minimum amount of electricity trade with the neighboring countries would be in a fully renewable Switzerland. As described in section A.3.4, the average import power during winter would lie between 1 GW and 2 GW, depending on the winter environmental conditions. This required import would occupy a reasonably small fraction of the 12 GW line capacity between Switzerland and the neighboring countries, leaving sufficient space for the trading described above.

This paper is the first in a series. In the near future we will extend our work to a spatially explicit analysis of the impact of PV and wind on the Swiss electricity system. Combining geo-located representations of the hydropower system and of the electricity network at transmission level with a power flow model, we will model different placement scenarios of wind and PV installations to answer the following questions:

- How does the spatially explicit model compare with the lumped analysis?
- Is the current transmission network equipped to handle the new challenges of electricity flow in a fully renewable system?
- How does the placement, orientation and sizing of PV panels affect the renewable mix and can it be optimized in combination with wind power installations in order to take advantage of spatial variability of resource?

Acknowledgments

This work was funded by the Swiss Competence Center for Energy Research, Supply of Energy (SCCER-SOE).

A.5 Add-on: Optimized formulation for the energy storage

In the case of an energy storage with infinite capacity, it is possible to compute more rapidly the remaining power mismatch time series $\Delta_2(t)$ after the short-term storage is invoked.
The input power mismatch is positive when non-dispatchable generation exceeds consumption.
As a reminder, and to complete the formulation presented in Equation A.1, the evolution of the storage level from time $t-1$ to time t can be expressed as: (in the case of a finite storage capacity and for the case b, where discharging power is adjusted such that the storage exactly compensates the instantaneous power deficit). $\forall\, t \in [1, N]$, the storage level update rule is as follow:

$$S(t) = S(t-1) + \begin{cases} \eta_{ch} \cdot \min(\Delta(t), P_{max_{ch}}, \frac{S_{max} - S(t-1)}{\eta_{ch}\tau}) \cdot \tau, & \text{if } \Delta(t) \geq 0 \\ -\frac{1}{\eta_{disch}} \cdot \min(-\Delta(t), P_{max_{disch}}, \frac{\eta_{disch} S(t-1)}{\tau}) \cdot \tau & \text{if } \Delta(t) < 0 \end{cases} \tag{A.5}$$

$\Delta(t)$ is the power mismatch, S_{max} is the energy storage capacity, η_{ch} and η_{disch} are the charging and discharging efficiencies, and τ is the timestep (15 min).

After storage has been invoked, the final mismatch $\Delta_2(t)$ remains the same as in Equation A.1:

$$\Delta_2(t) = \Delta(t) - \begin{cases} \frac{1}{\eta_{ch}}(S(t) - S(t-1)) & \text{if } \Delta(t) \geq 0 \\ \eta_{disch}(S(t) - S(t-1)) & \text{if } \Delta(t) < 0 \end{cases} \tag{A.6}$$

The optimized formulation (Equation A.7 to Equation A.9) is valid for the case of unlimited storage capacity ($S_{max} = \infty$). It limits the iterations only to the times of negative power mismatch, when the short-term storage can possibly get discharged. All calculation that occur before the iterations are performed in a vectorized manner, making the new method 3 to 5 times faster than the previous one.

$$\begin{cases} \Delta_{pos}(t) & = max(0, min(\Delta(t), P_{max_{ch}})) \\ S(t) & = \sum_{i=1}^{t} \Delta_{pos}(i) \cdot \eta_{ch} \\ \Delta_2(t) & = \Delta(t) - \Delta_{pos}(t) \end{cases} \qquad \forall\, t\ in [1, N] \tag{A.7}$$

$$\begin{cases} T_{neg} & = \{t \in [1, N] \mid \Delta(t) < 0\} \\ S_{neg} & = \{\eta_{disch} S(t) \mid t \in T_{neg}\} \\ \Delta_{neg} & = \{min(-\Delta(t), P_{max_{disch}}) \mid t \in T_{neg}\} \end{cases} \tag{A.8}$$

Then, for t in [0, $N_{T_{neg}}$], starting with $s_{drain} = 0$:

$$\begin{cases} s & = min(\Delta_{neg}(t), S_{neg}(t) - s_{drain}) \\ s_{drain} & = s_{drain} + s \\ \Delta_2(T_{neg}(t)) & = \Delta_2(T_{neg}(t)) + s \end{cases} \tag{A.9}$$

Bibliography

[1] Stuart John Bartlett, Bert Kruyt, Annelen Kahl, and Michael Lehning. Risks and Reliability in a Fully Renewable Switzerland. In *European Safety and Reliability Conference 2015*, 2015.

[2] Sarah Becker, Bethany A. Frew, Gorm B. Andresen, Timo Zeyer, Stefan Schramm, Martin Greiner, and Mark Z. Jacobson. Features of a fully renewable US electricity system: Optimized mixes of wind and solar PV and transmission grid extensions. *Energy*, 72:443 – 458, 2014.

[3] Philip E. Bett and Hazel E. Thornton. The climatological relationships between wind and solar energy supply in Britain. *Renewable Energy*, 87, Part 1:96 – 110, 2016.

[4] P. de Jong, A.S. Sánchez, K. Esquerre, R.A. Kalid, and E.A. Torres. Solar and wind energy production in relation to the electricity load curve and hydroelectricity in the northeast region of Brazil. *Renewable and Sustainable Energy Reviews*, 23:526 – 535, 2013.

[5] Ebubekir Firtin, Önder Güler, and Seyit Ahmet Akdağ. Investigation of wind shear coefficients and their effect on electrical energy generation. *Applied Energy*, 88(11):4097 – 4105, 2011.

[6] G Galanis. Smoothing out the wind power production patterns by connecting different countries within Europe. Master's thesis, Utrecht University, 2014.

[7] F. Geth, T. Brijs, J. Kathan, J. Driesen, and R. Belmans. An overview of large-scale stationary electricity storage plants in Europe: Current status and new developments. *Renewable and Sustainable Energy Reviews*, 52:1212 – 1227, 2015.

[8] G Giebel. *On the benefits of distributed generation of wind energy in Europe.* PhD thesis, University of Oldenburg, 2000.

[9] Dominik Heide, Martin Greiner, Lüder von Bremen, and Clemens Hoffmann. Reduced storage and balancing needs in a fully renewable European power system with excess wind and solar power generation. *Renewable Energy*, 36(9):2515 – 2523, 2011.

[10] Dominik Heide, Lueder von Bremen, Martin Greiner, Clemens Hoffmann, Markus Speckmann, and Stefan Bofinger. Seasonal optimal mix of wind and solar power in a future, highly renewable Europe. *Renewable Energy*, 35(11):2483 – 2489, 2010.

[11] Christina E. Hoicka and Ian H. Rowlands. Solar and wind resource complementarity: Advancing options for renewable electricity integration in Ontario, Canada. *Renewable Energy*, 36(1):97 – 107, 2011.

[12] James Honaker, Gary King, Matthew Blackwell, et al. Amelia ii: A program for missing data. *Journal of statistical software*, 45(7):1–47, 2011.

[13] S Jafari, T Sommer, N Chokani, and RS Abhari. Wind resource assessment using a mesoscale model: the effect of horizontal resolution. In *ASME Turbo Expo 2012: Turbine Technical Conference and Exposition*, pages 987–995. American Society of Mechanical Engineers, 2012.

[14] Willett Kempton, Felipe M. Pimenta, Dana E. Veron, and Brian A. Colle. Electric power from offshore wind via synoptic-scale interconnection. *Proceedings of the National Academy of Sciences*, 107(16):7240–7245, 2010.

[15] Bert Kruyt, Michael Lehning, and Annelen Kahl. Potential contributions of wind power to a stable and highly renewable Swiss power supply. *Applied Energy*, 192:1–11, 2017.

[16] T.M. Letcher. *Storing energy: With special reference to renewable rnergy sources*. Elsevier Science, 2016.

[17] M. Castelli and R. Stöckli and D. Zardi and A. Tetzlaff and J.E. Wagner and G. Belluardo and M. Zebisch and M. Petitta. The HelioMont method for assessing solar irradiance over complex terrain: Validation and improvements. *Remote Sensing of Environment*, 152:603 – 613, 2014.

[18] MeteoSchweiz. Automatisches Messnetz, 2016.

[19] F. Monforti, T. Huld, K. Bódis, L. Vitali, M. D'Isidoro, and R. Lacal-Arántegui. Assessing complementarity of wind and solar resources for energy production in Italy. A Monte Carlo approach. *Renewable Energy*, 63:576 – 586, 2014.

[20] Swiss Federal Office of Energy. Füllungsgrad der Speicherseen. http://www.bfe.admin.ch/themen/00526/00541/00542/00630/index.html?lang=en&dossier_id=00766., 2014.

[21] Swiss Federal Office of Energy. Statistik der Wasserkraftanlagen der Schweiz. http://www.bfe.admin.ch/themen/00490/00491/index.html?, 2015.

[22] Prognos. Die Energieperspektiven für die Schweiz bis 2050, 2012.

[23] Morten Grud Rasmussen, Gorm Bruun Andresen, and Martin Greiner. Storage and balancing synergies in a fully or highly renewable pan-European power system. *Energy Policy*, 51:642 – 651, 2012.

[24] S. Koller and T. Humar. Windpotentialanalyse für Windatlas.ch; Jahresmittelwerte der modellierten Windgeschwindigkeit und Windrichtung; Schlussbericht, 2016.

[25] Swiss Federal Office of Energy. Bundesamt für Energy (BFE), Die Energieperspektiven für die Schweiz bis 2050 Anhang 3, 2012.

[26] Swiss Federal Office of Energy. Gesamte Erzeugung und Abgabe elektrischer Energie in der Schweiz. http://www.bfe.admin.ch/themen/00526/00541/00542/00630/index.html?lang=en&dossier_id=00769, 2014.

[27] Swiss Federal Statistical Office. Statistik der Bevölkerung und der Haushalte. http://www.bfs.admin.ch/bfs/portal/fr/index/dienstleistungen/geostat/datenbeschreibung/volks-__gebaeude-0.html., 2014.

[28] Swissgrid. Energy Statistics Switzerland 2014. https://www.swissgrid.ch/swissgrid/en/home/reliability/griddata/load.html, 2014.

[29] Greg Wetstone, Kane Thornton, Rainer Hinrichs-rahlwes, Steve Sawyer, Marietta Sander, Richard Taylor, David Rodgers, Marcel Alers, Harry Lehmann, Michael Eckhart, and David Hales. *Renewables 2016 global status report 2016.* 2016.

[30] J. Widen. Correlations between large-scale solar and wind power in a future scenario for Sweden. *IEEE Transactions on Sustainable Energy*, 2(2):177–184, April 2011.

B Optimized market value of alpine solar photovoltaic installations

Optimized market value of alpine solar photovoltaic installations

Jérôme Dujardin[1,2], Moritz Schillinger[3], Annelen Kahl[1,2], Jonas Savelsbergt[4], Ingmar Schlecht[5] and Rebecca Lordan-Perret[3]

[1]School of Architecture, Civil and Environmental Engineering, Swiss Federal Institute of Technology in Lausanne (EPFL), Lausanne, 1015, Switzerland

[2]Institute for Snow and Avalanche Research (SLF), Swiss Federal Institute for Forest, Snow and Landscape Research (WSL), Davos 7260, Switzerland

[3]University of Basel, Forschungsstelle Nachhaltige Energie- und Wasserversorgung, 4002 Basel, Switzerland

[4]ETH Zurich, Centre for Energy Policy and Economics (CEPE), 8092 Zurich, Switzerland

[5]ZHAW School of Management and Law, Center for Energy and Environment, 8400 Winterthur, Switzerland

Abstract

Solar photovoltaic (PV) is the most rapidly expanding renewable resource worldwide. Yet, its full potential may be hindered by mismatches with market demand and correlated production profiles. In this research, we explore a case study of innovative PV placements in alpine regions using two, soft-linked optimization models of Switzerland's electricity system. Using Swissmod, an electricity dispatch and load-flow model, and OREES, an electricity system model employing evolution strategy to optimize PV placement, we simulate market prices of optimized PV placements given multiple years of weather data, various CO2 prices, and considering future electricity infrastructure developments across Europe. Mountain placements result in higher market value and less required area relative to lower-altitude PV placement strategies. The higher market value is driven by better alignment with demand, particularly during winter when demand is highest. We found that optimized alpine placements offer revenues of panel capacity (EUR/kW/year) that are on average 20% higher than revenues from urban PV installations. Furthermore, the Swiss mountains could host more than 1 GW of capacity with even greater revenues (33%). Alpine PV installations, with their higher market values and increased value factors, can potentially be very profitable investments and are also valuable from a system perspective. *Keywords*: Photovoltaic, Market value, Dispatch model, Optimization, Mountain solar, Evolution strategy

This chapter was submitted to the journal *Renewable Energy*

J.D investigated the research question, developed the model, performed the simulations, analyzed the results, and contributed to the writing of the paper.

B.1 Introduction

The Paris Agreement and legislative climate policy packages such as the European Commission's "Fit-for-55" package call for energy systems to decarbonize by 2050 (11). The electricity sector will play leading roles both directly and indirectly in decarbonizing energy systems worldwide. First, countries will replace fossil-fuel generation technologies with renewable generation technologies in their electricity systems, accounting for a large direct reduction in carbon emissions. Second, once the electricity sector has been decarbonized, other sectors historically relying on fossil fuels (e.g., transportation and heating) will be decarbonized through electrification, further reducing CO_2 emissions.

Countries have already begun expanding their share of renewable technologies in the electricity sector. The International Energy Agency expects that solar photovoltaic (PV) panels will make the largest contribution to expanding global renewable capacities in the coming decades (21). Indeed, PV is being installed at the highest rate of all renewable technology options (22) due to its rapidly falling investment costs that are expected to decrease further (37). Solar power is now less expensive than coal and gas in most countries, according to IEA estimates (21).

However, there are two challenges that arise at high levels of installed PV: a temporal mismatch between electricity demand and PV production (within the day and seasonally), and the so-called "cannibalization" effect (reduced market value induced by the introduction of more correlated PV generation in the market). In this paper, we explore the innovative PV placements proposed in Kahl et al. (24) and show how placing PV at higher altitudes can help address these issues, making PV potentially a more attractive investment opportunity.

Temporal mismatch within a day occurs because solar generation is highest around noon whereas electricity demand peaks at different times. Summer-peaking systems such as most North American power systems experience their demand peaks in the late afternoons, while winter-peaking systems such as the interconnected European power system experience their peaks in evening hours, both not matching the peak around noon of solar electricity generation. This results in electricity prices often being depressed in hours of peak solar infeed (as in the case of the Californian "duck curve" of summer electricity prices). Such daily mismatches can be addressed by short-term storage options such as batteries and pumped-storage hydropower, partly mitigating the cannibalization effect.

Seasonal mismatches occur where demand is highest in the colder, darker winter months[1] while solar generation is highest in the summer (Figure B.1). Seasonal mismatch requires seasonal storage options, grid expansion, other generation options (e.g., wind power) to compensate for PV production shortfalls during winter months.

[1] This is the case for example in Northern and Central European countries such as Germany, France or Switzerland. Warmer countries such as Italy or Spain, but also in parts of the US including California, have their peak in summer.

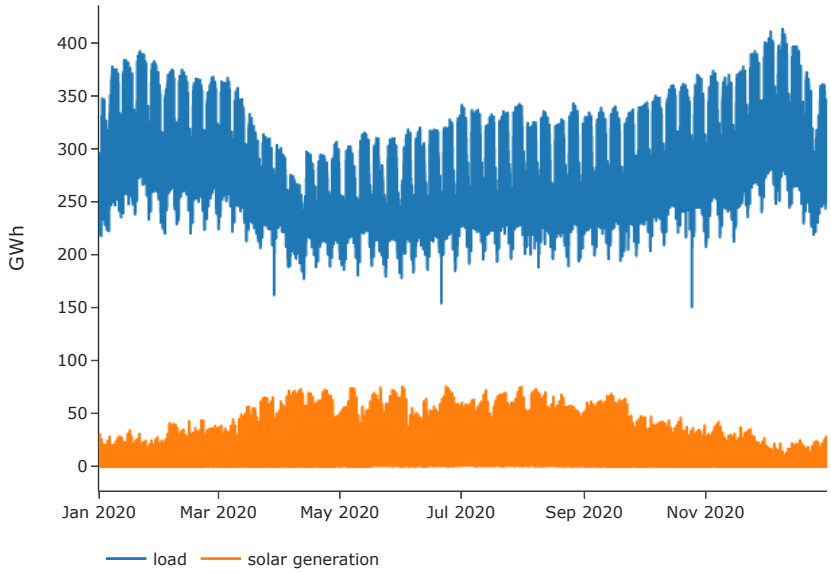

Figure B.1: Hourly solar power generation and load in EU-28 in 2020 (ENTSO-E2021).

PV cannibalization is when the market value of PV production declines as more PV comes online because the production of PV panels are correlated one with another. Cannibalization in turn depresses PV investment. However, PV cannibalization can also be addressed to some degree by storage options, which will however never fully compensate the effect due to the costs of storage investments and the energetic losses in storage operation.

Besides storage, innovative PV placements and configurations proposed in Kahl et al. (24) are another, promising way of dealing with cannibalization and the temporal mismatch of demand and production, particularly in places where storage options or public acceptance of alternative generation are limited. Kahl et al. (24) propose PV panel placements in locations that facilitate higher winter production. Using Switzerland as a case study, they show that PV panels placed at higher elevations can take advantage of higher winter irradiance, ground-reflected radiation from snow, and greater tilt angles to improve winter yield, all resulting in more electricity generation during the peak winter demand, and generation that is less correlated to pre-existing PV installations. Furthermore, Kahl et al. quantify the solar potential for Switzerland with these previously dismissed locations and find a more optimistic potential, rising from previous estimates between 7-19 TWh/year to more than 25 TWh/year. These results are exciting for mid-latitude regions like Switzerland; however, it remains to be seen whether there is an economic case for such placements.

In this paper, we use the market value approach (see e.g. (19; 23) for the approach and (20; 13; 26; 11; 4) for more recent applications) to estimate the market viability of innovative PV panel placements and geometries proposed by Kahl et al.(24). Following (19), we define

market value as the average market price per MWh of output (EUR/MWh) over all hours. In doing so, we account for the fact that the value of electricity depends on the time and location of the production and that generation profiles can be correlated through their dependence on weather patterns (e.g., 19) (insights that the traditional Levelized Cost of Electricity (LCOE) approach cannot capture). We also consider average panel revenue, a measure of the financial viability of new capacities (EUR/kW/year). To this end, we couple two complementary numerical models to explore economically viable placements of PV, both allowing and forbidding alpine locations. Our soft-linked models find optimal placements given local variations in the climate; electricity production and consumption; power transmission capacity; and market prices.

Switzerland is an interesting case study for a few reasons. First, in 2017 the Swiss passed a new Energy Strategy (ES 2050) (5) that requires the share of renewable generation to expand dramatically as the country phases-out nuclear generation. Second, Switzerland has significant potential for solar power (much more than its potential for other renewables (3)) and will continue to invest heavily in expanding this capacity. To date, the vast majority of solar panels are installed on rooftops of private homes and commercial buildings. Third, the Swiss electricity market exhibits similar seasonal patterns to other markets in Europe; therefore, these results are relevant for other countries. Switzerland has an additional constraint and advantage: its large share of hydropower generation (56%) in the electricity mix. In spring and summer, the country is a net exporter due to increased hydro production from snow melt. In fall and winter, it is a net-importer.

We proceed with this paper as follows: In section B.2, we outline the relevant literature. In section B.3, we explain our modeling method, scenario framework, and associated input data. In section B.4, we present our results. Finally, in section B.5, we discuss our results in context and discuss their broader policy implications.

B.2 Literature Review

In order to value the in-feed from intermittent energy sources more equitably, researchers and policymakers have turned away from levelized-cost comparisons to market value estimations (23). Market value is particularly important for estimating the financial viability of renewable energy sources with intermittent in-feed because market value acts as a proxy for the time-varying energy system balance: Higher prices at time t indicate that additional in-feed will benefit the system; lower prices indicate that additional in-feed is not as beneficial to the system at that time. Borenstein (6) uses simulated and historic wholesale market prices that incorporate average transmission losses and investment costs to quantify the cost-benefit market value comparison of a 10-kW solar installation in California. Comparing the time-varying value of solar to its constant counterfactual and considering the costs of investment and maintenance, he finds that PV did not have a compelling financial case in California, though he admittedly does not attempt to incorporate un-priced market externalities (e.g.,

environmental and social benefits) nor model the whole energy system.

Using different time and spatial resolutions, other researchers have used market value estimations to measure changes to both the supply and demand sides of energy systems. Hirth (19) uses an open market model to understand supply dynamics in the medium and long-term as the penetration of solar and wind increases and policy levers are adjusted. As the author increases solar and wind penetration in his model, the market value (value factor or value relative to a constant source of electricity) decreases for both solar and wind power, leaving both technologies noncompetitive. He also finds that changes in fuel prices, conventional capacity, interconnection investments, and CO_2 prices influence the value factors of these renewables, though not necessarily in intuitive directions. Winkler et al. (36) also show using econometric methods that fuel prices, conventional capacity, and CO_2 prices are some of the main drivers of changes in market value. Again, these drivers change in importance depending on the penetration rate: At lower shares of renewables, fuel prices, conventional capacity and CO_2 prices are most important while flexibility options become more important as penetration increases. Engelhorn and Müsgens (12) use historical in-feed data on existing wind installations to show the large variation in individual wind turbines' market value relative to the fleet; that is, even if the overall fleet does not have a high market value, individual turbines can have high market values. The author also quantifies the market value variation within Germany due to differences in in-feed price correlations and the consistency of the production yield, showing how regional production can vary significantly.

There are increasingly more studies considering alternative placements and orientations of renewables that could improve their market value prospects. Zipp (39) explores demand-oriented configurations, rather than orientations maximizing gross production, using historical data. He finds that solar orientations in Germany are largely driven by policies that do not consider market value. These results, and those in (6) that consider different panel orientations in California, suggest that load-response investment would improve market values of solar if supported by appropriate policies.

We contribute to the literature in several ways. First, we quantify the market value of placing solar PV panels in mountainous areas. Second, we endogenously consider feedback effects between electricity prices and solar placement to ensure that the resulting market values are not subject to cannibalization effects. Third, we optimize the market value of solar PV placements in alpine and non-alpine regions under different weather scenarios and CO_2 price scenarios.

B.3 Methods

To calculate the market value of PV placement strategies, we soft link two models: OREES (Optimized Renewable Energy by Evolution Strategy) (10; 2) and Swissmod (30; 1). We couple the models to leverage the strengths of each and iterate one with the other until the prices and placements converge to an equilibrium (Figure B.2). For reasons detailed in B.3.1.1 and

B.3.1.2, the two models cannot be combined into a unique entity.

We organize our analysis by comparing two main optimization scenarios (mountain and no-mountain placements) that we compare to a business as usual scenario. Both scenarios begin with the same initial conditions (step 1 in Figure B.2): time series of observed market prices (17). Those time series are fed into the objective function of OREES that explores the feasible space of PV locations in Switzerland and identifies the placements that generate the most revenue given grid constraints. The optimization includes or excludes mountain locations, creating the two scenarios.

For each scenario, when the optimal PV placement is found (step 2), the corresponding power generation time series is used by Swissmod to compute resulting electricity prices as well as other market related indicators (step 3). The new market prices are then used by OREES to optimize the PV placements once again. We repeat this process until the models converge: The PV placement and corresponding revenues reach an equilibrium and do not change significantly anymore between iterations.

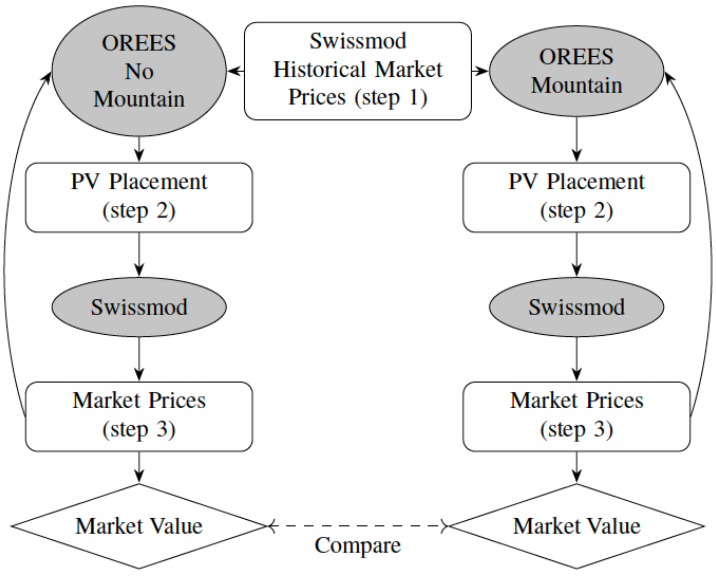

Figure B.2: Model Iterations

B.3.1 Models

B.3.1.1 Swissmod

Swissmod (30; 1) is an electricity market dispatch and load-flow model that represents the Swiss wholesale electricity market in a high spatial (nodal) and temporal (hourly) resolution. In its original formulation, Swissmod represents the entire transmission network of Switzerland (220 and 380 kV), the interconnections with Switzerland's neighboring countries as well as the cross-border connections in Europe (207 nodes and 450 lines) using a DC load flow approach

(31; 25)[2]. In this paper, Swissmod is used as a zonal model in an aggregated way. Each country is represented by a single node, with commercial import-export structures between interconnected countries being limited by net transfer capacities (NTCs). This results in a single market clearance and a single price (compared to multiple nodal prices) per country, which better reflects the current design of electricity markets in Europe.

The objective of the model is to minimize total generation costs under given demand levels. The model is deterministic, assumes a perfectly competitive market with perfect foresight and considers a whole year in hourly resolution. Due to the high dependence of the Swiss electricity market on hydropower, the model contains a detailed hydropower operation model of individual hydro power plants (run-of-river, storage and pumped-storage) and their interaction within cascade structures (interconnection and water flow).

Swissmod is coded in GAMS (General Algebraic Modeling System) and solved using the IBM CPLEX solver and the Gurobi Optimizer. A detailed model description can be found in (30; 1; 8).

The advantage of using Swissmod in combination with the OREES model (see next section) is on the one hand that Swissmod allows the simulation of future price developments, which are needed to simulate revenue-maximizing PV placements under future conditions. On the other hand, Swissmod enables the consideration of possible feedback effects of PV placements on market prices.

B.3.1.2 OREES

OREES shares many features with Swissmod: the high-voltage transmission grid of Switzerland and connections with the neighboring countries, the distributed electricity consumption and production from hydropower facilities, and a representation of the water inflow into the hydropower infrastructure. OREES does not consider the electricity market and is thus much faster at simulating an entire year, which is essential for the optimization of PV placement described below. Like Swissmod, we run OREES with an hourly resolution for each considered year. The model uses spatially distributed hourly time series of electricity consumption, production from run-of-river plants and PV panels, water inflow into the hydroelectric reservoirs and the hydropower plants specifications. Bartlett et al. (2) describe in detail how these data are fed into the optimal power flow algorithm of the MATPOWER library (38).

OREES has an external optimization layer that allows to explore the feasible space for PV placements (10). Based on evolution strategy, this layer successively generates PV placement scenarios of a specified total production; computes the corresponding spatially distributed production time series; and using the power flow model, simulates the behavior of the electric and hydropower systems given these choices of PV placements. Only solutions that are

[2] In addition to Switzerland, the countries considered in Swissmod include Austria, Germany, France, Italy, Belgium, Denmark, Spain, Great Britain, Luxembourg, the Netherlands, Norway, Poland, Portugal, Sweden, Slovenia, Slovakia, the Czech Republic, Hungary and the United Kingdom.

compatible with the grid infrastructure are allowed.

Concretely, the evolution strategy iteratively displaces fragments of the installed capacity of PV connected to each electric grid node, decreasing the amount on certain nodes and increasing it on others. Starting from a quasi-homogeneous distribution of installed capacities, the algorithm relocates them in order to maximize our objective function: the country-wide averaged market value of panel capacity. This evolution occurs across 169 electric nodes and on a spatial grid of 1.6x2.3 km which corresponds to the satellite-derived radiation data. The total installed capacity varies at each optimization step to keep an annual production of 25 TWh. The local geometry of PV panels (tilt and azimuth in each grid cell) is optimized once and for all at the initialization phase. In each location, tilt and azimuth are chosen to maximize revenue, given the initial market prices (step 1 in Figure B.2). More detail concerning the panel geometry is provided in B.3.2.

Dujardin et al. (10) used this optimization scheme to minimize the amount of required import in Switzerland by optimizing generation mix and location of PV and wind installations. In the present work, we only optimize PV location to maximize the average revenue of panel capacity under the constraint of a fixed total production of 25 TWh for each considered year.

B.3.2 Scenarios

B.3.2.1 Scenario setup

To quantify the impact of different PV placement strategies (business as usual, no-mountain, and mountain) on the market value of PV, we apply the scenario setup shown in Table B.1. Aside from differing the PV placement space, in each scenario setup we also take additional factors that can influence the market value of PV into account and do some robustness checks. That is, we consider changes to the European and Swiss electricity system, the price of carbon, and the weather (e.g., (19)). As a starting point, we consider the future European and Swiss electricity systems in 2025. In order to take into account the continuous change in generation structures as part of the energy transition (less conventional technologies, more renewables), we also analyzed the system in 2040. To account for the significant impact of the CO_2 prices on the marginal costs of fossil power plants and thus on the wholesale electricity price, we use the three CO_2 price scenarios described in B.3.2.2 . To consider the impact of weather on PV generation and the resulting impact on market values, the weather years 2013 to 2015 are analyzed. These years were chosen because they capture a range of weather conditions such that we feel confident in the robustness of our results. Since the model iteration process used in this paper is resource intensive, we do not calculate all possible cross-combinations (of system year, CO_2 price scenario and weather year).

System	CO_2 price (EUR/t CO_2)	Weather	PV placement
2025	BE (= 25.7)	2013	BAU
			No-Mountain
			Mountain
		2014	BAU
			No-Mountain
			Mountain
		2015	BAU
			No-Mountain
			Mountain
	G2C (= 56)	2015	BAU
			No-Mountain
			Mountain
	GCA (= 126)	2015	BAU
			No-Mountain
			Mountain
2040	GCA (= 126)	2015	BAU
			No-Mountain
			Mountain

Table B.1: Scenario setup

B.3.2.2 Input data

In this paper, we consider the Swiss and European electricity system in 2025 and 2040 based on the TYNDP 2018 (14) "Best Estimate" (BE) and "Sustainable Transition" scenarios. Accordingly, in Swissmod, we base the generation capacities, in-feed (except PV in CH) and demand on TYNDP 2018 (14). For Switzerland, we replace 25 TWh of nuclear generation (rounded 20-year average (32)) with the same amount of solar PV generation, for which we consider various placement scenarios from the OREES model. With regard to demand, in-feed profiles from renewable energies, and water inflows for Swiss hydropower, we run our models with three weather years: 2013, 2014, and 2015. These years represent average (2015), above-average (2013) and below-average (2014) years for Switzerland in terms of the annual electricity demand relative to the average over the last 10 years (32). To generate the corresponding Swissmod data for the three weather years for the future system, we scale the profiles and relative annual differences for demand (15; 27) and renewable in-feed (except for PV in CH) (28) for the years 2013, 2014 and 2015 to TYNDP 2018 (14) values. For Swiss PV, we use the simulated values from the SUNWELL/OREES models for the respective weather years (see below), and for the water inflows, we rely on the data generated by (1).

To limit cross-border trade in Swissmod, we use the NTC values for all European countries included in the model from TYNDP 2018 (14), matching to the closest available year in the source dataset. With regard to fuel prices, we also rely on the data from TYNDP, taking into account three sensitivities with respect to the CO_2 price, a scenario where coal is before gas in

the merit order (BE scenario, CO_2 price of 25.7 EUR/t CO_2 (14)), a scenario where gas is before coal in the merit order (G2C scenario, CO_2 price of 56 EUR/t CO_2 (16)) and a scenario in which "Global Climate Action" (GCA scenario, CO_2 price of 126 EUR/t CO_2 (14)) is undertaken.

We generated all input time series needed by OREES (solar radiation, hydropower, demand) using the procedure described in (2) and (9). These data correspond to the historical data for 2013, 2014, and 2015. Power generation from PV panels for each hour of the considered years is computed by the SUNWELL model (24) on a 1.6 x 2.3 km grid given the (annual) optimal geometry used in each grid cell. OREES uses this grid for the optimization, choosing the amount of panel capacity installed in each grid cell. "Optimal geometry" refers to the panel tilt and azimuth angles that generate the highest revenue. The optimal geometry depends on the temporal patterns of electricity prices, on the regional weather patterns, and local topography. High production at times of high prices is desirable. Furthermore, azimuth angles deviating from south are advantageous if preferential cloud cover or shading persistently diminish the direct solar irradiance during some part of the day. The optimal tilt angle favors production during the time of the year that provides the most energy at times of highest electricity prices. Local conditions such as cloud cover and surface albedo (especially in the presence of snow) have a strong effect on this dynamic.

B.3.2.3 Mountain, No-Mountain and BAU scenarios

As mentioned in B.3.1.2, OREES generates maps of installed PV capacity on a 1.6x2.3 km grid. The solution space we explore in the optimization is constrained by the maximum amount of PV panel area that can be installed in each grid cell. The Mountain and No-Mountain scenarios are created using different maps of available PV panel area.

For the Mountain scenario, we use the same map as the one described in Dujardin et al.(10). This map was constructed with a Geographical Information System (GIS) analysis at 50 m resolution. Using datasets (34; 33) from the Swiss Federal Office of Topography, we include locations that are: lower than 2700 meters-above-see-level (m.a.s.l), at least 150 m away from slopes steeper than 30 degrees, within 500 m of a road. We exclude the Swiss national park and north facing slopes and only consider the following surface cover types suitable (as defined by The Corine Land Cover inventory (7)): urban fabric; industrial or commercial units; non-irrigated arable land; permanently irrigated land; pasture; heterogeneous agriculture areas; natural grasslands; bare rocks; and sparsely vegetated areas. In each permitted location, we allow a maximum coverage of 5%, corresponding to a national potential PV area of 600 km^2. This high-resolution map of PV potential is then aggregated to the coarser 1.6x2.3 km grid.

For the No-Mountain scenario, we lower the elevation limit to 800 m.a.s.l, which reduces the PV potential area to 450 km^2. The PV potentials for both scenarios are depicted in Figure B.3.

In addition to optimizing PV installations for the Mountain and No-Mountain cases, we computed the market value generated by a business-as-usual (BAU) scenario in which PV

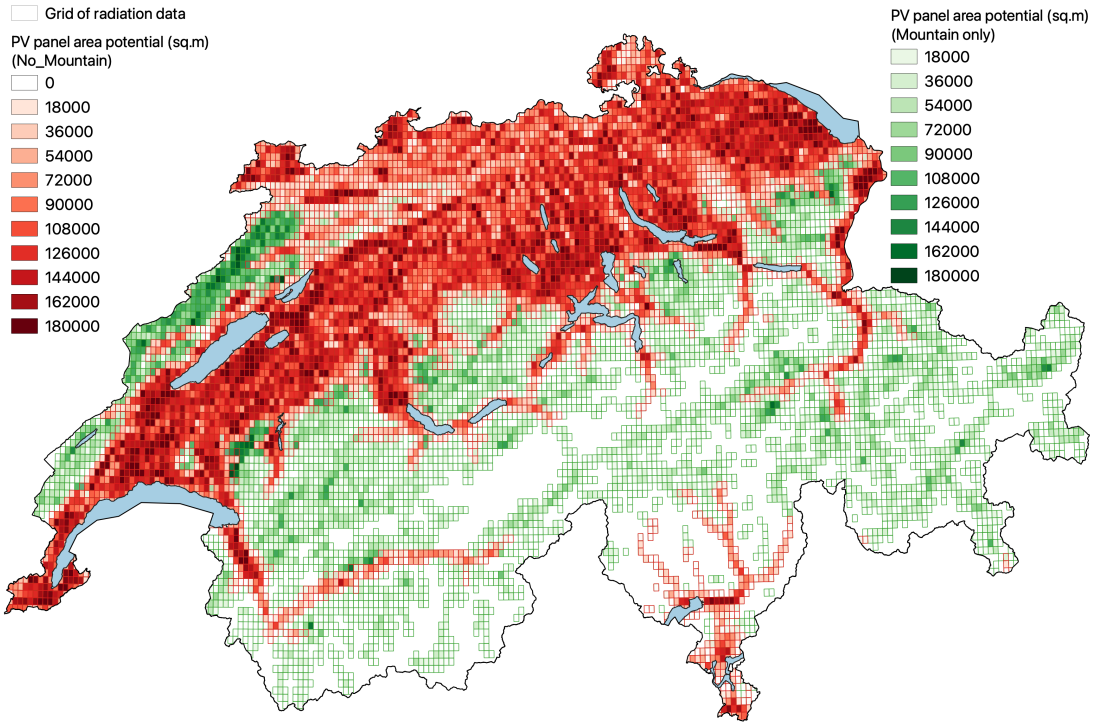

Figure B.3: Potential for PV installation in the Mountain and No-Mountain scenarios.

installations are homogeneously distributed in urban areas (Figure B.4) and have a typical south-facing and 23°-tilt geometry. This third scenario does not need to be optimized by ORESS as the PV placements are predefined. Swissmod directly uses the time series of power generation by this particular constellation of PV to compute the associated market value. We consider BAU as representative of the conventional, currently adopted strategy of PV installation on rooftops and compare it to the optimized scenarios in the analysis.

We used the weather year 2015 for an initial and extended analysis of our 2-model approach. More specifically, we used the three different (CO_2) price scenarios from TYNDP (BE, G2C and GCA) and iterated the two models four times in order to validate the stability of the procedure. Between the first iteration of the 2-model approach and all consecutive iterations, the variations in market values and PV placements were smaller than 0.2%. The 2-model approach is thus stable and the changes in electricity generation from PV in Switzerland from one iteration to the next do not impact sufficiently the electricity market to require multiple iterations in order to reach an equilibrium. After only one iteration, a solution sufficiently close to the global optimum is reached. Consequently, for the weather years 2013 and 2014, we iterated the models only twice. Similar to 2015, only small variations of 0.1 to 0.4% were observed between those two iterations.

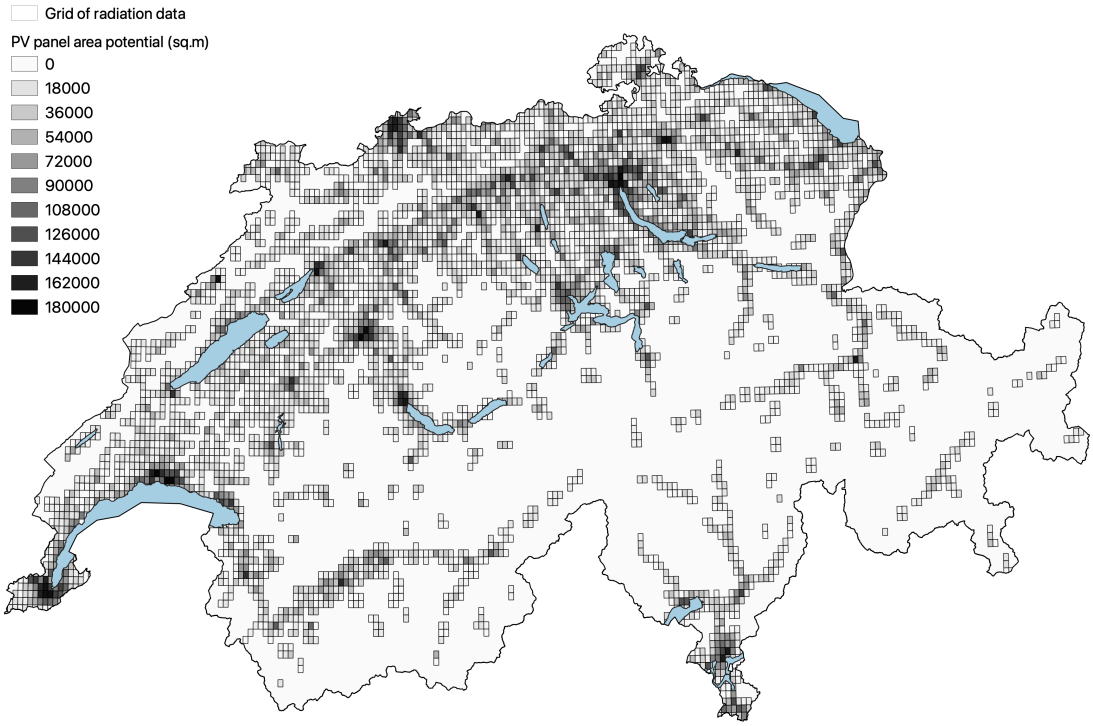

Figure B.4: PV panels installed in the Business As Usual scenario

B.4 Results

In this section, we first present the results for the weather year 2015, given the three CO_2 price scenarios and the two system conditions (2025 and 2040) and then present the results for 2013 and 2014 for the BE price scenario and the system in 2025 only. Finally, we analyze the inter-annual variations and their link to weather patterns.

B.4.1 Increased market value

As shown in Table B.2, the optimized scenarios (No-Mountain, Mountain) have higher market values than the BAU scenario. The increase in market value of energy is moderate (between 1.29% and 6.55%) and is due to a better alignment of production with demand, that is, more production in winter when demand (and accordingly prices) are higher. The increase in market value of capacity is however quite large (between 8.10% and 21.98%) and can be explained by the higher yield of panels in alpine areas. We can also observe that the No-Mountain scenario is positioned between the BAU and alpine scenarios in terms of performance. Additionally, the generation of the targeted 25 TWh in 2015 requires 120.21 km^2 of PV panel area (considering an efficiency of 15%) or 18.03 GW_{peak} under the BAU scenario and 104.04 km^2 or 15.61 GW_{peak} under the mountain scenario (and BE prices). In general, our results show that the altitude

constraint that limits our scenarios has a strong impact on the economic performance of the panels: the higher, the better.

CO_2 price/ System	Placement scenario	Market value of energy from PV (EUR/MWh)	Value Factor	Market value of panel capacity (EUR/kW/yr)
BE/ 2025	BAU	43.55 (reference)	0.82 (reference)	60.37 (reference)
	No-Mountain	44.17 (+1.42%)	0.83 (+1.89%)	65.3 (+8.16%)
	Mountain	44.95 (+3.23%)	0.85 (+4.37%)	72.01 (+19.27%)
G2C/ 2025	BAU	60.89 (reference)	0.86 (reference)	84.42 (reference)
	No-Mountain	61.68 (+1.29%)	0.88 (+1.33%)	91.26 (+8.10%)
	Mountain	62.76 (+3.07%)	0.89 (+3.33%)	100.75 (+19.34%)
GCA/ 2025	BAU	96.25 (reference)	0.84 (reference)	133.44 (reference)
	No-Mountain	97.93 (+1.75%)	0.85 (+1.63%)	144.77 (+8.49%)
	Mountain	100.26 (+4.17%)	0.87 (+3.90%)	160.59 (+20.35%)
GCA/ 2040	BAU	55.42 (reference)	0.66 (reference)	76.84 (reference)
	No-Mountain	57.26 (+3.31%)	0.68 (+3.62%)	83.83 (+9.10%)
	Mountain	59.05 (+6.55%)	0.71 (+7.12%)	93.73 (+21.98%)

Table B.2: Market value of PV installations (weather year 2015) for the 3 placement scenarios, 3 CO_2 price scenarios and 2 system years

We can see by looking at the value factors that PV has a market value below the average market price in all scenarios (value factor < 1). However, the value factors increase with optimal placement of the panels, especially when alpine areas are also allowed. It is important to note that value factors can also be increased by more demand flexibility, reducing certain price peaks outside of solar generation hours. Accordingly, a better representation of demand side flexibility could result in value factors closer to 1.

Comparing the three CO_2 price scenarios for the system in 2025, the market values for energy and capacity increase as CO_2 prices (and consequently electricity prices) rise. The added value of PV in the mountains (compared to the BAU scenario) is greatest in the GCA scenario, the scenario with the highest CO_2 price. However, as shown for the market value of energy, a higher CO_2 price does not necessarily increase the added value of alpine solar. Comparing the G2C scenario and the BE scenario, the increase in the market value of energy by allowing

alpine PV placement is higher in the BE scenario (although in a similar range). Looking at the value factors for the 2025 system, the highest increase compared to the BAU scenario is observed in the BE scenario, the scenario with the lowest CO_2 price. This suggests that the increase in the value factor is not driven solely by the electricity price level, but rather by the structure and dynamics of the underlying merit order (i.e., steepness (19)).

Comparing the system in 2025 and 2040 (for the GCA CO_2 price scenario), absolute market values fall in 2040. With less fossil plants (especially about 65% less coal generation) and more renewable generation (about +75%) in the system in 2040, the high CO_2 price is less relevant to market prices. More importantly, the high share of renewables lowers price levels, market values and value factors (also called "cannibalization effect", e.g., (29)). However, allowing mountain PV in 2040 shows the highest relative increase in market values (and value factors) compared to the BAU scenario. In a system with more renewable energies, mountain solar has a higher value.

Year	Placement scenario	Market value of energy from PV (EUR/MWh)	Value Factor	Market value of panel capacity (EUR/kW/yr)
2013	BAU	44.63 (reference)	0.82 (reference)	56.41 (reference)
	No-Mountain	45.59 (+2.14%)	0.84 (+2.49%)	61.27 (+8.63%)
	Mountain	46.88 (+5.03%)	0.87 (+5.74%)	70.25 (+24.54%)
2014	BAU	43.01 (reference)	0.82 (reference)	56.01 (reference)
	No-Mountain	43.16 (+0.33%)	0.82 (+0.42%)	59.25 (+5.77%)
	Mountain	43.92 (+2.10%)	0.84 (+2.48%)	63.80 (+13.90%)

Table B.3: Market value of PV installations (weather year 2013 and 2014) for the 3 placement scenarios under the TYNDP Best Estimate CO_2 price scenario for the system in 2025

For the weather years 2013 and 2014, we optimized the location of PV panels only under the TYNDP Best Estimate CO_2 price scenario, which is more in line with the current market conditions. Similar to 2015, the market value of energy from PV is increased by 5.03% and 2.10% for 2013 and 2014 respectively, between the BAU and Mountain scenario (Table B.3). This increase is of 24.54% and 13.90% for the market value of panel capacity. We can observe significant changes between each of the three years, with 2014 (the year with the lowest demand) showing the least improvement in the transition from an urban to a mountain placement scenario. The year 2013, which has the highest demand especially in winter, was the weather year with the biggest improvement. This result confirms the role of mountain solar for winter production.

B.4.2 Spatial distribution of PV installations

Figure B.5 depicts the spatially distributed results for the three considered years, for the Mountain and No-Mountain scenarios. The color gradient shows the market value of panel capacity in every grid cell, computed with the market price time series of the considered year and the local PV production time series computed by SUNWELL. The areas shaded in blue indicate the locations selected by OREES. As described in Dujardin et al.(10), in the region surrounding each electric grid node, OREES fills the best grid cells first (to their potential) until the optimal installed capacity connected to the node is reached. Consequently, the map of PV installations (surface area per grid cell) is equivalent to overlaying the blue areas of Figure B.5 with the installation potentials of Figure B.3. For this reason, we did not incorporate an additional figure. We can observe in Figure B.5 that some selected areas are common between the two scenarios, and throughout the three years: the Rhone Valley in the south-west and the south part of Ticino (populated Italian border) in the south. Both offer rather high market values and are located below our elevation threshold (800 m.a.s.l). The first benefits from particularly good weather conditions in winter, with the low-altitude clouds (stratus) being trapped further north on the Swiss plateau. The second exhibits a quasi-Mediterranean climate, also favoring high winter radiation (compared to the rest of the country).

Another important observation concerns the overall market value distribution across the country: The Alps exhibit high values compared to the Swiss plateau. Kahl et al. (24) showed that PV panels located in the Alps can produce much more electricity in winter than anywhere else in Switzerland. Higher winter solar radiation and higher ground reflection from snow can be exploited with steeper installations geometry to maximize winter production. In addition, the fact that market prices are higher in winter than in summer explains why the Alps show such high market values. In the Mountain scenario, OREES places as much PV as possible in the Alps, given the land availability and the grid constraints. In 2015, for the TYNDP Best Estimate CO_2 price scenario, 79% of the PV panels are located above 800 m.a.s.l, occupying 52.6% of the potential available above this elevation.

2014 shows the lowest market values of the three years and requires 114 km^2 and 121 km^2 of PV panel area for the Mountain and No-Mountain scenarios, respectively. Those values are 111 km^2 and 124 km^2 for 2013, and 104 km^2 and 113 km^2 for 2015. As described below, 2014 had an above-average cloudiness, especially in the Alps. More PV surface area is thus needed to reach the total production target. Despite the interannual change in PV capacity that is required to reach the desired production target, 78.9% of the installations are common between 2013 and 2015. This value is 75.2% between 2014 and 2015. This indicates that most installations are considered optimal for all years, and thus optimal for a range of weather situations.

We can summarize the PV placement dynamics as follows: The Alps offer the highest market values, independent of the inter-annual weather variations. If installations in certain high-altitude areas are not allowed, some specific valleys should be considered as alternatives. The

region surrounding Lake Geneva offers a lot of installation potential and higher market values than other Swiss urban centers.

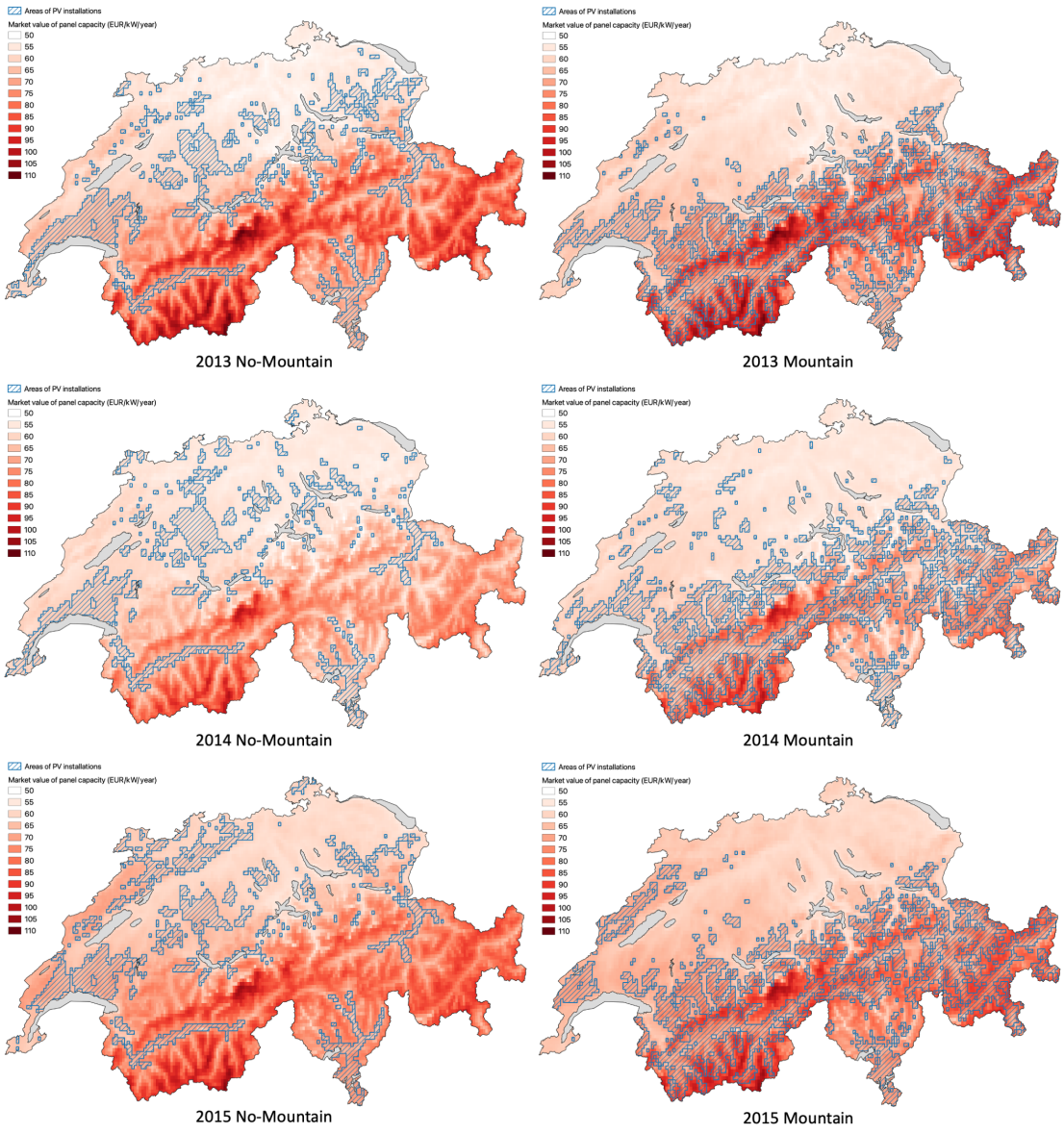

Figure B.5: Market value of panel capacity and optimized location for PV installations for the 3 considered years and the 2 placement scenarios

B.4.3 Weather driven performance

Of all three years, 2013 shows the biggest contrast in market value between alpine and non-alpine regions, as we can observe in Figure B.5. 2014 is characterized by overall lower values, across the entire country, with a more expressed decrease in the mountain regions. Finally, 2015 is characterized by overall high values in both regions. Those trends are confirmed in

Figure B.6 which depicts a temporally more detailed picture of the weather conditions for our considered period. The biggest difference between mountain and non-mountain areas occur in each season of 2013. The summer of 2014 and end of the year show particularly low radiation values. We can conclude that the market value of panel capacity is strongly driven by the weather patterns occurring on seasonal timescales and that our optimization of PV placements took advantage of the differences between regions to increase this market value.

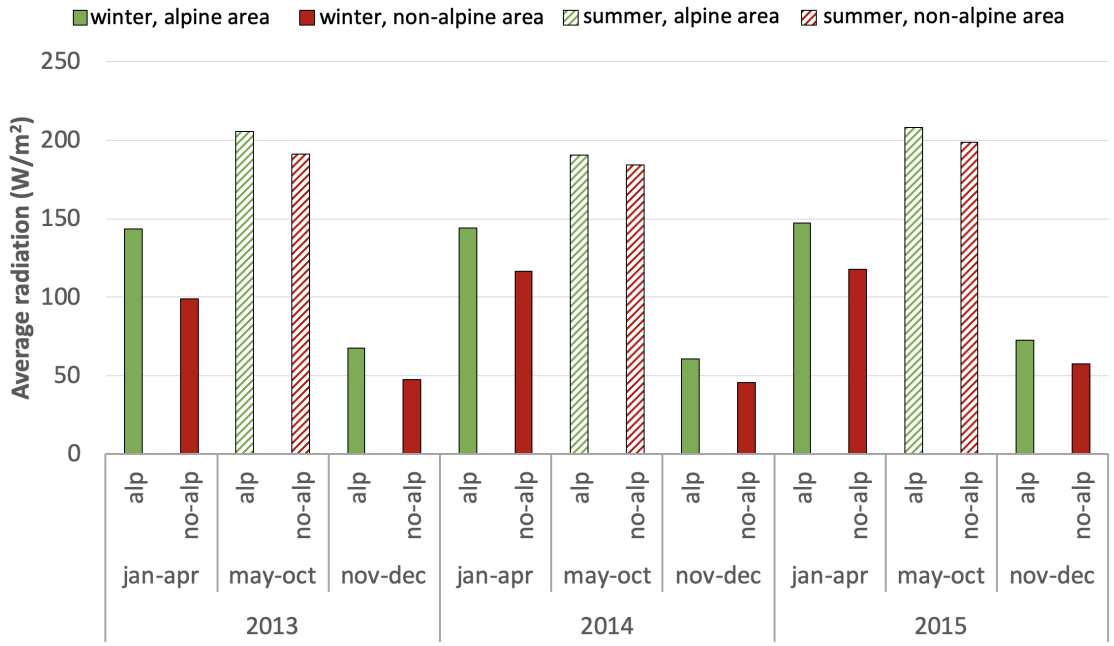

Figure B.6: Average horizontal solar radiation for alpine and non-alpine areas

B.4.4 Spatial heterogeneity of market value

Table B.2 and Table B.3 show the average performances of the three scenarios. Figure B.7 and Figure B.8 depict a disaggregated view of these performances, with the distributions of the market value of all PV panels in 2015. The panels in the BAU scenario, represented in grey, show an almost Gaussian distribution of revenues, centered around 43.2 EUR/MWh and 61 EUR/kW/year. For the market value of energy, we can see a clear separation between the distributions of the three scenarios. The No-Mountain scenario exhibits a long tail, indicating that some panels have the same market value of energy as panels from the Mountain scenario. As already observed in Table B.2, the relative differences between scenarios are small.

The distribution of market value of panel capacity for the Mountain scenario reveals an important piece of information. The long tail towards high revenues indicates that a considerable amount of installed capacity offers much higher revenues than the average value of the scenario, which is already 19.27% higher than the one from BAU. More than 1 GW of capacity offers revenues higher than 81 EUR/kW/year. This should be compared to the 61 EUR/kW/year that conventional urban PV panels offer during the same time.

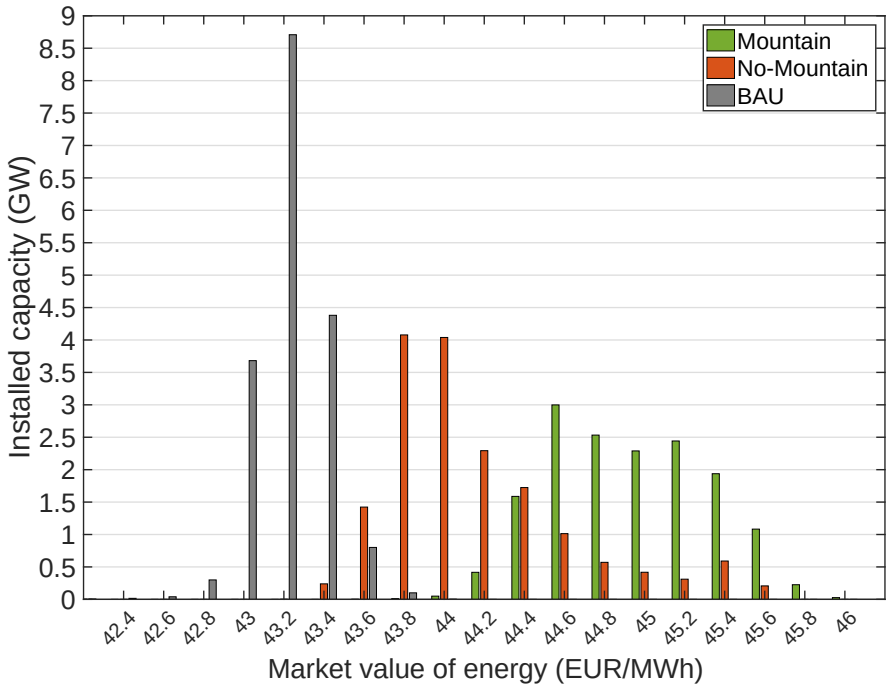

Figure B.7: Distribution of the market values of energy for the optimized PV placements of the three scenarios under the TYNDP Best Estimate CO_2 price for 2015.

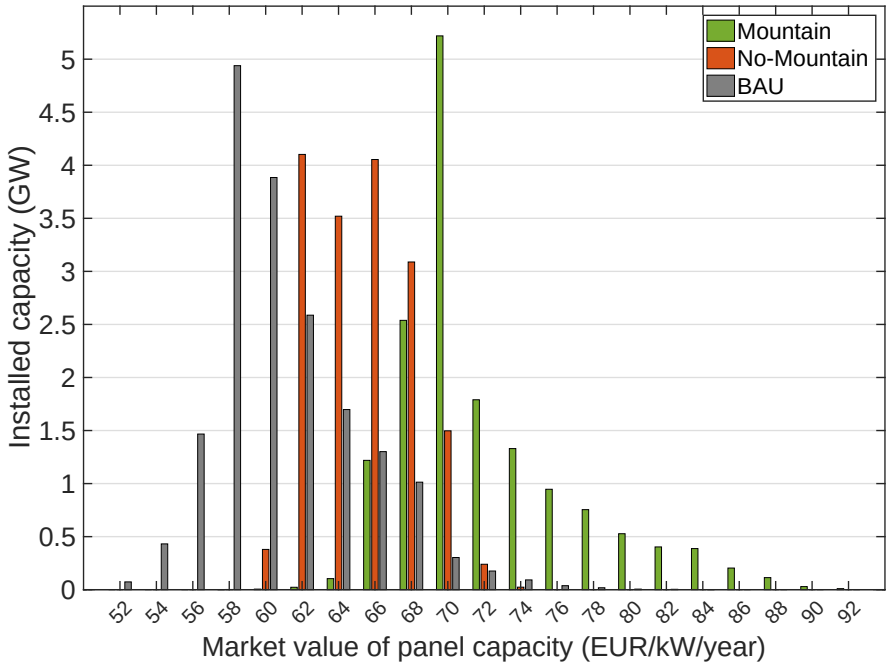

Figure B.8: Distribution of the market values of panel capacity for the optimized PV placements of the three scenarios under the TYNDP Best Estimate CO_2 price for 2015.

B.5 Discussion and conclusion

In this work, we explored the increased market value of PV panels located in the alpine regions of Switzerland. Furthermore, we showed that higher elevation is synonymous with higher revenues. This is particularly true for the revenue of panel capacity, which has an average value of 72.82 EUR/kW/year (2015, TYNDP Best Estimate CO_2 price scenario) for the selected placements located above 800 m.a.s.l. This is already 19.6% higher than the revenue from urban installations. We also saw that at least 1 GW of capacity could be installed in places offering revenues above 81 EUR/kW/year: another 13.4% increase. The future role for mountain solar looks promising based on our results since the highest increase in value factor can be observed for a system with a high share of renewable generation (2040 system). However, it is important to consider that we have limited mountain solar placement to Switzerland.

Our approach is subject to some limitations which should be addressed by future research. One of the main limitations of our study is the limited representation of demand side flexibility. While improved demand side management will increase the value factor and thereby the system value of non-dispatchable generation, it will at the same time reduce some of the gains from mountain solar generation. Another limitation is that we do not allow for curtailment of PV when determining the optimal placement of PV panels. However, from an economic perspective, some degree of curtailment may be socially optimal (e.g., (18)). If we would allow some curtailment, the share of alpine PV would be even higher. Hence, this likely results in an underestimation of the potential of alpine PV in this study. Another limiting factor in our modeling approach is the rather coarse resolution (1.6x2.3 km) of the radiation data, which is not sufficient to accurately account for all the topographic shading in the Alps. This results in an underestimation of the potential in certain, well exposed, locations and in an overestimation in other locations that have strong shading. We expect that the overall performance of the scenarios remains essentially the same if higher resolution datasets would be available and used. However, with such resolution, the tail of the distribution of market value of panel capacity for the alpine placements (green in Figure B.8) is expected to be even longer, with some locations offering even higher revenues. Furthermore, for a holistic cost-benefit calculation of mountain solar, an important question remains: What is the additional investment cost of such installations? Specifically, it is important to know if, for example, an alpine installation offering 33% more revenue than an urban one would require less than 33% additional investment, which would then be economically competitive. Such installation costs are very difficult to calculate in a generic manner, especially in alpine environments. Road access and proximity to existing electric infrastructure, as well as project size, have a strong impact on the investment cost per kW. Given the well-developed road and grid infrastructures in Switzerland, many locations could offer great competitiveness, but it remains to quantify such installation costs in a spatially distributed way. The construction of PV plants in the Alps also raises the question of the social acceptance of such projects. However, at least for Switzerland, a relatively high level of social acceptance can be observed, whereby the

environmental impact, ownership and design of the PV panels can have a major influence on social acceptance (35). Furthermore, Switzerland's alpine areas are already widely impacted by civilization, offering considerable surface area where the addition of PV panels would not be the only "disturbance". Based on our results, we see an important role for mountain solar placements in improving the system value of solar generation.

Acknowledgments

This work was funded by Innosuisse through Swiss Competence Centers for Energy Research: SCCER Supply of Electricity, SCCER Competence Center for Research in Energy, Society and Transition, and SCCER Joint Activity Scenarios and Modeling.

Bibliography

[1] Jan Abrell, Patrick Eser, Jared B. Garrison, Jonas Savelsberg, and Hannes Weigt. Integrating economic and engineering models for future electricity market evaluation: A swiss case study. *Energy Strategy Reviews*, 25:86 – 106, 2019.

[2] Stuart Bartlett, Jérôme Dujardin, Annelen Kahl, Bert Kruyt, Pedro Manso, and Michael Lehning. Charting the course : A possible route to a fully renewable Swiss power system. *Energy*, 2018.

[3] Christian Bauer, Stefan Hirschberg, Y. Bauerle, S. Biollaz, A. Calbry-Muzyka, Brian Cox, Thomas Heck, M. Lehnert, A. Meier, H.-M. Prasser, Warren Schenler, K. Treyer, F. Vogel, H.C. Wieckert, X. Zhang, M. Zimmerman, V. Burg, G. Bowman, M. Erni, M. Saar, and M.Q. Tran. Potentials, costs and environmental assessment of electricity generation technologies. https://www.psi.ch/ta/PublicationTab/Final-Report-BFE-Project.pdf, 2017.

[4] Christiane Bernath, Gerda Deac, and Frank Sensfuß. Impact of sector coupling on the market value of renewable energies – a model-based scenario analysis. *Applied Energy*, 281:115985, 2021.

[5] BFE. Energiestrategie 2050. https://www.bfe.admin.ch/bfe/de/home/politik/energiestrategie-2050.html, 2020.

[6] Severin Borenstein. The Market Value and Cost of Solar Photovoltaic Electricity Production. 2008.

[7] Copernicus European Earth Monitoring. Corine Land Cover inventory. https://land.copernicus.eu/pan-european/corine-land-cover/clc2018, 2018.

[8] T. Demiray, H. Weigt, G. Beccuti, I. Schlecht, J. Savelsberg, and M. Schillinger. Modellierung der System Adequacy in der Schweiz im Bereich Strom. 2017.

[9] Jérôme Dujardin, Annelen Kahl, Bert Kruyt, Stuart Bartlett, and Michael Lehning. Interplay between photovoltaic, wind energy and storage hydropower in a fully renewable Switzerland. *Energy*, 135:513–525, sep 2017.

[10] Jérôme Dujardin, Annelen Kahl, and Michael Lehning. Synergistic optimization of renewable energy installations through evolution strategy. *Environmental Research Letters*, 16(6):064016, 2021.

[11] Manuel Eising, Hannes Hobbie, and Dominik Möst. Future wind and solar power market values in germany — evidence of spatial and technological dependencies? *Energy Economics*, 86:104638, 2020.

[12] Thorsten Engelhorn and Felix Müsgens. How to estimate wind-turbine infeed with incomplete stock data: A general framework with an application to turbine-specific market values in Germany. *Energy Economics*, 72:542–557, 2018.

[13] Thorsten Engelhorn and Felix Müsgens. How to estimate wind-turbine infeed with incomplete stock data: A general framework with an application to turbine-specific market values in germany. *Energy Economics*, 72:542–557, 2018.

[14] ENTSO-E. Ten Year Network Development Plan 2018. https://tyndp.entsoe.eu/tyndp2018/, 2018.

[15] ENTSO-E. Power Statistics. https://www.entsoe.eu/data/power-stats/, 2020.

[16] ENTSO-E,ENTSOG. Fuel Commodities and Carbon Prices. https://www.entsos-tyndp2020-scenarios.eu/fuel-commodities-and-carbon-prices/, 2020.

[17] EPEXSPOT. Market data. https://www.epexspot.com/en/market-data, 2020.

[18] Arthur Henriot. Economic curtailment of intermittent renewable energy sources. *Energy Economics*, 49:370–379, 2015.

[19] Lion Hirth. The market value of variable renewables: The effect of solar wind power variablility on their relative price. *Energy Economics*, 38:218–236, 2013.

[20] Lion Hirth and Simon Müller. System-friendly wind power: How advanced wind turbine design can increase the economic value of electricity generated through wind power. *Energy Economics*, 56:51–63, 2016.

[21] IEA. World Energy Outlook 2020 -Summary. *Report*, 2020.

[22] IRENA. Renewable Capacity Higlights 2021. https://www.irena.org/-/media/Files/IRENA/Agency/Publication/2021/Apr/IRENA_-RE_Capacity_Highlights_2021.pdf?la=en&hash=1E133689564BC40C2392E85026F71A0D7A9C0B91, 2021.

[23] Paul L. Joskow. Comparing the Costs of Intermittent and Dispatchable Electricity Generating Technologies. *American Economic Association*, 101(3):238–241, 2011.

[24] Annelen Kahl, Jérôme Dujardin, and Michael Lehning. The bright side of PV production in snow-covered mountains. *Proceedings of the National Academy of Sciences of the United States of America*, 116(4):1162–1167, 2019.

[25] Florian U. Leuthold, Hannes Weigt, and Christian von Hirschhausen. A Large-Scale Spatial Optimization Model of the European Electricity Market. *Networks and Spatial Economics*, 12(1):75–107, mar 2012.

[26] Javier López Prol, Karl W. Steininger, and David Zilberman. The cannibalization effect of wind and solar in the california wholesale electricity market. *Energy Economics*, 85:104552, 2020.

[27] Open Power System Data. A free and open data platform for power system modelling. https://open-power-system-data.org/, 2020.

[28] Stefan Pfenninger and Iain Staffell. Long-term patterns of European PV output using 30 years of validated hourly reanalysis and satellite data. *Energy*, 114:1251–1265, 2016.

[29] Javier López Prol, Karl W. Steininger, and David Zilberman. The cannibalization effect of wind and solar in the california wholesale electricity market. *Energy Economics*, 85:104552, 2020.

[30] Ingmar Schlecht and Hannes Weigt. Swissmod-A Model of the Swiss Electricity Market. 2014.

[31] Fred C. Schweppe, Michael C. Caramanis, Richard D. Tabors, and Roger E. Bohn. *Spot Pricing of Electricity*. Kluwer Academic, Boston, 1988.

[32] SFOE. Schweizerische Elektrizitätsstatistik 2019. https://pubdb.bfe.admin.ch/de/publication/download/10112, 2020.

[33] Swisstopo - Federal Office of Topography. swissAlti3D: The high precision digital elevation model of Switzerland. https://www.swisstopo.admin.ch/en/geodata/height/alti3d.html.

[34] Swisstopo - Federal Office of Topography. swissTLM3D: The large-scale topographic landscape model of Switzerland. https://www.swisstopo.admin.ch/en/geodata/landscape/tlm3d.html.

[35] Pascal Vuichard, Alexander Stauch, and Rolf Wüstenhagen. Keep it local and low-key: Social acceptance of alpine solar power projects. *Renewable and Sustainable Energy Reviews*, 138:110516, 2021.

[36] Jenny Winkler, Martin Pudlik, Mario Ragwitz, and Benjamin Pfulger. The market value of renewable electricity - Which factors really matter? *Applied Energy*, 184:464–481, 2016.

[37] Mengzhu Xiao, Tobias Junne, Jannik Haas, and Martin Klein. Plummeting costs of renewables - Are energy scenarios lagging? *Energy Strategy Reviews*, 35:100636, 2021.

[38] Ray D. Zimmerman, Carlos E. Murillo-Sánchez, and Robert J. Thomas. MATPOWER's extensible optimal power flow architecture. *2009 IEEE Power and Energy Society General Meeting, PES '09*, (2):1–7, 2009.

[39] Alexander Zipp. Revenue prospects of photovoltaic in Germany-Influence opportunities by variation of the plant orientation. *Energy Policy*, 81:86–97, 2015.

Curriculum Vitae

Personal data

Name, first name	Dujardin, Jérôme
Date (DD.MM.YYY)	06.09.1985
Nationality	French
Languages	French, English
E-Mail	jerome.dujardin@epfl.ch, jerome.dujardin@slf.ch

Professional and Research Interests

- Renewable energy system modeling
- Atmospheric science and numerical weather modeling
- Machine learning for environmental data
- Instrumentation, optical measurements, automation

Education

2002-2004	Preparatory classes in Mathematics and Physics (CPGE) – Faidherbe, Lille, France.
2004-2007	École Nationale Supérieure de Physique de Strasbourg (now Télécom Physique Strasbourg) – ENSPS, Strasbourg, France. Engineering degree and Master's degree in Physics.
2017-2021	Ph.D. – Swiss Federal Institute of Technology in Lausanne (EPFL), ENAC, CRYOS laboratory and WSL Institute for Snow and Avalanche Research SLF, Snow and Atmosphere, Snow processes.

Work Experience

2017-2021	Ph.D. on wind downscaling and renewable energy modeling - Electric system modeling with emphasis on hydropower, solar and wind - Optimization with heuristic methods - Deep learning applied to the downscaling of wind in complex terrain
2016-2017	Research assistant – EPFL, CRYOS - Power and energy balance model of Switzerland
2015	Automation and metrology engineer – Microcube SARL, Crissier, Switzerland - Integration of automated 3D measurement in industrial robots - Automation of a 3D microscope

Publication record

J. Dujardin and M. Lehning, "*Wind-Topo: Downscaling near-surface wind fields to high-resolution topography in highly complex terrain with deep learning*", 2021, submitted to Quarterly Journal of the Royal Meteorological Society

J. Dujardin, M. Schillinger, A. Kahl, J. Savelsbergt, I. Schlecht, and R. Lordan-Perret, "*Optimized market value of alpine solar photovoltaic installations*", 2021, submitted to Renewable Energy

J. Dujardin, A. Kahl, and M. Lehning, "*Synergistic optimization of renewable energy installations through evolution strategy*", 2021, Environmental Research Letters

J. Dujardin, A. Kahl, B. Kruyt, S. Bartlett, and M. Lehning, "*Interplay between photovoltaic, wind energy and storage hydropower in a fully renewable Switzerland*", 2017, Energy (citations: 58)

A. Sigmund, J. Dujardin, F. Comola, V. Sharma, H. Huwald, D. Brito Melo, N. Hirasawa, K. Nishimura, and M. Lehning "*Evidence of Strong Flux Underestimation by Bulk Parametrizations during Drifting and Blowing Snow*", 2021, Boundary-Layer Meteorology

A. Kahl, J. Dujardin, and M. Lehning, "*The bright side of PV production in snow-covered mountains*", 2019, PNAS (citations: 14)

S. Bartlett, J. Dujardin, A. Kahl, B. Kruyt, and M. Lehning, "*Charting the course: A possible route to a fully renewable Swiss power system*", 2018, Energy (citations: 10)

B. Kruyt, J. Dujardin, and M. Lehning, "*Improvement of Wind Power Assessment in Complex Terrain: The Case of COSMO-1 in the Swiss Alps*", 2018, Frontiers in Energy Research (citations: 5)

P. Manso, B. Monay, J. Dujardin, and A. Scheiss, "*Assessing the potential increase of seasonal energy storage to mitigate the impact of climate change in Switzerland: Case study of the Grande Dixence dam*", 2017, conference paper Hydro 2017 (citations: 1)

Teaching

2017 -	Assistant, Atmospheric Physics and Chemistry EPFL, BA (5 ECTS)
2004 - 2007	Mathematics, high school level

Supervision of theses

2019	Master's thesis on wind downscaling with machine learning

Expeditions

2018/2019	Setup of an autonomous measurement station for blowing snow and surface mass balance at S17, Showa station, JARE60 expedition